UNIVERSITÉ DE LORRAINE

Ecole Doctorale BioSE (Biologie, Santé, Environnement)

Thèse

Présentée et soutenue publiquement pour l'obtention du titre de

DOCTEUR DE L'UNIVERSITE DE LORRAINE

Mention: 《Science de la Vie et de la Santé》

par **Chaohua DENG**

Titre: Modification du phénotype des chondrocytes dans la plaque de croissance et le cartilage articulaire: de la physiologie à la pathologie

Title: Modification of chondrocyte phenotype in growth plate and articular cartilage : from physiology to pathology

---

Soutenue le 28 Juin 2017

Membres de jury :

Rapporteurs :

Mme Laurence LEGEAI-MALLET	Directeur de recherche, Imagine Institute, INSERM U1163, Paris, France
Mr Francis BERENBAUM	PU-PH, INSERM UMR_S938, Hôpital Saint-Antoine, Paris, France

Examinateurs :

Mme Maria-Christina ZENNARO	Directeur de recherche, UMR_S970, Hôpital Européen Georges Pompidou, Paris, France
Mr Arnaud BIANCHI	Ingénieur de recherche, UMR 7365 CNRS, Nancy, France (Directeur de thèse)
Mr Hervé KEMPF	Chargé de recherche, UMR 7365 CNRS, Nancy, France (Co-directeur de thèse)
Mme Anne PIZARD	Chargé de recherche, INSERM CIC 1433, INSERM UMRS 1116, Nancy, France (Co-directrice de thèse)

UMR 7365 CNRS, Ingénierie Moléculaire et Physiopathologie Articulaire (IMoPA),
9 Avenue de la Forêt de Haye, Biopôle de l'Université de Lorraine,
54505 Vandœuvre-lès-Nancy, France

Remerciements

À madame le Docteur **Laurence Legeai-Mallet**, monsieur le Professeur **Francis Berenbaum**, et madame le Docteur **Maria-Christina Zennaro** les membres de mon jury de thèse, pour avoir accepté de juger mon travail de doctorat. Je leur exprime mes sincères remerciements et ma profonde reconnaissance.

À monsieur le Professeur **Jean-Yves Jouzeau** et monsieur le Professeur **Bruno Charpentier**, pour m'avoir accueillis dans leur unité UMR 7365 CNRS IMoPA (Ingénierie Moléculaire et Physiopathologie Articulaire) et pour m'avoir permis d'y accomplir ma thèse.

À mon directeur de thèse, monsieur le Docteur **Arnaud Bianchi** ou **"NoNo"**, pour son aide scientifique et humaine au cours de ma thèse. Merci de m'avoir encouragé, fait confiance, fait des petites fiches pour planning mes manips et donné l'indépendance nécessaire pour mon project de thèse.

À mon co-directeur de thèse monsieur le **Docteur Hervé Kempf** ou **"Greg House"** tout spécialement, pour son aide et enseignement scientique au cours de mon séjour en France pendant la thèse, pour sa soutien importante et son aide pendant mon depart pour les congrès, et mon retour l'entretien de travail. Ses conseils et son avis (souvent critique) ont été indispensables pour l'aboutissement de mes travaux de thèse et des articles scientifiques. Merci pour toutes les discussions "scientifique et non scientifique" très agréables.

À mon co-directrice de thèse madame le Docteur **Anne Pizard** spécialement (qui est la première de toujours essayer appeller mon nom chinoise, la langue plus difficile du monde…)**,** je souhaiterais lui exprimer toute ma reconnaissance et ma gratitude pour m'avoir guidée et conseillée tout au long de mon travail de thèse. San elle, cette thèse et les belles publications sur BJP et ARD n'aurait pas pu voir le jour. Du coté non scientifique, ses "Home made" gateaux sont très délicieux et nous (ma femme et moi) aiment beaucoup.

À monsieur le Docteur **Xavier Houard** et madame le Docteur **Sandra Kaminski**, pour avoir accepté d'être mon comité de suivi de thèse. Je les remercie du temps

consacré à évaluer mes travaux et me donner des conseilles importants et je leur en suis reconnaissante.

À **la gouvernement chinoise et la service de l'Éducation**, Ambassade de Chine en France qui a financé ma thèse.

À **la SFBTM** pour son soutien

À tous les membres de équipe 4-IMoPA, Pascal, Fred, David, Meriem, Pascale, Julie, Cécile, Nathalie……,

À **tous amis chinois de l'Université Wuhan** à Nancy, Wang Yingying, Cai Huili, Wu Xianglei, Li Zhen, Liu Yihua, Yan Xu, Duan Jie, Hu yong, Luo Yun, Tu Qian, Li Yueying, Xu Song, Dan Pan, Liu Mengmeng, Pan Xiaomeng, Liang Shiheng, Peng Lu, Xu Yong, Xie Zhe, Zhang Lin, Xie Yu, Qian Chongsheng, Zhang Ganggang, Wei Chaojie, Liu Xing, Yu hao, Sun Zhen, Li Jie, Gong Caifeng**,** qu'ils sachent leur présence, leur soutien et leur encouragement m'ont été importants.

À **Nathalie Presle** spécialement, pour l'enseignement de histologie de l'OA au cours de mon project de thèse et les corrections pendant ma rétaction de thèse. Qu'il sache que son support a été très précieux.

À **Cécile Guillaume** spécialement, pour son support de l'organisation de tous les matériaux biomoléculaires, cellulaires… et son aide pour la continuation de mes expérimentations pendant mes absences.

À **ma femme Zhang Yuying** très très spécialement, pour sa soutien et encouragement dans les moments les plus difficiles jusque l'aboutissement de ma thèse.

À **ma petite fille Eva**, pour son gentillement pendant les soirs et les moments sympathiques qu'elle a apporté.

À **tous mes chère familles**, pour avoir cru en moi et pour m'avoir soutenue, encouragée et supportée dans les moments les plus difficiles jusque l'aboutissement de ma thèse.

Résumé de la thèse

Résumé de la thèse

MODIFICATIONS DU PHÉNOTYPE DES CHONDROCYTES DANS LA PLAQUE DE CROISSANCE ET LE CARTILAGE ARTICULAIRE: DE LA PHYSIOLOGIE À LA PATHOLOGIE

Dans les conditions physiologiques, les chondrocytes qui sont les cellules présentes dans la plaque de croissance et le cartilage articulaire, ont un phénotype stable qui leur permet d'assurer leur rôle au sein du tissu cartilagineux. Toutefois, des altérations de ce phénotype peuvent conduire à l'apparition de maladies touchant le squelette ou les articulations. Dans ce contexte, mon projet de thèse a eu pour objectif d'étudier les modifications du phénotype chondrocytaire survenant lors du développement de deux pathologies :

1. l'achondroplasie dans un modèle de souris déficientes en Matrix Gla Protein (MGP), un puissant inhibiteur de minéralisation.
2. l'arthrose associée aux troubles métaboliques en utilisant des rats SHHF$^{cp/cp}$ qui présentent une mutation du récepteur de la leptine et développent une obésité, une résistance à l'insuline, une dyslipidémie et une hypertension caractéristiques d'un syndrome métabolique.

1. Phénotype des chondrocytes et achondroplasie

Les souris déficientes en MGP présentent non seulement une calcification vasculaire massive mais également une minéralisation anormale de divers cartilages, notamment celui de la trachée ou celui de la plaque de croissance, à l'origine d'un nanisme de type achondroplasique (Luo et al., 1997). Si notamment du fait de leurs conséquences léthales précoces les calcifications vasculaires ont été largement étudiées, à l'inverse, les effets d'une déficience en Mgp sur la minéralisation du cartilage et des modifications du phénotype chondrocytaire n'ont que peu été abordés.

C'est dans ce contexte que j'ai entrepris chez les souris *Mgp*$^{-/-}$ des études

morphologiques, histologiques et moléculaires pour essayer de comprendre les mécanismes à l'origine des altération affectant les chondrocytes trachéaux et principalement de la plaque de croissance qui pourrait expliquer le retard de croissance.

Les résultats obtenus par ces différentes approches démontrent que l'absence de MGP conduit :

1. dans la trachée, à:

- l'accélération de la différenciation hypertrophique des chondrocytes trachéaux à l'origine de la minéralisation du cartilage du tronc respiratoire,

Une publication rassemblant l'ensemble de ces résultats est en cours de soumission (article #1):

- Tabcheh L*, Marulanda J*, **Deng C***, Bianchi A, Kraft T, Jouzeau JY, Murshed M, Kempf H. *MINERALIZATION OF THE MOUSE TRACHEA IS A SUDDEN AND EARLY PHYSIOLOGICAL EVENT, ACCELERATED BY THE ABSENCE OF MATRIX GLA PROTEIN*. *equal contribution

2. dans la plaque de croissance, à:

- l'apparition d'une zone hypertrophique raccourcie et perturbée dès 7 jours après la naissance (P7),
- la formation accélérée du centre d'ossification secondaire,
- une perturbation de l'expression des gènes impliqués dans la différenciation endochondrale qui prend place dans la plaque de croissance au cours du développement squelettique postnatal.

L'ensemble de ces modifications explique l'apparition du nanisme visible à partir de P21. De plus, mes derniers résultats suggèrent qu'une altération du mécanisme de régulation de l'autophagie pourrait être impliquée dans les défauts de la plaque de croissance, potentiellement lié à une augmentation de la signalisation FGF

Une publication rassemblant l'ensemble de ces résultats est en cours de préparation

(article #2):

- **Deng C**, Gemble A, Guillaume C, Bianchi A, Kempf H. *Growth plate postnatal development is compromised by matrix gla protein deficiency in mice: potential role of autophagy inhibition and elevated FGF signaling*.

Perspectives

L'activation du récepteur FGFR3 est connue pour entrainer une achondroplasie plus ou moins sévère chez l'homme et la souris (Shiang et al., 1994). Ce même récepteur a plus récemment été également impliqué dans la régulation du processus autophagique dans la plaque de croissance (Wang et al., 2015). Il serait par conséquent intéressant de déterminer si l'expression ou l'activation du récepteur FGFR3 est modifiée chez les souris *Mgp*$^{-/-}$ et si de tels changements peuvent être à l'origine de l'apparition des anomalies du phénotype observées dans les plaques de croissance des souris déficientes en MGP. Si nos résultats mettent en évidence un rôle essentiel de FGFR3, il paraît intéressant d'évaluer à plus long terme l'intérêt thérapeutique d'une modulation de ce récepteur pour le traitement des achondroplasies induites par une mutation perte de fonction de Mgp ou plus généralement induites par une modification de l'activité autophagique dans la plaque de croissance.

2. Phénotype chondrocytaire et arthrose métabolique

Un nombre croissant d'études epidémiologiques et expérimentales indique que le Syndrome Métabolique (SMet) qui se caractérise par le développement d'une obésité, d'une résistance à l'insuline, d'une dyslipidémie et d'une hypertension, est un facteur de risque important pour l'arthrose. Afin de mieux comprendre la contribution de ce syndrome dans cette arthropathie dégénérative, j'ai utilisé un modèle de rat SHHF (Spontaneously Hypertensive Heart Failure) qui comporte à la fois des rats maigres

témoins ($SHHF^{+/+}$) et des rats obèses ($SHHF^{cp/cp}$) atteints de SMet (Youcef et al., 2014).

Une étude à laquelle j'ai participé a permis de démontrer qu'un traitement chronique de ces rats $SHHF^{cp/cp}$ par de l'éplérénone, un antagoniste des récepteurs aux minéralocorticoïdes, améliore le profil métabolique de ces rats atteints de SMet (Youcef et al., 2016).

Fort de ces résultats, j'ai cherché à évaluer :

- le rôle du SMet dans les modifications du phénotype chondrocytaire ainsi que dans l'apparition des atteintes histologiques de l'articulation,
- l'effet de l'amélioration du SMet par l'éplérénone sur le développement d'atteintes articulaires,
- la contribution individuelle et combinatoires de 2 composants du SMet, à savoir l'hyperglycémie et la dyslipidémie représentée par un acide gras saturé (le palmitate), dans les modifications du phénotype chondrocytaire chez le rat.

Les données obtenues démontrent que :

- seuls les rats $SHHF^{cp/cp}$ atteints de SMet, c'est-à-dire ceux âgés de 12,5 mois, développent une arthrose sévère du genou avec une érosion importante du cartilage, une inflammation de la synoviale et la formation d'ostéophytes,
- le traitement chronique des rats $SHHF^{cp/cp}$ par l'éplérénone prévient l'apparition de ces lésions articulaires,
- le palmitate induit une réponse inflammatoire et dégénérative dans des chondrocytes de rats en culture, qui est augmentée par l'hyperglucidie et qui est sans doute reliée à une altération du mécanisme de l'autophagie. Le traitement des cellules par un acide gras polyinsaturé permet de prévenir les effets du palmitate.

L'ensemble de ces résultats très originaux confirme le rôle essentiel du SMet dans l'arthrose et offre des perspectives thérapeutiques intéressantes pour le traitement de l'arthrose d'origine métabolique. Ces travaux sont rapportés dans deux manuscrits publiés (articles # 3 & #4), un autre en préparation (article # 5) :

- Youcef G, Olivier A, Nicot N, Muller A, **Deng C**, Labat C, Fay R, Rodriguez-Guéant RM, Leroy C, Jaisser F, Zannad F, Lacolley P, Vallar L, Pizard A *Preventive and chronic mineralocorticoid receptor antagonism is highly beneficial in obese SHHF rats*. **Br J Pharmacol.** 2016;173(11):1805-1819.
- **Deng C**, Bianchi A, Presle N, Moulin D, Koufany M, Kempf H, Pizard A**.** *Eplerenone treatment alleviates the development of joint lesions in a new rat model of spontaneous metabolic associated osteoarthritis.* **Ann Rheum Dis. 2017** May 5. doi: 10.1136/annrheumdis-2016-210700. [Epub ahead of print]
- **Deng C**, Gemble A, Guillaume C, Pizard A, Bianchi A, Kempf H. *Eicosapentaenoic acid attenuates the inflammatory and degenerative response of rat chondrocyte to palmitate and hyperglycemia via regulation of autophagy.* **Manuscrit en préparation.**

Le potentiel thérapeutique des antagonistes du récepteur minéralocorticoïde est quant à lui protégé par un dépôt de brevet:

- Dépôt de Brevet # 16 305 964.5 *"Methods and pharmaceutical compositions for the treatment of osteoarthritis"*

Perspectives

Les perspectives de ces travaux sont nombreuses. A court terme, il serait intéressant de préciser la cinétique d'apparition de la pathologie arthrosique chez les rats SHHF. L'analyse de biomarqueurs présents dans les prélèvements urinaires et sanguins collectés au cours de nos expériences chez les rats SHHF devrait permettre de répondre à cette question. Le rôle du récepteur aux minéralocorticoïdes pourra également être précisé *in vitro* sur des chondrocytes en culture ainsi que sur des échantillons de tissus articulaires prélevés chez des patients atteints d'arthrose.

Avant Propos

Avant Propos

Au cours de ma thèse intitulée «*Modification of chondrocyte phenotype in growth plate and articular cartilage: from physiology to pathology»,* je me suis intéressé aux modifications du phénotype chondrocytaire qui peuvent survenir au niveau de la plaque de croissance et ainsi perturber le développement postnatal, et dans le cartilage articulaire pour conduire à une arthropathie dégénérative comme l'arthrose.

Je me suis d'abord consacré à l'étude des effets d'une délétion du gène *Mgp* sur le phénotype cartilagineux au cours du développement postnatal chez la souris. J'ai ainsi participé à la première caractérisation du processus de minéralisation de la trachée qui s'accompagne d'une modification de phénotype des chondrocytes trachéaux vers une différenciation terminale de type hypertrophique. D'autre part, concernant le cartilage du squelette appendiculaire,, des résultats inattendus ont été obtenus : j'ai pu fournir des preuves morphologiques, histologiques et moléculaires solides montrant que le nanisme observé chez les souris déficientes en Mgp est probablement dû à la surexpression de FGFR3 dans la plaque de croissance et à la perturbation concomitante du mécanisme d'autophagie, deux facteurs—impliqués dans l'achondroplasie.

Parallèlement, je me suis intéressé aux modifications du phénotype chondrocytaire rencontrées au cours de l'arthrose et notamment celles induites par le syndrome métabolique (SMet). Mon travail a permis pour la première fois de décrire un modèle d'arthrose spontanée associée à un SMet chez des rats de la souche SHHF. En utilisant ce modèle, j'ai pu démontrer qu'un traitement chronique avec un antagoniste du récepteur aux minéralocorticoïdes, l'eplerenone, peut entraver le développement des lésions arthrosiques. Pour compléter cette étude réalisée *in vivo*, j'ai également effectué des expériences *in vitro* pour mieux caractériser les rôles individuels ou combinés de certains facteurs de risque associés au SMet, tels que l'hyperglycémie et la dyslipidémie, sur la modification du phénotype des chondrocytes.

A travers ces travaux que j'ai menés de front, j'ai du appréhender des domaines très divers et des modèles variés (souris, rats, culture de chondrocytes d'origine différente, ...). Ces années de recherche ont par conséquent été aussi passionnantes que difficiles à mener. Il en résulte une thèse probablement atypique notamment pas son aspect hétéroclite bien que son fil directeur reste les altérations du phénotype chondrocytaire, un thème cher à mon équipe d'accueil. En conséquence, le mémoire qui suit pourra apparaitre peu classique au moins dans son format puisqu'il est divisé en deux chapitres indépendants composés chacun d'une introduction propre, des résultats expérimentaux (papiers acceptés, soumis ou en préparation) et des perspectives de chaque travail. Ces parties indépendantes sont précédées par un court premier chapitre introductif présentant les deux tissus d'intérêt très brièvement car très bien discuté dans d'autres thèses du laboratoire ou des revues de la littérature.

Considérant les domaines divers et complexes abordés au cours de ma thèse, ce manuscrit n'a donc aucunement la prétention de présenter toutes les notions de façon exhaustive mais de donner les informations que j'ai pensées nécessaires et suffisantes pour exposer le cheminement scientifique qui mène aux différentes hypothèses à l'origine de ce travail de thèse.

En espérant que ces choix vous conviendront, je vous souhaite une bonne lecture...

Table of Contents

REMERCIEMENTS **2**

RÉSUMÉ DE LA THÈSE **5**

AVANT PROPOS **11**

LIST OF FIGURES **16**

LIST OF TABLES **17**

ABBREVIATIONS **18**

CHAPITRE 1 ..... **20**

GENERAL INTRODUCTION **20**

1.1 PHYSIOLOGIC MODIFICATION OF CHONDROCYTE PHENOTYPE IN CARTILAGE 21

1.1.1 Growth plate cartilage *21*

1.1.2 Articular cartilage *24*

1.2 PATHOLOGICAL MODIFICATION OF CHONDROCYTE PHENOTYPE IN CARTILAGE 26

CHAPTER 2 ..... **27**

MODIFICATION OF CHONDROCYTE PHENOTYPE INDUCED BY MATRIX GLA PROTEIN DEFICIENCY IN THE GROWTH PLATE DURING SKELETAL DEVELOPMENT **27**

2.1 MATRIX GLA PROTEIN 28

2.1.1 Brief introduction on Gla protein *28*

2.1.2 Discovery of MGP *29*

2.1.3 MGP mutation in human: Keutel Syndrome *30*

2.1.4 Function of MGP: an inhibitor of calcification *31*

2.1.5 MGP in skeletal development *33*

2.2 SKELETAL DYSPLASIAS 34

2.2.1 Achondroplasia *34*

2.2.2 Role of FGFR3 in skeletal development *35*

2.2.3 FGFR3 signaling in growth plate *36*

2.3 ROLE OF AUTOPHAGY IN SKELETAL DEVELOPMENT 39

CONTEXTE ET HYPOTHÈSE 42

ARTICLE NO.1: MGP AND CHONDROCYTE PHENOTYPE IN TRACHEAL CARTILAGE 43

ARTICLE NO.2 (IN PREPARATION): MGP AND CHONDROCYTE PHENOTYPE IN GROWTH PLATE CARTILAGE 44

CONCLUSION 64

DISCUSSION & PERSPECTIVE 65

I. No apparent skeletal abnormalties between MGP WT and KO during embryonic stages *65*

II. Compensatory role of GRP in MGP KO mice ? *65*

III. Are there treatments to rescue the skeletal phenotypes in MGP KO mice? *67*
III-A Treatment targeting MGP 67
III-B Treatment targeting MGP downstream signaling 71

CHAPTER 3 73

MODIFICATION OF CHONDROCYTE PHENOTYPE INDUCED BY METABOLIC FACTORS IN THE DEVELOPMENT OF OSTEOARTHRITIS 73

CHAPTER 3A 74

METABOLIC SYNDROME ASSOCIATED OSTEOARTHRITIS: STUDY ON ANIMAL MODEL 74

3A.1 METABOLIC SYNDROME ASSOCIATED OSTEOARTHRITIS 75
3A.1.1 Osteoarthritis 75
3A.1.2 Metabolic syndrome 77
3A.1.3 Metabolic syndrome and Osteoarthritis 78
3A.2 MINERALOCORTICOID RECEPTOR AND METABOLIC SYNDROME 81
3A.2.1 Brief introduction on mineralocorticoid receptor 81
3A.2.2 Mineralocorticoid Receptor Antagonists 82
3A.2.3 Mineralocorticoid receptor in metabolic syndrome 83
MR and Obesity 83
MR and Insulin resistance 83
3A.2.4 Critical mechanisms involved in MR activation 85
MR and oxidative stress 85
MR and fibrosis 86
MR and Inflammation 87
3A.3 ANIMAL MODELS OF METABOLIC SYNDROME 89
SHHF rat model 89
CONTEXTE ET HYPOTHÈSE 91
ARTICLE NO.3: SHHF RATS-A GOOD MODEL OF METS 92
ARTICLE NO.4: MRA TREATMENT REDUCES METS-ASSOCIATED OA IN SHHF RATS 93
CONCLUSIONS 94
DISCUSSION & PERSPECTIVE 95
I. The preventive effects of eplerenone on MetS-associated OA changes: indirect or direct? 95
II. Does Eplerenone have effects on the subchondral bone of the rats? 98
III. SHHF rat model can serve a instrumental tool for the study of MetS-associated OA? 99
IV. Eplerenone may constitute a preventive therapeutic strategy for MetS patients at increased risk of developing OA 100
V. MR is a potential target for the treatment of OA? 101

CHAPTER 3B 103

METABOLIC SYNDROME COMPONENTS AND OSTEOARTHRITIS: STUDY ON CHONDROCYTES 103

3B.1 OBESITY AND OA 104

Mechanical loading *104*
Metabolic stress *105*
3B.2 DIABETES AND OA 105
Hyperglycemia *106*
Insulin resistance *107*
3B.3 HYPERTENSION AND OA 107
3B.4 DYSLIPIDEMIA AND OA 108
ARTICLE NO.5 (IN PREPARATION): EPA REDUCES INFLAMMATION VIA AUTOPHAGY 110
CONCLUSIONS 125
DISCUSSION & PERSPECTIVE 126
I. Omega-3 fatty acid : a potential therapeutic choice for OA? *126*
II. Autophagy will be critical therapeutic target in OA? *129*
REFERENCES 132

List of Figures

Figure 1 The stages of endochondral bone formation in the developing mouse hindlimb. 22

Figure 2 Summary of regionalized gene expression in the growth plate. 23

Figure 3 A shematic representation of articular cartilage. 24

Figure 4 Vitamin K-dependent γ-glutamylcarboxylation. 28

Figure 5 Schematic presentation of MGP structure. 30

Figure 6 Clinical characteristics of KS patients. 31

Figure 7 Schematic representation of MGP in the regulation of mineralization. 32

Figure 8 Achondroplasia phenotypes at different ages. 35

Figure 9 FGFR3 expression (in situ hybridization) in proliferating and prehypertrophic chondrocytes and trabecular osteoblasts in a 21-day-old mouse tibia. 36

Figure 10 Schematic representation of FGFR3 downstream signaling in chondrocytes. 37

Figure 11 Different types of autophagy. 39

Figure 12 Proposed schematic representation of FGF18-dependent regulation of autophagy in growth plate chondrocytes. 41

Figure 13 Quantitative PCR results for the expression of GRP in MGP KO femur and primary chondrocytes. 67

Figure 14 Quantitative PCR results for the expression of MGP and BMP2 in the primary chondrocytes from MGP WT and KO pups. 69

Figure 15 STS has no preventive effect on vascular calcification, but impairs skeletal development. 70

Figure 16 Schematic representation of summarized therapeutic approaches targeting FGFR3 signaling for ACH. 71

Figure 17 Articular structures that are affected in OA. 75

Figure 18 Multivariate logistic regression analysis of the Odds ratios for occurrence and progression of knee OA during the 3-year follow-up period vs the number of MetS components. 79

Figure 19 MR expression in human tissues. 81

Figure 20 Summarized potential mechanisms of MR activation induced insulin resistance. 85

Figure 21 Mechanisms by which aldosterone/MR activation induces oxidative stress. 86

Figure 22 Shematic presentation for the effects of cell-specific MR activation. ..88

Figure 23 Schematic representation for the mutation of leptin receptor in SHHF$^{cp/cp}$ rat. 90

Figure 24 Follow-up of animal body weight during eplerenone treatment. 96

Figure 25 MR gene expression in femoral head cartilage of SHHF rats. 97

Figure 26 Quantitative PCR results performed mRNA from femoral head cartilage of SHHF rats. 98

Figure 27 Omega-3 fatty acids and the GPR120 signaling pathway. 127

Figure 28 Effect of agonists and antagonists of GPR40 and GPR120 on the expression of COX-2 induced by palmitate and high glucose. 128

Figure 29 Regulation and execution of autophagy. 130

List of Tables

Table 1 Proposal for different clinical phenotypes of OA. 76

Table 2 Frequently used definitions of MetS. 78

Table 3 Summary of epidemiological studies regarding the association between serum cholesterol levels and OA. 109

Abbreviations

ACH	Achondroplasia
AGEs	Advanced glycation end products
ATF6	Activating transcription factor 6
BGP	Bone Gla protein
BMPs	Bone morphogenetic proteins
CHOP	C/EBP homologous protein
Col10a1	Collagen, type X, α1
Col2a1	Collagen, type II, α1
CTX-II	Compare C-Telopeptide of Type II Collagen
DAMPs	Danger-associated molecular pattern molecules
DHA	Docosahexaenoic acid
DM	Diabetes mellitus
DMOADs	Disease-modifying OA drugs
ECM	Extracellular matrix
ECMM	Extracellular matrix mineralization
EGIR	European Group for the Study of Insulin Resistance
ELISA	Enzyme-linked immunosorbent assay
EPA	Eicosapentaenoic acid
ER	Endoplasmic reticulum
FFA	Free fatty acids
FGFR3	Fibroblast growth factor receptor 3
Gla	γ-carboxyglutamate
Glu	Glutamate
GLUT-1	Glucose transporter 1
GPCRs	G-protein-coupled receptors
GRP	Gla-rich protein
HDL	High-density lipoprotein
HF	Heart failure
IDF	International Diabetes Federation
IHH	Indian hedgehog
IL-6	Interleukin-6
InsR	High affinity insulin receptor
KS	Keutel syndrome
LC3	Microtubule-associated protein light chain 3
LDL	Low-density lipoprotein
LRP6	Low-density lipoprotein receptor-related protein 6
MetS	Metabolic syndrome
MGP	Matrix Gla protein
MMP13	Matrix metalloproteinase 13
MR	Mineralocorticoid receptor

MRA	Mineralocorticoid receptor antagonist
MRI	Magnetic resonance imaging
mTOR	Mammalian target of rapamycin
NCEP ATP III	National Cholesterol Education Program-Third Adult Treatment Panel
OA	Osteoarthritis
OPN	Osteopontin
OR	Odds ratio
PA	Palmitate
PCR	Polymerase chain reaction
PGE2	Prostaglandin E2
PRGP	Proline rich Gla protein
PTHrP	Parathyroid hormone-related protein
ROAD	Research on Osteoarthritis/ osteoporosis Against Disability
ROS	Reactive oxygen species
SHHF	Spontaneously Hypertensive Heart Failure
STAT1	Signal Transducer and Activator of Transcription 1
STS	Sodium thiosulfate
TNF-α	Tumor necrosis factor-α
TOF-SIMS	Time of flight-secondary ion mass spectrometry
VEGF-A	Vascular endothelial growth factor A
VKA	Vitamin K antagonist
VKDPs	Vitamin K-dependent proteins
VSMCs	Vascular smooth muscle cells
WHO	World Health Organization
µCT	Micro-computed tomography
ω-3 PUFAs	Omega-3 polyunsaturated fatty acids

Chapitre 1

General introduction

1.1 Physiologic modification of chondrocyte phenotype in cartilage

Cartilage is a unique tissue characterized by an abundant extracellular matrix (ECM) and a single cell type, the chondrocyte. Modifications of chondrocyte phenotype, such as proliferation and hypertrophy, are physiological events occuring during skeletal development in growth plate cartilage and matrix remodeling in adult articular cartilage. In growth plate cartilage, chondrocytes play a central role in endochondral bone formation, through a combination of proliferation, ECM secretion and hypertrophy. In articular cartilage, the chondrocytes are distributed throughout distinct regions and maintain the balance between production and degradation of ECM components.

1.1.1 Growth plate cartilage

The growth plate is a highly specialized and dynamic cartilage structure, located between the metaphysis and epiphysis of long bones. The growth plate consists of several layers of chondrocytes, including resting, proliferating and hypertrophic chondrocytes that temporally and spatially follows a highly regulated developmental program. Longitudinal bone growth is driven by the proliferation and differentiation of chondrocytes in the growth plate, a process known as endochondral ossification (Kozhemyakina et al., 2015) (**Figure 1**).

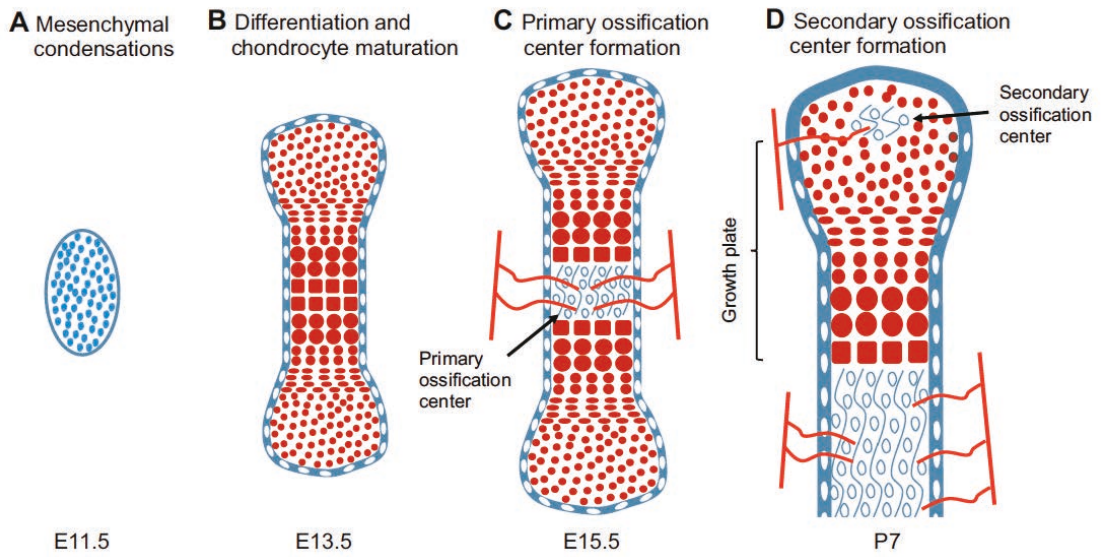

Figure 1 The stages of endochondral bone formation in the developing mouse hindlimb.
A. Mesenchymal cells (blue) begin to form condensation at E11.5 in the hindlimb buds. B. At E13.5, mesenchymal cells differentiate into chondrocytes (red), and the maturation of chondrocyte initiates. C. By around E15.5, the primary ossification forms with vascularization (red lines) and endochondral bone formation (open circles). D. By around 7 days of postnatal life (P7), the secondary ossification center forms. (Kozhemyakina et al., 2015)

In early stages of embryonic development, mesenchymal progenitors that originate from the lateral plate mesoderm contribute to the formation of growth plate. Condensations of the mesenchymal cells express the transcription factor Sox9, a key regulator of chondrogenesis, and give rise to cartilage primordia consisting of round immature chondrocytes (Akiyama et al., 2002; Bi et al., 1999). Then, the cells lying within the central regions of the cartilage primordia undergo proliferation and differentiation. Chondrocytes withdraw from the cell cycle, increase tremendously in volume and give rise to hypertrophic chondrocytes. Then the hypertrophic chondrocytes are subsequently replaced by bone in the region known as primary ossification center. A secondary ossification center then arises within the epiphysis, separating the growth plate from the distal ends of long bones.

During endochondral ossification, the molecular expression profiles of chondrocytes in the growth plate change progressively with the chondrocyte phenotype (**Figure 2**).

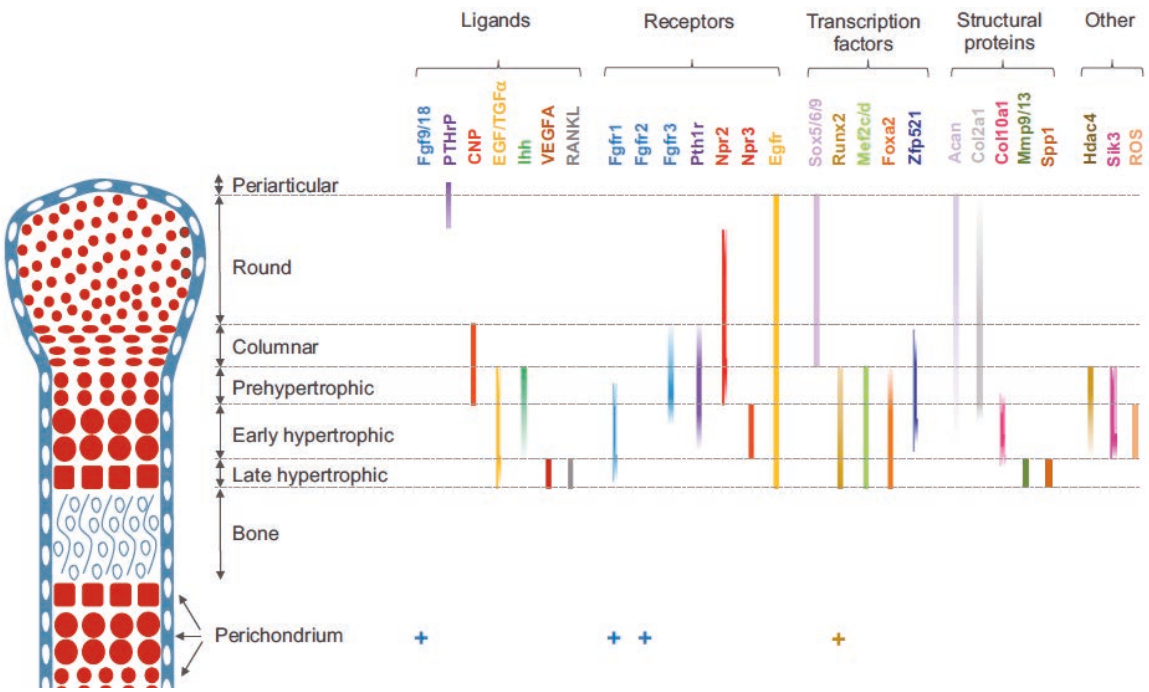

Figure 2 Summary of regionalized gene expression in the growth plate.
Schematic representation of the various zones of chondrocyte in a mouse long bone growth plate at around E15.5. The expression of various classes of genes and/or proteins is displayed. (Kozhemyakina et al., 2015)

Within the growth plate, immature proliferating chondrocytes express the transcription factor Sox9 and the structural proteins collagen, type II, α1 (Col2a1). The maturation of proliferating chondrocytes into prehypertrophic chondrocytes is marked by the expression of Indian hedgehog (IHH). This is followed by maturation into early hypertrophic chondrocytes that express collagen, type X, α1 (Col10a1). Finally, Col10a1-expressing cells progress to become late hypertrophic chondrocytes, which express vascular endothelial growth factor A (VEGF-A), matrix metalloproteinase 13 (MMP13) and osteopontin (OPN). The subsequent invasion of growth plate by endothelial cells, osteoblast precursors and osteoclasts remodel the growth plate matrix to form trabecular bone.

1.1.2 Articular cartilage

In healthy state, the articular cartilage provides two essential properties for the functions of joint: (1) the extremely low coefficient of friction during joint motion; (2) regulating the distribution of the mechanical forces across the joint. On the basis of studies of cartilage samples from different species and different joints, articular cartilage has been shown to compose a complex ECM that is highly organized and can be distinguished into four distinct zones, each with its own characteristic matrix appearance (Wong and Carter, 2003) (**Figure 3**).

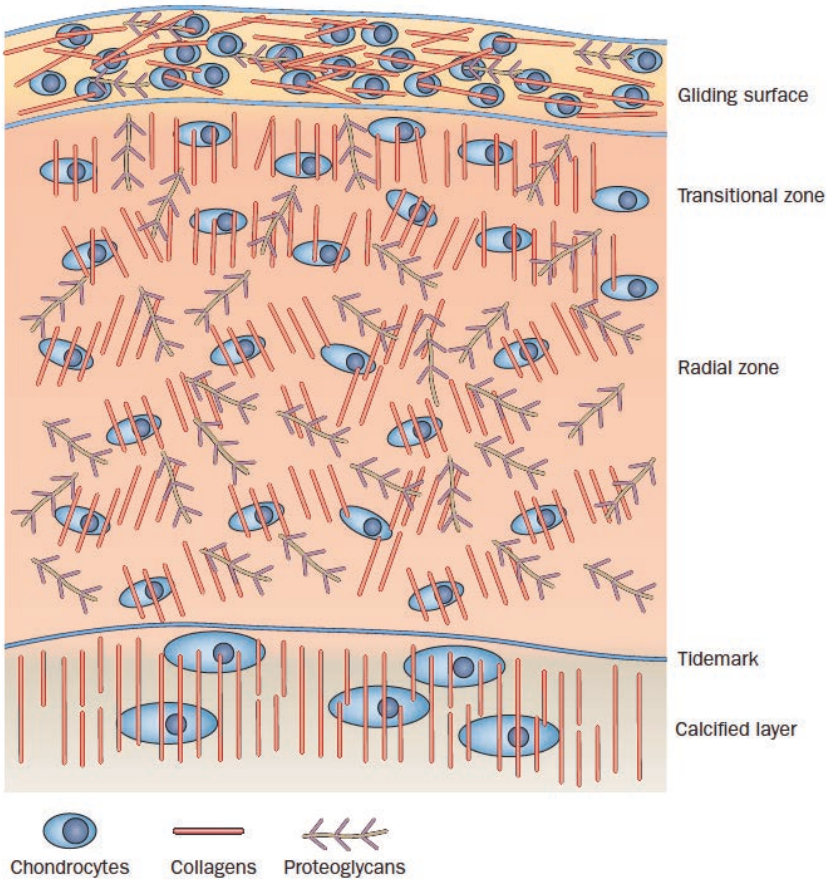

Figure 3 A shematic representation of articular cartilage.
Articular cartilage is organized into four different zones: the gliding surface, the transitional zone, the radial zone and the calcified layer. (Hardin et al., 2015)

The superficial zone, also known as the gliding surface, is composed of a layer of intertwined type I and type II collagen fibres oriented in parallel to the surface, which favours the distribution of joint compressive loads. This superficial zone

contains the highest amount of chondrocytes, which promote matrix synthesis and tissue repair. The second layer, or transitional zone, and the third layer, or radial zone have a low density of chondrocytes and their collagen fibres are organized obliquely and radially to the joint surface to increase resistance to compressive forces. The tidemark demarcates the radial zone from the calcified cartilage, which anchors the collagen fibrils to the subchondral bone. Chondrocytes are rare and mostly hypertrophic in the fourth zone, the calcified layer, which is located between the tidemark and the subchondral bone.

1.2 Pathological modification of chondrocyte phenotype in cartilage

Pathological alterations of chondrocyte phenotype could lead to numerous human skeletal and articular diseases, including dwarfism and osteoarthritic diseases.

In this context, my PhD project was designed to study the modifications of chondrocyte phenotypes:

(1) in the gowth plate, in a model of mild dwarfism caused by genetic deficiency in Matrix gla protein. This will be presented in the Chapter 2;

(2) in the articular cartilage, in a context of metabolic syndrome. In vivo and in vitro results will be described in the Chapter 3.

Chapter 2

Modification of chondrocyte phenotype induced by Matrix gla protein deficiency in the growth plate during skeletal development

2.1 Matrix Gla protein

2.1.1 Brief introduction on Gla protein

Gla proteins, also known as vitamin K-dependent proteins (VKDPs), have a common domain which is characterized by having modified glutamic acid residues, denominated γ-carboxyglutamate (Gla) residues. The biological activity of these proteins requires the conversion of glutamate (Glu) into Gla by a post-translational modification, known as γ-glutamylcarboxylation, which requires vitamin K as a cofactor (Bandyopadhyay et al., 2002) (**Figure 4**).

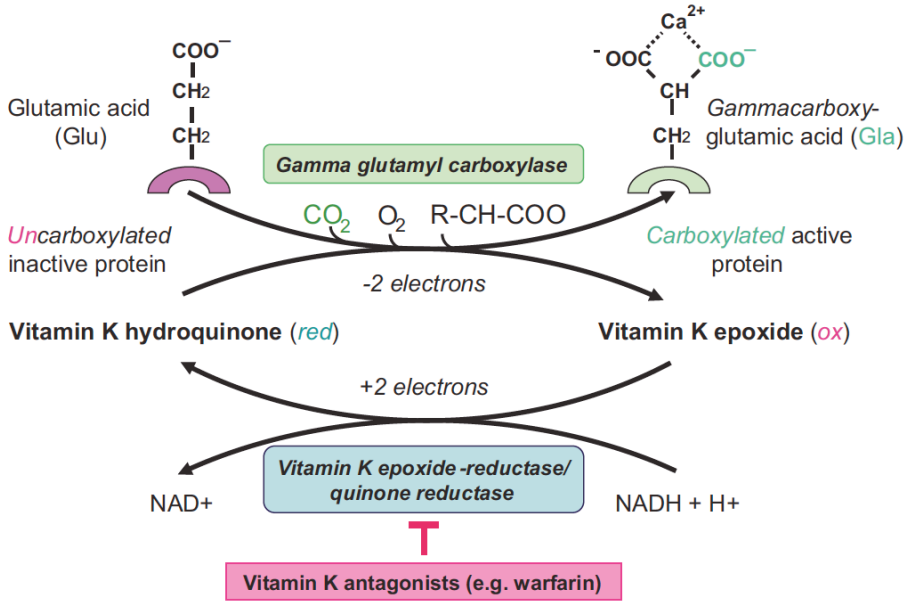

Figure 4 Vitamin K-dependent γ-glutamylcarboxylation.
(Gröber et al., 2014)

VKDPs can be categorized into two groups: hepatic and extrahepatic VKDPs. Hepatic VKDPs are mainly involved in the coagulation pathway by bridging their Gla residues through calcium (Ellison and Castellino, 1998; Sunnerhagen et al., 1996). Extrahepatic VKDPs were found in other tissues, such as the proline rich Gla protein (PRGP) 1 and 2 respectively in the spinal cord and thyroid (Kulman et al., 1997).

VKDPs were also found in calcified tissues and involved in the mineralization, such as matrix Gla protein (MGP), bone Gla protein (BGP) and a recently identified

Gla protein, the Gla-rich protein (GRP).

2.1.2 Discovery of MGP

MGP was first described in 1983 by Price et al, who purified it from the bovine bone matrix (Price et al., 1983). It is a 14 kDa secretory and structural protein of the ECM which belongs to a large family of extracellular mineral-binding proteins called Gla proteins. After its discovery in bone, MGP was also found to be synthesized in cartilage, lung, heart, kidney, arteries, skin, and calcified atherosclerotic plaques (Fraser and Price, 1988; Gheduzzi et al., 2007; Hale et al., 1988; Shanahan et al., 1999). The mature MGP protein consists of 84 amino-acids and contains three sites of serine phosphorylation and five sites of γ-carboxylation which can undergo two types of posttranslational modification: γ-glutamate carboxylation and serine phosphorylation (Hackeng et al., 2001) (**Figure 5**). To date, the conversion of five Glu residues into Gla in a vitamin K-dependent reaction, generating calcium binding sites, is the best-studied modification. Phosphorylation occurs at serine residues 3, 6, and 9, enabled by the tandemly repeated Ser-X-Glu motif within MGP and is carried out by the Golgi casein kinase (Price et al., 1994). The function of serine phosphorylation is not precisely known. Recent study suggest that it plays a role in regulating the secretion of proteins into the extracellular environment: phosphorylated MGP exits vascular smooth muscle cells (VSMCs) via the secretory pathway, whereas non-phosphorylated MGP is only partially secreted and appears in the cytosol (Wajih et al., 2004).

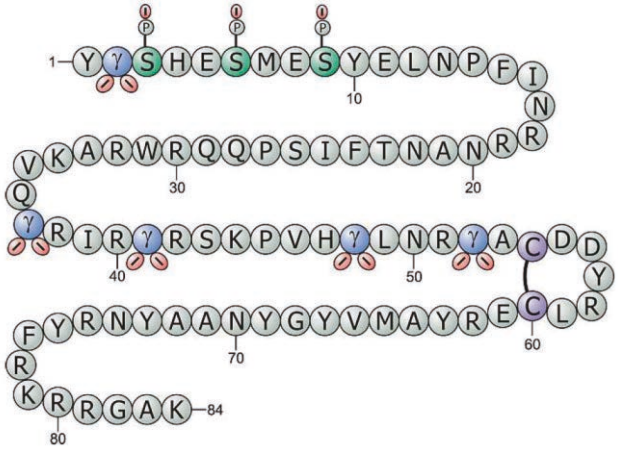

Figure 5 Schematic presentation of MGP structure.
(Schurgers et al., 2008)

2.1.3 MGP mutation in human: Keutel Syndrome

Keutel syndrome (KS, MIM 245150) is an autosomal recessive disorder first reported by Keutel in 1971, and characterized by abnormal cartilage calcification, peripheral pulmonary stenosis and midfacial hypoplasia (Keutel et al., 1971). Clinical characteristics of KS patients include abnormal calcification in laryngal, tracheobronchial, auricular, nasal and rib cartilage, brachytelephalangism and facial abnormalities such as mid-facial hypoplasia, depressed nasal bridge and reduced alae nasi (**Figure 6**) (CRANENBURG et al., 2011; Hur et al., 2005; Sun and Chen, 2012; Ziereisen et al., 1993).

Further symptoms include mild to severe unilateral or bilateral hearing loss, multiple peripheral pulmonary artery stenosis, mental retardation and dyspnoea. Long-term follow-up studies have revealed that KS patients develop skin lesions after 30 years of age (Khosroshahi et al., 2014) and suffer chronic and progressive respiratory disease caused by gradual laryngotrachebronchial calcification and stenosis (Meier et al., 2001).

It is well established that KS is due to loss-of-function mutations in the gene encoding the human MGP gene (Munroe et al., 1999).

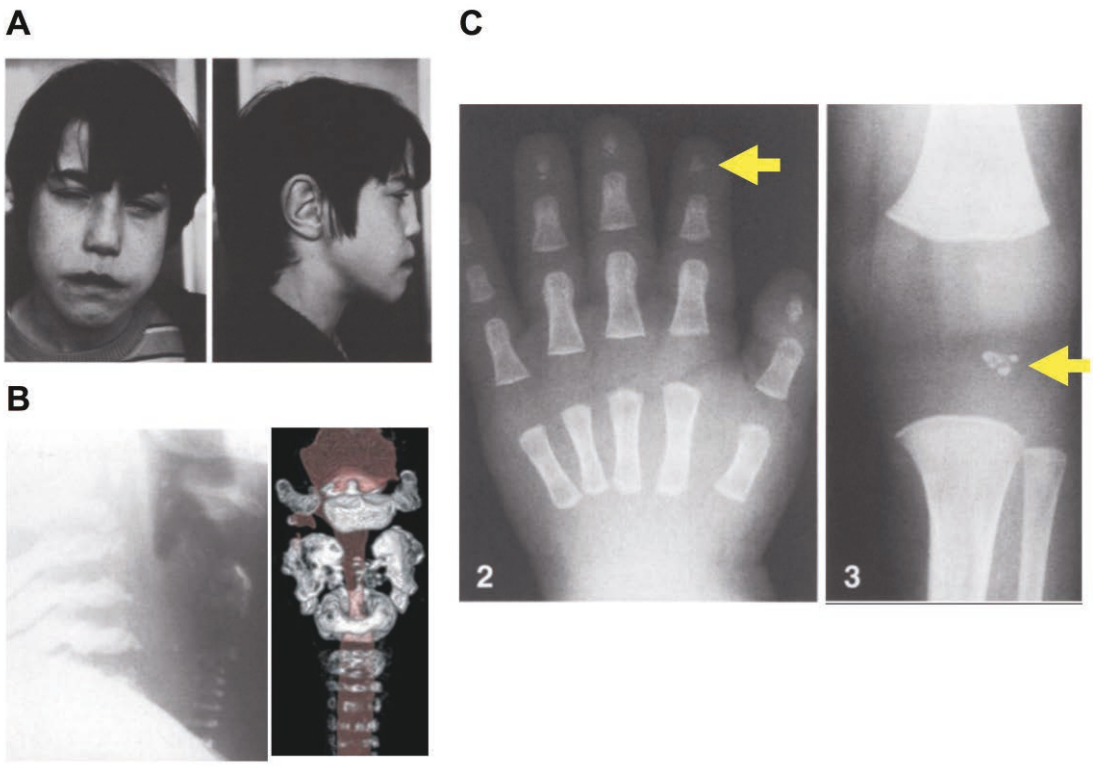

Figure 6 Clinical characteristics of KS patients.
A. The craniofacial appearance of the patients at the age of 13 years. B. Lateral film and three-dimensional CT scan reconstructions illustrate the calcification in the tracheal ring cartilage. C. Anteroposterior film of the left hand (2) showing shortness of the distal phalanges and stippled calcification in the first four distal phalanges; anteroposterior view of the left knee (3) showing stippled calcification in the patella (shown by yellow arrows). Adapted from (Fryns et al., 1984; Ziereisen et al., 1993)

2.1.4 Function of MGP: an inhibitor of calcification

The first clue for the role of MGP came from rats treated with vitamin K antagonist (VKA) warfarin. The warfarin-treated rats developed excessive cartilage calcification, leading to impaired growth, maxillonasal hypoplasia and reduction in the length of nasal bones (Feteih et al., 1990; Howe and Webster, 1992; Price et al., 1982). The role of MGP as an inhibitor of calcification was definitely confirmed, through the development of MGP-deficient mouse model (Luo et al., 1997). MGP knock-out mice develop massive calcification of the media, leading to the rupture of aorta and consequently the death of mice between six to eight weeks after birth (Luo et al., 1997). However, in contrast to MGP knockout mice, with the exception of only one clinical case (CRANENBURG et al., 2011; Meier et al., 2001), vascular

calcification has not been observed in KS patients, whereas high levels of circulating phosphorylated MGP was found. This suggests that the variable clinical features observed in KS patients may be explained by the altered levels of the different MGP species.

During the last decade, the role of MGP as an inhibitor of calcification in VSMCs has been largely studied (**Summarized in Figure 7**) (Schurgers et al., 2013), and will not be described here.

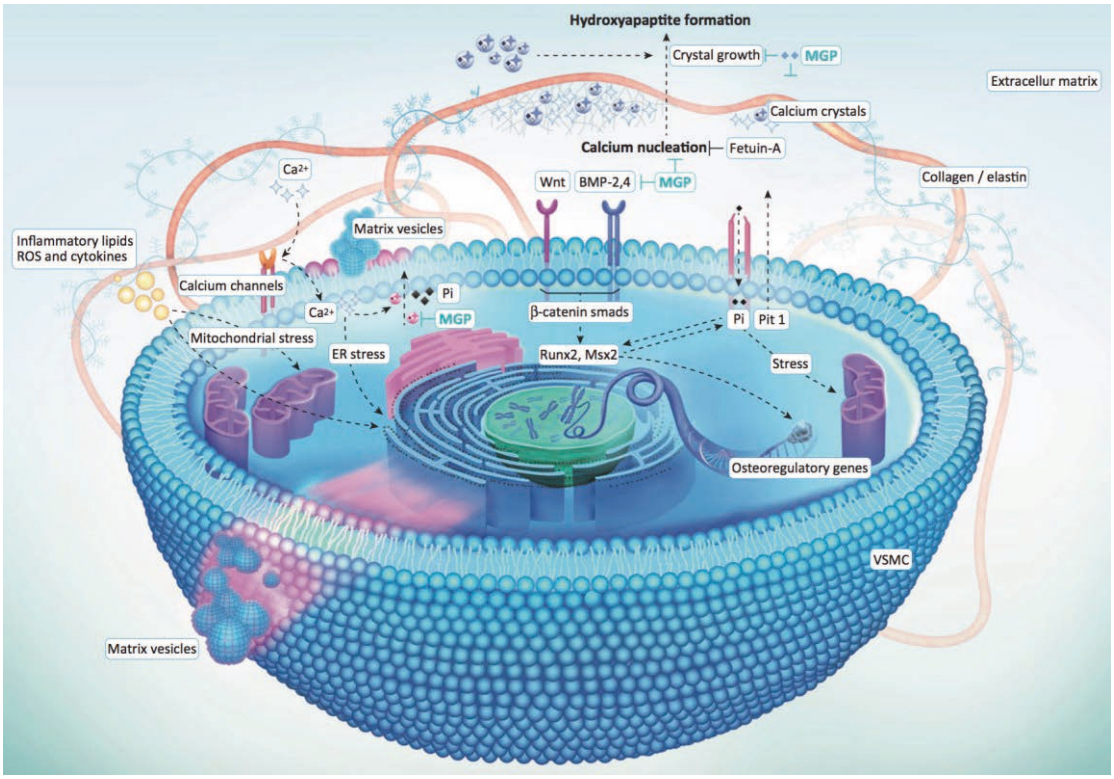

Figure 7 Schematic representation of MGP in the regulation of mineralization. (Schurgers et al., 2013)

In contrast, in the next part of the chapter, I will discuss the involvement of MGP deficiency in the pathologic mineralization of different cartilaginous tissues, focusing on the tracheal cartilage and the growth plate cartilage which is the orginal research work of my PhD project.

2.1.5 MGP in skeletal development

As mentioned earlier in Chapter 2.1.3, in most KS patients, we can observe brachytelephalangia of the fingers and abnormal calcification of patella (**Figure 6**). In a chick model, overexpression of MGP in the developing chick limbs could delay the maturation of chondrocytes and block endochondral ossification, while MGP inactivation could trigger the mineralization of cultured hypertrophic chondrocytes (Yagami et al., 1999). In addition, the original study reporting the MGP knock-out mice, the authors have described a short stature and abnormal mineralization of cartilage(Luo et al., 1997). All these observations suggest that MGP may play a role in bone and cartilage development during skeletogenesis.

However, in contrast to the vascular defects largely studied by different groups (Leroux-Berger et al., 2011; Luo et al., 1997; Murshed et al., 2004), no one described in detail the (tracheal and) skeletal defects observed in MGP KO mice leading to the dwarfism of these mice, that results from growth retardation.

2.2 Skeletal dysplasias

The skeletal dysplasias are generalized disorders of the skeleton and are diagnosed based on radiographic, clinical and molecular criteria (Krakow, 2015; Offiah, 2015). The 2015 Nosology and Classification of Genetic Skeletal Disorders listed 436 conditions, of which approximately 50 are perinatally lethal, and 316 are associated with one or more of 364 genes (Bonafe et al., 2015). The skeletal dysplasias for which the underlying gene defect is known can be found listed in a recent review (Krakow and Rimoin, 2010).

According to the molecular basis of the disease, the skeletal dysplasias are divided into 8 groups of conditions, including those related to fibroblast growth factor receptor 3 (FGFR3), type 2 collagen, type 11 collagen, sulfation disorders, perlecan, aggrecan, filamin, and Transient receptor potential cation channel subfamily V member 4 (TRPV4). The other 34 groups are organized according to their clinical and radiographic presentation (Bonafe et al., 2015).

Growth retardation disorders are certainly the most frequent and studied skeletal dysplasias. Briefly, besides growth-hormone deficiency that leads to extreme short stature, most dwarfisms are due to genetic deficiency in a restricted set of genes, implicated in growth plate formation. These include β-integrins (Bengtsson et al., 2005), the short stature homeobox gene (SHOX) (Marchini et al., 2016), or the most implicated and studied FGFR3 (Ornitz and Legeai-Mallet, 2017).

2.2.1 Achondroplasia

Achondroplasia (ACH) is the most common form of short-limb dwarfism in humans, affecting more than 250000 individuals worldwide. ACH is an autosomal dominant genetic disease and is estimated to occur in between one in 10000 and one in 30000 livebirths (Orioli et al., 1986).

ACH patient is characterized by short long bones, disproportional shortening of

the proximal skeletal segments (rhizomelia), impaired elbow extension, tibial bowing, exaggerated lumbar lordosis, shortening of the vertebral pedicles and narrowing of the lumbar interpedicular distance, shortening of the femoral head, macrocephaly, midface hypoplasia, frontal bossing, hearing loss, and a reduced size of the foramen magnum (Horton et al., 2007; Ornitz and Legeai-Mallet, 2017) (**Figure 8**). More than 95% of ACH patients have a mutation in the gene for FGFR3 (Ornitz and Legeai-Mallet, 2017).

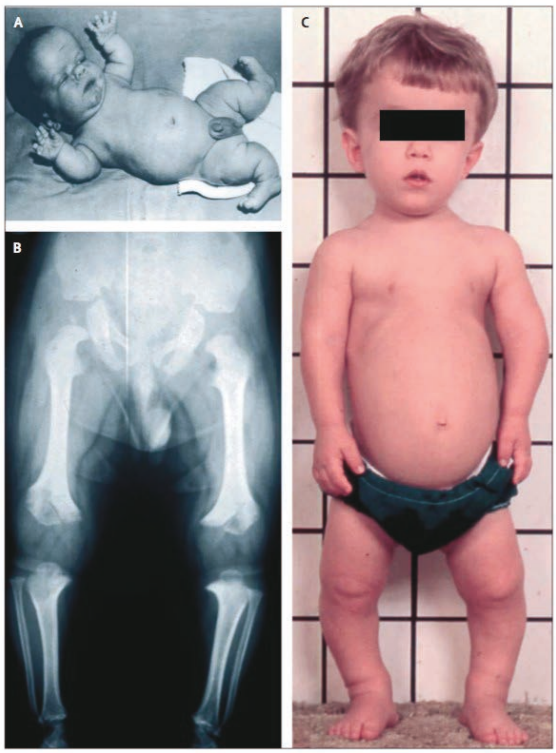

Figure 8 Achondroplasia phenotypes at different ages.
A. Infant with macrocephaly, frontal bossing, midface hypoplasia, small chest, rhizomelic shortening of all the limbs, redundant skin folds, and extreme joint laxity. B. Typical radiography of a child with achondroplasia. C. 3-year-old child with achondroplasia with typical features listed in A. (Horton et al., 2007)

2.2.2 Role of FGFR3 in skeletal development

FGFR3 is one of four high-affinity receptors for canonical FGF ligands, including FGF1-10, 16-18, 20 and 22 (Ornitz and Marie, 2015). FGFR3 is expressed in proliferating and prehypertrophic chondrocytes during embryonic and postnatal

development (Ornitz and Legeai-Mallet, 2017) (**Figure 9**).

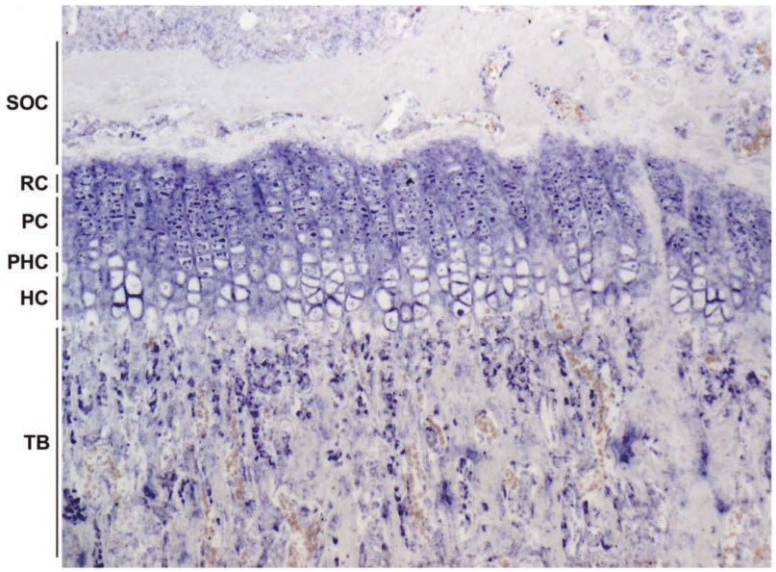

Figure 9 FGFR3 expression (in situ hybridization) in proliferating and prehypertrophic chondrocytes and trabecular osteoblasts in a 21-day-old mouse tibia.
SOC, secondary ossification center; RC, reserve chondrocyte zone; PC, proliferating chondrocyte zone; PHC, prehypertrophic chondrocyte zone; HC, hypertrophic chondrocyte zone; TB, trabecular bone. (Ornitz and Legeai-Mallet, 2017)

During the formation of growth plate in early embryonic stages of skeletal development, FGFR3 signaling promotes chondrogenesis (Iwata et al., 2000). Conversely, during postnatal skeletal growth, FGFR3 signaling inhibits chondrocyte proliferation and differentiation (Iwata et al., 2000). The paradoxical effect of FGFR3 in chondrogenesis underlies the etiology of ACH in which gain-of-function mutations in FGFR3 suppress the proliferation and differentiation of chondrocytes during prepubertal skeletal growth (Chen et al., 1999; Colvin et al., 1996; Deng et al., 1996; Li et al., 1999; Naski et al., 1996; Pannier et al., 2010).

2.2.3 FGFR3 signaling in growth plate

In growth plate, FGFR3 activates several intracellular signaling pathways, including Signal Transducer and Activator of Transcription 1 (STAT1), ERK1/2, p38 branches of the MAPK pathway and Snail1 (Chen et al., 1999; de Frutos et al., 2007; Legeai-Mallet et al., 2004; Li et al., 1999; Raucci et al., 2004; Su et al., 1997) (**Figure**

10). Recent studies demonstrated that mutant activated FGFR3 (FGFR3K650E) induces a differentiation block in growth plate chondrocytes by inducing persistent expression of Sox9, the master regulator of chondrogenesis. This dysregulation of Sox9 level is an underlying mechanism in the Thanatophoric Dysplasia, an extreme case of ACH caused by the K650E mutation of the FGFR3 gene (Shung et al., 2012; Zhou et al., 2015).

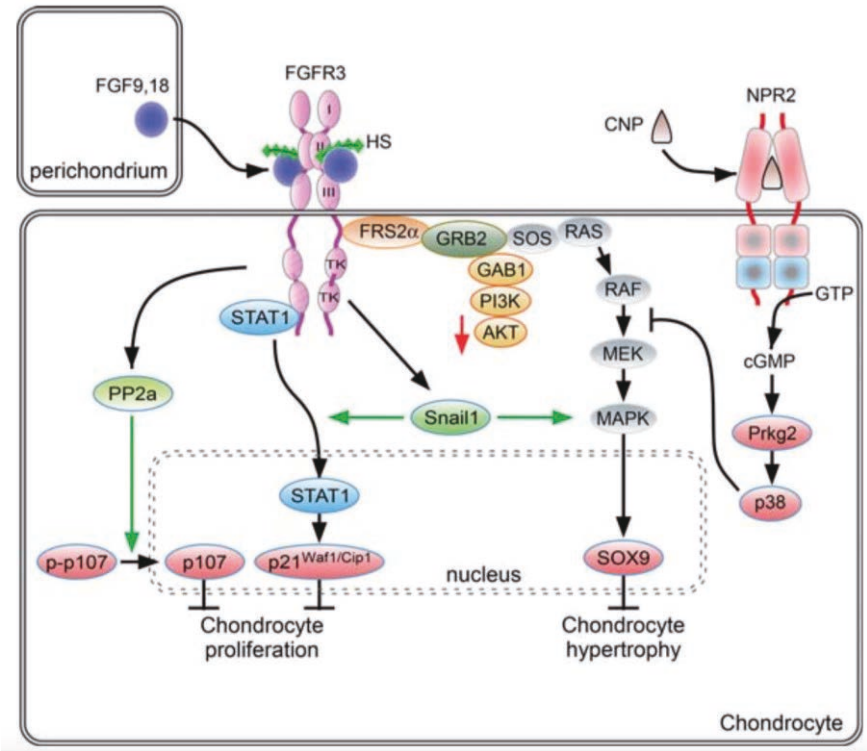

Figure 10 Schematic representation of FGFR3 downstream signaling in chondrocytes.
Activation of FGFR3 by FGF9 and FGF18, derived from the perichondrium and surrounding tissue, activates the STAT1 and MAPK signaling pathways. Activation of downstream signals, p107, $p21^{Waf1/Cip1}$, and Sox9 regulates chondrocyte proliferation and differentiation to hypertrophic chondrocytes. (Ornitz and Marie, 2015)

FGFR3 signaling may indirectly regulate other growth factor signaling pathways in chondrocytes, including PTHrP (parathyroid hormone-related protein), BMPs (bone morphogenetic proteins), IHH and Wnt signaling pathway. In mice with FGFR3 activating mutations, FGFR3 downregulated the Ihh signaling, the PTHrP signaling and BMP4 expression in growth plate chondrocytes (Chen et al., 2001; Naski et al., 1998). In addition, in a chondrocytic cell line, overexpression of FGFR3

downregulated the expression of PTH/PTHrP receptor gene (Li et al., 2010). FGFR3 could activate canonical Wnt/β-catenin pathway in chondrocytes via Erk MAP kinase-mediated phosphorylation of Wnt co-receptor LRP6 (Low-density lipoprotein receptor-related protein 6) and functions to suppress chondrocyte differentiation (Buchtova et al., 2015; Krejci et al., 2012). Finally, it has also been shown that FGFR3 can induce the degradation of BMPR1a, a BMP receptor essential in growth plate formation (Qi et al., 2014).

Recently, Wang et al. showed that activated FGFR3 signaling inhibits autophagic activity in chondrocytes, both in vivo and in vitro, leading to cartilage growth retardation in ACH. Autophagy inhibitors could suppress the cartilage development that resembles the inhibited chondrogenesis by activated FGFR3 signaling (Wang et al., 2015). These results indicate the essential role of autophagy in the pathogenesis of FGFR3-related ACH.

2.3 Role of Autophagy in skeletal development

Autophagy is the major intracellular degradation system by which cytoplasmic materials are delivered to and degraded in the lysosome in animal cells. There are roughly three classes of autophagy: macroautophagy, microautophagy, and chaperone-mediated autophagy (Mizushima and Komatsu, 2011) (**Figure 11**). Although different, the purpose of all three autophagic processes is to enable the cell to adapt to all types of stress. Macroautophagy is thought to be the major type of autophagy and has been studied most extensively. Therefore, macroautophagy is often simply refered as ‘‘autophagy’’.

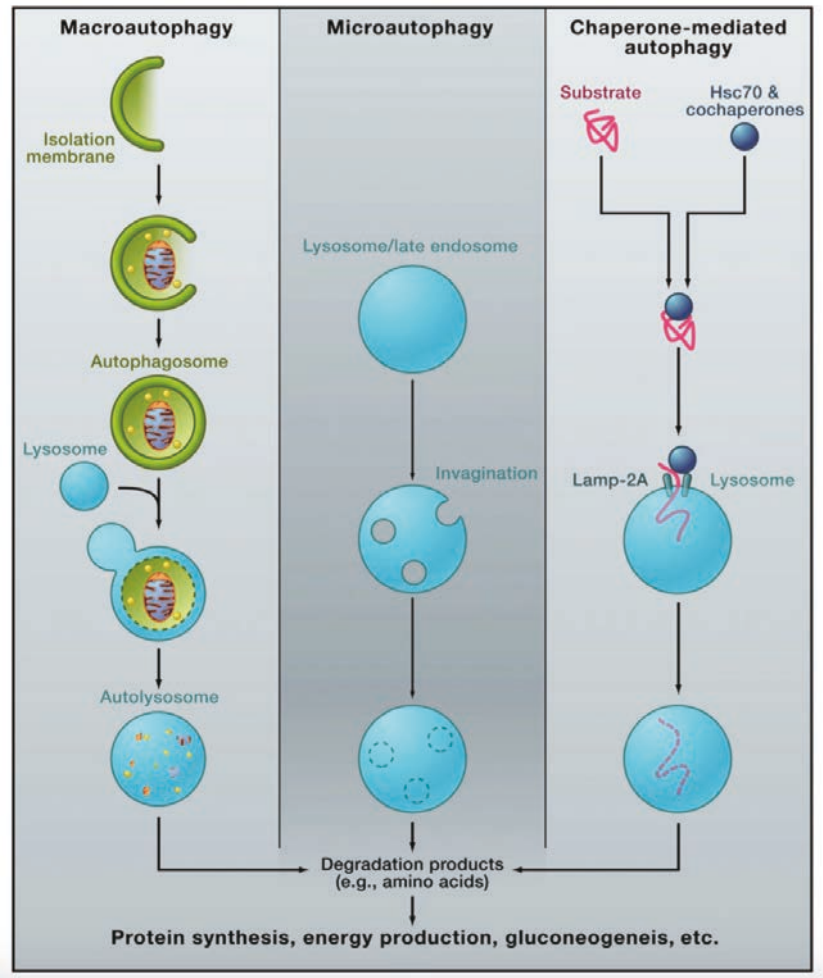

Figure 11 Different types of autophagy.
(Mizushima and Komatsu, 2011)

During growth plate development, autophagy regulates the maturation and the

hypertrophy of chondrocytes (Shapiro et al., 2014). A genome-wide association study showing link between autophagy and adult height in the Han Chinese population (Pan et al., 2010), suggests that autophagy may be involved in skeletal development. Autophagy is induced in growth plate chondrocytes during postnatal development and regulates the secretion of Col2, which is the major component of cartilage ECM (Cinque et al., 2015). Targeted deletion of autophagy genes Atg5 or Atg7 in chondrocytes lead to mild growth retardation associated with enhanced chondrocyte cell death and decreased cell proliferation (Vuppalapati et al., 2015).

The link between autophagy and FGF signaling regulated chondrogenesis has recently been identified by several research groups.

Wang et al. showed that activated-FGFR3 signaling inhibits autophagic activity in chondrocytes, both in vivo and in vitro, by decreasing the protein level of ATG12-ATG5 conjugate (Wang et al., 2015). Autophagy in FGF18 knockout mice is completely suppressed in growth plate from embryonic stage, while FGF18 heterozygous mice and FGFR4 knockout mice failed to induce autophagy during postnatal development and showed decreased type II collagen expression in the growth plate. This phenotype is regulated by FGF18-dependent regulation of autophagy in chondrocytes (Cinque et al., 2015) (**Figure 12**).

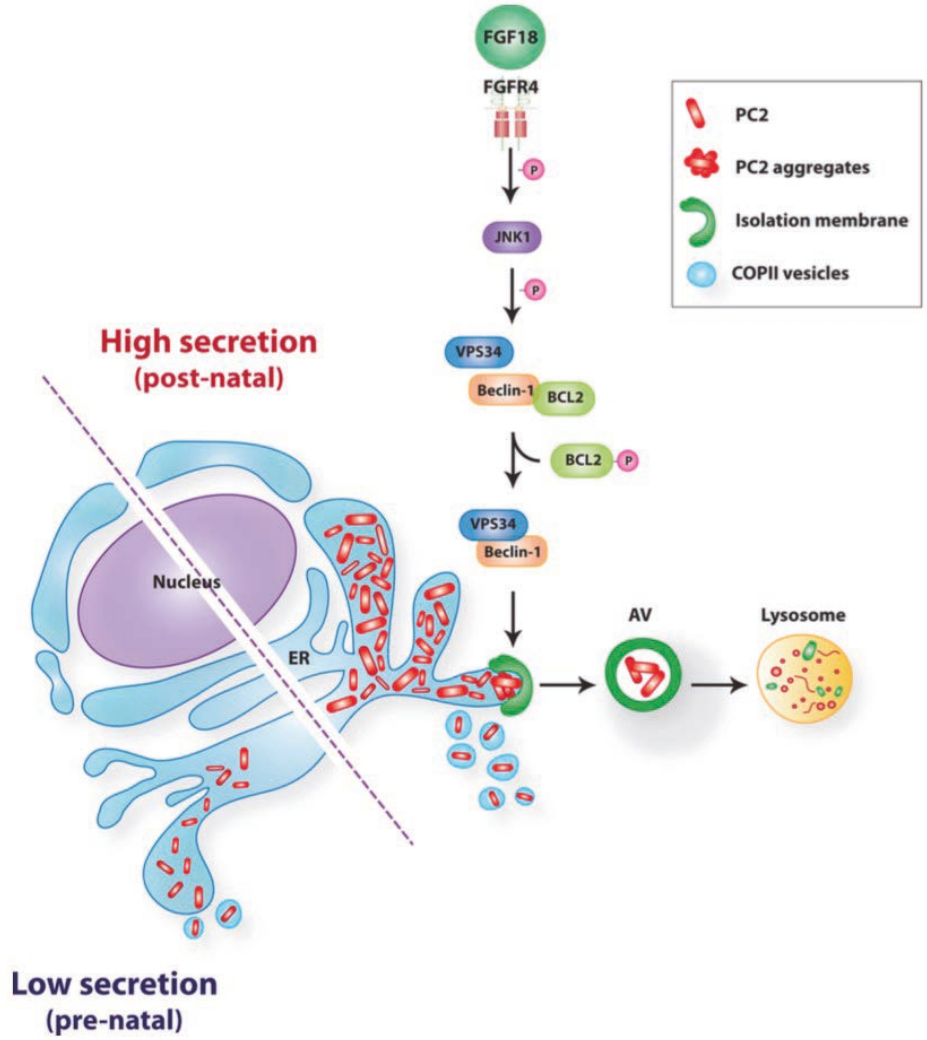

Figure 12 Proposed schematic representation of FGF18-dependent regulation of autophagy in growth plate chondrocytes.
During early postnatal stages of skeletal development, FGF18 induces the activation of FGFR4 and JNK kinase, which phosphorylates BCL2 and activates the VPS34-beclin1 autophagy complex. This process induces autophagy, which maintains PC2 (type II procollagen) homeostasis by preventing accumulation of PC2 in the ER. (Cinque et al., 2015)

Contexte et Hypothèse

Dans mon travail de thèse, j'ai décrit et étudié le rôle du MGP dans la minéralisation pathologique. La minéralisation de la matrice extracellulaire peut être physiologique ou pathologique. La minéralisation physiologique est un processus essentiel dans les os, les dents et le cartilage hypertrophique où la matrice extracellulaire souple est convertie en un matériau rigide capable de maintenir la force mécanique. La minéralisation pathologique peut se produire dans les artères, le cartilage et d'autres tissus mous, et peut causer une grande variété de symptômes selon le tissu où la minéralisation se produit.

Le MGP a été largement étudié et reconnu comme un inhibiteur de la calcification dans les tissus cardiovasculaires, le média et l'intima ded l'aorte, et le valve cardiaque.

L'absence de MGP chez la souris entraîne une minéralisation trachéale massive et accélérée chez la souris, qui ressemble à la calcification pathologique de la trachée chez les patients atteint du syndrôme de keutel ou les patients traités par la warfarine. Le mécanisme à l'origine ce phénomène a été étudié chez les souris déficientes en MGP (***voir l'article N°1: MGP et la minéralisation trachéale***).

La déficience en MGP entraîne également un nanisme (achondroplasie) qui n'a pas été étudié. L'objectif de mon projet principal de thèse est d'étudier le mécanisme sous-jacent de la minéralisation de la matrice extracellulaire anormal dans le cartilage de plaque de croissance de souris déficiente en MGP (***voir l'article N°2: MGP et développement squelettique***).

Article No.1: MGP and chondrocyte phenotype in tracheal cartilage

MINERALIZATION OF THE MOUSE TRACHEA IS A SUDDEN AND EARLY PHYSIOLOGICAL EVENT, ACCELERATED BY THE ABSENCE OF MATRIX GLA PROTEIN

Lina Tabcheh[1,#], Juliana Marulanda Montoya[2,#], **Chaohua Deng[1,#]**, Arnaud Bianchi[1], Tabea Kraft[1], Jean-Yves Jouzeau[1], Monzur Murshed[2,*] and Hervé Kempf[1,*]

1. UMR 7365 CNRS–Université de Lorraine, IMoPA, Vandoeuvre-lès-Nancy 54500, France

2. Department of Medecine, Faculty of Dentistry, McGill University, H3A 1G1, Montreal, Canada

 # These authors contributed equally to this work.

*** Corresponding authors**

Direct Submission/Classification BIOLOGICAL SCIENCES Cell Biology

MINERALIZATION OF THE MOUSE TRACHEA IS A SUDDEN AND EARLY PHYSIOLOGICAL EVENT, ACCELERATED BY THE ABSENCE OF MATRIX GLA PROTEIN.

Lina Tabcheh[1,#], Juliana Marulanda Montoya[2,#], Chaohua Deng[1,#], Arnaud Bianchi[1], Tabea Kraft[1], Jean-Yves Jouzeau[1], Monzur Murshed[2,*] and Hervé Kempf[1,*]

1. UMR 7365 CNRS–Université de Lorraine, Laboratoire d'Ingeniérie Moléculaire et Physiopatholgie Articulaire, IMoPA, Faculté de Médecine, Vandoeuvre-lès-Nancy 54500, France

2. Department of Medecine, Faculty of Dentistry, McGill University, H3A 1G1, Montreal, Canada

Running Title: Mineralization of the mouse trachea

# these authors contributed equally to this work.

*Corresponding authors:

Hervé Kempf

UMR 7365 CNRS-Université de Lorraine, Ingénierie Moléculaire et Physiopathologie Articulaire (IMoPA), Biopôle de l'Université de Lorraine, Campus biologie-santé, Faculté de Médecine

9 Avenue de la Forêt de Haye – CS 50184

54505 Vandœuvre-lès-Nancy Cedex, FRANCE

tel. +33 3 83 685 426

e-mail: herve.kempf@inserm.fr

Monzur Murshed

Departement of Medecine, McGill University, 1003 Boulevard Décarie, H4A 0A9, Montreal, Canada

tel. 1(514)282-8255

e-mail: monzur.murshed@mcgill.ca

KEYWORDS:

Trachea, cartilage, mineralization, mouse, matrix gla protein

ABSTRACT

Tracheal cartilage is a C-shaped hyaline cartilage known as permanent cartilage. Compliance and elasticity are the two features required for tracheal cartilage in order to fulfill its function in preventing airway collapse. Tracheal mineralization is a rare condition mostly found in the elderly population where the elasticity of the trachea is compromised leading patients to eventually suffer from dyspnea. In that context, we ought to understand the cellular and molecular mechanisms at the origin of tracheal mineralization that has been unexplored so far and investigate the role of the Matrix Gla Protein in the process, as genetic or pharmacological inhibition of this protein has been shown to induce abnormal tracheal mineralization in very young individuals.

Our morphological and histological studies show an unexpected early mineralization of the cartilage rings of the trachea that is detected at only 30 days after birth in wild-type mice. This mineralization extends in a rostro-caudal pattern, through a process involving terminal differentiation of tracheal chondrocytes. We further demonstrated that, via a similar pattern and comparable mechanism, deficiency of *Mgp* accelerates the overall mineralization of the mouse respiratory tract.

The present study is the first to describe mouse tracheal calcification and provide evidence that, in the mouse, contrary to the typical notion, tracheal cartilage is not a permanent hyaline cartilage throughout life. It also authenticates Matrix Gla protein as a key factor in abnormal mineralization of the tracheobronchial tree.

SIGNIFICANCE STATEMENT

The trachea is a very complex structure of the respiratory tract, composed of C-shaped cartilaginous rings, made of hyaline cartilage. Although this cartilage does not typically mineralize, tracheal mineralization has been reported in humans in the elderly population and in rare pathological cases involving the Matrix gla protein (Mgp).

In this context, this work seeked to understand the mechanisms at the origin of tracheal mineralization that has been unexplored so far and establish the role of Mgp in the process.

In the course of this study, unanticipated results were obtained as we provide solid morphological, and histological evidence showing that, in mice, in contrast to what has been commonly predicted, the mineralization of the trachea is an early physiological event, that is indeed hastened when Mgp is defective.

INTRODUCTION

The trachea is a very complex structure of the respiratory tract, composed of C-shaped cartilaginous rings, made of hyaline cartilage. In contrast to other intensely studied cartilages such as the ones found in the developing growth plate or in the adult joints, very little information is available on the innate propensity of this structure to mineralize.

In the growth plate, the chondrocytes, sole type of cells of the cartilage tissue, have a transient phenotype: they first proliferate, then mature into hypertrophic cells, and are finally replaced by osteoblasts during endochondral ossification. In contrast, chondrocytes present in articular cartilage, laryngeal cartilage, tracheal and bronchial rings, nasal septum, costal cartilage, and intervertebral disks do not enter the maturation process. As a result, these structures persist throughout life and, as such, are viewed as permanent cartilage. However, this definition disregards the fact that, in humans, it has been reported that, on occasion, these 'permanent' cartilages, including that of the windpipe, undergoes mineralization with increasing age.

Tracheal calcification is considered a common finding in elderly patients. Indeed, it is seen almost exclusively in patients aged 40 years and older, especially in woman. Although visually remarkable by standard chest radiography, this is of no clinical significance. Nevertheless, patients with severe mineralization of the tracheobronchial tree can occasionnaly complain from stridor, wheezing and dyspnea (1). A radiologic study including 105 elderly individuals showed that 19% displayed subtle to severe calcifications in the cartilage rings of the trachea and bronchi (2). In the same line, it has been shown that phosphorus and calcium concentration in trachea reach their highest levels at seventieth, while the magnesium concentration remains stable and the sulfur concentration decreases with age (3). This suggested that during aging the calcifications of the trachea are due to the deposition of calcium-phosphate crystals, similar to those found in bones or in the vessel wall when patients develop vascular calcifications.

Extensive tracheobronchial mineralization may occur more often and be more severe in patients who have taken long-term anticoagulation therapy, such as Warfarin, after prosthetic heart valve replacement (4). Indeed, the percentage of tracheobronchial calcification is estimated to be 47% in adults receiving warfarin sodium compared to the 19% in age-matched control subjects (2). Noteworthy, although considered a very rare occurrence in young individuals always associated with stridor (5), several recent case reports have shown that this is not infrequent in children that underwent valve replacement to treat mitral valvular disease (6) or after Fontan surgery for single-ventricle palliation (7) and placed under Warfarin treatment. Patients with Keutel syndrome, a rare autosomal disease with less than 30 cases reported notably from Turkey and the Middle East, present prominent tracheobronchial calcification, sometimes associated with tracheobronchial stenosis (8) (9)

mostly leading to distressing dyspnea. Interestingly, altogether these clinical radiographic findings point up the potential role of the potent vitamin K-dependent calcification inhibitor called Matrix Gla Protein (MGP), as MGP activity is altered by anti-Vitamin K medication and the *Mgp* gene is mutated in Keutel Syndrome patients.

Besides these clinical studies in humans, there are hardly no data regarding tracheal mineralization in animal models. To our knowledge, tracheobronchial mineralization in the aged mice has not been studied. Moreover, if the potential role of Mgp has been suggested in the original paper describing the Mgp KO mice (10), it has never been investigated further since.

In this study, we thus carried out a thorough anatomical and histological analysis in order to determine the spatiotemporal onset and progression of trachea mineralization first in aging wild-type mice and in *Mgp*-deficient mice. This extensive and straightforward analysis led to very unanticipated results. Indeed, in contrast to what has been described in humans, our data undeniably demonstrate that, in the mouse, tracheal mineralization initiates in the cartilaginous rings as early as one month after birth and progresses through a rostrocaudal direction throughout the trachea to eventually spread in the bronchi after only 2 months. This process seems to be accompanied by the terminal differentiation of the chondrocytes of the rings. Additionnaly, we demonstrate that an absence of functional MGP, accelerates the process, although not as critically as in humans. Altogether, this study notably demonstrates that the tracheal cartilage cannot be considered a permanent hyaline cartilage in the windpipe, as it undergoes a maturation similar to that observed in the growth plate, which is facilitated by a lack of Matrix Gla Protein.

RESULTS

Tracheal mineralization in C57BL/6J wild-type mice follows a specific spatiotemporal pattern.

To identify the precise spatio-temporal occurence of tracheal mineralization in wild-type mice, we dissected and sequentialy stained with Alcian Blue and Alizarin Red the whole respiratory tract of C57BL/6J mice at different ages.

As anticipated, a broad and initial morphological analysis first revealed that, if newborn mice (P0 to P7) displayed no evidence of mineralization in the airway cartilage, the oldest (6-month old) specimens examined exhibited strong mineralization along the whole respiratory system (data not shown).

Thus, we undertook a more thorough investigation covering a narrower range of ages between P14 and P60. Alizarin red staining revealed that the thyroid cartilage of the larynx shows the first signs of mineralization at P17 (Fig. 1*A*). The mineralization spreads to the entire laryngeal cartilage over time (Fig.1*B*-*G*) with the cricoid cartilage being one of the last laryngeal structure to be mineralized at P30 (Fig. 1*F*). With regard to the trachea itself, if occasional and rare spots of AR staining could be found in the very first rings of P29 individuals, extensive mineralization of the trachea spontaneously starts at P30, as the first 5 or 6 cartilage rings display strong to very strong AB staining (Fig.1*F*), and slowly progresses to adjacent distal rings in a rostro-caudal direction (Fig. 1*G*) to fully cover the whole trachea and even extend within the two main bronchi after 2 months (Fig. 1*H*). Noteworthy, there does not seem to exist any sexual dimorphism in the mineralization process of the tracheal structures as we found similar pattern of initiation and progression between individuals, irregardless of their gender (Fig. S1). Interestingly, the number of rings affected and their degree of mineralization observed at P30 were virtually uniform between littermates and moderately variable between distinct litters (data not shown).

Altogether, these morphological observations suggest that there is a very short period of time around P30 where tracheal mineralization initiates in C57BL/6J mice.

Tracheal cartilage mineralization comparably happens in mice of different strains.

To confirm that these observations were not specific to the C57BL/6J strain and that tracheal mineralization comparably happens in mice of different strains, identical experiments were repeated in mice of a different background: the BALB/cJ mice (Fig. S2). Alcian Blue/Alizarin Red double staining on trachea collected from mice of the BALB/cJ strain revealed a spatiotemporal pattern of occurence and progression similar to that found for the C57BL/6J strain (Fig. S2*A*-*F*). However, in contrast to C57BL/6J mice, where the first patches of mineralization appeared at P17 in the larynx and affected the first upper cartilage rings at P30 (Fig. 1*F*), the mineralization of the trachea appeared even earlier in BALB/cJ mice.

Indeed, the very first rings are already weakly AR positive at P21 (Fig. S2*A*) and 5-7 rings are already mineralized as early as P25 (Fig. S2*A*). The tracheal mineralization is consequently completed earlier than what has been observed for C57BL/6J mice, as BALB/cJ trachea are already entirely AR positive at P45 (Fig. S2*F*).

Tracheal mineralization affects the core of the cartilage rings.

To validate and strengthen our morphological observations, histological experiments consisting of double staining Von-Kossa/Alcian blue were performed on longitudinal (Fig. 2) and transversal (Fig. S3) sections of trachea from C57BL/6J mice at different ages.

According to our morphological findings (Fig. 1), the thyroid cartilage mineralization can be noticed as early as P17 (Fig. 2*A*) and spreads all over the thyroid cartilage overtime (Fig. 2*A-F* and Fig. S3*B,C*). Cricoid cartilage mineralization can be observed starting at P29 (Fig. 2*I*). Trachea mineralization cannot be significantly detected in mice younger than 30-days old, neither in the upper part (Fig. 2*M-O* and Fig. S3*F*) nor in the lower part (Fig. 2*S-U* and Fig. S3*G*). Starting at P30, mineralization initiates in the upper part of the trachea (Fig. 2*P*) and intensifies thereafter (Fig. 2*Q,R*). No or faint mineralization can be detected in the lower part of the trachea from P31 onwards (Fig. 2*S-X* and Fig. S3*H*), although it fully calcifies only later in time (data not shown).

It is also important to note that longitudinal and transversal sections also reveal that tracheal mineralization occurs in the core of the cartilage rings, where chondrocytes become larger with time suggesting that they may undergo hypertrophy.

Chondrocyte terminal differentiation precedes tracheal mineralization.

To further characterize the process of tracheal mineralization, qPCR analysis of various potential genes potentially implicated in chondrocyte mineralization was performed on P20 to P30 samples isolated from upper or lower regions of C57BL/6 trachea (data not shown).

Among those genes differentially expressed between upper and lower trachea, *Collagen X* (*Coll X*) showed a marked difference between the two regions at any time point (Fig. 3). Compared to lower region, *Coll X* expression started to be significantly upregulated in the upper region at P20 (not shown) and continued to increase in this region at P25 and P30 (Fig. 3).

To verify that the *Coll X* upregulation observed by qPCR was qualitatively and geographically related to an upregulation of the marker in the mineralized region, we looked at its mRNA expression by *in situ* hybridization in the trachea of C57Bl/6J mice at P25 and P30. Interestingly, *Coll X* expression can be detected at low level at P25 and strong level at P30 in longitudinal (Fig. 3) and transversal (Fig. S4) sections of each region analyzed. Indeed, *Coll X* can be detected at P25 in the thyroid region that is already mineralized (compare Fig. 3A

and 3B), but also in regions that are not yet mineralized such as in the cricoid (Fig. 3E,F) and tracheal rings, with a decreasing gradient between upper cartilage rings (Fig. 3I) and lower cartilage rings (Fig. 3M) in agreement with qPCR results. At P30, *CollX* is strongly expressed in all respiratory regions analyzed, even in lower cartilage rings that are still devoid of mineralization at this stage (Fig. 3 and Fig. S4).

MGP-deficiency accelerates mineralization of the tracheal cartilaginous structures

To investigate the potential role of Mgp in mouse tracheal mineralization, we next compared its spatio-temporal progression between $Mgp^{+/+}$, $Mgp^{+/-}$ and $Mgp^{-/-}$ mice (Fig. 4). $Mgp^{+/+}$ mice, backcrossed in a pure C57BL/6J background, display a pattern of tracheal mineralization analogous to that of C57BL/6J wild type mice (compare Fig. 4 with Fig. 1). There was also no sign of major alteration of the pattern in mice heterozygous for the mutation. In contrast, *Mgp*-deficient mice showed an earlier and prompter mineralization of the respiratory tract. Indeed, in these mice, mineralization is initiated in the upper tracheal rings at P14, which happens to be 2 weeks earlier than $Mgp^{+/+}$ (or $Mgp^{+/-}$) mice. The ensuing spreading of the mineralization of the cartilage rings followed a rostro-caudal progression identical to that observed in control mice (WT or $Mgp^{+/+}$ mice) but completed in a week of time (Fig. 4), when it requires about a month in $Mgp^{+/+}$,$Mgp^{+/-}$ and wild-type mice (Fig. 1).

Comparison of in situ hybridization signals and Von Kossa staining allowed to confirm that, as in wild-type mice, hypertrophy of tracheal chondrocytes precedes mineralization, with upper rings being calcified before lower rings (Fig. 5*B,C*). At P21, a stage where mineralization is absent from the entire respiratory tract of $Mgp^{+/+}$ mice but on the contrary covers all the tract of $Mgp^{-/-}$ mice, qPCR confirmed that *Coll X* expression is higher when the mineralization is already engaged (Fig. 5*A*). Noteworthy, *Coll X* expression is confined in the core of the rings that initiates hypertrophy and surrounded by non-hypertrophic *Coll II* positive chondrocytes (Fig. 5*C*).

Mgp-deficiency induces extra-cartilaginous mineralization in the trachea.

Surprisingly, a diffuse extra-staining in a tissue that does not appear cartilaginous on the lumen side of the trachea is also appearing in $Mgp^{-/-}$ tracheal preparation (Fig. 4 and Fig. 5*B,C*). This signal is lacking in mice that are not deficient in *Mgp*, even at stage where the level of mineralization is maximum and spread all over the respiratory tract at P60 (Fig. 1H). Von Kossa staining clearly uncovered that, in addition to the mineralization that is located in the cartilage rings, there is also in $Mgp^{-/-}$ mice a strong and extended signal in the tracheal epithelium, which concomitantly displays a curvated structure and thus is very different from the normal linear and non-mineralized structure present in wild-type or $Mgp^{+/+}$ mice (arrows in Fig. 4, Fig. 5*B* and Fig6*B*).

Local MGP overexpression in cartilage partially rescues the tracheal calcification phenotype in *Mgp*$^{-/-}$ rings.

In further experiments, we wanted to better understand how Mgp is involved in tracheal mineralization (Fig. 6). To tackle this question, we examined the status of tracheal mineralization in various transgenic mice either restoring Mgp expression in vasculature or cartilage respectively or reducing systemic Pi level.

In *Mgp*$^{-/-}$;*SM22-Mgp* mice, in contrast to calcification of the vasculature which is totally rescued (11) (and data not shown), tracheal mineralization of the rings appears unaffected when compared to that observed in *Mgp*$^{-/-}$ mice (compare Fig. 6B and Fig. 6C). In *Mgp*$^{-/-}$;*Col2-Mgp* mice, in which no effect on vasculature was observed (12) (and data not shown), Mgp overexpression in cartilage cells partially prevent the accelerated mineralization affecting the cartilage rings observed in *Mgp*$^{-/-}$ mice (compare Fig. 6B and Fig. 6D). Finally, in *Mgp*$^{-/-}$*;Hyp* mice, where systemic phosphate levels are lowered by approximately 50% (13), no amelioration of the tracheal cartilage mineralization phenotype could be observed (Fig. 6E). Altogether, these results suggest that tracheal ring mineralization is most likely autonomously regulated and cannot be overcome by non-cartilaginous overexpression of Mgp or through Pi homeostasis regulation (Fig. 6).

Strikingly, whereas the mineralization occurring in the tracheal rings is only rescued in *Mgp*$^{-/-}$;*SM22-Mgp*, that affecting the epithelium is rescued in all the three compound mice analyzed (Fig. 6*C-E*). Together with the protection against mineralization, the epithelium structure is also realigned in the three different lines (Fig. 6*C-E*) and ressembles the wild-type epithelieum (Fig. 6*A*). This suggests that this abnormal epithelium phenotype is due to the modification of systemic phosphate concentration in *Mgp*$^{-/-}$ mice.

DISCUSSION

To investigate in vivo tracheal mineralization during mouse aging, we performed an extensive and straightforward study to reveal the precise time and location at which mineralization occurs and tried to understand the molecular mechanisms responsible for this process.

Interestingly and surprisingly, we discovered that, in contrast to the current concept that defines tracheal cartilage as a permanent hyaline cartilage, mineralization of the trachea is an early and sudden phenomenon in mice. Indeed, we found that mineralization starts around P30 in C57BL/6J mice in the upper rings immediately down the larynx, and through a rostro-caudal progression, spreads into the whole trachea and bronchi that become eventually completely calcified at P60. An identical pattern was also found in BALB/cJ mice, although it initiates even earlier in this strain, as we could detect the mineralization of the first rings as early as P25. Despite an exhaustive scrutiny of the literature, we could not find any tracheal differences reported between these two strains that could explain this difference in timing other than submucus gland distribution (14, 15). Although the implication of this structural element (with secretory function) in tracheal mineralization is obviously unconfirmed, it remains a disputable but possible hypothesis considering numerous reports showed that defects in one of the components of the trachea can lead to defects in others as in asthma (16) and cystic fibrosis (17, 18). Thus, although we have absolutely no evidence, we cannot rule out that submucus gland repartition may have a role in the timing variation observed in the occurrence of tracheal mineralization between the two strains studied.

In view of this striking phenotype, it is retrospectively very surprising that, except our current study, there has been no report of tracheal mineralization in early individuals in the mouse model. Our data are however in agreement and thus confirm and strengthen rather ancient data obtained in birds and rats. The tendency of the cartilage of avian vocal and respiratory systems to mineralize has been shown in the early 80's, when Hogg performed an extensive characterization of the timing and pattern of the mineralization process in syringeal, laryngeal and tracheal cartilages (19). He showed that the first tracheal ring start to mineralize at 126 days post-hatching. Interestingly, apart from the shape (complete in avian) and the number (>100), there are some major differences in term of mineralization with what we observed in the mouse: i) the process follows a caudo-rostral pattern, ii) it is incomplete as the tracheal rings at the cranial end tend to remain lightly to not mineralized, iii) the mineralization is due to the ossification of the cartilage rings (19). With regard to the only 3 reports by Bonnuci *et al*. in 1974 (20) and Sasano *et al.* in the mid-90's (21, 22) that studied mineralization in the rat, they all agree that mineralization of the tracheal cartilage can be seen in rather young

individuals. However, they only show Von Kossa staining in 10-week old rats, whereas they clearly detect hypertrophic chondrocytes in the central region of the tracheal rings at 4 weeks in postnatal rats. This is rather consistent with our results, although we observed earlier occurrence of Von Kossa (and Alizarin Red) staining since we can detect those in the upper cartilage of P30 WT mice. So, among rodents, there seem to have a clear shift towards early stages for the physiological mineralization in mice versus rats. However in both case, chondrocyte hypertrophy and calcified cartilage are responsible of the mineralization observed (21, 22), which is different from the ossification process noticed in birds (19) or even opposite to what occurs in the nasal septum mineralization of the very same *Mgp*-deficient mice (12). This propensity of tracheal chondrocyte to engage into terminal differentiation in rodents is further demonstrate at the molecular level. Indeed, we observed a progressive upregulation of *Coll X* mRNA expression in the cartilaginous rings of upper and lower regions, revealed both by qPCR and in situ hybridization. This is to some extent contradictory to previous work (22) performed on rats, where COLL X protein was detected in the developing tracheal ring of rats, but outside of the mineralized or hypertrophic zones, as immunoreactivity was localized in the uncalcified peripheral region of the trachea in all age groups included in the study (4,8 and 10 week old rats) (22).

Mgp is known as a potent mineralization inhibitor. In addition to the extensive mineralization of their arterial trunk, Mgp KO mice were also reported to develop abnormal early tracheal mineralization (10). Because we found that early tracheal mineralization was a physiological process in mice, we sought to revisit the potential effect of MGP deficiency in tracheal mineralization by comparing the tracheal phenotype of $Mgp^{+/+}$, $Mgp^{+/-}$ and $Mgp^{-/-}$ C57BL/6 mice. We found that the tracheal phenotype differs from $Mgp^{-/-}$ to their WT ($Mgp^{+/+}$) littermates since mineralization are more pronounced and more extended in the *Mgp*-deficient tracheal cartilage. When no mineralization was detected in the trachea of $Mgp^{+/+}$ mice at P28 postnatal, the trachea of $Mgp^{-/-}$ mice at the same age was already fully mineralized.

These morphological results suggest that MGP may play a role in the appearance of tracheal mineralization but this role in mice is more limited than originally thought based on observations in humans. Indeed our herby results strikingly contrast with its major role in humans, since patients with defective MGP expression or activity (Keutel syndrome or warfarin therapy) show enhanced calcification at very early ages, several decennia before aging-related mineralization. Further molecular analysis of the regulation of the genes potentially involved in the mineralization of the trachea between the three genotypes may help to decipher the role of Mgp in this process. However, we believe its role as a BMP inhibitor is important in the process. If as observed in WT mice, BMP2 peak at P26 is involved in the mineralization process (data not shown), it is reasonable to think that the

partial or complete absence of one of the inhibitor of the BMP signaling in the *Mgp*$^{+/-}$ and *Mgp*$^{-/-}$ trachea respectively may accelerate the mineralization process. Further investigations including crossing BMP2-conditionnal KO mice with *Mgp*$^{+/+}$, *Mgp*$^{+/-}$ and *Mgp*$^{-/-}$ mice would tremendously help understand the initiation of mineralization in the trachea.

In order to assess if the role of Mgp was autonomous or systemically regulated, we made use of transgenic mice that restore Mgp expression in either smooth muscle cells or in chondrocytes. If overexpression of Mgp in smooth muscle cells could not impede the appearance of tracheal mineralization, overexpression of Mgp in chondrocytes of the trachea resulted in a partial rescue of the phenotype. As the same strategy in the same transgenic line led to a complete rescue of the Mgp-deficiency dependent mineralization in the nasal septum, this difference in the penetrance of the rescue may be attributable in diverse transgene expression levels in the two types of cartilages. As a matter of fact, the tracheal cartilage has been shown to differ from other hyaline cartilage by expressing different levels or types of molecules (miRNAs, fibronectin or Snail). In addition, our preliminary and unpublished data demonstrate that the level of *Coll II* mRNA present in tracheal cartilage is lower than that present in other types of cartilage such as femoral or sternal cartilages. This low expression of *Coll II* might thus explains that the *Col2-Mgp* transgene is less effective in inducing high level of local *Mgp* in tracheal chondrocytes, where Coll2 activators are probably either less efficient or different and consequently activate the *Col2-Mgp* transgene

As Mgp deficiency is well known to induce spontaneous and massive calcification of the smooth muscle cells of the arteries (10, 11, 13, 23), one can wonder if it might also induce calcification of the tracheal smooth muscle cells that compose the dorsal muscular element of each ring. Although those tracheal smooth muscle cells are able to mineralize *in vitro* when treated with high concentration of Pi (24), no sign of mineralization of the trachealis muscle has been observed in *Mgp*$^{-/-}$ mice. This suggests that all smooth muscle cells are not prone to mineralize in absence of Mgp. If tracheal smooth muscle was immune to mineralization, we however uncovered that, in absence of Mgp production, the tracheal epithelium displays an ectopic mineralization and abnormal structure. This mineralization of this extra-cartilaginous tissue in *Mgp*-deficient mice is puzzling. This is not only rescued by *SM22-Mgp* overexpression when this has no effect on tracheal cartilage mineralization, but is also impeded in *Mgp*$^{-/-}$;*Col2-Mgp* and *Mgp*$^{-/-}$;*Hyp* mice. These results strongly suggest that, in contrast to the mineralization occuring in the tracheal chondrocytes, this is a mineralization that is systemically regulated. The existence of this epithelial mineralization is particularly interesting as it may have a crucial unsuspected role in tracheal function. Noteworthy, Keutel patients suffer from dyspnea, coughing, wheezing but also respiratory infections that most often are the cause of their hospitalization and the fortuitous disclosure of their syndrome.

However, although commonly thought and presented by clinicians as the origin of their symptoms, the mineralization of the tracheal rings may not be the genuine cause, which may rather be attributable to epithelial dysfunction. Indeed, the present study brings surprising but clear evidence that wild-type mice do mineralize very early their tracheal cartilage rings. Unless largely overlooked, wild-type mice bred massively worldwide has never been reported to have symptomatic respiratory problems. A similar reasoning can be made for birds that also mineralize and even ossify their trachea early in life (19). So, as in the avian or rodent species, it seems plausible that mineralization of the tracheal cartilage rings is not sufficient enough to cause respiratory trouble and infections, whereas mineralization occuring in the tracheal epithelium may favor those complications. Indeed, by affecting (reducing or even abolishing) its “mobility”, it is likely that the epithelium might be defective in its functions that include mucus production and movement. This impairement of critical physiological functions of the epithelium would thus lead to coughing and a drastic decrease in protection against pathogens responsible for increased susceptibility to infections. In this context, although beyond the scope of the present study, it would be worth to more precisely identify the epithelial cells that mineralize (probably cilitated cells) and investigate the alteration in the functions of the tracheal epithelium when mineralized. *Mgp*$^{-/-}$ mice have a short lifespan, due to the lethal vascular phenotype caused by massive vascular calcifications (10). However, as mineralization is appearing at P14, these mice may be a good model to investigate further the respiratory epthelium phenotype and provide clinicians with a novel possible explanation for the symptoms associated with tracheobranchial mineralization in warfarin-treated or Keutel patients.

Altogether our results demonstrate a very specific and early timing and pattern of calcification of the trachea in mice that display subtle to very substantial differences with other species (19-22). The most striking dissimilarity is that observed with humans, who in normal conditions display tracheal mineralization solely in very aged people (1). Also, if there seems that Matrix Gla Protein likely plays an important role in the precocious abnormal appearance of tracheobronchial calcifications in children with Keutel Syndrome (8, 9) or subjected to warfarin therapy (4, 6, 7), the role that was also potentially attributed in the development of trachea calcification observed in young *Mgp*-deficient mice (10) might has been somehow revisited. We bring evidence that its absence certainly accelerates the process. Moreover and more importantly, we also uncover a new tissue affected by Mgp-deficiency, the tracheal epithelium, which may explain the symptomatic affections suffered by Keutel patients, previously and possibly erroneously attributed to the mineralization of the tracheal cartilage

MATERIAL AND METHODS

Animals

C57BL6/J and BALB/cJ wild-type mice, originally supplied by Charles River (Charles River, France), were locally inbred. *Mgp*$^{+/+}$, *Mgp*$^{+/-}$, *Mgp*$^{-/-}$, *Mgp*$^{-/-}$*;SM22-Mgp*; *Mgp*$^{-/-}$*;Col2-Mgp*, *Mgp*$^{-/-}$*;Hyp* mice were described elsewhere (10-13). Mice were housed in conventional animal rooms under constant humidity (55 ± 10%) and temperature (22 ± 2ºC) in 12h light-dark cycle conditions. They were fed *ad libitum* with standard food diet (Scientific Animal Food & Engineering, France) and had free access to water. Mice were placed in reproductive conditions whenever necessary in order to maintain the colony or provide the sufficient number of mice for each experiments. For all the following procedures, adult mice were euthanized with CO_2 in an appropriate chamber (Minerva) and newborn or very young animals were euthanized by decapitation. All animal protocols were in accordance with the guideline set by the relevant animal care committee.

Whole-mount Alcian Blue (AB) and Alizarin Red (AR) staining

Euthanized mice were beheaded, skinned, and eviscerated from their internal organs with the exception of their full-length respiratory tract (trachea, bronchi and lungs). The specimens were then fixed in ethanol 95% for at least 2 days till the day of the experiments. Collected specimens were incubated in Alcian Blue 8GX (AB, Sigma A3157) solution (0.03% AB, 80% of 96% EtOH, 20% acetic acid) for approximately 18 hours. AB solution was replaced with 95% EtOH solution for at least 6 hours followed by 2% KOH solution until tissues are cleared out. Specimens were transferred to Alizarin Red S (AR, Sigma A5533) solution (0.003% in KOH 1%) until dark staining of the skeletal bones. Staining was then stopped at the very same time for all specimens in 1% KOH-20% glycerol solution while agitating. To store specimens for long periods of time, they were passed through glycerol/ethanol solutions (50/50, 80/20) and photographed in 100% glycerol solution.

Histology and in situ hybridization

Tracheas were collected promptly after animal euthanasia. They were fixed in sterile 4% paraformaldehyde solution (prepared in RNase-free PBS) overnight at 4° and kept in 70% EtOH for at least 24 hours at 4°C. Specimens were then dehydrated via routine procedures using a Tissue processor (Leica ASP 300S) and embedded in paraffin. Blocks were then sectioned with a manual rotary microtome (Leica RM 2135) and sections where positioned on Superfrost+ glass slides (Fisher, Germany). Images were taken with a Leica DMD 108.

For Von Kossa/Alcian Blue staining, sections were dewaxed and rehydrated through standard procedure. They were incubated for 1 hour in 2% silver nitrate (Normapur, VWR) solution (prepared in deionized water) under the light of a 60-Watt lamp, washed twice in

deionized water for 3 minutes, once in 1% acetone for 3 minutes, and finally incubated for 15 minutes in Alcian Blue solution (0.02% Alcian Blue, 70% ethanol, 30 ml acetic acid). They were then washed for 1 minute in 1% acetone, 2 minutes twice in water, dehydrated (3 minutes in 25% ethanol (EtOH), 3 in 50% EtOH and 3 in 75% EtOH), counterstained with 0.1 % eosine for 30 seconds, destained twice for 3 minutes in 100% EtOH, washed twice with xylene for 5 minutes and mounted using Petrex®.

Non-radioactive ISH was performed on 7µm-thick paraffin embedded longitudinal or transversal sections of mouse trachea specimens mounted on Superforst + glass slides (Fisher).

Sections were subjected to acid hydrolysis (0.2 N HCl, 15 min), proteinase K treatment (5 µg/ml in PBS, 15 min), postfixation (4% PFA, 5 minutes) and acetylation (0.25% acetic acid, 15 min). Each of these steps was followed by two 5-minute washes with PBS. After the last PBS wash, slides were rinsed with dH2O and air-dried, before a 2-hour prehybridization step, at 65°C, in hybridization solution [50% formamide, 10 mM Tris (pH 7.6), 200 µg/ml Torula yeast RNA, 1xDenhardt's solution, 10% dextran sulfate, 600mM NaCl, 0.25% SDS, 1 mM EDTA (pH 8.0)]. Hybridization with digoxygenin-labeled *Collagen II* (*Coll II*) and *Collagen X (Coll X*) RNA probes was performed overnight at 65°C. Posthybridization, slides were rinsed briefly in 5x SSC at 65°C, washed with 1x SSC, 50% formamide (65°C, 30 minutes), subjected to RNase A digestion to reduce nonspecific hybridization, and washed at increasing stringency with SSC buffers (final wash at 55°C with 0.2xSSC). Bound probes were detected with an alkaline phosphatase-conjugated anti-DIG antibody (Roche) and revealed with BM purple substrate (Roche).

RNA extraction and Quantitative-PCR

Wild-type and *Mgp*-deficient mice were sacrificed when they reach the demanded age, then trachea were dissected immediately following their death.

Tracheas were dissected in two parts: the upper part consisting of the first seven cartilage rings and the lower part from the eighth ring to the carina. Dissected parts were rinsed with PBS and directly frozen in liquid nitrogen and conserved at -80°C till the day of RNA extraction procedure.

Total RNA from upper or lower parts of the trachea was isolated using the RNeasy Plus Mini kit (Qiagen) according to manufacturer's instructions. Extracted RNA was reverse transcribed into cDNA by Reverse transcription reaction using the M-MLV enzyme (Invitrogen, 28025-013) and an adequate mix (dNTP, Buffer, random hexaprimer, DTT). cDNAs were then amplified and quantified by Real-time PCR, performed using the StepOne Plus technology

(Applied Biosystems) with primers specific to the genes of interest (sequences available upon request) and the iTAQ SYBRgreen master mix (Biorad) according to the manufacturer's instructions.

Melting curve was performed to determine melting temperature of the specific PCR products After amplification, the product size was checked on a 1% agarose gel stained with 0.5µg/ml GelRed^{TM} Nucleic Acid Gel Stain (Interchim). Each run included positive and negative reaction controls. S29 housekeeping gene was determined in parallel for each sample. Quantification was determined using the ΔΔCT method and the results were expressed as fold change over control.

Statistics

All experiments were repeated at least 3 times. All data are reported as means ± S.E.M. with statistical significance defined as $p<0.05$(*) using two-tailed distribution with equal variance student's t-test evaluated with Prism6 software (GraphPad).

ACKNOWLEDGMENTS

This study was funded through grants from the Fondation pour la Recherche Médicale local committee and by the Région Lorraine, Université de Lorraine and CNRS. This work was also supported by operating grants from the Canadian Institutes of Health Research (CIHR) Fund. Support for L.T was provided by a stipend from the Middle East Institute of Health (Dr Norman Makdissy), Tripoli, Lebanon. J.M received a studentship form RSBO. C.D was funded by the China Scholarship Council (CSC) graduate program. T.K was granted through a studentship from the University of Münster. M.M. is an FRQS chercheur-boursier.

We thank the members of both teams for their technical help and valuable discussions. We also thank the SFBTM for its continuous support.

REFERENCES

1. Jo S-H, et al. (2008) Tracheal calcification. *CMAJ* 179(3):291.

2. Moncada RM, et al. (1992) Tracheal and bronchial cartilaginous rings: warfarin sodium-induced calcification. *Radiology* 184(2):437–439.

3. Tohno S, et al. (2000) Age-dependent changes of elements in human trachea. *Biol Trace Elem Res* 77(2):131–138.

4. Thoongsuwan N, Stern EJ (2003) Warfarin-induced tracheobronchial calcification. *J Thorac Imaging* 18(2):110–112.

5. Rifkin MD, Pritzker HA (1984) Tracheobronchial cartilage calcification in children. Case reports and review of the literature. *The British journal of radiology* 57(676):293–296.

6. Golding LP, Walsh MJ, Sumner TE, Nakagawa TA (2013) Tracheobronchial calcifications in children. *Pediatric radiology* 43(8):937–940.

7. Eckersley L, Stirling J, Occleshaw C, Wilson N (2014) Two cases of warfarin-induced tracheobronchial calcification after Fontan surgery. *Pediatr Cardiol* 35(6):954–958.

8. Meier M, Weng LP, Alexandrakis E, Rüschoff J, Goeckenjan G (2001) Tracheobronchial stenosis in Keutel syndrome. *Eur Respir J* 17(3):566–569.

9. Sun L-F, Chen X (2012) Tracheobronchial stenosis in Keutel syndrome. *Indian Pediatr* 49(9):759.

10. Luo G, et al. (1997) Spontaneous calcification of arteries and cartilage in mice lacking matrix GLA protein. *Nature* 386(6620):78–81.

11. Murshed M, Schinke T, Mckee MD, Karsenty G (2004) Extracellular matrix mineralization is regulated locally; different roles of two gla-containing proteins. *J Cell Biol* 165(5):625–630.

12. Marulanda J, et al. (2017) Matrix Gla Protein Deficiency Impairs Nasal Septum Growth Causing Midface Hypoplasia. *Journal of Biological Chemistry*:jbc.M116.769802.

13. Murshed M, Harmey D, Millán JL, Mckee MD, Karsenty G (2005) Unique coexpression in osteoblasts of broadly expressed genes accounts for the spatial restriction of ECM mineralization to bone. *Genes Dev* 19(9):1093–1104.

14. Innes BA, Dorin JR (2001) Submucosal gland distribution in the mouse has a genetic determination localized on chromosome 9. *Mamm Genome* 12(2):124–128.

15. Widdicombe JH, et al. (2001) Distribution of tracheal and laryngeal mucous glands in some rodents and the rabbit. *J Anat* 198(Pt 2):207–221.

16. Jeffery PK (2004) Remodeling and inflammation of bronchi in asthma and chronic obstructive pulmonary disease. *Proceedings of the American Thoracic Society* 1(3):176–183.

17. Regamey N, et al. (2008) Increased airway smooth muscle mass in children with asthma, cystic fibrosis, and non-cystic fibrosis bronchiectasis. *Am J Respir Crit Care Med* 177(8):837–843.

18. Wallace HL, Southern KW, Connell MG, Wray S, Burdyga T (2013) Abnormal tracheal smooth muscle function in the CF mouse. *Physiol Rep* 1(6):e00138.

19. Hogg DA (1982) Ossification of the laryngeal, tracheal and syringeal cartilages in the domestic fowl. *J Anat* 134(Pt 1):57–71.

20. Bonucci E, Cuicchio M, Dearden LC (1974) Investigations of ageing in costal and tracheal cartilage of rats. *Z Zellforsch Mikrosk Anat* 147(4):505–527.

21. Sasano Y, et al. (1993) The process of calcification during development of the rat tracheal cartilage characterized by distribution of alkaline phosphatase activity and immunolocalization of types I and II collagens and glycosaminoglycans of proteoglycans. *Anat Embryol* 188(1):31–39.

22. Sasano Y, et al. (1998) Type X collagen is not localized in hypertrophic or calcified cartilage in the developing rat trachea. *Anat Embryol* 197(5):399–403.

23. Leroux-Berger M, et al. (2011) Pathologic calcification of adult vascular smooth muscle cells differs on their crest or mesodermal embryonic origin. *J Bone Miner Res* 26(7):1543–1553.

24. Tabcheh L, Bianchi A, Clément A, Jouzeau J-Y, Kempf H (2014) Phosphate-induced mineralization of tracheal smooth muscle and cartilage cells. *Biomed Mater Eng* 24(1 Suppl):37–45.

FIGURE LEGENDS

Figure 1. Kinetic of tracheal mineralization in the C57BL/6J mouse strain.

Representative Alcian-blue/Alizarin red staining of the trachea of C57BL/6J individuals at P17 (A), P21 (B), P25 (C), P27 (D), P29 (E), P30 (F), P31 (G), and P60 (H). Mineralization of the respiratory tract initiates at P17 in the thyroid cartilage in the laryngeal prominence (A) and progresses over time to cover the whole larynx (A-H). At P30, mineralization appears in the first five rings of the trachea (F). At P60, the trachea and the bronchi are fully mineralized (H).

Figure 2. Laryngeal and tracheal longitudinal sections of C57BL6 mice stained with Von-Kossa/ Alcian-blue.

Longitudinal sections of the thyroid cartilage (A-F), the cricoid cartilage (G-L), a representative upper tracheal cartilage ring (M-R) and a lower tracheal cartilage ring at P17 (A,G,M and S), P25 (B,H,N and T), P29 (C,I,O and U), P30 (D,J,P and V), P31 (E,K,Q and W) and P33 (F,L,R and X). All thyroid samples panels are markedly stained with black due to mineralized cartilage (A-F). Cricoid mineralization can be detected at P29 (I) and intensifies with time (J-L). Mineralization in the upper tracheal cartilage can only be seen at P30 onward (P-R). No mineralization was detected in the lower part of the trachea at any time point (S-X).

Figure 3. Collagen X expression is spatiotemporally expressed throughout the airways

CollX mRNA expression studied by qPCR or *in situ* hybridization (A-P). Expression of *CollX* assesses by qPCR is upregulated in upper versus lower tracheal regions. Longitudinal sections of the thyroid cartilage (A-D), the cricoid cartilage (E-H), a representative upper tracheal cartilage ring (I-L) and a lower tracheal cartilage ring at P25 (A-B,E-F,I-J and M-N) and P30 (C-D,G-H,K-L and O-P). *CollX* expression starts to be visible by in situ hybridization in all P25 samples (A,E,I and M) and is markedly induced at P30 in the larynx (C,G) and the trachea (K,O). Von Kossa staining appears through a time-dependent rostrocaudal pattern.

Figure 4. Kinetic of tracheal mineralization in Mgp-deficient mice.

Representative Alcian-blue/Alizarin red staining of the trachea of $Mgp^{+/+}$ and $Mgp^{-/-}$ littermates at P0 (A), P7 (B), P10 (C), P14 (D), P21 (E), P28 (F) and P35 (G). Mineralization of the respiratory tract of $Mgp^{+/+}$ and $Mgp^{+/-}$ mice initiates at P17 in the thyroid cartilage in the laryngeal prominence (A) and progresses over time to cover the whole larynx (A-H). In

contrast, mineralization of the trachea of *Mgp*$^{-/-}$ mice start earlier as it is already present at P14 in the upper cartilage rings and is complete at P21.

Figure 5. Tracheal mineralization in Mgp-deficient mice is accelerated in cartilage and broadened to the epithelium.

Representative Alcian-blue/Alizarin red staining of the trachea of *Mgp*$^{+/+}$ and *Mgp*$^{-/-}$ littermates at 3 weeks of age.

Figure 6. Tracheal mineralization in Mgp-deficient mice is autonomously regulated

A. Representative Alcian-blue/Alizarin red staining of the trachea of *Mgp*$^{+/+}$, *Mgp*$^{-/-}$, *Mgp*$^{-/-}$ *;SM22-Mgp, Mgp*$^{-/-}$ *;Col2-Mgp, Mgp*$^{-/-}$ *;Hyp* mice littermates at 3 weeks of age.

SUPPLEMENTARY DATA

Supplemental Figure 1. Tracheal mineralization displays no gender difference in C57BL/6J mice.

Alcian blue/alizarin red staining done on trachea of male and female C57BL6mice aged of 30 days shows no difference in the mineralization pattern with sex variation, panel A represents the trachea of female mice while in panel B the trachea of male mice is presented, in both trachea the mineralization revealed by red staining is localized in the cartilage of the upper part of the trachea.

Supplemental Figure 2. Tracheal mineralization in BALB/cJ.

Representative Alcian-blue/Alizarin red staining of the trachea of BALB/cJ individuals at P20 (A), P25 (B), P27 (C), P29 (D), P30 (E), and P45 (F). Mineralization of the larynx is well advanced at P17, a time where faint patches of mineralization can already be observed in the first two tracheal rings (A). At P25, mineralization has progressed in the first seven rings of the trachea (B). At P45, the whole tracheobronchial tree is mineralized (F).

Supplemental Figure 3. Von-Kossa/ Alcian-blue staining in transversal section of C57BL6J trachea.

Transversal sections of the thyroid cartilage (A-C), the cricoid cartilage (I), a representative upper tracheal cartilage ring (D-F) and a representative lower tracheal cartilage ring (G-I) at P29 (A,D and G), P30 (B,E and H) and P31 (E,K,Q and W) and P33 (F,L,R and X). At P29 no mineralization can be detected in the upper tracheal cartilage (D), while at P30 (E) and P31 (F) mineralization can be detected in the first cartilage rings of the upper region of the trachea. No mineralization can be detected in the lower tracheal cartilage at any time point.

Supplemental Figure 4. Collagen X expression in P30 larynx and trachea.

Adjacent transversal sections of the thyroid cartilage (A-D), the cricoid cartilage (E-H), a representative upper tracheal cartilage ring (I-L) and a representative lower tracheal cartilage ring (M-P) at P30 hybrized with DIG-labelled *CollX*-riboprobe or double stained with Alcian Blue and Von Kossa.

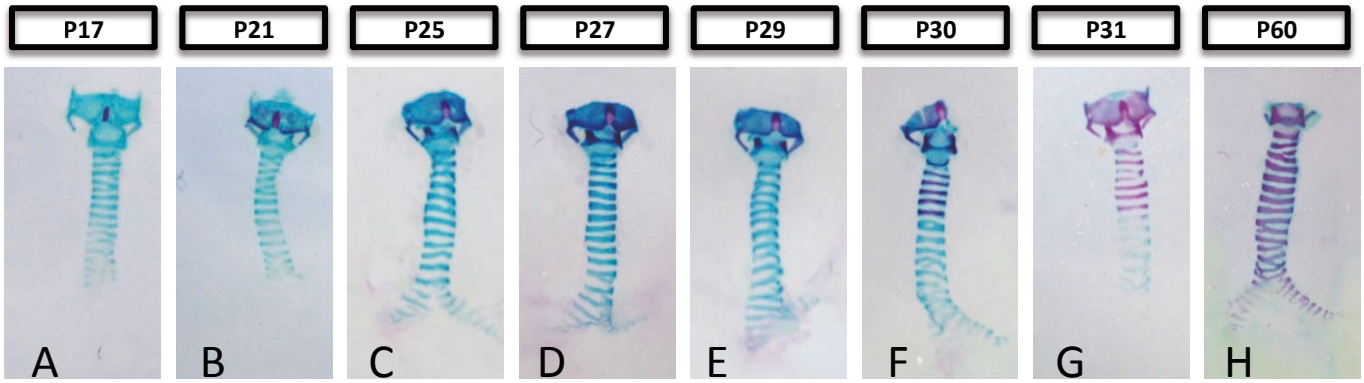

Figure 1. Kinetic of tracheal mineralization in the C57BL/6J mouse strain.
Representative Alcian-blue/Alizarin red staining of the trachea of C57BL/6J individuals at P17 (A), P21 (B), P25 (C), P27 (D), P29 (E), P30 (F), P31 (G), and P60 (H). Mineralization of the respiratory tract initiates at P17 in the thyroid cartilage in the laryngeal prominence (A) and progresses over time to cover the whole larynx (A-H). At P30, mineralization appears in the first five rings of the trachea (F). At P60, the trachea and the bronchi are fully mineralized (H).

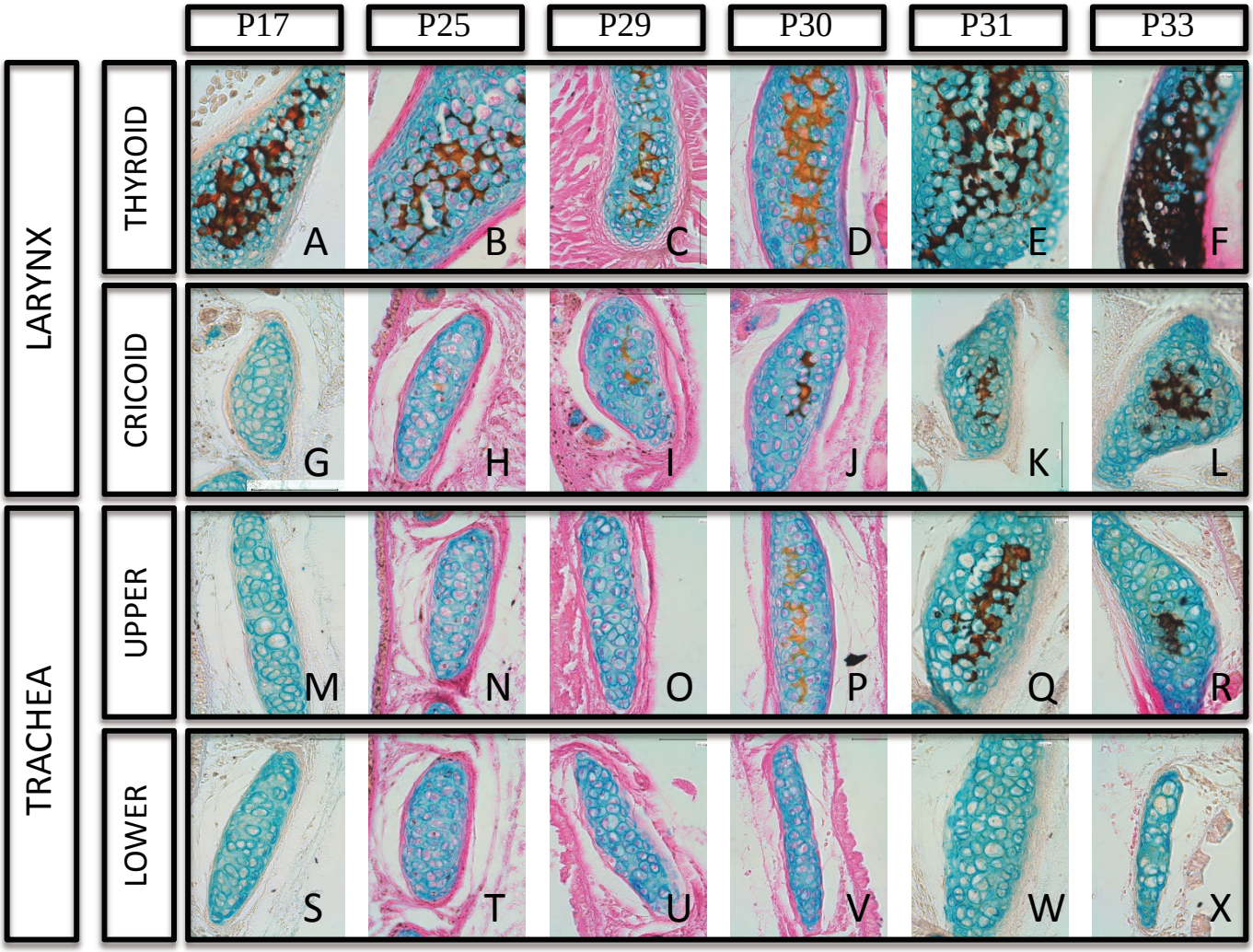

Figure 2. Laryngeal and tracheal longitudinal sections of C57BL6 mice stained with Von-Kossa*l* Alcian-blue.

Longitudinal sections of the thyroid cartilage (A-F), the cricoid cartilage (G-L), a representative upper tracheal cartilage ring (M-R) and a lower tracheal cartilage ring at P17 (A,G,M and S), P25 (B,H,N and T), P29 (C,I,O and U), P30 (D,J,P and V), P31 (E,K,Q and W) and P33 (F,L,R and X). All thyroid samples panels are markedly stained with black due to mineralized cartilage (A-F). Cricoid mineralization can be detected at P29 (I) and intensifies with time (J-L). Mineralization in the upper tracheal cartilage can only be seen at P30 onward (P-R). No mineralization was detected at the lower part of the trachea at any time point (S-X).

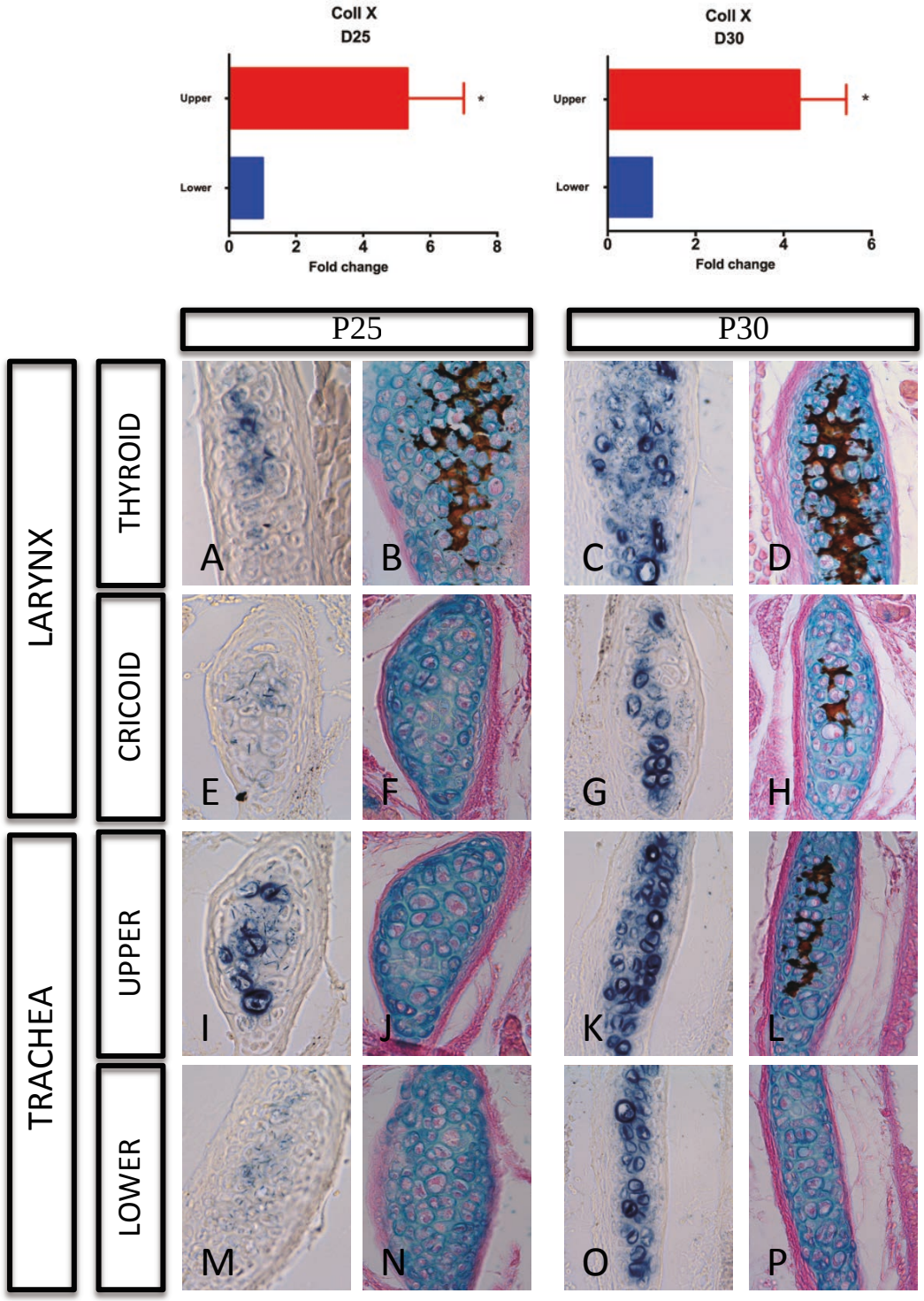

Figure 3. Collagen X expression is spatiotemporally expressed throughout the airways
CollX mRNA expression studied by qPCR or *in situ* hybridization (A-P). Expression of *CollX* assesses by qPCR is upregulated in upper versus lower tracheal regions. Longitudinal sections of the thyroid cartilage (A-D), the cricoid cartilage (E-H), a representative upper tracheal cartilage ring (I-L) and a lower tracheal cartilage ring at P25 (A-B,E-F,I-J and M-N) and P30 (C-D,G-H,K-L and O-P). *CollX* expression starts to be visible by in situ hybridization in all P25 samples (A,E,I and M) and is markedly induced at P30 in the larynx (C,G) and the trachea (K,O). Von Kossa staining appears through a time-dependent rostrocaudal pattern.

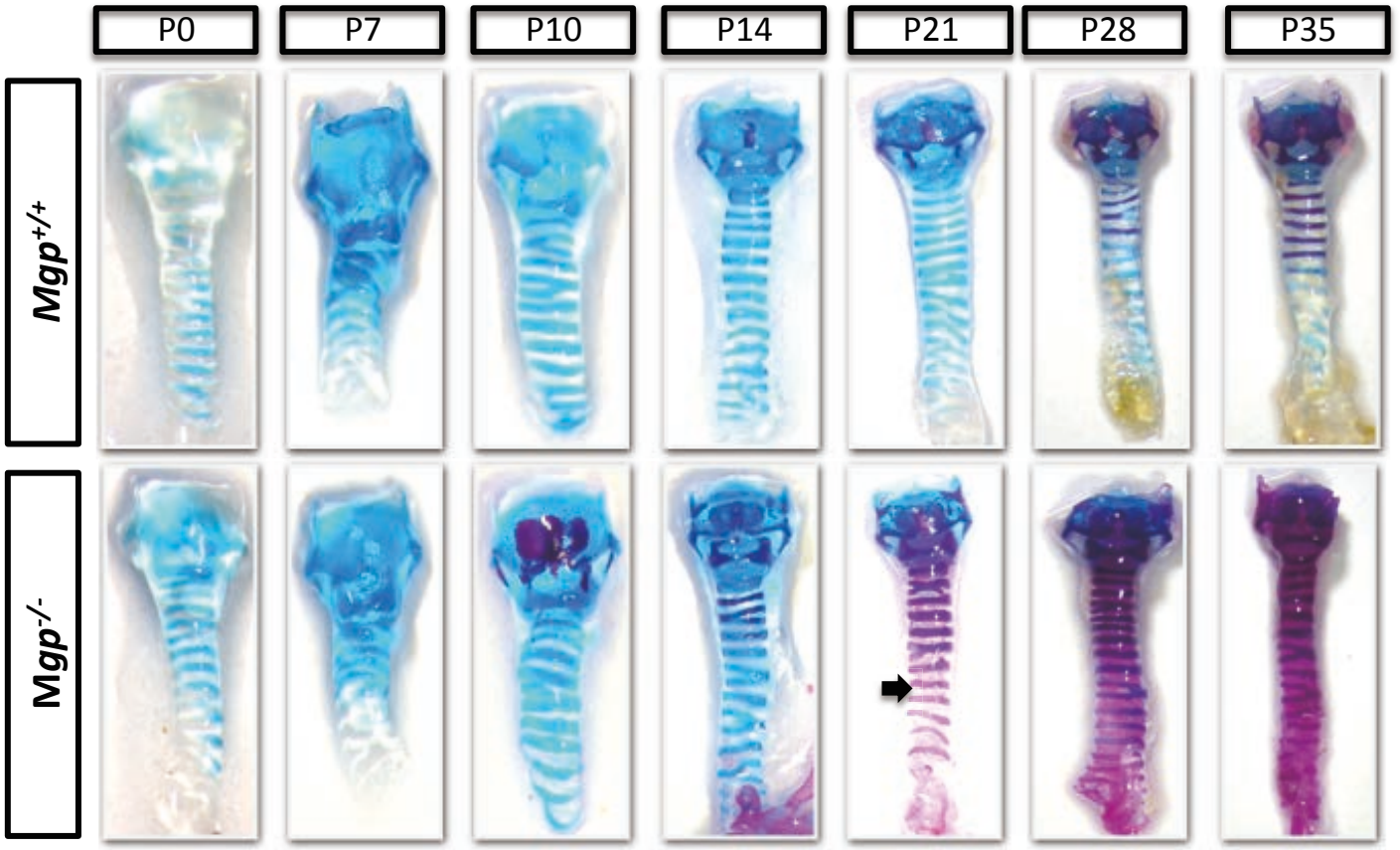

Figure 4. Kinetic of tracheal mineralization in Mgp-deficient mice.
Representative Alcian-blue/Alizarin red staining of the trachea of *Mgp*$^{+/+}$ and *Mgp*$^{-/-}$ littermates at P0 (A), P7 (B), P10 (C), P14 (D), P21 (E), P28 (F) and P35 (G). Mineralization of the respiratory tract of *Mgp*$^{+/+}$ mice initiates at P17 in the thyroid cartilage in the laryngeal prominence (A) and progresses over time to cover the whole larynx (A-H). In contrast, mineralization of the trachea of *Mgp*$^{-/-}$ mice start earlier as it is already present at P14 in the upper cartilage rings and is complete at P21.

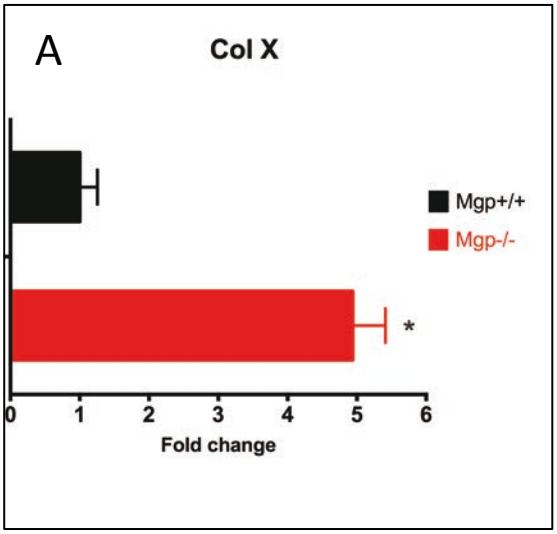

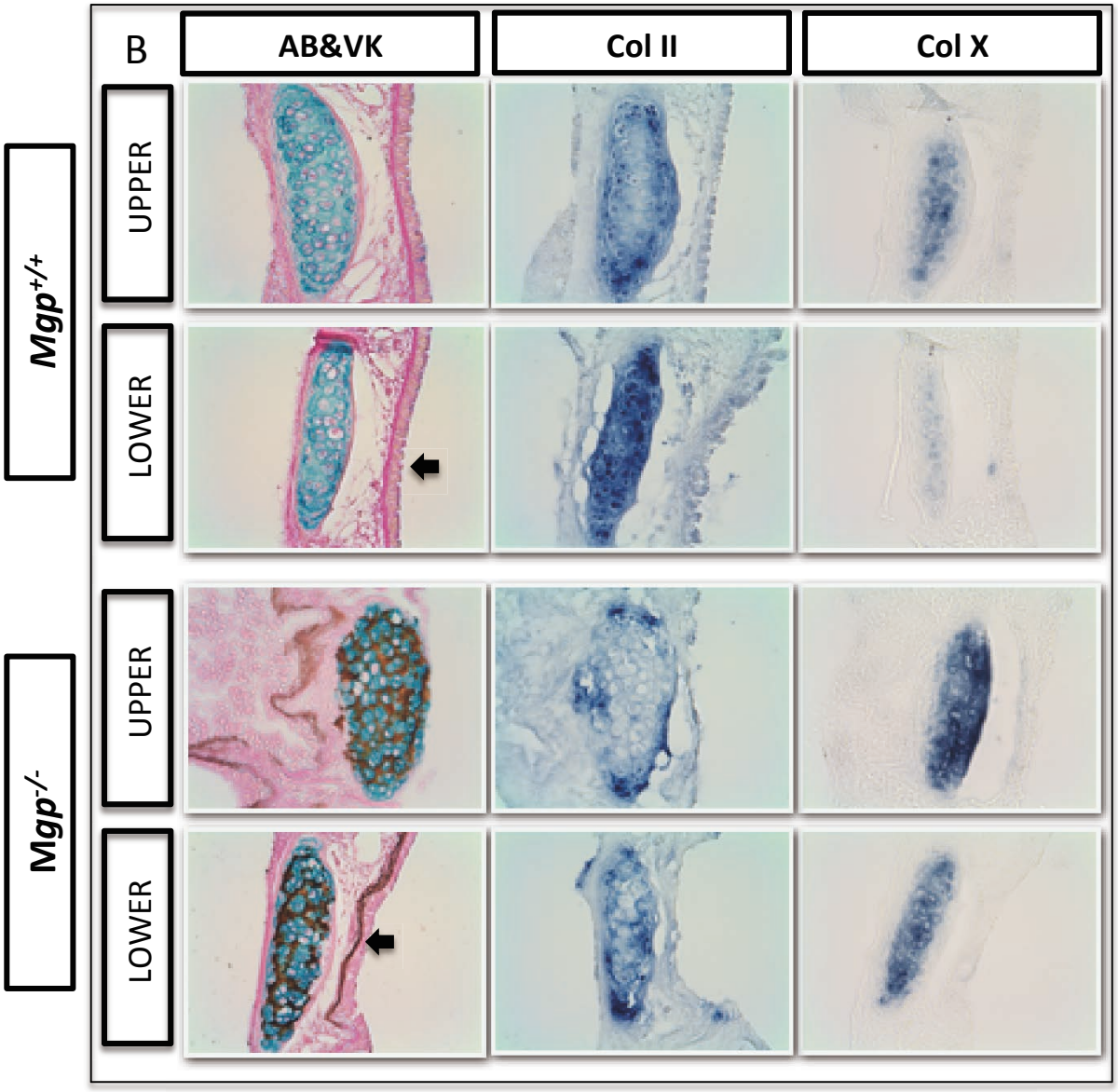

Figure 5. Tracheal mineralization in Mgp-deficient mice is accelerated.
Representative Alcian-blue/Alizarin red staining of the trachea of *Mgp*$^{+/+}$ and *Mgp*$^{-/-}$ littermates at 3 weeks of age.

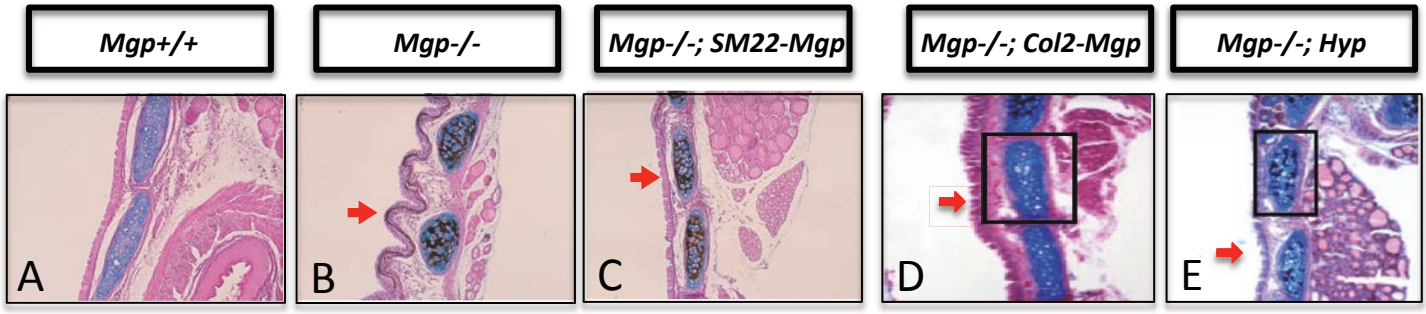

Figure 6. Tracheal mineralization in Mgp-deficient mice is autonomously regulated
A. Representative Alcian-blue/Alizarin red staining of the trachea of *Mgp*$^{+/+}$, *Mgp*$^{-/-}$, *Mgp*$^{-/-}$*;SM22-Mgp, Mgp*$^{-/-}$*;Col2-Mgp, Mgp*$^{-/-}$*;Hyp mice* littermates at 3 weeks of age.

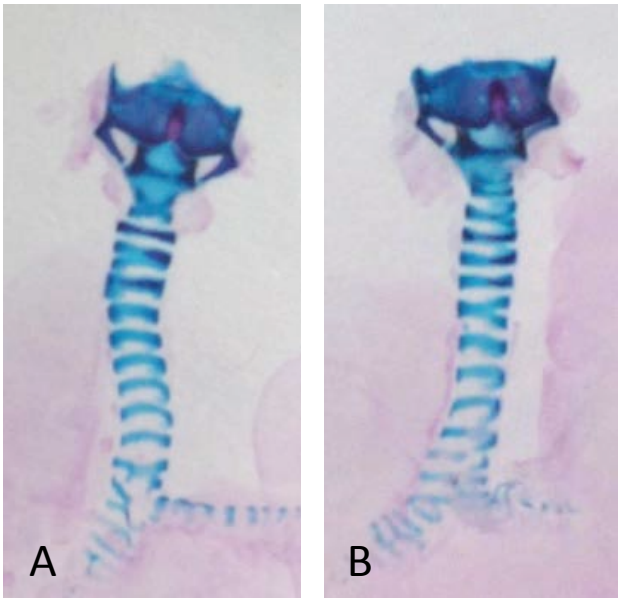

Supplemental Figure 1. Tracheal mineralization displays no gender difference in C57BL/6J mice.

Alcian blue/alizarin red staining done on trachea of male and female C57BL6mice aged of 30 days shows no difference in the mineralization pattern with sex variation, panel A represents the trachea of female mice while in panel B the trachea of male mice is presented, in both trachea the mineralization revealed by red staining are localized in the cartilage of the upper part of the trachea.

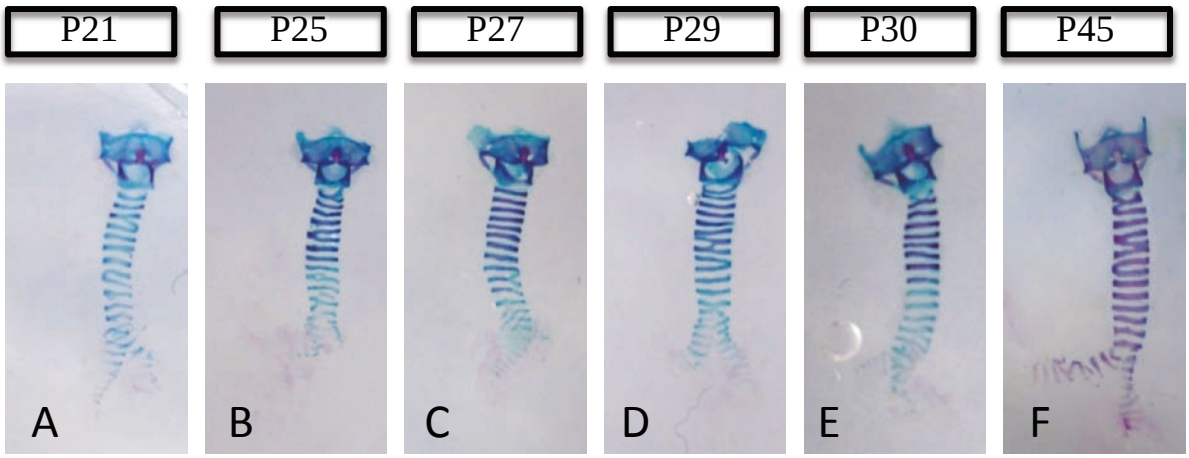

Supplemental Figure 2. Tracheal mineralization in BALB/cJ Representative Alcian-blue/Alizarin red staining of the trachea of BALB/cJ individuals at P20 (A), P25 (B), P27 (C), P29 (D), P30 (E), and P45 (F). Mineralization of the larynx is well advanced at P17, a time where faint patches of mineralization can already be observed in the first two tracheal rings (A). At P25, mineralization has progressed in the first seven rings of the trachea (B). At P45, the whole tracheobronchial tree is mineralized (F).

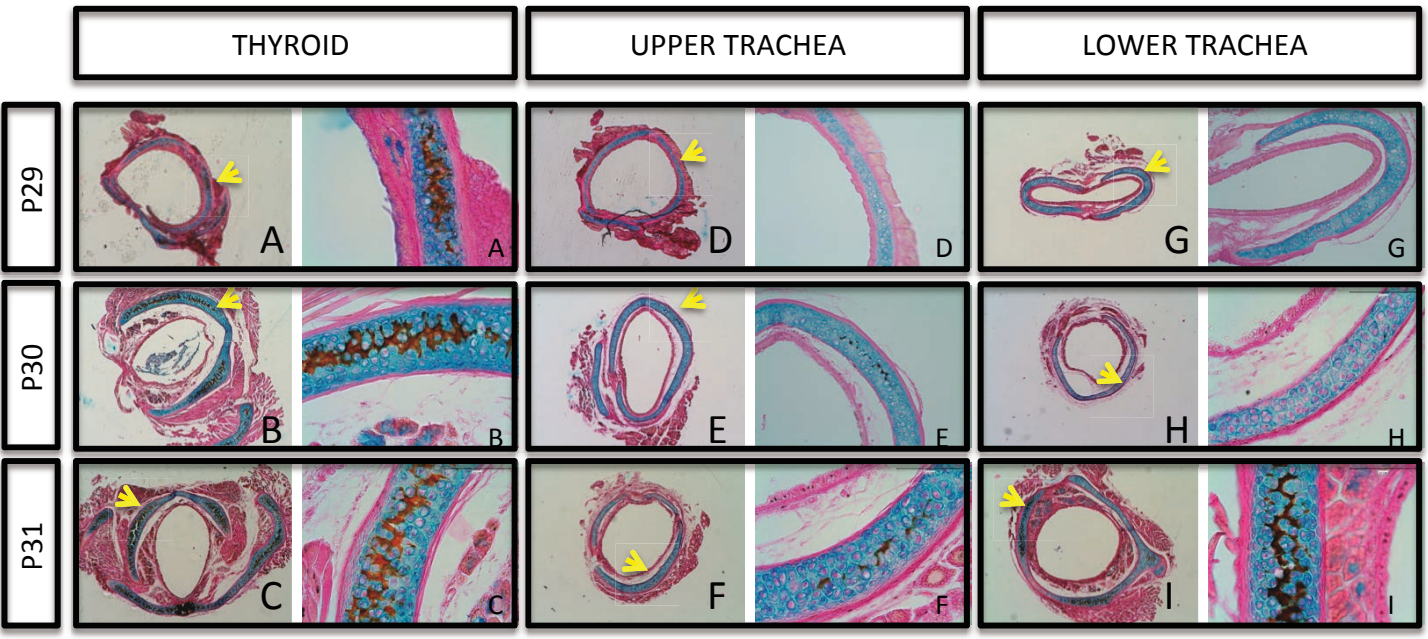

Supplemental Figure 3. Von-Kossa/ Alcian-blue staining in transversal section of C57BL6J trachea.

Transversal sections of the thyroid cartilage (A-C), the cricoid cartilage (I), a representative upper tracheal cartilage ring (D-F) and a representative lower tracheal cartilage ring (G-I) at P29 (A,D and G), P30 (B,E and H) and P31 (E,K,Q and W) and P33 (F,L,R and X). At P29 no mineralization can be detected in the upper tracheal cartilage (D), while at P30 (E) and P31 (F) mineralization can be detected in the first cartilage rings of the upper region of the trachea. No mineralization can be detected in the lower tracheal cartilage at any time point. Mineralized cricoid cartilage is mineralized at P31.

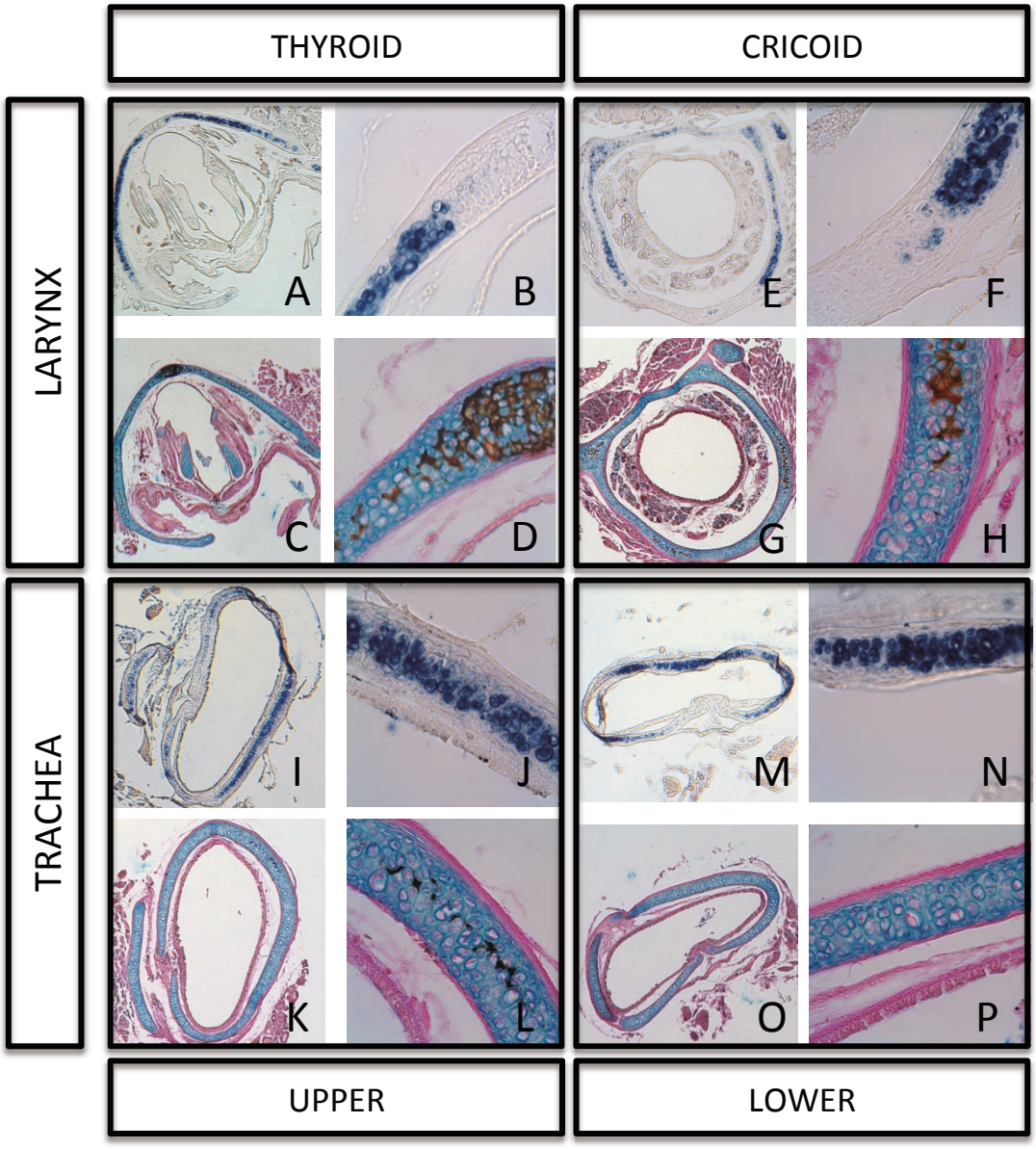

Supplemental Figure 4. Collagen X expression in P30 larynx and trachea
Adjacent transversal sections of the thyroid cartilage (A-D), the cricoid cartilage (E-H), a representative upper tracheal cartilage ring (I-L) and a representative lower tracheal cartilage ring (M-P) at P30 hybrized with DIG-labelled CollX-riboprobe or double stained with Alcian Blue and Von Kossa.

Article No.2 (in preparation): MGP and chondrocyte phenotype in growth plate cartilage

Growth plate postnatal development is compromised by matrix gla protein deficiency in mice: potential role of autophagy inhibition and elevated FGF signaling

Chaohua Deng[1], Aurore Gemble[1], Cécile Guillaume[1], Arnaud Bianchi[1], and Hervé Kempf[1,*]

1. UMR 7365 CNRS–Université de Lorraine, IMoPA, Vandoeuvre-lès-Nancy 54500, France

***Corresponding author**

Longitudinal bone growth takes place in a structure termed growth plate, which contains the chondrocytes at different stages of differentiation. Within the growth plate, chondrocytes can be divided into different anatomic zones according to their morphology, components of the extracellular matrix, enzyme activity, and expression of growth factors and relevant receptors: the resting zone, proliferative zone, prehypertrophic zone, early and late hypertrophic zone (Kozhemyakina et al., 2015).

Briefly, early hypertrophic chondrocytes express specific extracellular matrix molecules, such as Col 10a1, with loss of Sox 9, Col 2a1 and Aggrecan expression (Dy et al., 2012; Leung et al., 2011). Subsequently, Col 10a1-expressing chondrocytes differentiate to late hypertrophic chondrocytes, which express VEGF-A (Gerber et al., 1999), MMP13 (Inada et al., 2004; Stickens et al., 2004), and OPN (Chen et al., 1993). The late hypertrophic chondrocytes work together with endothelial cells, osteoclasts and osteoblast precursors from the perichondrium (Maes et al., 2010) to induce the mineralization of ECM (ECMM) to form trabecular bone (Yang et al., 2014).

Physiological ECMM is an essential process in bone, teeth, and hypertrophic cartilage where the soft extracellular matrix is converted into a rigid material capable of sustaining mechanical force (Behonick and Werb, 2003). However, ECMM can also be pathological. Pathological ECMM can occur in arteries, cartilage and other soft tissues, and may cause a large variety of symptoms or diseases depending on the tissue where mineralization occurs. To date, human and mouse genetic studies have identified several proteins acting as inhibitors of ECMM, including MGP (Luo et al., 1997).

MGP is a 14-kDa secretory and structural protein of the extracellular matrix, which belongs to the family of extracellular mineral-binding proteins called Gla proteins. Gla proteins contain several glutamic acid residues that can be γ-carboxylated by a specific γ-carboxylase, whose function is controlled post-transcriptionally by vitamin K (Schurgers et al., 2013). The modified amino acids, called Gla residues, confer on these proteins a high affinity for calcium ions and hydroxypatite crystals (O'Young et al., 2011). This enables MGP to bind mineral crystals, thereby actively inhibiting mineralization of the soft tissues in which it is mainly synthesized and expressed, such as chondrocytes, vascular smooth muscle cells, endothelial cells and fibroblasts. In the last decade, MGP has been widely investigated and accepted as playing a critical role in preventing vascular

mineralization (Proudfoot and Shanahan, 2006), whereas its role in skeletal development has hardly been studied.

The original study reporting the MGP knock-out mice, describes a short stature, massive vascular calcification, and abnormal mineralization of cartilage (Luo et al., 1997). The vascular phenotype has been largely studied (El-Maadawy et al., 2003; Kaartinen et al., 2007; Leroux-Berger et al., 2011; Luo et al., 1997; Murshed et al., 2004). Recent studies have also demonstrated the nasal phenotype (Marulanda et al., 2017) and tracheal phenotype (***Article N°1***). However, the underlying mechanism of abnormal ECMM in the growth plate of MGP knockout mice still remains unknown. In our study, we performed serial morphological, histological and molecular analysis on MGP knockout mouse model, at different time-points during postnatal development, to detect the role of MGP in endochondral ossification. We also performed in vitro assays on the primary immature articular chondrocytes from the MGP wild type and knockout pups, to detect their proliferation and mineralization ability.

Our work suggests that the growth retardation at age of P21 caused by MGP deficiency in KO mice is due to shortened hypertrophic zone and accelerated secondary ossification formation from P7 onwards. Furthermore, the growth retardation may result from disturbed FGF signaling and consequent inhibition of autophagy.

Materials and Methods

(This section will used in the part of manuscript)

Mouse models

MGP heterozygous mice were a kind gift from Dr. Monzur Murshed (McGill University, Canada). Experiments were performed on the $MGP^{+/+}$ and $MGP^{-/-}$ mice, which were obtained from the intercross of $MGP^{+/-}$ parent mice. Genotypes were confirmed by polymerase chain reaction (PCR), using the specific designed primers. Mice were housed in conventional animal rooms under constant humidity (55 ± 10%) and temperature (22 ± 2ºC) in 12h light dark cycle conditions. They were fed ad libitum with standard food diet (Scientific Animal Food & Engineering, France) and had free access to water. For all the following procedures, adult mice were euthanized with CO2 in an appropriate chamber (Minerva) and newborn or very young animals were euthanized by decapitation. All experimental protocols were reviewed and approved by the Animal Care and Ethic Committee of University of Lorraine.

Whole-mount Alcian Blue (AB) and Alizarin Red (AR) staining

Whole-mount Alizarin Red/Alcian Blue skeletal staining were performed on fetal, newborn, and early post-natal skeletons of $Mgp^{+/+}$, $Mgp^{+/-}$ and $Mgp^{-/-}$ mice, as decribed previously (Ovchinnikov, 2009). Briefly, the mice were carefully dissected with forceps and scissor to peel off the skin and to eviscerate the bodies, including the contents of the peritoneal and pleural cavities. Then, the skeletons were fixed in 95% ethanol for at least 24 h before being replaced by filtered Alcian Blue solution (0.03% wt/vl Alcian Blue powder, 80% ethanol 95%, 20% acetic acid) for about 24 h staining of cartilage under weak agitation. The skeletons were washed with ethanol 95% for 6-8 h, transfered to 2% potassium hydroxide and kept until all the tissues are adequately cleared. The skeletal bones were counterstained by Alizarin Red solution (0.003% wt/vl Alizarin Red powder dissolved in 1% potassium hydroxide) for 12h to 48h (younger mice take less time) and cleared by placing them in 1% potassium hydroxide/20% glycerol for 2 d or more. When the samples are appropriately cleared, they were placed in 100% glycerol for storage. The Alcian Blue/Alizarin Red stained

skeletons were photographed by Canon 600D reflex camera. The length of skeletal elements were analyzed and calculated by Photoshop CS6 software.

Histology

For histological examination, knee samples were fixed in 4% paraformaldehyde (PH 7.4) overnight. Then they were processed with decalcification in 10% EDTA (PH 7.4), dehydration and embedding with paraffin. Paraffin sections (5 μm) were stained with Hematoxylin and Eosin (H&E), Alcian Blue or Safranin O as described (Schmitz et al. 2010). The images were obtained by Leica DMD108 system.

In situ hybridization

Sections (5 μm-thick) were subjected to acid hydrolysis (0.2 N HCl, 15 min), proteinase K treatment (5 μg/ml in PBS, 15 min), postfixation (4% PFA, 5 minutes) and acetylation (0.25% acetic acid, 15 min). Each of these steps was followed by two 5-minute washes with PBS. After the last PBS wash, slides were rinsed with dH2O and air-dried, before a 2-hour prehybridization step, at 65°C, in hybridization solution [50% formamide, 10 mM Tris (pH 7.6), 200 μg/ml Torula yeast RNA, 1xDenhardt's solution, 10% dextran sulfate, 600mM NaCl, 0.25% SDS, 1 mM EDTA (pH 8.0)]. Hybridization with digoxygenin-labeled RNA probes was performed overnight at 65°C. Posthybridization, slides were rinsed briefly in 5x SSC at 65°C, washed with 1x SSC, 50% formamide (65°C, 30 minutes), subjected to RNase A digestion to reduce nonspecific hybridization, and washed at increasing stringency with SSC buffers (final wash at 55°C with 0.2xSSC). Bound probes were detected with an alkaline phosphatase-conjugated anti-DIG antibody (Roche) and revealed with BM purple substrate (Roche).

Primary chondrocyte culture

Primary chondrocytes from the joints of 5 day old Mgp wild type and Mgp knock-out pups were isolated as described with slight modifications (Gosset et al., 2008). Briefly, articular cartilage was excised from femoral condyles and tibial plateaus with a scalpel and placed in 1X PBS. Cartilage fragments were digested using 3mg/ml Collagenase D (Roche) in 3 ml Dulbecco's modified Eagle's

medium (DMEM) (Gibco) for 45 min at 37 C° in a thermal incubator under 5% CO2 in a 50-ml flacon. Then, discard the digestion solution and add new 3ml of 3mg/ml Collagenase D digestion solution for 45 min. Add 9 ml of DMEM medium to the tube, and make a Collagenase D solution at 0.75 mg/ml (4X dilution). Incubate maximum 24h at 37C° in a thermal incubator under 5% CO_2. Pass the solution through 25-, 10-, 5-, 2-ml Pasteur pipettes successively to disperse any cell aggregates. This yields a suspension of isolated cells. Then centrifuge for 10 min at 400g. Resuspend it with 15 ml of DMEM medium supplemented with 10% fetal bovine serum (Thermo Fisher Scientific) supplemented with 1 mg/ml penicillin and 0.1 mg/ml streptomycin (Sigma Aldrich).

RNA extraction and Quantitative PCR analysis

Total RNA was isolated from primary articular chondrocytes or fresh growth plate cartilage using an RNeasy plus kit (Qiagen), according to the manufacturer's instructions. Extracted RNA was transcribed into cDNA by Reverse transcription reaction using the M-MLV enzyme (Invitrogen) and adequate mix (dNTP, transcription buffer, random hexaprimer, DTT). cDNA were then amplified and quantified by ViiA™ 7 Real-Time PCR System (Applied Biosystem) and the iTaq SYBR Green supermix (Biorad) according to the manufacturer's instructions. Mouse specific PCR primers were designed and are available upon request. RPS29 housekeeping gene was determined in parallel for each sample. Comparative ΔΔCT method was used for quantification and the results were expressed as fold change over control.

Protein extraction and Western blot

Femoral and tibia cartilages were microdissected and lysed using a TissueLyser (Qiagen) in RIPA buffer supplemented with 1mM PMSF (Cell signaling). Samples were incubated for 30min on ice, briefly sonicated on ice and the soluble fraction was isolated by centrifugation at 14000 r.p.m. for 10min at 4°C. Total protein concentration in tissue extracts was measured using the colorimetric BCA protein assay.

Cells were washed twice with PBS and then scraped in lysis buffer (Laemmli 1x). Cell lysates were incubated on ice for 20min, then the soluble fraction was isolated by centrifugation at 14000 r.p.m. for 10min at 4°C.

Protein extracts, seperated by SDS-PAGE and transferred onto PVDF membranes, were probed with antibodies against LC3A, LC3B, p-P38, P38, p-ERK, ERK1/2, p-mTOR, mTOR (Cell signaling), actin (Sigma-Aldrich). Proteins of interest were detected with horseradish peroxidase (HRP)-conjugated goat anti-mouse or anti-rabbit IgG antibody (1:2000, Cell signaing) and visualized with Clarity Western ECL substrate (Bio-Rad), according to the manufacturer's protocol. The western blotting images were acquired using ChemiDoc imaging system (Bio-Rad) and band intensity was calculated using Image J software using the 'Gels and Plot lanes' plug-in.

Statistics

Unpaired two-tailed t-test was performed with Prism6 software (GraphPad) when comparing two groups of mice or different primary chondrocyte preparations. All experiments were repeated at least 3 times. All data are reported as means ± S.E.M. with statistical significance defined as $p<0.05$(*), $p<0.01$(**) or $p<0.001$ (***).

Results

(This section will be summarized and used in the manuscript)

No apparent difference in skeletal phenotype between MGP WT and KO embryos in embryonic stage

MGP gene expression is detectable from 10.5 day of embryonic stage (E10.5), and is predominantly expressed in mesenchymal epithelial interphase in lung and limb buds (Luo et al., 1995). Although Mgp is expressed during embryogenesis, the MGP KO mice displayed no fetal mortality (Luo et al., 1997). In order to characterize the effect of MGP absence on skeletal development and morphology, we performed whole-mount Alizarin Red/Alcian Blue skeletal staining. No difference in the skeleton size was found from early embryonic stage (E14.5) to birth (P0) (**Fig1A**). We also performed Von kossa/Alcian Blue staining on the histological sections of E18.5 embryos, and no obvious differences of mineralization in the skeleton between MGP WT and KO embryos were noticed, including metatarsal, humerus and vertebrae (**Fig1B**).

Dwarfism of MGP KO mice appeares during postnatal skeleton development

We thus performed whole-mount Alizarin Red/Alcian Blue skeletal staining in postnatal stages up to P28. In accordance to the original description of MGP KO mice (Luo et al., 1997), we showed and confirmed the dwarfism of MGP KO mice is substantially noticeable at day 21 of postnatal life (P21) (**Fig2A**). There is neither difference between $MGP^{+/-}$ and $MGP^{+/+}$ mice, or difference beween male or female mice (data not shown). The dwarfism of MGP KO mice persists at P28 (**Fig2B**) and then these mice started to die, due to pathological calcification of aorta and subsequent hemorrage(Luo et al., 1997). The body weight of MGP KO mice is significantly smaller than $Mgp^{+/-}$ and $Mgp^{+/+}$ mice at P21 (**Fig2C**).

Then we dissected the Alizarin Red/Alcian Blue stained skeleton into different parts, such as skull, vertebra and tail. Surprisingly, all the skeletal elements of MGP KO mice are smaller than their WT littermates (**Fig3A**), which indicated the

impairement of both endonchondral and intramembranous ossification. Measurement of each skeletal element length confirmed the noticeable retarded skeletal phenotype at P21 (**Fig3B**).

Shortened hypertrophic zone and accelerated formation of secondary ossification center in MGP KO mice

In order to reveal the underlying mechanism of the abnormal endochondral ossification process in the MGP KO mice, we performed serial histological analysis at different time-points of postnatal life. Safranin O staining showed that a significantly shortened and disturbed hypertrophic zone in MGP KO mice when compared to that of MGP WT mice could be observed as early as P4 (**Fig4A**).

Later at P7 and P21, the shortened hypertrophic zone is still present in the growth plate of MGP KO mice (**Fig4B&D**). Interestingly, we found that the formation of secondary ossification center (SOC) is accelerated in Mgp KO mice compared with MGP WT littermates at P14 (**Fig4C**). At age P21, we can see a reduced and impaired hypertrophic zone in both growth plate and SOC (**Fig4D**).

The morpholocial phenotypes of growth plate in MGP KO mice have been confirmed by in situ hybridization with the specific probe Col 2, marker of the proliferating chondrocytes and probe Col 10, marker for the hypertrophic chondrocytes (**Fig5**). There is a slight decreased expression of Col2 in the resting and proliferating zones in MGP KO mice compared with those of WT littermates (**Fig5A**). In addition, the bone formation in the MGP KO mice seems to be disturbed, as the trabecular bone in SOC is abnormal and different from the MGP WT littermate (**Fig4D**) and a significant impaired Col10-positive hypertrophic zone in both growth plate and SOC (**Fig5B**).

MGP deficiency leads to slight decreased proliferation, increased apoptosis and excessive mineralization in growth plate chondrocytes

MGP is particularly expressed in the resting, proliferating and late hypertrophic chondrocytes in growth plate, as shown by in situ hybridization with the probe MGP

on the tibia sections of P7 mice (**Fig6A**). We thus hypothesize that Mgp may play a role in proliferation and maturation of chondrocytes in growth plate.

To detect the proliferation ability of chondrocytes in the growth plate, we performed an immunohistochemistry staining with Ki67, which is a specific marker for the proliferative cells. Even if, due to limited number of samples, we could not do the statistical quantification for the moment, we still noticed the mild decreased number of Ki67-positive cells in the resting and proliferating regions (**Fig6A**). With the colony formation assay performed on primary chondrocytes, we confirmed the decreased proliferation ability in the chondrocytes from MGP KO mice (**Fig6B**). Importantly, we also found increased number of apoptotic cells with TUNEL staining in the hypertrophic zone of MGP KO mice at P7, compared to that of WT littermate (**Fig6C**).

When we performed the Von kossa/Alcian Blue staining on the early stages of postnatal life, particularly at P4, in addition to the confirmation of shortened and disturbed hypertrophic zone observed with Safranin O staining (**Fig4A**), we also found that the mineralization of this region and the following subchondral region seem to be more intense (**Fig7A**). Then we dissected out the growth plate cartilage from the pups of about age P5, according to a well-established protocol (Gosset et al., 2008), to isolate the chondrocytes with Collagenase D digestion and put them in primary culture for 7 days. We performed Alizarin red and Alcian blue staining on the cultured chondrocytes from MGP WT and KO pups, and we found more excessive mineralization in MGP KO chondrocytes with increased glycosaminoglycan production (**Fig7B**).

MGP deficiency results in disturbed expression of cartilage and bone markers

In the objective to explore the mechanisms underlying the morphological and histological results in the MGP KO mice, we further analyzed the gene expression profile from the total femur and cranium. Quantitative PCR on the RNA extracted from these two skeletal elements at P21 confirmed the absent expression of Mgp and showed the significant lower expression of Col 1 and Col 10 in the femur from MGP

KO mice (**Fig8A**). The same results were obtained on the cranium (**Fig8B**). However, we did not find the signicant change in the expression of Col 2 in both tissues (**Fig8A&B**).

MGP deficiency results in decreased autophagic activity and disruption of related signaling pathway

Interestingly, among other genes detected in the MGP KO mice, we have noticed an increased expression of fibroblast growth factor receptor 3 (FGFR3) in the RNA extracted from femur at P21 (**Fig9A**), the stage when the dwarfism appears significant. FGFR3 is a negative regulator of endochondral ossification. Gain-of-function mutations in FGFR3 are responsible for achondroplasia, the most common genetic form of dwarfism in humans (Li et al., 1999; Shiang et al., 1994) (Ornitz and Legeai-Mallet, 2017)(See also the Chapter 2.2). Recent study revealed that FGFR3 inhibits the autophagic activity by decreasing the ATG5-ATG12 conjugate level, leading to the delay of cartilage development in achondroplasia (Wang et al., 2015). This prompted us to determine whether MGP deficiency affects the autophagic activity.

First, we determined the protein level of LC3, a classic marker for autophagosomes localized on the phagophore and autophagosome membrane (Klionsky et al., 2016), in growth plate chondrocytes. The immunohistochemistry analysis showed that LC3 expression was remarkably reduced in MGP KO mice compared with that of WT control at P4 (**Fig9A**). Then, the protein of fresh articular cartilage isolated from MGP KO and WT littermates at P4 was analyzed by western blot. The results showed that the ratio of LC3-II/-I, an indicator of autophagic activity, was decreased in MGP KO mice. The phosphorylation of Erk1/2 is also decreased; meanwhile the phosphorylation of Akt has a tendency to increase (**Fig9B**).

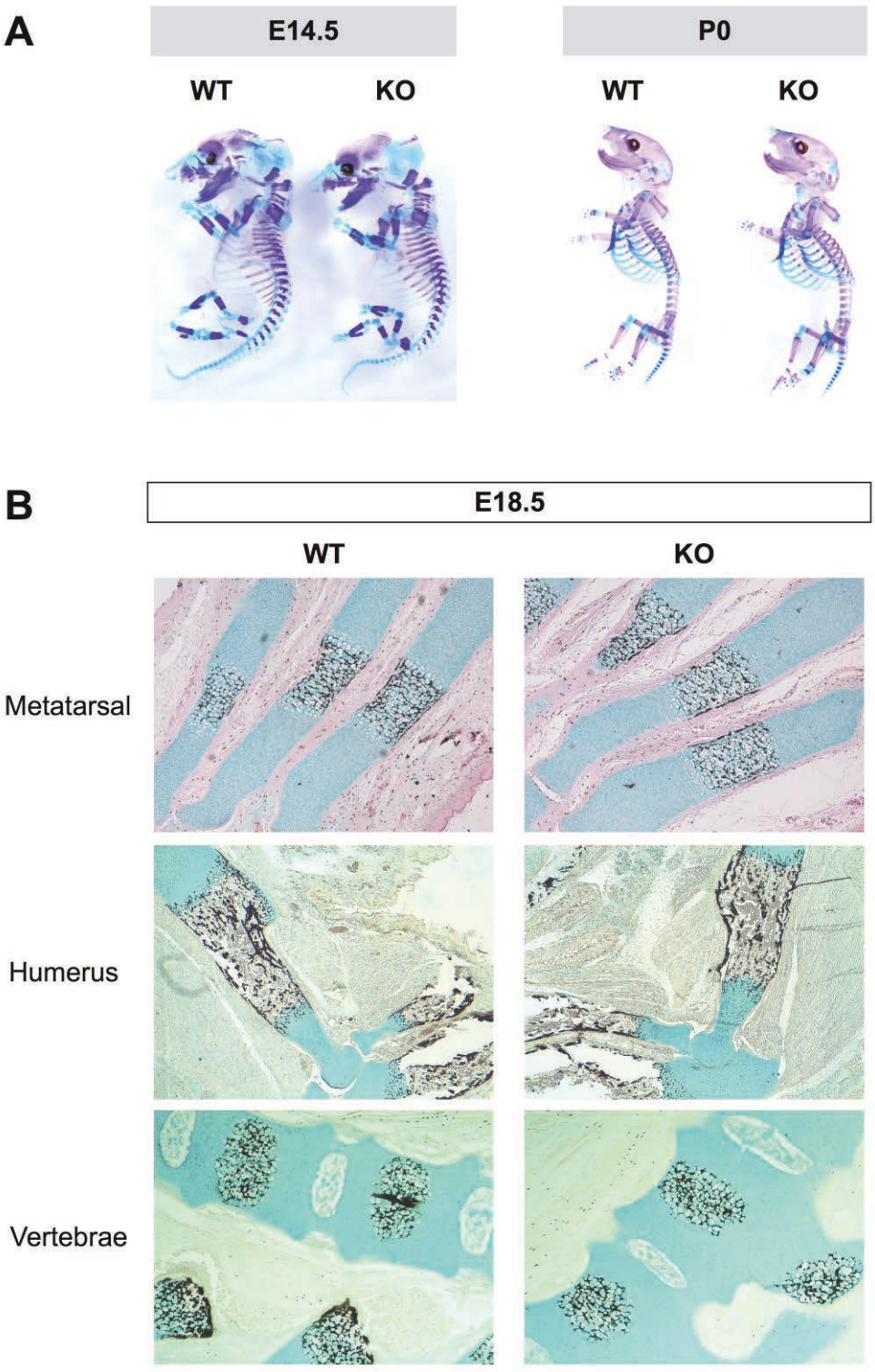

Figure 1. No difference in mineralization between MGP WT and KO embryos. A. Whole-mount Alcian blue/Alizarin red staining of skeletal preparations from embryonic stage (E14.5) and newborn pups (P0). B. Von kossa/Alcian Blue staining on the histological sections of metatarsal, humerus and vertebrae from E18.5 embryos.

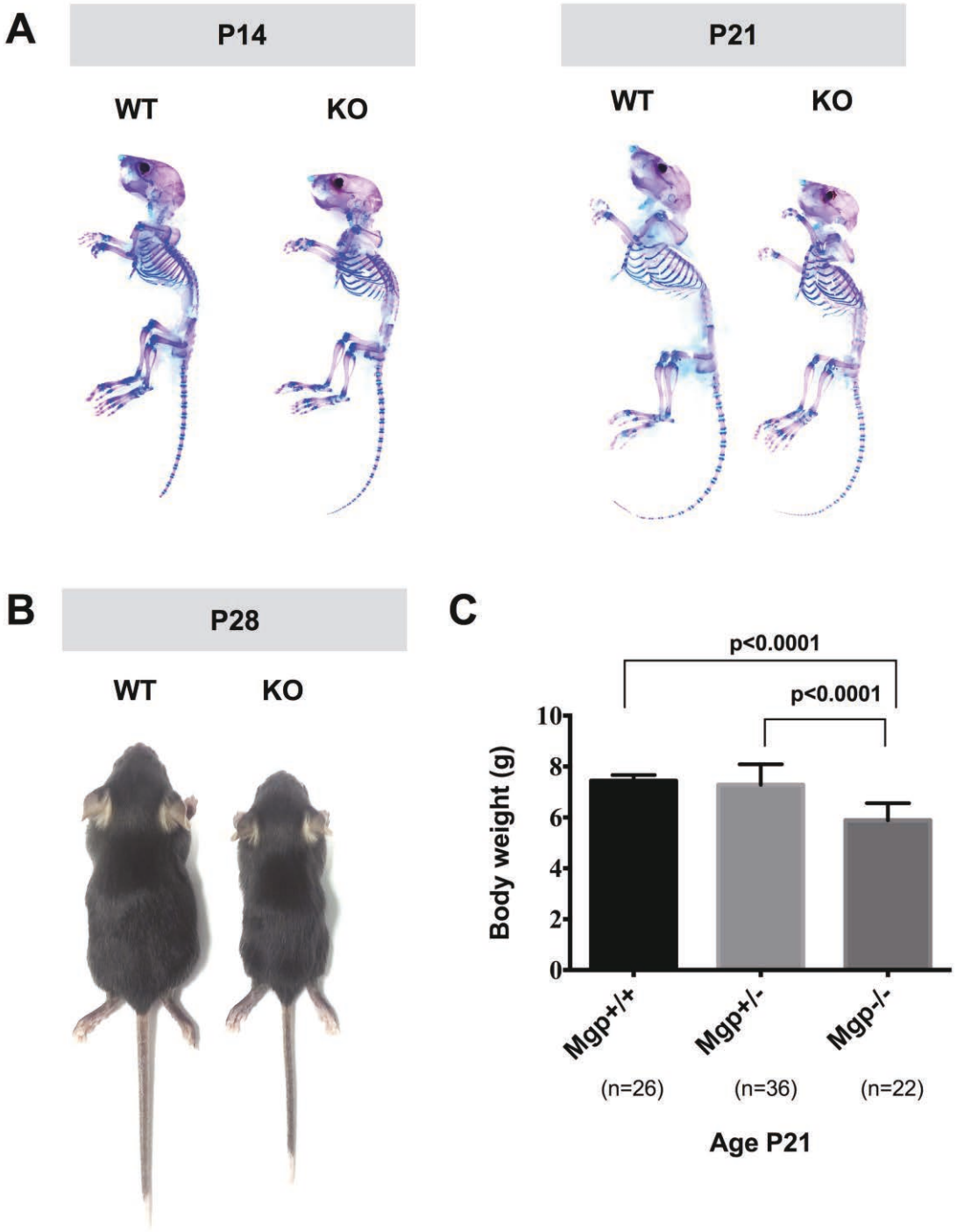

Figure 2. MGP deficiency results in dwarfism at P21. A. Whole-mount Alcian blue/Alizarin red staining of skeletal preparations from postnatal stages (P14 and P21). B. The gross appearances of mice at 4 weeks after birth (P28). MGP KO mice showed smaller size than Mgp WT mice. C. The body weight between $MGP^{+/+}$ (n=26), $MGP^{+/-}$(n=36) and $MGP^{-/-}$(22) mice at age P21. Values represent mean±SD. Unpaired two-tailed t-test was used.

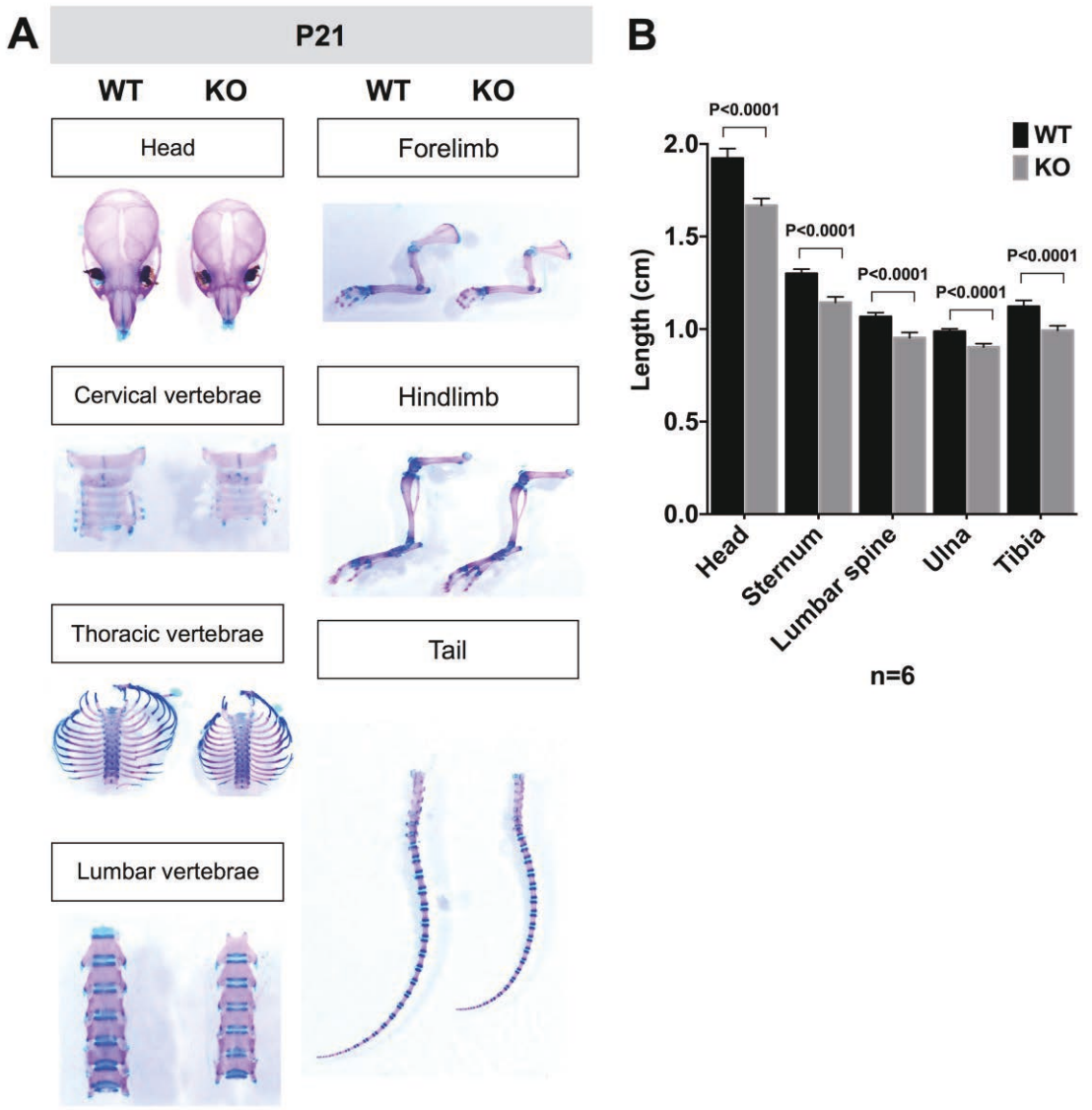

Figure 3. Quantification of skeleton elements at P21. A. The different skeletal elements of MGP WT and KO mice at age P21 were analyzed, including head, cervical vertebrae, thoracic vertebrae, forelimb, hindlimb and tail. B. Quantitative measurement of the skeletal elements by using Image J. Values represent mean±SD. Paired two-tailed t-test was used. N=6.

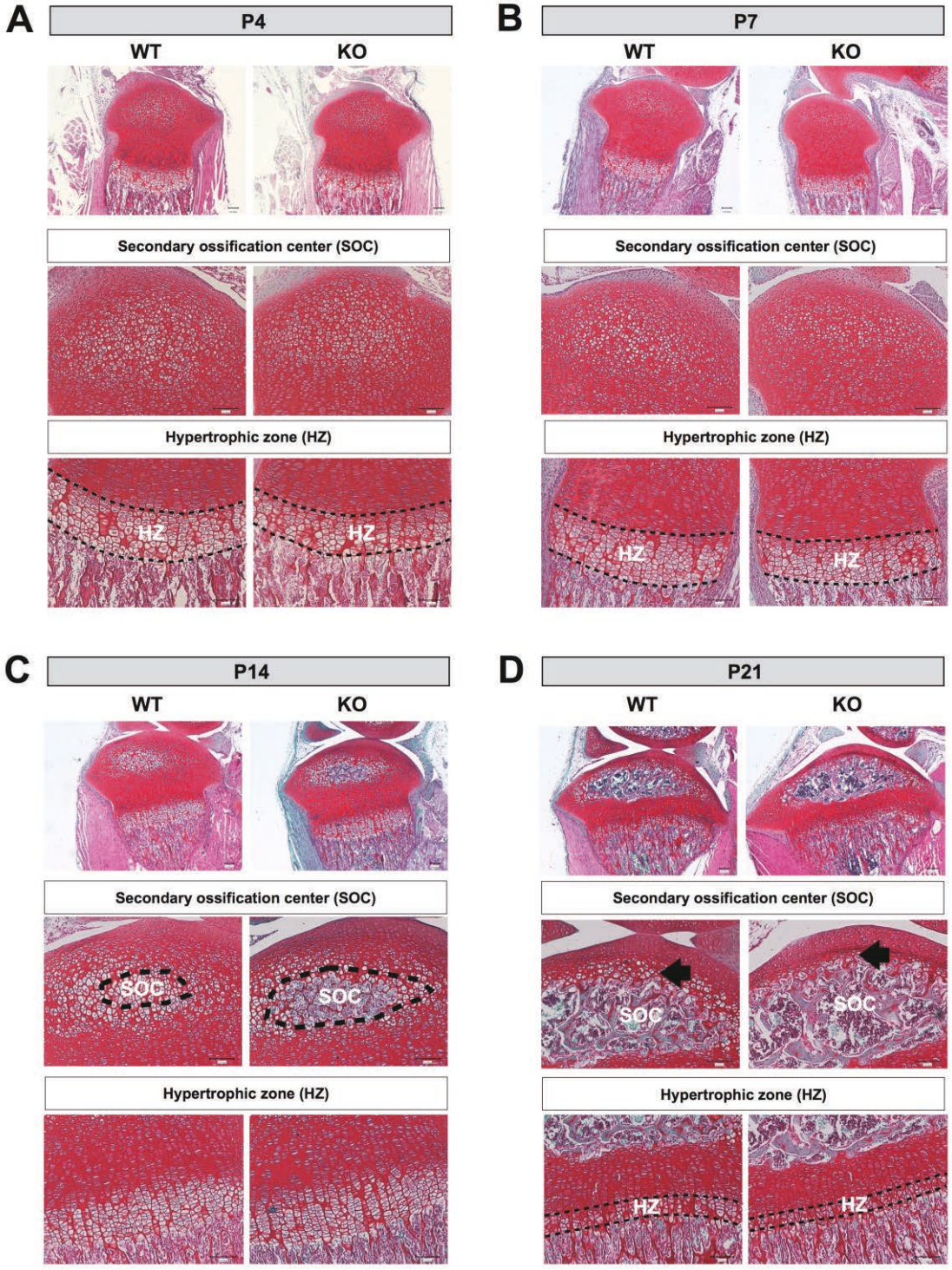

Figure 4. MGP deficiency results in impaired growth plate structure. Safranin O staining of the tibia sections at P4, P7, P14 and P21 of postnatal stages. A&B. The shortened HZ in MGP KO mice was obeserved as early at P4. C. Accelerated SOC was observed in MGP KO mice from P14 onwards. D. Impaired HZ in the SOC of MGP KO mice at P21 was noticed (black arrow). SOC: secondary ossification center; HZ: hypertrophic zone.

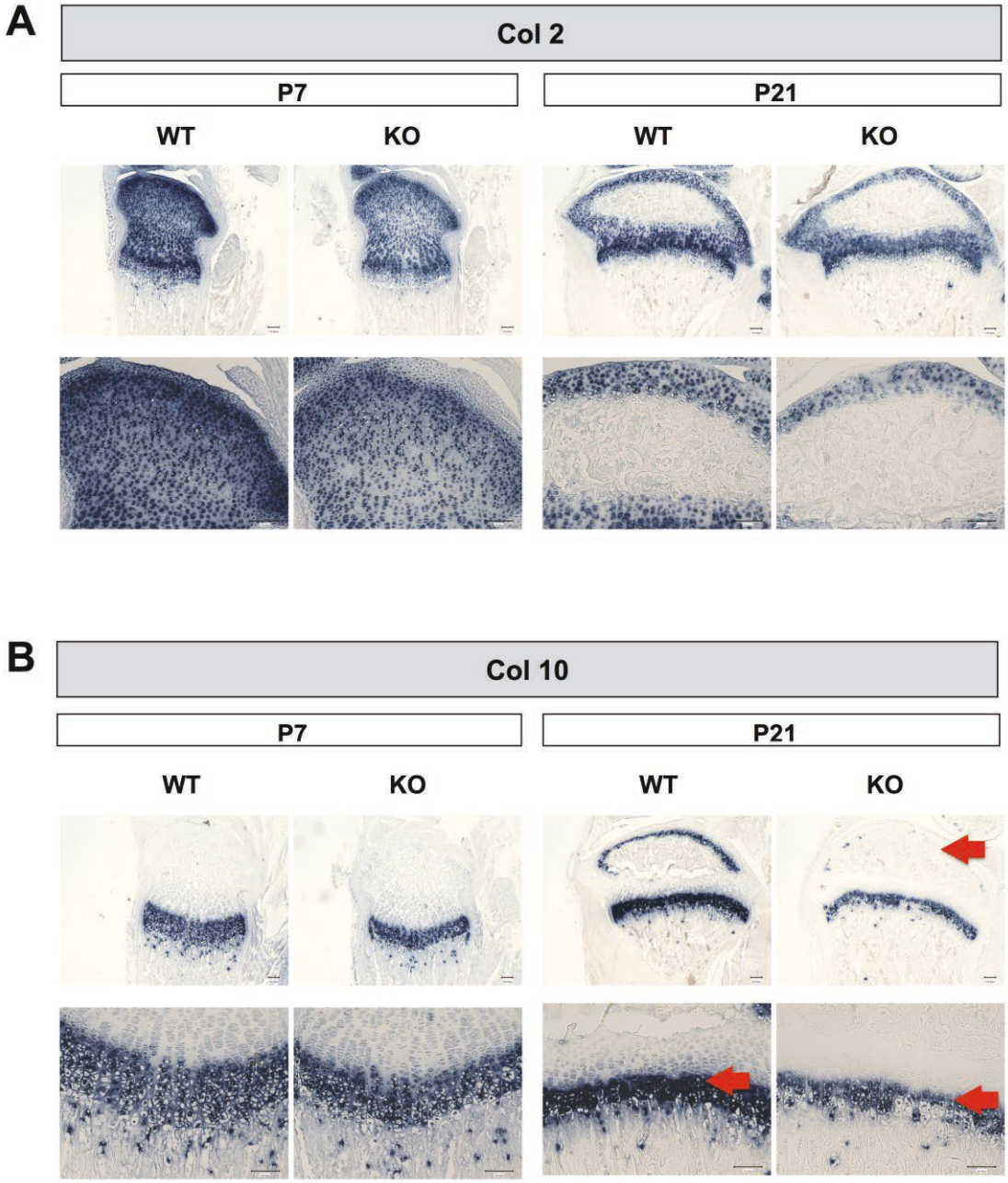

Figure 5. MGP deficiency results in shortened hypertrophic zone and disturbed ossification center. A. Slightly decreased expression of Col 2 was observed on the tibia sections from P7 and P21 MGP KO mice. B. Smaller size of Col 10-positive region was noticed in MGP KO mice at P7 and decreased expression of Col 10 was observed at P21 in the hypertrophic zone and secondary ossification center (red arrow).

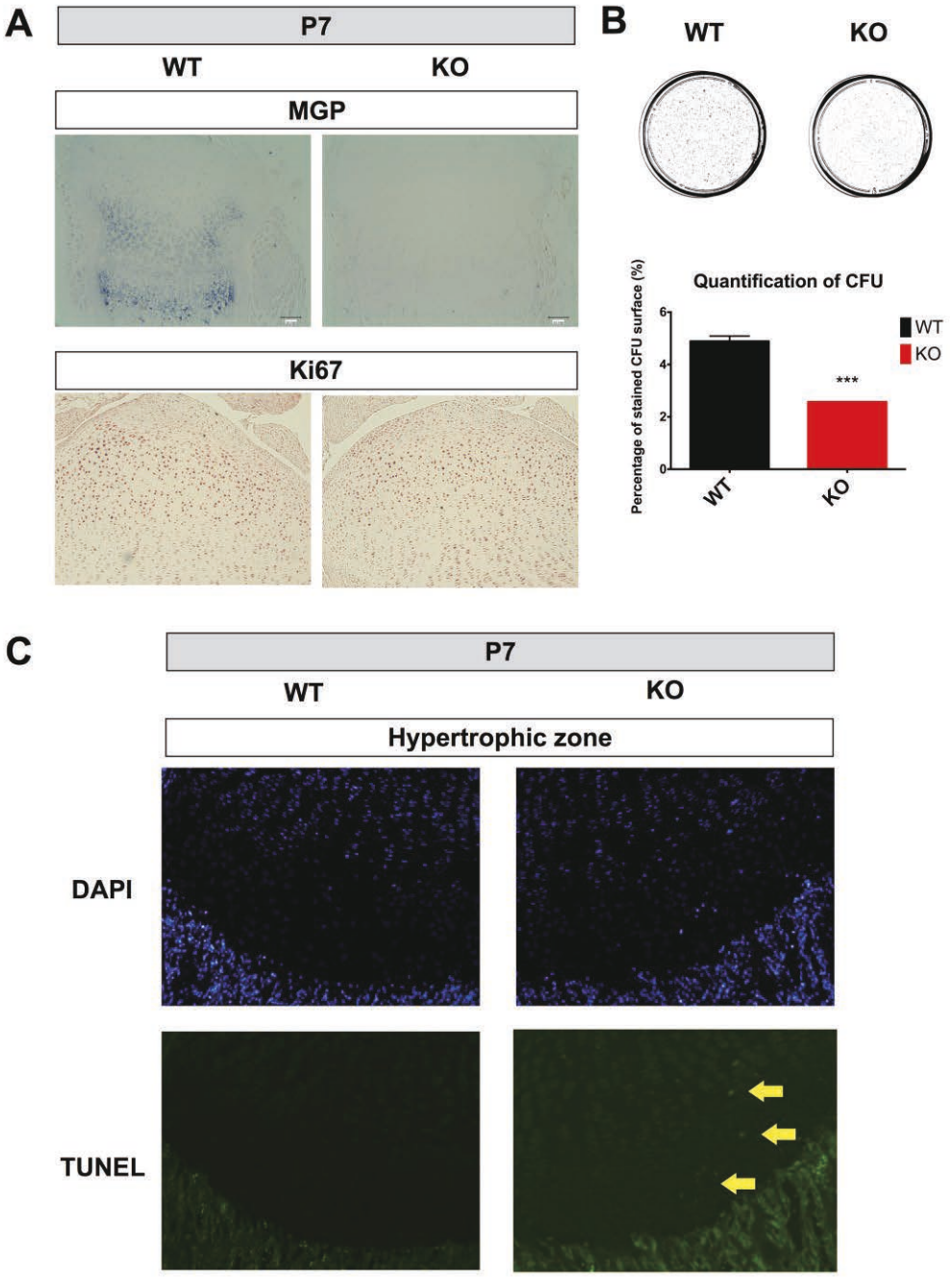

Figure 6. MGP deficiency results in decreased chondrocyte proliferation and increased apoptosis. A. Expression of MGP mRNA by in situ hybridization and expression of Ki67 by immunohistochemistry was performed on tibia sections from P7 pups. B. Colony formation assay was performed on the primary chondrocytes with 5000 cells per petri dish. The scanned macro view of colony wes presented and the result was analyzed and quantified by Image J. Values represent mean±SD. Unpaired two-tailed t-test was used. ★★★, $p<0.001$. C. Measurement of apoptotic cells by TUNEL system on tibia sections from P7 pups showed increased number of apoptotic cells (Green) in hypertrophic zone of MGP KO mice.

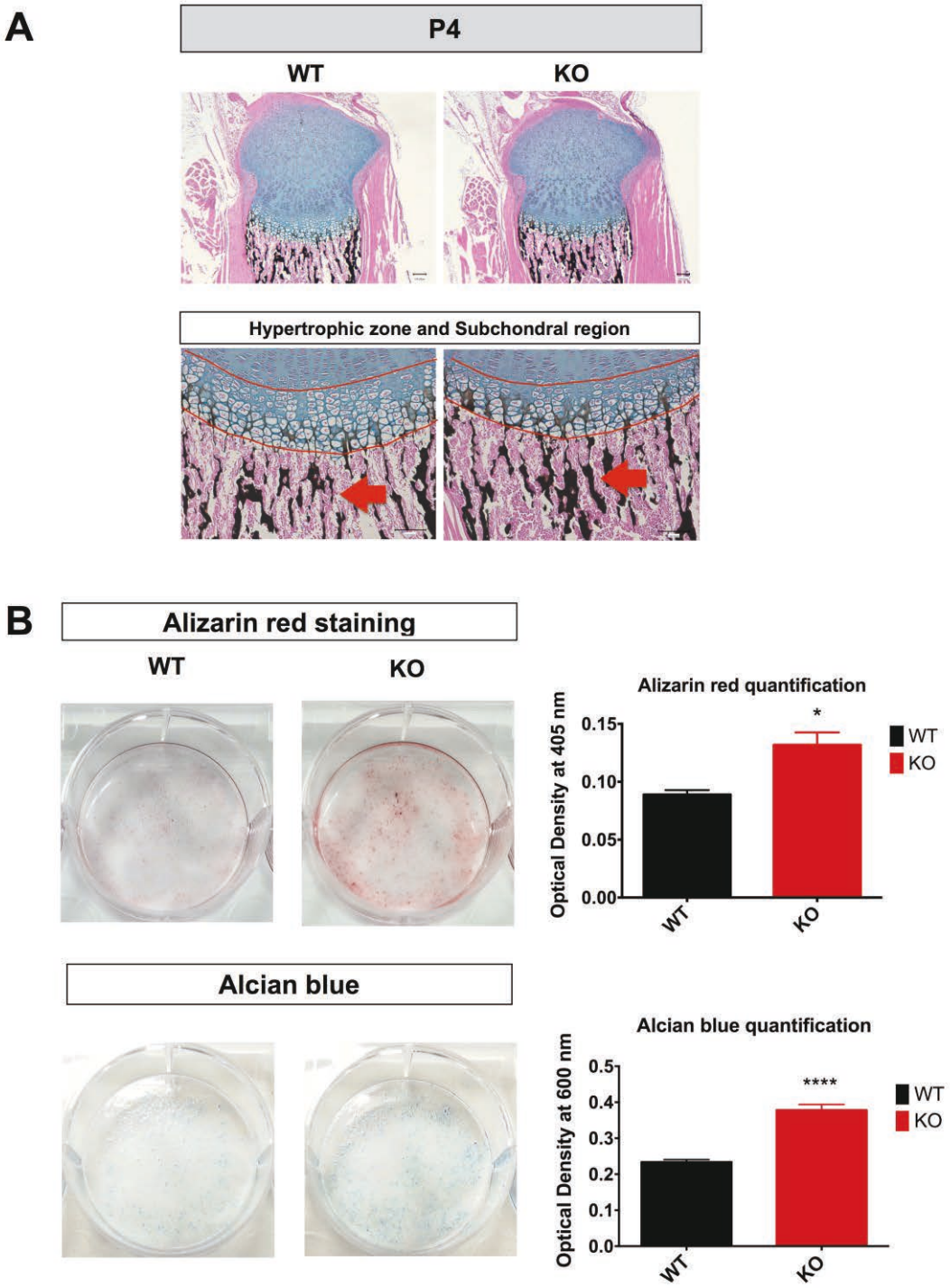

Figure 7. MGP deficiency leads to excessive mineralization. A. Von kossa/Alcian Blue staining on the histological sections of tibia from P4 pups showed more excessive mineralization of subchondral region in MGP KO mice compared with that of MGP WT mice. B. Alizarin red and Alcian blue staining on the primary chondrocytes from MGP WT and KO pups showed more excessive mineralization in MGP KO chondrocytes with increased glycosaminoglycan production. Quantification of staining was performed with Varioskan at 405 nm and 600nm. Values represent mean±SD. Unpaired two-tailed t-test was used. ★, $p<0.05$; ★★★★, $p<0.0001$.

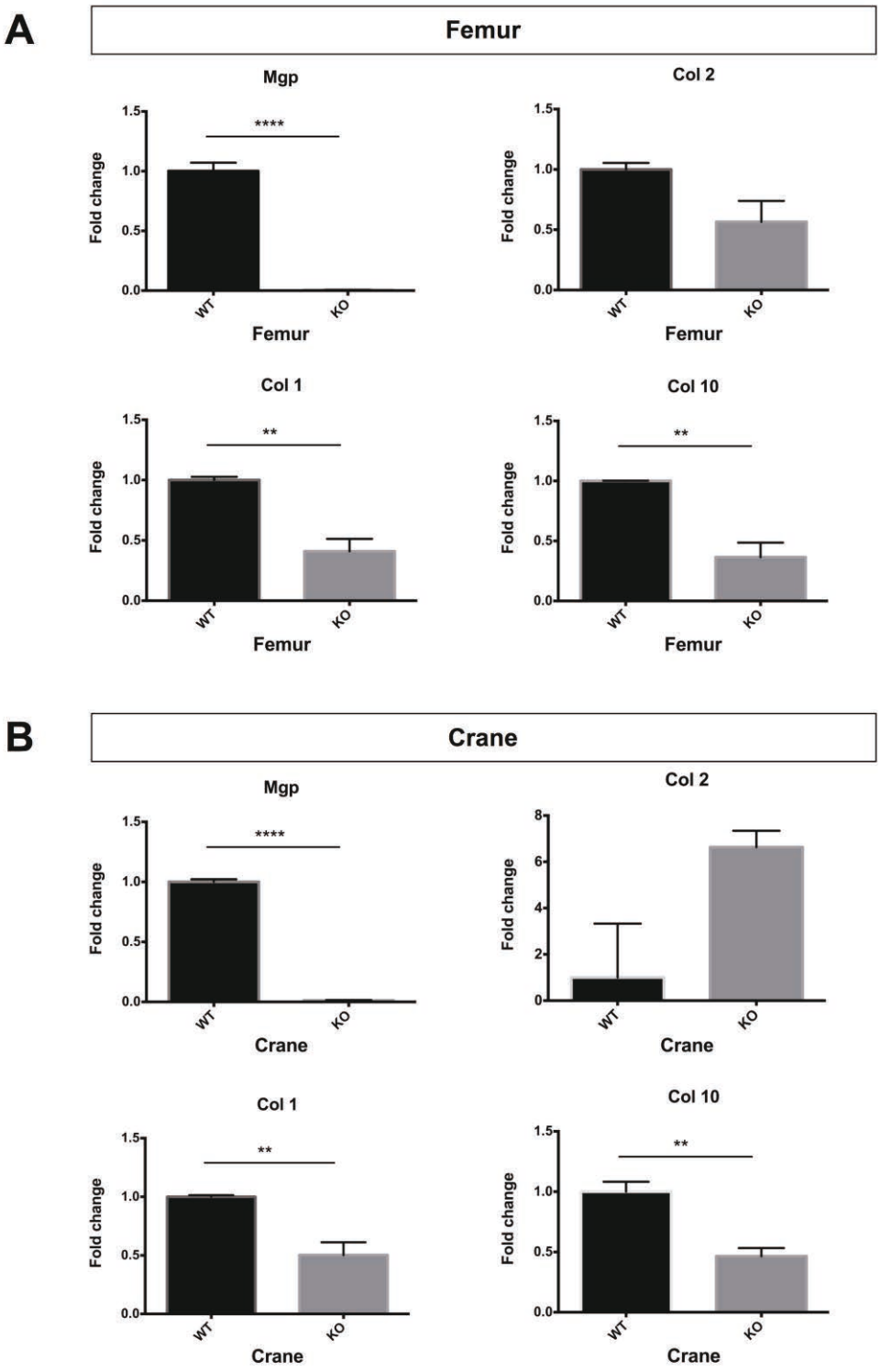

Figure 8. Disturbed expression profile of bone and cartilage markers in MGP KO mice. Quantitative PCR on the RNA extracted from femur (A) and cranium (B) at P21 showed a significant lower expression of Col 1 and Col 10 in the MGP KO mice. Values represent mean±SD. Unpaired two-tailed t-test was used. ★★, $p<0.01$; ★★★★, $p<0.0001$.

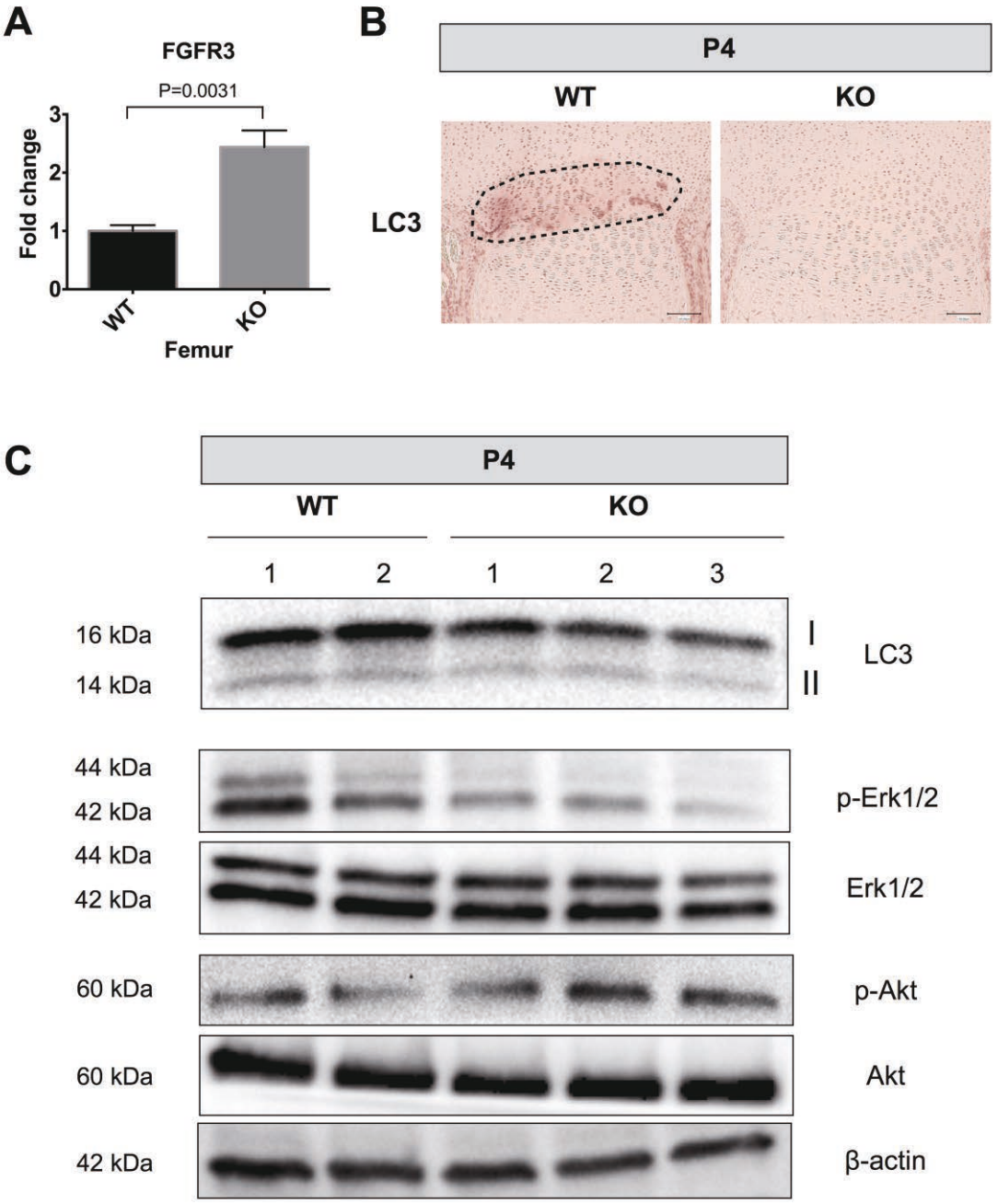

Figure 9. MGP deficiency results in increased expression of FGFR3 and decreased autophagic activity. A. Quantitative PCR on the RNA extracted from femur at P21 showed an increased expression of FGFR3 in MGP KO mice. B. Immunohistochemistry analysis of autophagy marker LC3 in the tibia sections of P4 MGP WT and KO mice. C. Western blot analysis of total protein from the growth plate cartilage of P4 MGP WT and KO mice.

Conclusion

Our study suggests that MGP plays critical roles in regulating chondrocyte proliferation and the timing of maturation and mineralization during postnatal endochondral ossification.

Absence of MGP leads to shortened hypertrophic zone of growth plate from around P4 onwards, accelerated formation of secondary ossification center, significant dwarfism at P21 and decreased autophagic activity.

Discussion & Perspective

I. No apparent skeletal abnormalties between MGP WT and KO during embryonic stages

Although MGP gene expression is detectable during embryonic development (Luo et al., 1995), MGP KO mice do not display any skeletal abnormalties. Vascular, tracheal and skeletal phenotypes only appear postnatally. Due to the massive vascular calcification in MGP KO mice, they died between six to eight weeks after birth before the sexual maturation, due to the rupture of the large arteries and hemorrhage (Luo et al., 1997). To obtain MGP KO mice, only a cross between MGP heterozygous mice is possible.

In addition, MGP is a secreted circulating protein. Interestingly, BGP, the same family member of Gla protein, has been already proved to cross the placenta during pregnancy and rescue the abnormalities in the BGP knockout progeny (Oury et al., 2013). Altogether, these prompted us to suppose that circulating MGP from the pregnant mother MGP heterozygous mice may pass through the placenta to restore the absence of MGP in the MGP KO embryons.

II. Compensatory role of GRP in MGP KO mice ?

In 2008, a novel Gla-containning protein was initially identified from the calcified cartilage of adriatic sturgeon (Viegas et al., 2008), and also detected in other species, such as human (Rafael et al., 2014; Viegas et al., 2009; Viegas et al., 2015), mouse (Rafael et al., 2014; Surmann-Schmitt et al., 2008; Tagariello et al., 2008), rat (Viegas et al., 2009) and zebrafish (Neacsu et al., 2011) through independent studies. It is named Gla-rich protein (GRP) after its high content in Gla residues.

Since most relevant levels of GRP gene expression were observed in cartilaginous tissues and associated with chondrocytes, it suggests a potential role of GRP in chondrogenesis and skeletal development.

GRP was shown to accumulate at the sites of ectopic mineralization in human skin and vascular tissues in cases of dermatomyositis, pseudoxanthoma elasticum (PXE), and chronic kidney disease, supporting the association of GRP with calcification processes (Viegas et al., 2009). Recent study revealed that GRP acts as an inhibitor of vascular and valvular calcification and its function may be associated with prevention of calcium-induced signaling pathway and direct binding to inhibit crystal formation (Viegas et al., 2015).

Furthermore, GRP was shown to be involved in pathological calcification in OA. Uncarboxylated GRP (inactive form) was the predominant form in OA-affected tissues, colocalizing at sites of ectopic calcification (Rafael et al., 2014). Cavaco and colleagues further showed that treatment of articular cells with γ-carboxylated GRP inhibited extracellular matrix mineralization (Cavaco et al., 2016). GRP can act as a cartilage-derived factor that stimulates bone remodelling during experimental OA, while the underlying mechanism still warrants further investigation (Onuora, 2017; Stock et al., 2017).

In summary, GRP has been demonstrated to accumulate at the sites of ectopic mineralization in vascular tissues and act as an inhibitor of vascular calcification (Viegas 2015). All these functions of GRP are similar with those of MGP, suggesting and leading us to study the potential link between them.

During skeletal development, even if GRP was specifically detected in adult growth plate cartilage, no significant impairement of skeleton was observed in GRP knockout mice (Eitzinger et al., 2012). In contrast, one of the two forms of GRP in zebrafish, GRP-2 is required for zebrafish skeletal development and knockdown of GRP-2 leads to severe growth retardation and perturbance of skeletal development (Neacsu et al., 2011).

In MGP KO mice, we have detected the significant increased gene expression of GRP in the femur at P21 and primary chondrocytes (**Figure 13**). Our research collaborator Leonor Cancela (Faro, Portugal) has also found the increased gene and protein expression of MGP in the articular chondrocytes of GRP KO mice.

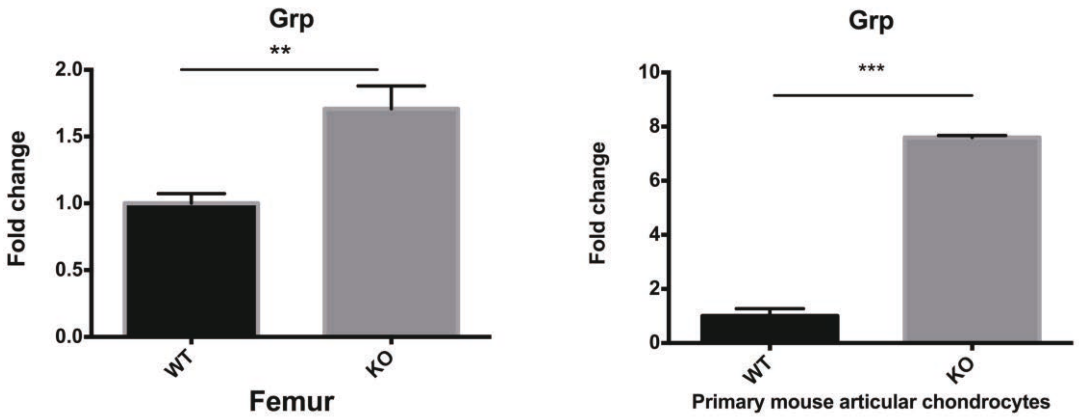

Figure 13 Quantitative PCR results for the expression of GRP in MGP KO femur and primary chondrocytes.
Values represent mean±SD. Unpaired two-tailed t-test was used. ★★, $p<0.01$; ★★★, $p<0.001$.

In the future, in order to detect the possible link and/or balance between MGP and GRP, a double KO mice may be an approach.

III. Are there treatments to rescue the skeletal phenotypes in MGP KO mice?

III-A Treatment targeting MGP

Sodium thiosulfate (STS, $Na_2S_2O_3$) is an agent with strong antioxidant properties and also probably chelates calcium to form soluble calcium thiosulfate complexes. Accumulating evidences have indicated that STS is a successful treatment for calciphylaxis, a disease characterized by abnormal calcium deposits in soft tissues (Brucculeri et al., 2005; Cicone et al., 2004; Fernandes et al., 2014; Meissner et al., 2006). STS also seems to have cardioprotective role on chronic heart failure by modulating endogenous H_2S generation in heart failure mouse model (Sen et al., 2008).

Recently, the role of STS had been extended to the prevention of vascular calcifications. In uremic rats model, the rats treated by sodium thiosulfate had no histological evidence of calcification in the aortic wall, whereas almost three-fourths

of untreated uremic rats showed aortic calcification. There was increased urinary calcium excretion and significantly reduced calcium content of aortic, heart, and renal tissue in the STS-treated rats compared to non-treated rats. The only side effect that they found in the study was lowered bone strength in the STS-treated rats compared to their normal controls (Pasch et al., 2008). In haemodialysis patients, progression of coronary artery calcification occurred in 25% of the STS-treated patients compared with 63% in the control group. These results indicated that STS can delay the progression of coronary artery calcification (Adirekkiat et al., 2010). Interestingly, a recent study showed that STS may protect human aortic smooth muscle cells from osteoblastic transdifferentiation via high-level phosphate and the MGP-BMP2-Cbfα-1 signal pathway (Zhong et al., 2013).

However, until today, the underlying mecanism of STS in preventing vascular calcification remains unclear. One possible mecanism is to induce hypercalciuria and excessive urinary excretion of calcium, preventing calcifications by its chelation properties. A second possible mechanism might be the induction of acidosis. The third possible mechanism, STS might change the availability or function of factors affecting the extracellular matrix, such as the calcification inhibitor MGP. The plasma MGP concentrations were higher in uremic STS-treated rats versus untreated rats, strongly suggesting the possibility of additional therapeutic effects of STS by modulating vascular calcification inhibitors (Pasch et al., 2008).

In this context, we aimed to study if STS can prevent or inhibit the pathological vascular calcification observed in MGP KO mice and its potential effects on skeletal development.

In contrast to a recent publication that showed anti-mineralization ability of STS in the primary murine chondrocytes (Nasi et al., 2016), we did not observe the same effect in our phosphate-induced mineralization culture model (data not shown) and we noticed the possible pro-mineralization ability of STS in primary chondrocytes from MGP WT and KO pups (**Figure 14**).

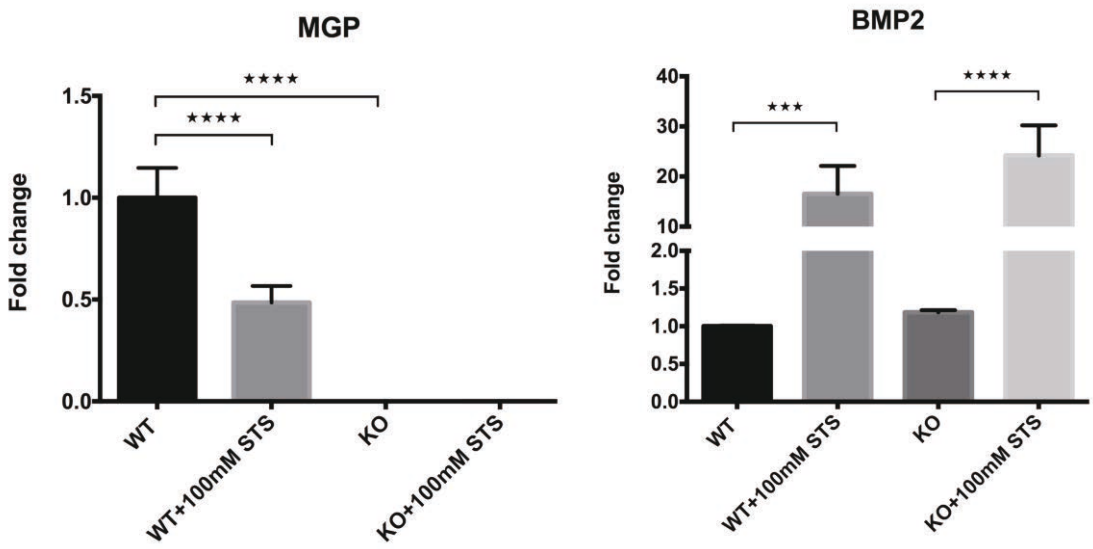

Figure 14 Quantitative PCR results for the expression of MGP and BMP2 in the primary chondrocytes from MGP WT and KO pups.
Values represent mean±SD. One-way ANOVA with bonferroni's correction was used. ★★★, $p<0.001$; ★★★★, $p<0.0001$.

We further investigated the effect of STS on mineralization in vivo by intraperitoneal injection or adminstration in drinking water, as presented in **Figure 15A**. Our results showed that both protocols of STS treatment did not rescue the abnormal vascular or skeletal phenotype in the MGP KO mice, as the calcification of aorta still persists (shown by red arrow, **Figure 15 B&C**). Interestingly, we also noticed the remarkably decreased skeleton size of MGP KO mice in both types of STS treatment when compared to that without STS treatment (**Figure 15 C**). The reduced skeleton size by STS treatment also exists in $MGP^{+/+}$ and $MGP^{+/-}$ mice (data not shown).

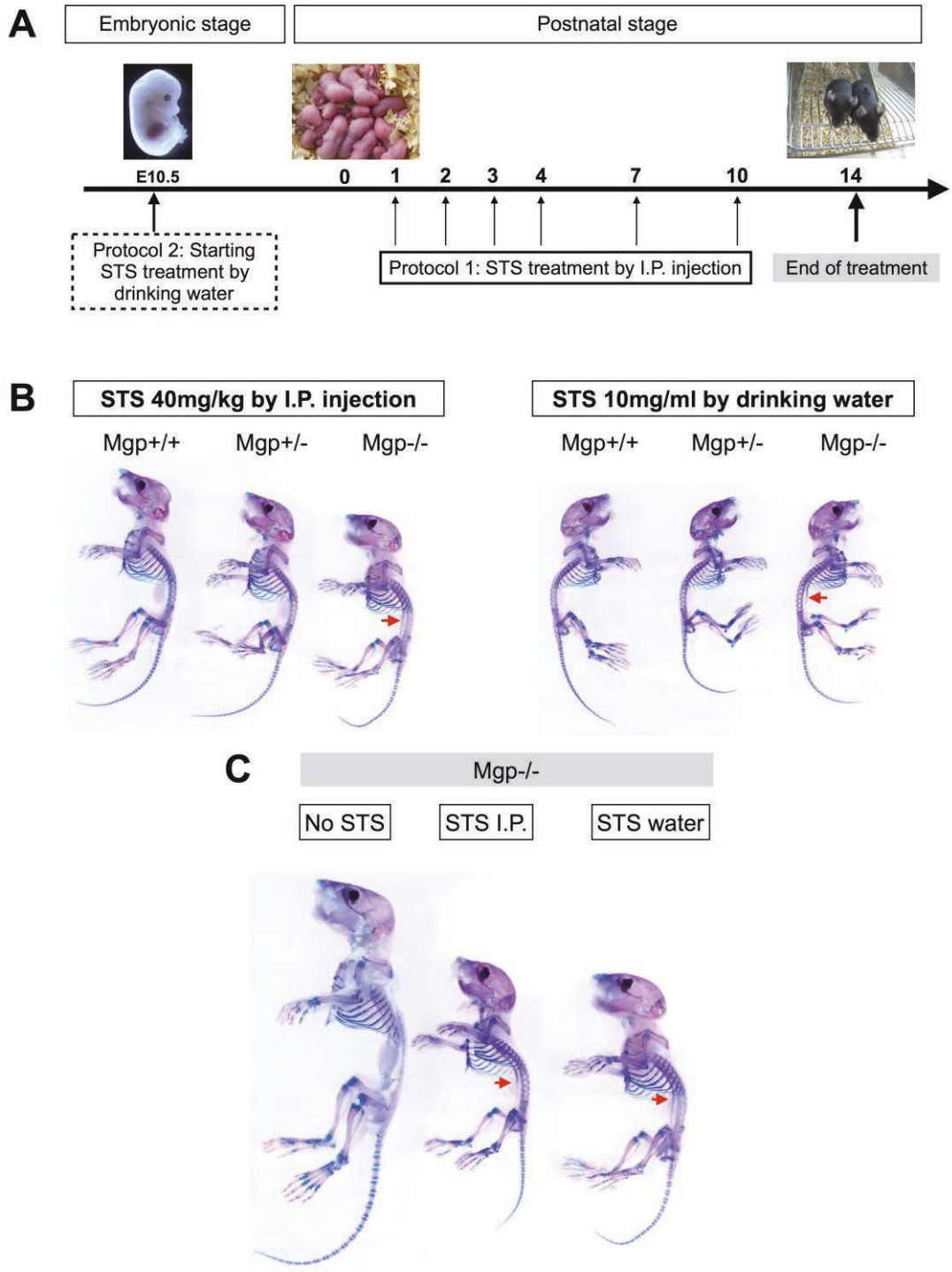

Figure 15 STS has no preventive effect on vascular calcification, but impairs skeletal development.

A. Schematic representation of STS treatment protocols. B&C. Whole-mount Alcian blue/Alizarin red staining of skeletal preparations at P14 from STS 40 mg/kg by I.P. injection or STS 10mg/ml by drinking water.

Taken together, these in vitro and in vivo results suggest a potential role of STS treatment in skeletal development. Actually, a collaboration project is ongoing with Dr.

Sonia Nasi and Pr. Nathalie Busso (Lausanne, Switzerland) to study the role of STS in chondrocyte phenotype in the growth plate during skeletal development.

III-B Treatment targeting MGP downstream signaling

If our preliminary results on FGFR3 and autophagy can be further confirmed by different approaches in MGP KO mice, it will be very interesting to test the inhibitors of FGFR signaling or activitor of autophagy, to see if we can rescue the dwarfism caused by MGP deficiency.

The therapeutic approaches targeting FGFR3 can be well summarized in a recent review (**Figure 16**) (Ornitz and Legeai-Mallet, 2017).

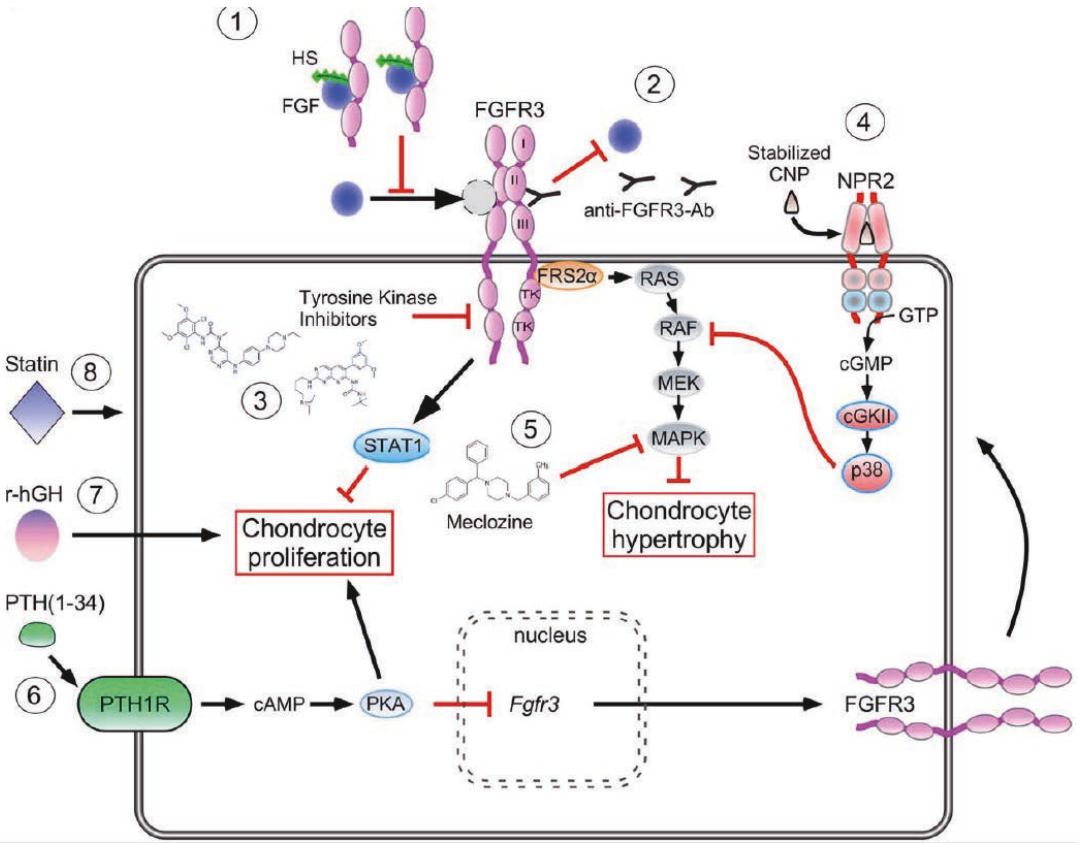

Figure 16 Schematic representation of summarized therapeutic approaches targeting FGFR3 signaling for ACH.
(1)sFGFR3: soluble FGFR3 extracellular domain decoy receptors; (2)Anti-FGFR3 antibodies; (3)TKIs: tyrosine kinase inhibitors; (4)Stabilized CNP (BMN-111); (5)Meclozine: suppresses high ERK1/2 phosphorylation; (6)PTH(1-34): increases chondrocyte proliferation and suppresses FGFR3 expression; (7)Indirect effect of r-hGH on bone growth; (8)Statin: promotes degradation of FGFR3.

Many pharmacological strategies have been proposed and tested, aiming at reducing excessive activation of FGFR3, including FGFR-selective small molecule tyrosine kinase inhibitors (TKIs) (CHIR-258, PD173074, SU5402, NVP-BGJ398), anti-FGFR3 antibodies and soluble FGFR3 extracellular domain decoy receptors (sFGFR3). As the balance between chondrocyte proliferation and differentiation is severely disrupted, other strategies have focused on the non-FGF signaling pathway that control chondrocyte proliferation and differentiation, including stabilized CNP.

As presented in Chapter 2.2, autophagy has been shown to play an important role in chondrocyte homeostasis during skeletal development and dysregulation of the autophagic response is involved in the pathogenesis of growth plate cartilage, including ACH. Our preliminary results presented in ***Figure 9 of Article N°2*** also suggest that in our MGP KO mice autophagy is altered. Hence, pharmacological activation of autophagy may serve as another strategy to rescue the skeletal defects observed in MGP KO mice.

Chapter 3

Modification of chondrocyte phenotype induced by metabolic factors in the development of osteoarthritis

Chapter 3A

Metabolic syndrome associated osteoarthritis: study on animal model

3A.1 Metabolic syndrome associated osteoarthritis

3A.1.1 Osteoarthritis

Osteoarthritis (OA) is a progressive degenerative joint disease, characterized by articular cartilage deterioration, and hyperplasia, fibrosis and inflammation of the synovial membrane (synovitis), as well as remodeling of the subchondral bone (Wieland et al., 2005) (**Figure 17**).

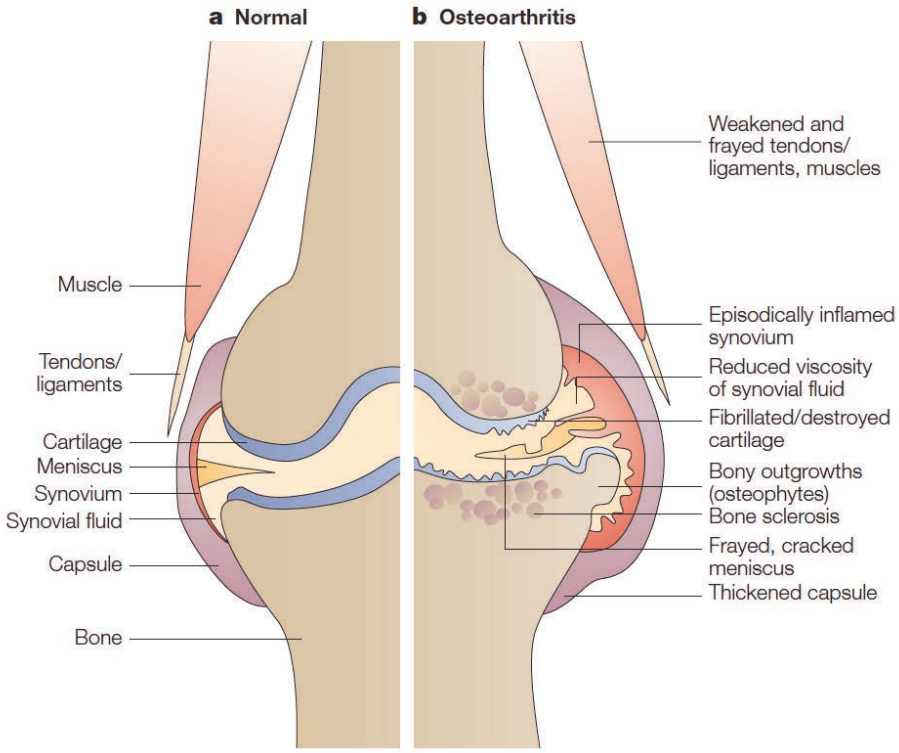

Figure 17 Articular structures that are affected in OA.
a. Normal healthy cartilage: without any fissures, no signs of synovial inflammation. b. OA lesions: synovial inflammation, 'fibrillated' cartilage, bony outgrowths (osteophytes), bone sclerosis, etc. (Wieland et al., 2005)

OA can occur in any joint but is most common in certain joints, including those of the hand, knee, foot and hip. Recent studies about its pathophysiology prompted the division of OA into distinguishable clinical phenotypes, including post-traumatic, ageing-related, genetic, pain-related and metabolic (Bijlsma et al., 2011) (**Table 1**).

	Post-traumatic (acute or repetitive)	Metabolic	Ageing	Genetic	Pain
Age	Young (<45 years)	Middle-aged (45–65 years)	Old (>65 years)	Variable	Variable
Main causative feature	Mechanical stress	Mechanical stress, adipokines, hyperglycaemia, oestrogen/ progesterone imbalance	AGE, chondrocyte senescence	Gene related	Inflammation, bony changes, aberrant pain perception
Main site	Knee, thumb, ankle, shoulder	Knee, hand, generalised	Hip, knee, hand	Hand, hip, spine	Hip, knee, hand
Intervention	Joint protection, joint stabilisation, prevention of falls, surgical interventions	Weight loss, glycaemia control, lipid control, hormone replacement therapy	No specific intervention, sRAGE/AGE breakers	No specific intervention, gene therapy	Pain medication, anti-inflammatory drugs

Osteoarthritis is not one disease, and might benefit from the recognition of its different phenotypes. AGE=advanced glycation endproducts. sRAGE=soluble receptor for advanced glycation endproducts.

Table 1 Proposal for different clinical phenotypes of OA.
(Bijlsma et al., 2011)

In the past few years, metabolic OA has been linked not only to obesity but also to other cardiovascular risk factors, including diabetes, dyslipidemia, hypertension and insulin resistance. All those risk factors constitute the metabolic syndrome (MetS), which has become a major worldwide health issue affecting more than 2 billion individuals across the globe (Shin, 2014; Zhuo et al., 2012).

3A.1.2 Metabolic syndrome

MetS is a widely used and accepted phenotype associated with an increased risk of cardiovascular disease, but it lacks a universe definition. The most frequently used definitions of MetS have been produced by the World Health Organization (WHO), the European Group for the Study of Insulin Resistance (EGIR), the National Cholesterol Education Program-Third Adult Treatment Panel (NCEP ATP III) and the International Diabetes Federation (IDF) (Zhuo et al., 2012) (**summarized in Table 2**). There are four central features in these definitions, comprising obesity, insulin resistance, dyslipidemia and hypertension.

Characteristics and studies	Published definitions			
	WHO (1998)[4]	EGIR (1999)[5]	NCEP ATP III (2005)[6]	IDF (2005)[7]
Criteria requirements	Insulin resistance plus two of the four others	Insulin resistance plus two of the three others	Any three of the five	Obesity plus two of the four others
Individual criteria				
Insulin resistance	IGT, IFG,T2D	Plasma insulin >75th percentile	Fasting glucose ≥5.6 mmol/l	Fasting glucose ≥5.6 mmol/l
Obesity	Waist/hip ratio: >0.90 (men); >0.85 (women) or BMI >30	Waist circumference: >94 cm (men); >80 cm (women)	Waist circumference: >94 cm (men); >80 cm (women)	Waist circumference: >94 cm (men); >80 cm (women)
Dyslipidemia (TG and HDL-C combined)	TG ≥1.7 mmol/l or HDL-C <0.9 mmol/l (men); <1.0 mmol/l (women)	TG >2.0 mmol/l or HDL-C <1.0 mmol/l	NA	NA
Dyslipidemia (TG)	NA	NA	TG >1.7 mmol/l	TG 1.7 mmol/l
Dyslipidemia (HDL-C)	NA	NA	HDL-C <1.03 mmol/l (men); < 1.29 mmol/l (women)	HDL-C <1.03 mmol/l (men); < 1.29 mmol/l (women)
Hypertension	≥140/90 mmHg	≥140/90 mmHg	≥130 mmHg systolic or ≥85 mmHg diastolic	≥130 mmHg systolic or ≥85 mmHg diastolic
Microalbuminuria	Urinary albumin excretion of 20 μg per min or albumin:creatinine ratio of 30 mg/g	Not included	Not included	Not included

*All values are in the absence of pharmacologic therapy. No definition yet includes metabolic osteoarthritis. Abbreviations: EGIR, European group for the study of Insulin resistance; HDL-C, HDL cholesterol; IDF, International Diabetes Federation; IFG, impaired fasting glucose; IGT, impaired glucose tolerance; NA, not applicable; NCEP ATP III; the US National Cholesterol Education Program Adult Treatment Panel III; T2D, type 2 diabetes; TG, triglycerides.

Table 2 Frequently used definitions of MetS.
(Zhuo et al., 2012)

3A.1.3 Metabolic syndrome and Osteoarthritis

MetS was shown to be prevalent in 59% of OA patients compared to 23% of the general population, based on data from the Third National Health and Nutrition Examination Survey in 2002 (Singh et al., 2002). Furthermore, in 2009, Puenpatom and Victor sugggested for the first time that, compared to OA patients without MetS, patients with MetS develop clinical symptoms of OA earlier in life and are subject to more generalised pathology, increased inflammation and augmented intensive pain in the joints (Puenpatom and Victor, 2009). Other cross-sectional studies confirmed the association between MetS and OA(Courties et al., 2015; Shin, 2014).

Interestingly, recent cohort studies showed that incidence and severity of OA were positively correlated with the number of MetS components. In the ROAD (Research on Osteoarthritis/ osteoporosis Against Disability) cohort of 1384 Japanese

individuals, the prevalence of knee OA significantly increased according to the number of MetS components. Logistic regression analyses after adjusting for potential risk factors revealed that the odds ratio (OR) for the occurrence of knee OA significantly increased according to the number of MetS components present (OR vs no component: one component, 2.33; two components, 2.82; ≥three components, 9.83). Similarly, the progression of knee OA significantly increased according to the number of MetS components present (OR vs no component: one component, 1.38; two components, 2.29; ≥three components: 2.80) (Yoshimura et al., 2012) (**Figure 18**).

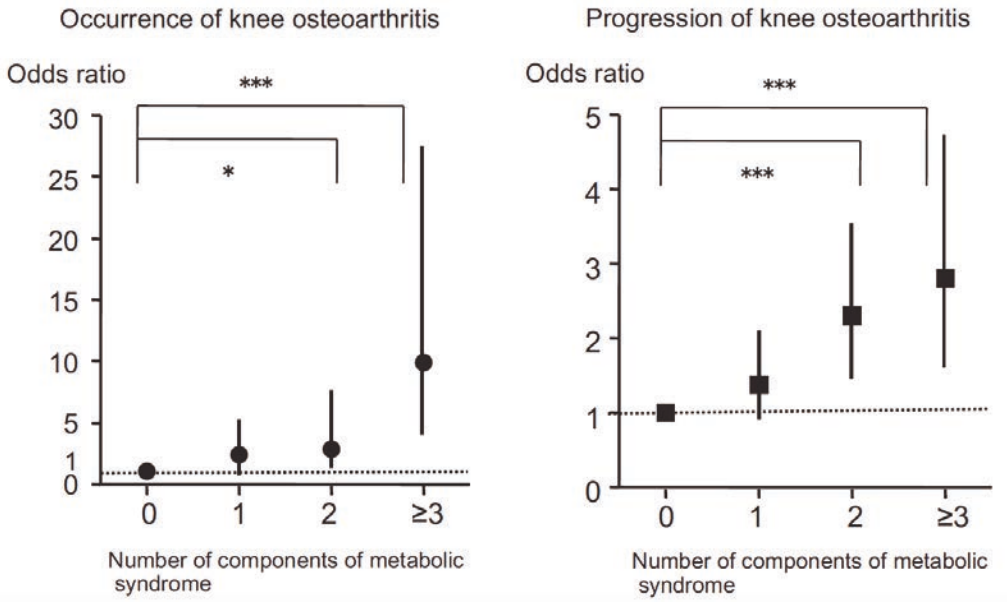

Figure 18 Multivariate logistic regression analysis of the Odds ratios for occurrence and progression of knee OA during the 3-year follow-up period vs the number of MetS components.
*: $p<0.05$, ***: $p<0.001$. (Yoshimura et al., 2012)

Taken together, all these epidemiologic studies show the clear associations between MetS and OA, and there is an urge to propose metabolic OA as one of the components of MetS. However, the contribution of MetS to the phenotype of OA joint is yet unclear and warrants further investigation in experimental models, as all these cross-sectional and longitudinal epidemiologic studies have high heterogeneity in the design (definition of MetS, sex selection, record of medication, etc) (Berenbaum et al., 2017; Courties et al., 2015).

Interestingly enough, aldosterone, the ligand of mineralocorticoid receptor (MR), has been shown to be associated with MetS. MetS present high circulating aldosterone concentration and epidemiological studies demonstrated that higher aldosterone concentrations are associated with a greater prevalence of MetS and its components in the subjects of African descent. In the Framingham Offspring Study, higher aldosterone levels was associated with the development of MetS and with longitudinal change of its components{Ingelsson:2007cn}. In addition, increasing experimental and clinical studies have reported aldosterone as a potential risk factor for MetS and its important role in the pathology of metabolic and cardiovascular diseases (Briet and Schiffrin, 2011; Cabandugama et al., 2017; Das, 2016; Musani et al., 2013; Whaley-Connell et al., 2010; Zennaro et al., 2009).

This role of aldosterone via MR in MetS and the link between MetS and OA inclined to look at the potential role MR in OA.

3A.2 Mineralocorticoid receptor and Metabolic syndrome

3A.2.1 Brief introduction on mineralocorticoid receptor

MR and its ligand aldosterone are the principal modulators of hormone-regulated renal sodium reabsorption and potassium excretion, therefore playing an important role in the control of blood pressure and extracellular volume homeostasis. Beside the aldosterone-sensitive distal nephron in the kidney, MR is expressed in several other cells and organs, in which its activation mediates pathologic changes, indicating potential therapeutic applications of pharmacological MR antagonism (Jaisser and Farman, 2016). (**Figure 19**)

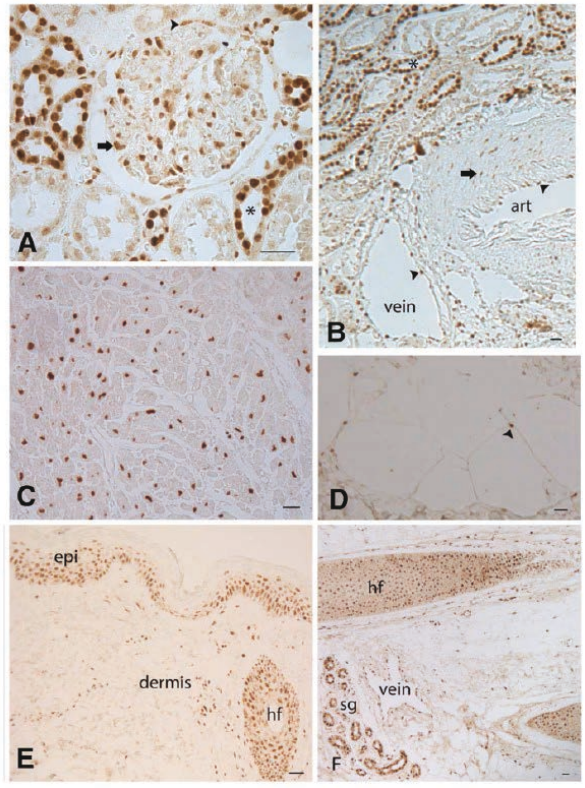

Figure 19 MR expression in human tissues.
A. Kidney: distal tubule and collecting duct cells (star), podocytes (arrow), and glomerular parietal epithelial cells (arrowhead). B. Artery: vascular smooth muscle cells (arrow) and endothelial cells (arrowhead). C. Heart: nuclei of atrial cardiomyocytes. D. Subcutaneous adipocytes. E&F. Skin : epidermis (epi), hair follicle (hf), sweat glands (sg).(Jaisser and Farman, 2016)

3A.2.2 Mineralocorticoid Receptor Antagonists

Spironolactone was the first steroidal mineralocorticoid receptor antagonist (MRA) developed by Searle Laboratories in 1959 and was approved as a diuretic and natriuretic drug for the treatment of hypertension, primary aldosteronism and heart failure (Ménard, 2004). Spironolactone is a competitive MRA but with low selectivity, and it also inhibits the androgen and progesterone receptors. At high concentrations, spironolactone may also interfere with the glucocorticoid receptor (GR) (Kolkhof and Borden, 2012).

Eplerenone is a second generation MRA, which was developed by Ciba-Geigy (Basel, Switzerland) and launched by Pfizer (New York) in 2002 for the treatment of hypertension and heart failure (Kolkhof and Borden, 2012; Ménard, 2004). Eplerenone is much more selective for MR than spironolactone, but with less potency (40× less), requiring high dosage to obtain similar MRA effect.

Spironolactone can rapidely metabolize into several active metabolites with a half-time of about 15 hours, whereas eplerenone has no active metabolite with a shorter half-life of less than 4 hours. Hyperkaliemia is a potential life-threatening side effects of MRA, because of their efficacy to decrease urinary potassium excretion. Even if the clinically relevant hyperkaliemia during the treatment with MRA is rare, close follow up of kaliemia is required, as well as regular monitoring of renal function.

In the last decade, the widely therapeutic applications of MRA in heart failure and possibly in kidney diseases, as well as the side effects of steroidal MRA due to the risk of hyperkaliemia, has stimulated the search for novel MRA with higher selectivity, high potency, and if possible, a reduced risk of hyperkaliemia. For example, BAY-94-8862 (finerenone), a third generation MRA, was used in phase 2a clinical trials in patients with heart failure and mild renal dysfunction (Pitt et al., 2013). Finerenone was shown to be safe with lower rate of hyperkaliemia than spironolactone. This benefit of finerenone over the steroidal MRA spironolactone and eplerenone may relay on the differential tissue distribution of the two compounds.

Low dose of finerenone may achieve sufficient MR antagonism in other tissues with less renal MR blockade (Kolkhof et al., 2014; Lentini et al., 2016).

Other nonsteroidal MRA such as PF-03882845 (Pfizer) and SM-368229 (Dainippon Sumitomo Pharma, Osaka, Japan) have been shown to be efficient in preclinical models and are going through clinical trials (Collin et al., 2014).

3A.2.3 Mineralocorticoid receptor in metabolic syndrome

MR and Obesity

The role of MR in adipose tissue has been highlighted. MR is involved in the plasticity of white adipocyte, and MRA leads to increased presence of brown adipocytes within the white adipose tissue, through direct control of autophagy promoting increased metabolic activity of adipose depots (Armani et al., 2014). Activation of MR by aldosterone influence adipocyte differentiation and the secretion of adipokines as well as proinflammatory markers (Caprio et al., 2007). In db/db mice, treatment with MRA eplerenone for 16 weeks could reverse obesity-related changes in adipose tissue, comprising the increased expression of leptin and proinflammatory cytokines with a concomitant reduction of adiponectin (Guo et al., 2008). Short-term eplerenone administration (3 weeks) in db/db and ob/ob mice also showed improved insulin sensitivity and restored dysregulation of adipose gene expression (Hirata et al., 2009). The specific role of MR in adipose tissue was recently studied using a transgenic mouse model, with inducible MR expression only in adipocytes. Increased MR expression in adipose tissues was associated with increased body weight, insulin resistance, and features of MetS (Urbanet et al., 2015).

MR and Insulin resistance

The relationship between MR and insulin resistance has been reported by many observational studies, which showed that high aldosterone levels and MR activation are present in human insulin resistant states and are associated with insulin resistance,

irrespective of race, blood pressure or body weight.

The the convincing evidence in favor of the contribution of MR to insulin resistance is that patients with primary aldosteronism have increased insulin resistance (Mosso et al., 2007) and removal of aldosterone by treatment improves insulin resistance, suggesting aldosterone as a main determinant of the alteration in insulin sensitivity (Catena et al., 2006; Giacchetti et al., 2007; Sindelka et al., 2000).

Aldosterone is also associated with insulin sensitivity in normal healthy individuals. In a study involving 483 African-Americans without any cardiovascular or renal disease, aldosterone levels correlated with insulin resistance independent of all other variables (MD et al., 2012). In another study of 1088 individuals, plasma aldosterone levels predicted insulin resistance. In addition, after 10 years of follow-up, insulin resistance developed more often in individuals with high baseline plasma aldosterone than in those with low baseline plasma aldosterone (Kumagai et al., 2011).

Numerous experimental studies have explored the potential mechanisms by which MR may contribute to insulin resistance, including a decreased transcription of the insulin receptor gene, increased degradation of insulin receptor substrates, interference with insulin signaling, decreased adiponectin production and increased oxidative stress and inflammation. These mechanisms have been well summarized in a recent review (**Figure 20**) (Garg and Adler, 2012).

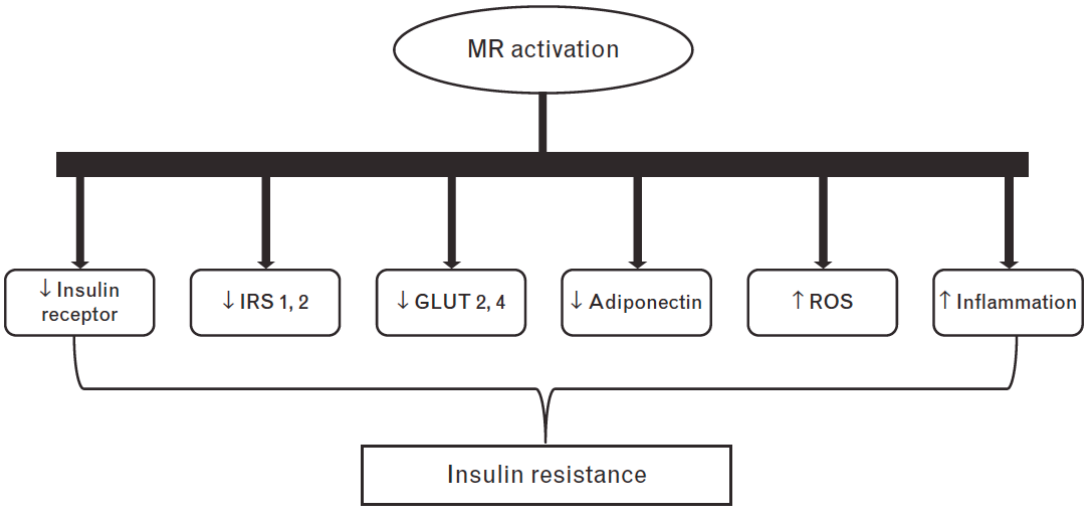

Figure 20 Summarized potential mechanisms of MR activation induced insulin resistance.
GLUT, glucose transporter; IRS, insulin receptor substrate; ROS, reactive oxygen species. (Garg and Adler, 2012)

3A.2.4 Critical mechanisms involved in MR activation

MR and oxidative stress

MR activation by aldosterone stimulates oxidative stress in target cells, such as collecting duct cells, cardiomyocytes, endothelial cells, adipocytes and macrophages (Brown, 2013; Queisser and Schupp, 2012). The induced oxidative stress by MR activation may lead to posttranslational modifications of important downstream pathways, including increased production of hydrogen peroxide, increased expression of NADPH oxidase subunits, mitochondrial dysfunction, and activation of the nuclear factor κB pathway (Brown, 2013; Mayyas et al., 2013). The consequences of oxidative stress consist inflammation and fibrosis (**Figure 21**) (Brown, 2013).

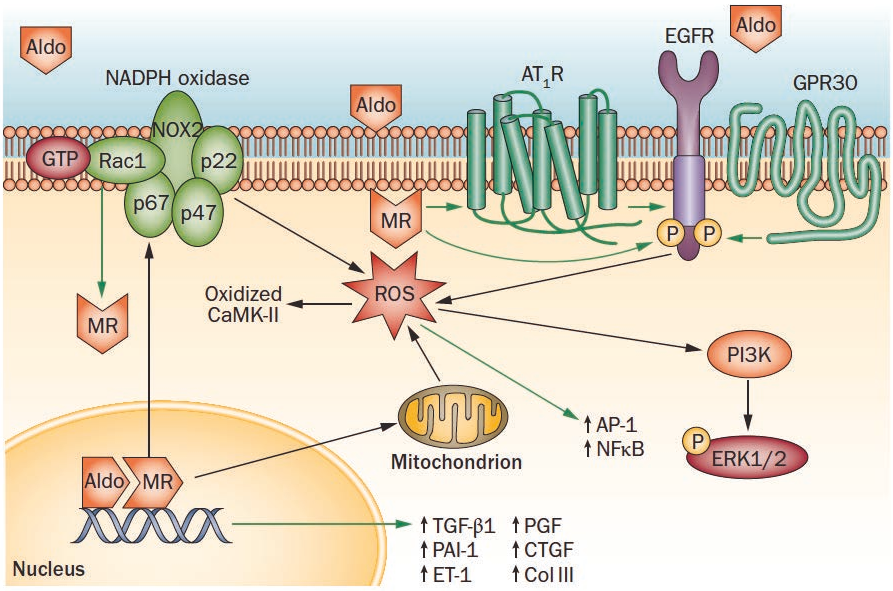

Figure 21 Mechanisms by which aldosterone/MR activation induces oxidative stress.
MR activation induces oxidative stress by both NADPH oxidase and mitochondria. MR activation can also cause rapid, nongenomic effects via transactivation of the EGFR, resulting in the generation of ROS. (Brown, 2013)

The link between MR and oxidative stress has been reviewed in excellent publications (Even et al., 2014; Queisser and Schupp, 2012).

MR and fibrosis

Increasing number of studies have indicated that MR plays a deleterious role in cardiovascular and renal diseases by promoting fibrosis (Thomas et al., 2009; Young and Rickard, 2012). MR activation has been shown to promote cardiovascular and renal tubulointerstitial fibrosis (Bauersachs et al., 2015). The profibrotic effect of MR activation has also been reported in other tissues, including liver (Pizarro et al., 2015), skin (Mitts et al., 2010), lung (Maron et al., 2014) and adipose tissue (Divoux and Clément, 2011).

In addition, MRA treatment can mitigate the fibrosis induced by MR activation. In heart failure, MRA treatment is beneficial associated with a reduction of fibrotic markers (Iraqi et al., 2009). MRA also showed beneficially effect in mice with nonalcoholic steatohepatitis (Pizarro et al., 2015), in limiting skin fibrosis (Mitts et al.,

2010), and in peritoneal fibrosis (MS et al., 2014; Zhang et al., 2014).

MR and Inflammation

Low-grade systemic inflammation is a hallmark of cardiovascular, metabolic and rheumatic diseases. Recently, macrophages, dendritic cells, and T lymphocytes were identified as MR target cells (Bene et al., 2014).

MR activation induces the expression of interleukin-6 (IL-6) and tumor necrosis factor-α (TNF-α) in both immune and non-immune cells (Bene et al., 2014). Vascular inflammation and the infiltration of arterial wall by immune cells is an early event after MR activation (Kasal and Schiffrin, 2012). MR activation promotes a switch in macrophage polarization toward a proinflammatory phenotype (Marzolla et al., 2014). Specific deletion of MR in macrophage protects against the pharmacological treatment induced cardiac fibrosis (Usher et al., 2010). T regulatory cells prevent the vascular injury induced by aldosterone in mice (Kasal et al., 2012).

Recent studies highlighted the potential role of danger-associated molecular pattern molecules (DAMPs), which can initiate and immune responses in noninfectious inflammatory states (Anders and Schaefer, 2014). In particular, several DAMPs have been identified as MR targets, including galectin-3, osteopontin, tenascine-C, and collagen/fibronectin peptides. In conclusion, as MR is activated during immune system and can modulate immune functions, it suggests that the beneficial therapeutic effects of MRA in cardiovascular, renal and metabolic diseases in part rely on their anti-inflammatory properties.

The effects of cell-specific activation of MR in different target cells, including T cells, endothelial cells, macrophage and cardiomyocyte, have been well summarized in the publication (Brown, 2013) and presented in the following schema (**Figure 22**).

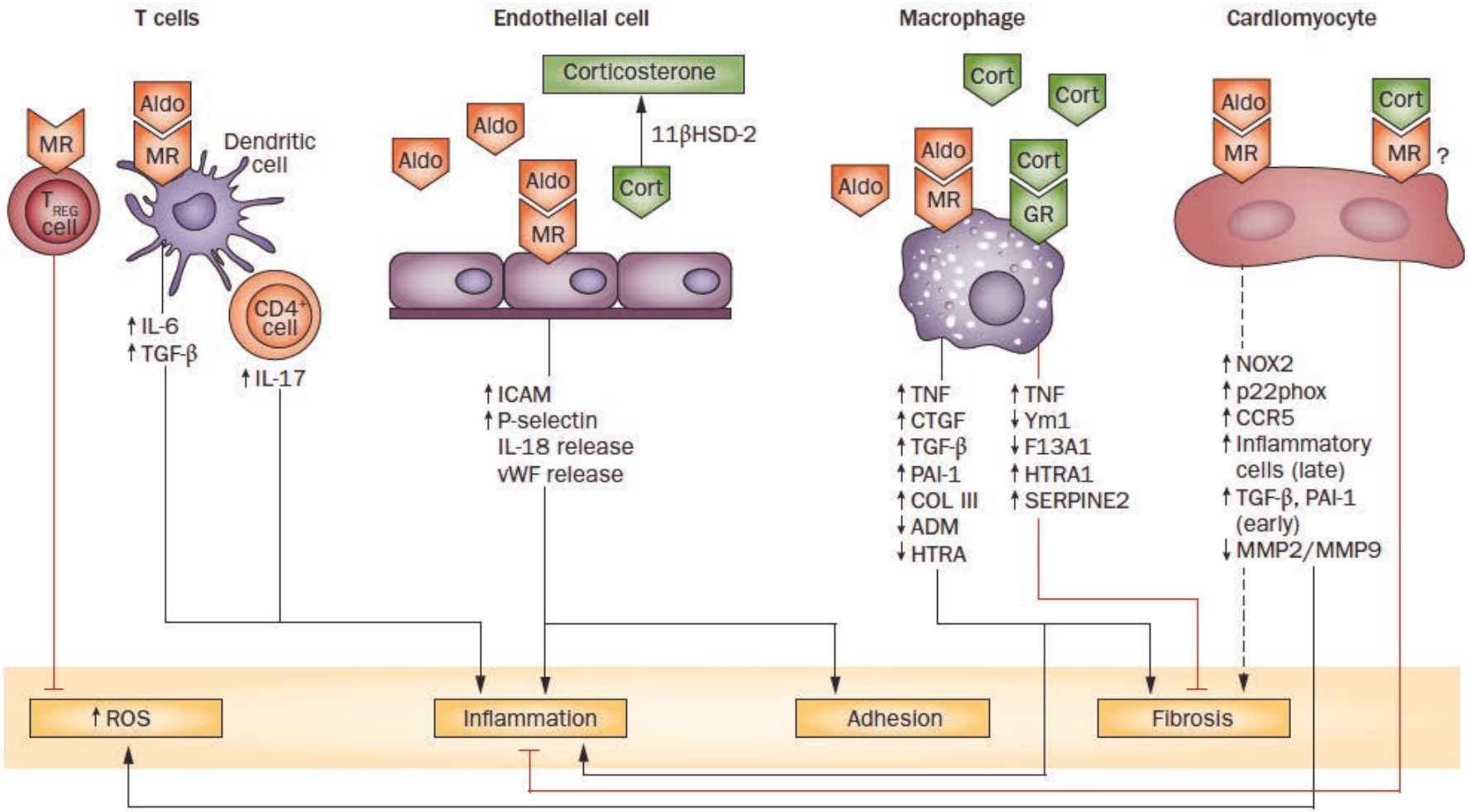

Figure 22 Shematic presentation for the effects of cell-specific MR activation.
For summary and review in details, please see the publication (Brown, 2013).

3A.3 Animal models of metabolic syndrome

Numerous epidemiological and clinical studies have highlighted the role of MetS in the incidence and progression of OA. These two pathologies have become a major public health issue since recent years and there is an urge need to study the contribution and pathophysiological effects of MetS in OA. In this context, animal models are essential and of high importance.

To date, the most common MetS models consist models induced by diets and models exhibiting a non-functional leptin pathway, which have been well reviewed recently (Berenbaum et al., 2017; Fellmann et al., 2013; Wong et al., 2016).

Benefiting from these animal models with MetS, many studies have been conducted to investigate the OA phenotype in the context of MetS or metabolic disorders.

In our present study, in order to study the impact of excessive activation of MR in the progression of MetS-associated heart failure and OA, the appropriate animal model should develop hyperaldosteronism, heart failure and MetS components, including obesity, dyslipidemia, insulin resistance and diabetes . In this context, the SHHF (Spontaneously Hypertensive Heart Failure) rat model meets well our need and objective.

SHHF rat model

SHHF rats were described for the first time in 1990 and the strain was obtained from the backcross between SHR/N-cp obese and SHR/N rats. The $SHHF^{cp/cp}$ rats exhibit MetS that is related to the presence of a homozygous mutation known as ‘cp’ (corpulent) in the leptin receptor gene which have appeared spontaneously in the SHR/N-cp strain. This mutation introduces a stop codon when translating the leptin receptor protein and results in the production of a non-functional truncated protein whose transmembrane and intracellular parts do not exist (**Figure 23**).

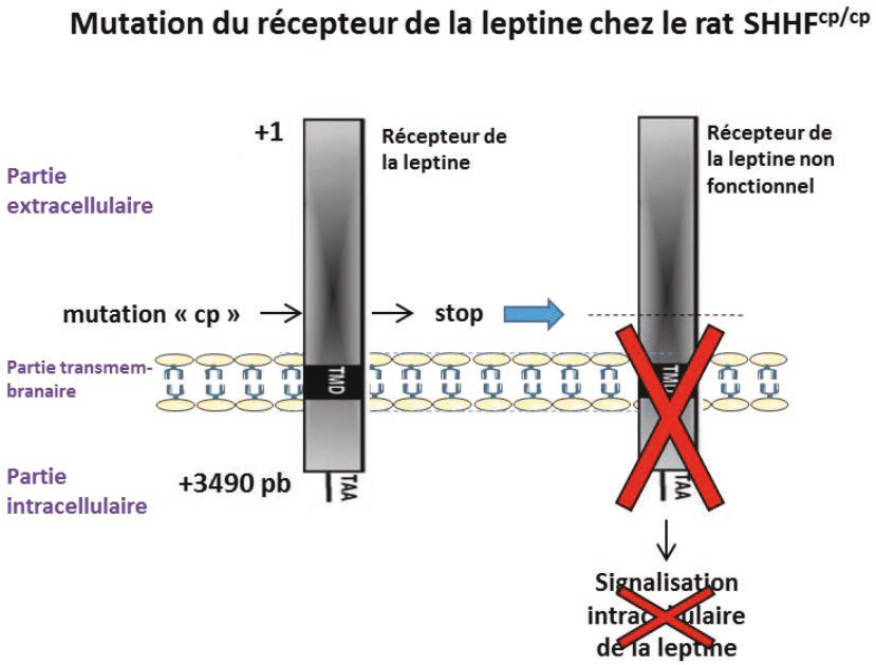

Figure 23 Schematic representation for the mutation of leptin receptor in SHHF$^{cp/cp}$ rat.
(Adapted from PhD thesis of Youcef G with permission.)

The SHHF$^{cp/cp}$ rats develop congestive heart failure, hypertension, obesity, insulin resistance, hyperinsulinemia, insulino resistance, hypertriglyceridemia, and hypercholesterolemia (Youcef et al., 2014). Thus, the SHHF rat model mimics the same pathophysiology of human MetS and heart failure.

In addition, the SHHF$^{cp/cp}$ obese rats also exhibit hyperaldosteronism compared with SHHF$^{+/+}$ lean rats, providing the possibilty to investigate the disease contributing effect of MR activation and the potential therapeutic effect of MRA in this MetS model.

Contexte et Hypothèse

De plus en plus d'études épidémiologiques et cliniques suggèrent que le syndrome métabolique (SMet) joue un rôle sur l'incidence et la progression de l'arthrose. Il n'existe cependant pas à l'heure actuelle de modèle expérimental d'arthrose associée au SMet qui permettrait d'étudier la contribution de ce syndrome dans l'initiation et/ou la progression de l'arthrose et d'autre part de determiner des outils pharmacologique capables de moduler le SMet et entrainer le développement de l'arthrose.

En l'absence d'un modèle expérimental d'arthrose associée au Smet satisfaisant, la contribution du SMet aux modifications du phénotype articulaire dans l'arthrose reste difficile à explorer.

Le modèle de rat SHHF est d'un grand intérêt pour notre étude car ces animaux développent une hypertension associée à l'obésité, une dyslipidémie et une résistance à l'insuline, et manifestent donc les caractéristiques du SMet.

De manière intéressante, le traitement chronique de ces rats par l'éplérénone, améliore les paramètres métaboliques et les protège des complications cardiovasculaires associées (***Voir le papier N°3***).

Notre étude présentée dans le papier N°4 avait donc un double objectif: le premier était d'examiner le rôle du SMet dans l'apparition d'atteints articulaires et le second était d'évaluer le bénéfice thérapeutique sur l'articulation d'une modulation du SMet par un traitement chronique de l'éplérénone (***Voir le papier N°4: MRA treatment alleviates MetS-associated OA***).

Article No.3: SHHF rats-a good model of MetS

Published in British Journal of Pharmacology on 2016

Preventive and chronic mineralocorticoid receptor antagonism is highly beneficial in obese SHHF rats

Youcef G[1,3], Olivier A[1], Nicot N[3], Muller A[3], **Deng C[2]**, Labat C[1], Fay R[4], Rodriguez-Guéant RM[5], Leroy C[1,4], Jaisser F[4], Zannad F[1,4], Lacolley P[1], Vallar L[4], Pizard A[1,4,*]

1. UMRS-Inserm U1116, Université de Lorraine, Vandoeuvre-les-Nancy, France
2. UMR7365 CNRS-Université de Lorraine, IMoPA, Vandoeuvre-les-Nancy, France
3. Genomics Research Unit, Luxembourg Institute of Health, Luxembourg
4. CIC 1433 Inserm, Pierre Drouin, Nancy, France
5. U954 Inserm, Nancy, France

***Corresponding author**

British Journal of Pharmacology

British Journal of Pharmacology (2016) **173** 1805–1819 1805

RESEARCH PAPER

Preventive and chronic mineralocorticoid receptor antagonism is highly beneficial in obese SHHF rats

Correspondence Anne Pizard, Inserm U1116, CHRU Nancy, rue du Morvan, Vandoeuvre-lès-Nancy 54500 France. E-mail: anne.pizard@inserm.fr

Received 10 December 2015; **Revised** 17 February 2016; **Accepted** 23 February 2016

G Youcef[1,2,3,4], A Olivier[1,2,3,5], N Nicot[4], A Muller[4], C Deng[2,3,6], C Labat[1,2,3], R Fay[5,7], R-M Rodriguez-Guéant[2,3,5,8], C Leroy[1,7], F Jaisser[5,7], F Zannad[1,2,3,5,7], P Lacolley[1,2,3,5], L Vallar[4] and A Pizard[1,2,3,5,7]

[1]UMRS U1116 Inserm, Nancy, France, [2]Fédération de Recherche 3209, Nancy, France, [3]Université de Lorraine, Nancy, France, [4]Genomics Research Unit, Luxembourg Institute of Health, Luxembourg, [5]CHU Nancy, Nancy, France, [6]UMR 7365 CNRS, Nancy, France, [7]CIC 1433 Inserm, Pierre Drouin, Nancy, France, and [8]U954 Inserm, Nancy, France

BACKGROUND AND PURPOSE

Mineralocorticoid receptor (MR) activation contributes to heart failure (HF) progression. Its overactivity in obesity is thought to accelerate cardiac remodelling and HF development. Given that MR antagonists (MRA) are beneficial in chronic HF patients, we hypothesized that early MRA treatment may target obesity-related disorders and consequently delay the development of HF.

EXPERIMENTAL APPROACH

Twenty spontaneously hypertensive HF dyslipidaemic obese SHHF$^{cp/cp}$ rats and 18 non-dyslipidaemic lean SHHF$^{+/+}$ controls underwent regular monitoring for their metabolic and cardiovascular phenotypes with or without MRA treatment [eplerenone (eple), 100 mg · kg^{-1} · day^{-1}] from 1.5 to 12.5 months of age.

KEY RESULTS

Eleven months of eple treatment in obese rats (SHHF$^{cp/cp}$eple) reduced the obesity-related metabolic disorders observed in untreated SHHF$^{cp/cp}$ rats by reducing weight gain, triglycerides and total cholesterol levels and by preserving adiponectinaemia. The MRA treatment predominantly preserved diastolic and systolic functions in obese rats by alleviating the eccentric cardiac hypertrophy observed in untreated SHHF$^{cp/cp}$ animals and preserving ejection fraction (70 ± 1 vs. 59 ± 1%). The MRA also improved survival independently of these pressure effects.

CONCLUSION AND IMPLICATIONS

Early chronic eple treatment resulted in a delay in cardiac remodelling and HF onset in both SHHF$^{+/+}$ and SHHF$^{cp/cp}$ rats, whereas SHHF$^{cp/cp}$ rats further benefited from the MRA treatment through a reduction in their obesity and dyslipidaemia. These findings suggest that preventive MRA therapy may provide greater benefits in obese patients with additional risk factors of developing cardiovascular complications.

Abbreviations

aldo, aldosterone; BMI, body mass index; BNP, brain natriuretic peptide; ^{cp}, mutant ^{cp} allele of the leptin receptor; CSAA, cross-sectional adipocyte area; EDT, E wave deceleration time; EDV, end-diastolic volume; EF, ejection fraction; Einc, elastic incremental modulus; eple, eplerenone; ESV, end-systolic volume; Fn1, fibronectin 1; HDL, high-density lipoproteins; HF, heart failure; HW, heart weight; IR, insulin resistance; IVRT, isovolumetric relaxation time; LDL, low-density lipoproteins; Lepr, leptin receptor; LV, left ventricle; LVID, Left ventricle internal diameter; MR, mineralocorticoid receptor; MRA, mineralocorticoid receptor antagonist; Nox4, NADPH oxidase 4; PWT, posterior wall thickness; RAAS, renin–-angiotensin–aldosterone system; SHHF, spontaneously hypertensive heart failure; SWT, septum wall thickness; TG, triglycerides; TL, tibia length; VAT, visceral adipose tissue; Vim, vimentin

DOI:10.1111/bph.13479

Tables of Links

TARGETS
Nuclear hormone receptors[a]
Mineralocorticoid receptor (MR; NR3C2)
Catalytic receptors[b]
Leptin receptor

LIGANDS	
Adiponectin	Fibronectin
Aldosterone	Insulin
BNP	TGFβ2
COL3A1	TGFβ3
Corticosterone	

These Tables list key protein targets and ligands in this article which are hyperlinked to corresponding entries in http://www.guidetopharmacology.org, the common portal for data from the IUPHAR/BPS Guide to PHARMACOLOGY (Pawson *et al.*, 2014) and are permanently archived in the Concise Guide to PHARMACOLOGY 2015/16 ([a,b]Alexander *et al.*, 2015a,b).

Introduction

Over 23 million patients are diagnosed with heart failure (HF) worldwide (McMurray *et al.*, 1998) among whom 32 to 49% are obese (body mass index, BMI $\geq$ 30 kg·m^{-2}) and 31 to 40% are overweight (25 $\leq$ BMI $<$ 30 kg·m^{-2}) (Clark *et al.*, 2014). Obesity, along with the ageing of the population and the increased prevalence of various underlying pathophysiological mechanisms, also referred to as HF modifier conditions (van Deursen *et al.*, 2014), are known to precipitate individuals towards fully developed HF phenotypes.

Adverse adaptive mechanisms such as overactivation of the renin–angiotensin–aldosterone system (RAAS) are recognized to contribute to HF. Extensive study of the RAAS has resulted in the development of several pharmacological strategies aimed at inhibiting its unbalanced signalling pathways in HF. Accordingly, the addition of mineralocorticoid receptor (MR) antagonists (MRA) to standard treatments has been proven to alleviate HF symptoms and clearly reduce mortality in HF patients (Greenberg *et al.*, 2006; Iraqi *et al.*, 2009). Although initially believed to mainly regulate body fluid volumes via its interaction with the renal MR, extrarenal pathophysiological effects of its ligands, namely, aldosterone and corticosterone, have been substantiated by the finding that MRs are expressed in the myocardium of the failing heart and in non-epithelial target tissues such as adipose tissue (Caprio *et al.*, 2007; Zennaro *et al.*, 2009; Caprio *et al.*, 2011; Marzolla *et al.*, 2012. Excessive MR activation and increased aldosterone concentration have been implicated in the development of co-morbidities that are highly prevalent in HF patients. Whether alone (obesity, insulin resistance, diabetes and hypertension) or in combination (metabolic syndrome, MetS), they participate in a rapid deterioration of myocardial structure (remodelling) and function. Because increased aldosterone concentrations have also been reported in MetS, increased MR stimulation is thought to accelerate the pathophysiological conditions that lead to the development of HF (De Keulenaer and Brutsaert, 2011). Thus, when endeavouring to prevent or delay the development of HF, abnormal MR activity in non-cardiac co-morbidities appears as a potentially valuable target for new personalized therapeutic strategies. Although it is clear that obesity is an important risk factor for HF development, data remain relatively scarce regarding the contribution of MRAs in the prevention of the development of HF in obese patients. Given the proven role of MR activation in adipogenesis (Guo *et al.*, 2008; Feraco *et al.*, 2013), we hypothesized that early MRA treatment with eple, one of the most selective MRAs to date, may delay or attenuate the adverse cardiac remodelling and subsequently prevent HF progression especially in obese rats.

Our previous characterization of spontaneously hypertensive heart failure obese rats (SHHF$^{cp/cp}$, homozygous for the defective mutant ^{cp} allele of the leptin receptor gene Lepr) (Youcef *et al.*, 2014) demonstrated that the onset of metabolic disorders (dyslipidaemia, overweight and insulin resistance) as well as pre-hypertension occurred within the first 3 months of the life of these animals. These alterations appeared in the absence of any sign of cardiac dysfunction but nonetheless contributed to the earlier onset of HF in SHHF$^{cp/cp}$ rats as compared with their lean controls SHHF$^{+/+}$. Considering that SHHF$^{cp/cp}$ rats also develop an exacerbated hyperaldosteronism compared with SHHF$^{+/+}$ rats, the present study investigated whether early antagonism of the MR could sustainably improve the cardiovascular function of ageing SHHF rats and whether the effects of this treatment were modulated by the presence of metabolic alterations in SHHF$^{cp/cp}$ rats. To this end, SHHF rats were treated for 11 months (initiated at 1.5 months of age) with either the MRA eple as a mono-therapy or its placebo. Our conclusions with regard to the beneficial effects of chronic MRA are strengthened by the results observed with this treatment of both dyslipidaemic obese SHHF$^{cp/cp}$ rats and their non-dyslipidemic lean SHHF$^{+/+}$ controls.

Methods

Animal model

Animal studies are reported in compliance with the ARRIVE guidelines (Kilkenny *et al.*, 2010; McGrath and Lilley, 2015). One-month-old SHHF male rat littermates (SHHF/MccGmiCrl-Lepr^{cp}, Charles River Laboratories, USA) were genotyped (Ishizuka *et al.*, 1998) to determine their homozygocity for the wild-type '+' allele or the mutant 'cp' allele that encodes a defective leptin receptor, thus identifying the animals as the SHHF$^{+/+}$ or SHHF$^{cp/cp}$ genotype respectively. The experimental protocols were carried out in our laboratory after a 2-week acclimatization period within the animal care facility where rats were allowed *ad libitum* access

to fluid and food (Purina Formulab chow 5008, Charles River, USA). This protocol was designed according to the ARRIVE guidelines (http://onlinelibrary.wiley.com/doi/10.1111/j.1476-5381.2010.00872.x/pdf). It was approved by the 'Comité d'Éthique Lorrain en Matière d'Expérimentation Animale' (CELMEA) under agreement no. 0.1886 and was performed in an authorized animal facility (agreement no. C 54–547-17). This agreement defined appropriate end-points, which limited the amount of pain an animal suffered during the development of the HF phenotype; end points (survival study) were set as being lack of mobility of the animal and the development of congestion. Changes in the behaviour of the animals were assessed daily and supported by their regular phenotyping. Animals with the most noticeable phenotype were intensely monitored but none of them needed to be killed.

Study design

The effect of MR activation during the development of obesity and related disorders was evaluated for its involvement in the transition towards HF. Animals of both genotypes ($SHHF^{cp/cp}$ and $SHHF^{+/+}$) were given the selective MRA eple (pure active molecule provided by *Pfizer*) from 1.5 months onwards (Figure 1A). This time point corresponds to the onset of metabolic disorders (dyslipidaemia, insulin resistance and overweight) and the pre-hypertensive stage in the absence of any apparent signs of cardiac dysfunction to date (Youcef *et al.*, 2014). Eple treatment was provided in drinking water at a final concentration of 100 $mg \cdot kg^{-1} \cdot day^{-1}$. The choice of this dosage was based on data from several reports (Lacolley *et al.*, 2002; Bayorh *et al.*, 2006; Rigsby *et al.*, 2007; Susic *et al.*, 2007; Baldo *et al.*, 2011; Fraccarollo *et al.*, 2011; Miana *et al.*, 2011; Watson *et al.*, 2013). Although much higher than that prescribed to patients with HF, the MRA concentration used herein is justified by the differences in drug metabolism and efficacy of the compounds between rats and humans. In order to minimize the effects of subjective bias when assessing results, each experimenter was blinded to the assignment of animals to the different treatment groups especially for echocardiography and haemodynamic evaluations.

In order to facilitate the description of the various experimental groups, the following nomenclature is used throughout the paper: the time (expressed in months) at which the observations/assays were performed is indicated as a number in front of the SHHF strain (for example, $^{1.5}SHHF$ refers to observations made at 1.5 months of age); the genotype is indicated by a sign after SHHF (as $SHHF^{+/+}$ or $SHHF^{cp/cp}$), while the treatment status with eple is indicated with the suffix 'eple'. The absence of eple indicates that these rats are part of a control placebo group.

Ten $SHHF^{cp/cp}$ and 10 $SHHF^{+/+}$ rats were allocated to the $^{1.5}SHHF$ group. From 1.5 to 12.5 months of age, the regular monitoring of the metabolic and cardiovascular parameters of the four experimental groups ($SHHF^{+/+}$eple, n = 8; $SHHF^{cp/cp}$eple, n = 11; $SHHF^{+/+}$, n = 10 and $SHHF^{cp/cp}$, n = 8) allowed the comparison of their respective phenotypes at different time points up to 11 months of follow-up (Figure 1a).

Echocardiography

Transthoracic echocardiographies were performed at 1.5, 3, 6, 9.5, 11.5 and 12.5 months of age on anesthetized rats (isoflurane, 5% at induction and 3% for maintenance, in 1.5 $L \cdot min^{-1}$ O_2) using a 12 MHz transducer (Sonos 5500 Ultrasound System, Philips) (Youcef *et al.*, 2014). Animals were positioned in left decubitus to acquire a short axis view of the left ventricle (LV) and an apical four-chamber view.

Morphological parameters of the LV were assessed using the two-dimensional (2D) M mode: LV internal diameter at the end diastole (LVIDd), at the end systole (LVIDs), posterior wall and septum thicknesses (PWT and SWT, respectively) were recorded to enable the calculation of LV mass according to the following equation, $LVmass = 1.04*[(PWT + SWT + LVIDd)^3 - (LVIDs)^3]$, where 1.04 is the estimated specific gravity of the myocardium.

LV systolic function was assessed by (i) 2D M mode to calculate the ejection fraction (EF) as follows: $EF\ (\%) = [(EDV - ESV)/EDV \times 100]$, where EDV and ESV correspond to the end-diastolic and end-systolic volumes respectively, and (ii) offline

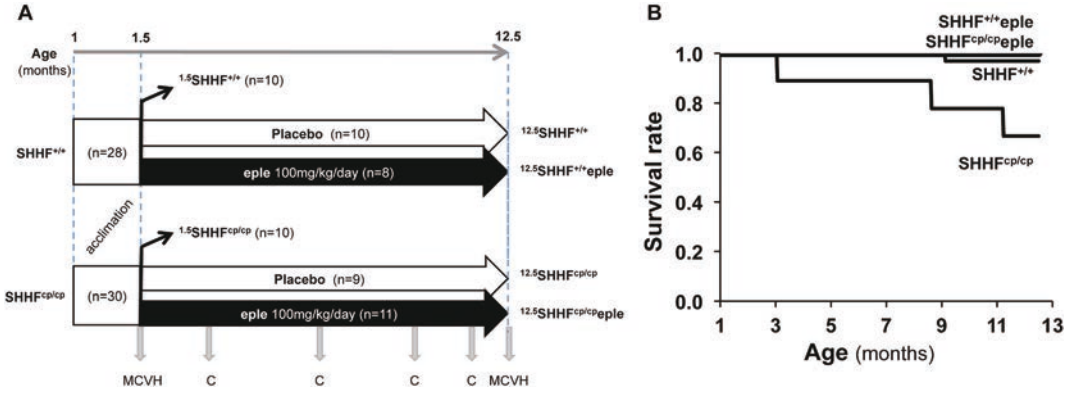

Figure 1

Study design and survival rate. (A) Thirty $SHHF^{cp/cp}$ and 28 $SHHF^{+/+}$rats were randomized either to the $^{1.5}SHHF$ group (1.5-month follow-up, n = 10 per genotype) or to the long-term follow-up group to receive either the selective MRA eplerenone (eple 100 $mg \cdot kg^{-1} \cdot day^{-1}$) ($^{12.5}SHHF^{+/+}$eple, n = 8 and $^{12.5}SHHF^{cp/cp}$eple, n = 11) or placebo ($^{12.5}SHHF^{+/+}$, n = 10 and $^{12.5}SHHF^{cp/cp}$, n = 9). Animals underwent metabolic (M), cardiac (C), vascular (V) and histological (H) phenotyping at the beginning and at the end of the study. Cardiac parameters were regularly monitored from 1.5 to 12.5 months of age. (B) Kaplan–Meier curves indicating the survival rate for each studied group.

tissue Doppler imaging at the lateral and septal mitral annulus in the apical four-chamber view which assesses longitudinal LV function and measures Sa wave velocity.

LV diastolic function and LV filling pressures were assessed by pulse wave Doppler performed on the apical four-chamber view. This allowed the measurement and calculation of the ratio of the early (E) to late (A) ventricular filing waves, the isovolumetric relaxation time (IVRT), the E wave deceleration time (EDT), while the e′ mitral wave by tissue Doppler imaging allowed the evaluation of diastolic function of the myocardium. The LV filling pressures were determined by the E/e′ ratio. All echocardiographic examinations were based on the calculation of the mean of three consecutive cardiac cycles and were performed by a single experienced sonographer. The group sizes varied along the follow-up due to loss of animals in untreated groups and to the restricted access to the echocardiographic transducer.

Fasting glycaemia, blood biochemical and hormonal assays

Blood samples were drawn from the carotid artery of killed 16 h-fasted animals. Sera were obtained after a 20-min incubation period at room temperature and centrifugation at 1000x *g* for 15 min. Serum lipid profiles [total cholesterol, triglycerides (TG), high-density and low-density lipoproteins (HDL and LDL respectively) and free fatty acids] were assessed by an automatic biochemistry analyser using enzymatic methods. Sodium and potassium (Na^+, K^+) were measured by a standardized indirect potentiometry technique. Adiponectin and insulin levels were determined by ELISA (adiponectin Rat ELISA kit #ab108784 and insulin Human ELISA kit, #ab100578, respectively).

Insulin resistance (IR) was estimated by the HOMA-IR index:

$$\text{HOMA-IR} = [\text{fasting plasma glucose } (\text{mmol}\cdot\text{L}^{-1}) \times \text{fasting plasma insulin } (\mu\text{IU}\cdot\text{mL}^{-1})]/22.5.$$

Plasma samples were obtained by adding sodium citrate anticoagulant to a subset of the blood samples immediately followed by centrifugation at 1700x *g* for 10 min and subsequent retrieval of the supernatant. Circulating levels of brain natriuretic peptide (BNP) were measured by ELISA (BNP 45 Rat ELISA Kit #ab108816). Aldosterone and corticosterone levels were measured on 24-h urine samples with commercial kits according to the manufacturer's recommendations (Siemens 06615154 Coat-A-Count RIA Aldosterone Kit and AssayMax Corticosterone ELISA Kit, Assaypro, St. Charles, MO, USA, respectively). Fasting glycaemia was measured on a drop of venous blood from conscious rats using a glucometer (Freestyle Papillon Easy, Abbott).

Total RNA isolation and RT qPCR assays

Total RNAs were isolated from a transverse section of the myocardium including portions of both ventricles (RNA Now, Ozyme) and their purity and integrity verified by spectrophotometry and capillary electrophoresis (NanoDrop® ND-1000 spectrophotometer and Agilent 2100 Bioanalyzer with RNA 6000 Nano assay kit respectively). Only RNAs with no sign of high levels of DNA contamination or marked degradation (RNA Integrity Number > 8) were considered of good quality and used for further analysis.

Briefly, reverse transcriptions (RT) of 400 ng of total RNA into cDNA were performed using the Qiagen RT^2 First Strand Kit according to the manufacturer's protocol. Real-time quantitative PCR (qPCR) was subsequently performed with Qiagen Custom RT^2 Profiler PCR Arrays on 2.27 ng of cDNA per well using Qiagen RT^2 SYBR Green Mastermixes. Triplicate assays were run for each gene of interest [fibronectin 1 (fn1; vimentin (vim); tissue growth factor 2, tgb2; tissue growth factor 3 (tgb3); collagen 3a1 (col3a1); NADPH oxidase 4 (Nox4)] in the ViiA7 PCR system (Life Technologies) using the default settings. Comparative threshold cycles (C_T) data were used to calculate relative gene expression values, by applying the RT^2 Profiler PCR Array Data Analysis software v3.5, available online at http://pcrdataanalysis.sabiosciences.com/pcr/arrayanalysis.php. C_T for Sdha, Actb and B2m genes, considered as housekeeping genes, were used for qPCR data normalization. Fold changes in the gene expressions studied (Qiagen reference upon request) were calculated as $2^{(-\Delta CT)}$. Results are expressed as the ratio of $2^{(-\Delta CTSHHFeple)}/2^{(-\Delta CTSHHF)}$ for each transcript in each genotype studied. The *P*-values were calculated using Student,*s t*-test.

Histology

Immediately after the animals had been killed, $^{12.5}$SHHF right carotid, heart and perirenal visceral adipose tissue (VAT) were rapidly dissected, rinsed in saline solution (NaCl 0.9%) and formalin fixed for further histological analysis. Perirenal location was preferred over other locations because it was always present even in the $^{12.5}$SHHF$^{+/+}$ rats where very few small VAT pads developed. Serial 5-μm sections of paraffin embedded tissues were prepared for heart and carotid while 10-μm sections were prepared for VAT. Carotids were stained using the Weigert's orcein-fuchsin method to determine the medial cross-sectional area by manually delineating the carotid edges of several serial carotid slides for each rat using the NIS-element software (Nikon). Hearts and perirenal VAT were stained with Sirius red to determine the degree of myocardial fibrosis and distribution of cross-sectional adipocyte area (CSAA) respectively using ImageJ software. Myocardial fibrotic area was analysed by measuring the % of fibrotic area (demonstrated as magenta staining) of whole heart sections. CSAA was measured for each adipocyte representing the VAT sections from each rat.

Statistical analysis

The data and statistical analysis comply with the recommendations on experimental design and analysis in pharmacology (Curtis *et al.*, 2015). However, some limitations apply: randomization was not used for *in vivo* experiments as the littermate status (genetic link) of the purchased rats was not known, and the group sizes varied in the follow-up due to the restricted access to the echocardiographic transducer and biochemistry laboratory.

All analyses were performed using SAS R9.3 software (SAS Institute, Cary, NC, USA). The overall two-tailed significance level was set at $P < 0.05$. Two-way ANOVA with genotype (SHHF$^{+/+}$ vs. SHHF$^{cp/cp}$) and treatment (placebo vs. eple) along with their interaction as fixed effects were performed, followed by four *post hoc* pairwise comparisons of interest

(when the overall probability of the model was significant) effect of treatment according to genotype (placebo vs. eple for each genotype) and effect of genotype according to treatment ($SHHF^{+/+}$ vs. $SHHF^{cp/cp}$ in each treatment group). The significance level for comparisons was adjusted for multiplicity in order to preserve the overall 5% error rate using the formula $\alpha' = 1 - (1 - \alpha)^{1/k}$, where α and α′ are the overall and adjusted significance levels respectively, and k is the number of comparisons (four comparisons; $^*P < 0.05$). Results are presented for each parameter and each time point as global results (sample size, *P*-values of the model and the fixed effects), adjusted means and SEM (mean values adjusted for the effect of other factors) and the four pairwise comparisons of interest for which the significance level has to be set to $P < 0.0127$ in order to preserve the overall 5% α error rate. Of note, pairwise comparison results were only considered in the cases of significant interaction ($P < 0.05$).

Statistical analysis of the CSAA measured in adipose tissue sections was performed using a Mann–Whitney test to compare the difference between $^{12.5}SHHF^{cp/cp}$ and $^{12.5}SHHF^{cp/cp}$ eple rats ($^*P < 0.05$). All results are expressed as adjusted means ± SEM.

To evaluate how variations in metabolic parameters may be associated with cardiac phenotypes, a statistical analysis of the raw data obtained from each group of animals were combined and computed in the COExpress software (Nazarov *et al.*, 2013). Pearson's test was conducted to calculate the correlation coefficients (*r*) and a *P*-value <0.05 was considered to identify the significant parameters that may associate together. Correlation coefficients rank from +1 to −1, where +1 means a strict positive correlation and −1 denotes a strict negative correlation.

Results

The present study design allowed the evaluation of the preventive effects of long-term eple treatment observed in the presence of metabolic disorders in obese $SHHF^{cp/cp}$ rats and to compare these effects with those observed in lean $SHHF^{+/+}$ rats (Figure 1A). Preventive effects were expected given that eple treatment was started before any cardiac symptoms were observed (1.5 months of age) in control lean $SHHF^{+/+}$ rats. The end point of the study (month 12.5) was chosen so as to maintain the number of surviving untreated $SHHF^{cp/cp}$ rats to an appropriate level to allow statistical comparison with the other groups of rats (Figure 1B). The effective delivery of eple was confirmed by the measurement of urinary excretions of aldosterone and corticosterone, which were significantly increased and decreased respectively, upon treatment in both genotypes (Supporting Information Table S1).

Haemodynamic and vascular parameters are not affected by eplerenone monotherapy

Mean blood pressure and pulse pressure calculations were based on the invasive measurement of central blood pressures (diastolic blood pressure and systolic blood pressure) of anaesthetized $^{12.5}SHHFeple$ and their genotype-matched untreated controls. The results demonstrated the presence of severe hypertension whose severity was independent of both genotype and of MRA treatment (Supporting Information Table S2). The distensibility-pressure curve as well as analysis of compliance, elastic incremental modulus (Einc) and wall stress values demonstrated that the intrinsic mechanical behaviour of the carotid wall was similar across all groups at 12.5 months of age (Supporting Information Table S2 and Fig. S1A and B). The lack of effect of eple on SBP (systolic blood pressure) was confirmed on conscious animals during plethysmographic evaluation of their peripheral blood pressure (Supporting Information Table S3).

Metabolic disorders accelerate adverse cardiac remodelling in $SHHF^{cp/cp}$ rats compared with $SHHF^{+/+}$ controls

Echocardiographic follow-up between 1.5 and 12.5 months of age revealed that $SHHF^{+/+}$-untreated rats developed LV concentric hypertrophic remodelling as evidenced by the stability of the LVIDd values (Figure 2A) and the diastolic

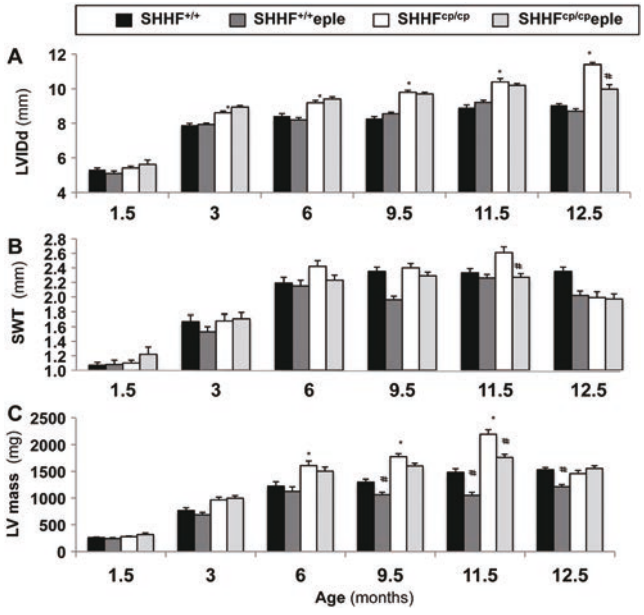

Figure 2

Chronic eple treatment alleviates cardiac remodelling. Cardiac remodelling of $SHHF^{+/+}$ (black), $SHHF^{+/+}$eple (dark grey), $SHHF^{cp/cp}$ (white) and $SHHF^{cp/cp}$eple (light grey) rats was evaluated by echocardiographic follow-up. At 1.5 months of age $n = 9$, $SHHF^{+/+}$ rats were evaluated then $n = 8$ of them at the other time points; $n = 8$ $SHHF^{+/+}$eple were evaluated at each time point; $n = 8$ $SHHF^{cp/cp}$ were evaluated at 1.5, 3 and 6 months, $n = 7$ of them at 9 months and $n = 6$ of them at 11.5 and 12.5 time points. Finally, $n = 10$ $SHHF^{cp/cp}$eple were evaluated from 1.5 to 11. 5 months of age and n = 11 of them at 12.5 months allowing the determination of (A) left ventricular internal diameter at end diastole (LVIDd), (B) septum wall thickness (SWT) and (C) calculation of left ventricular mass (LV mass). Two-way ANOVA with genotype ($SHHF^{+/+}$ vs. $SHHF^{cp/cp}$) and treatment (placebo vs. eple) was performed, and the significance level was set to $P < 0.0127$. $^*P < 0.0127$ for the comparison between the genotypes at the same age, $\#P < 0.0127$ for the comparison of the untreated and treated animals from the same genotype at the same age.

thickening of the septal wall (SWT) (Figure 2B) resulting in an increased LV mass (Figure 2C).

When compared with the lean rats, SHHF$^{cp/cp}$ animals exhibited worsened phenotypes. Only 60% of untreated SHHF$^{cp/cp}$ rats survived until 12.5 months of age, while 90% of SHHF$^{+/+}$ rats completed the protocol (Figure 1B). This observation was explained in part by sudden cardiac death due to the development of end-stage systolic dysfunction observed with ageing in this genotype. Compared with SHHF$^{+/+}$ rats, $^{11.5}$SHHF$^{cp/cp}$ rats developed LV eccentric remodelling characterized by a decrease in SWT and an increase in both LVIDd and LVmass (Figure 2A–C). In addition, in $^{12.5}$SHHF$^{cp/cp}$ LV dilation was exacerbated (Figure 2A), while SWT (Figure 2B) decreased. LV remodelling was accompanied by a greater interstitial fibrosis in $^{12.5}$SHHF$^{cp/cp}$ rats than in $^{12.5}$SHHF$^{+/+}$ rats (Figure 3A and B).

From 1.5 to 11.5 months of age, SHHF$^{cp/cp}$ rats exhibited a progressive alteration of their diastolic function (increased IVRT and EDT values over time, Figure 4A and B). By 12.5 months, SHHF$^{cp/cp}$ LV remodelling was exacerbated by concomitant functional alterations. $^{12.5}$SHHF$^{cp/cp}$ rats exhibited altered diastolic function and increased filling pressures (reduced IVRT and EDT values, Figure 4A and B) as well as a decline in systolic function (reduced EF values, Figure 4D) compared with $^{12.5}$SHHF$^{+/+}$ rats. The reduction in Sa (marker of an altered longitudinal shortening and lengthening of the myocardium) observed in $^{12.5}$SHHF$^{cp/cp}$ rats further characterized the decline in their systolic function ($^{12.5}$SHHF$^{cp/cp}$ Sa = 2.64 ± 0.10 cm·s^{-1} vs. $^{12.5}$SHHF$^{+/+}$ Sa = 3.41 ± 0.07 cm·s^{-1}; Figure 4C).

The accelerated decline in cardiac function in SHHF$^{cp/cp}$ rats in comparison with SHHF$^{+/+}$ rats arose in part from the early onset of drastic metabolic disorders. Already overweight at 1.5 months of age ($^{1.5}$SHHF$^{cp/cp}$ = 150 ± 4 g vs. $^{1.5}$SHHF$^{+/+}$ = 133 ± 2 g; Figure 5A), $^{1.5}$SHHF$^{cp/cp}$ rats exhibited dyslipidaemia that dramatically and significantly worsened with ageing when compared with SHHF$^{+/+}$ rats (Table 1). While the genotype did not influence fasting glycaemia, $^{12.5}$SHHF$^{cp/cp}$ insulin and adiponectin levels were increased by approximately fourfold and decreased by approximately twofold, respectively, when compared with $^{12.5}$SHHF$^{+/+}$ animals (Table 1). This paralleled the development of massive visceral obesity in SHHF$^{cp/cp}$ rats [body weight (BW), ^{12}SHHF$^{cp/cp}$BW = 787 ± 17 g vs. ^{12}SHHF$^{+/}$

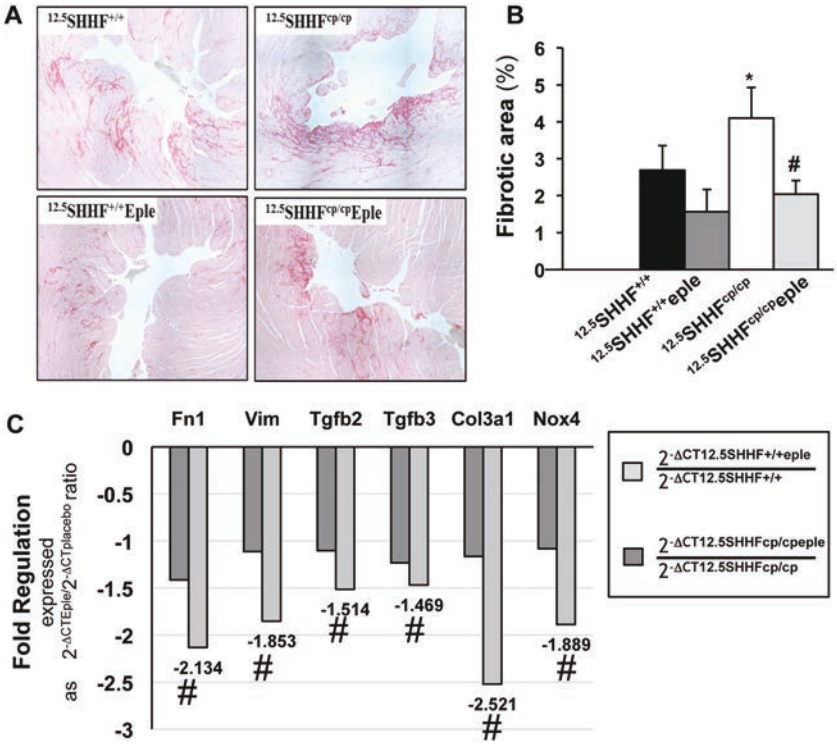

Figure 3

Chronic eple treatment reduces myocardial fibrosis. Myocardial fibrosis and the anti-fibrotic effects of eple were measured at the histological and molecular levels on rat myocardium. (A) Sections of paraffin-embedded hearts obtained from untreated (upper panels) and MRA-treated (lower panels) $^{12.5}$SHHF$^{+/+}$ and $^{12.5}$SHHF$^{cp/cp}$ animals ($^{12.5}$SHHF$^{+/+}$, n = 5; $^{12.5}$SHHF$^{+/+}$eple, n = 6; $^{12.5}$SHHF$^{cp/cp}$, n = 4; $^{12.5}$SHHF$^{cp/cp}$eple, n = 6) were stained with Sirius red enabling the identification of fibrotic areas (evidenced in magenta). (B) Fibrotic areas in each experimental group were quantified using ImageJ software and expressed as percentage of total section area. (C) The impact of eple on mRNA expression levels of genes involved in cardiac fibrosis and remodelling [fibronectin (Fn1), vimentin (Vim), transforming growth factor β2 and β3 (Tgfb2 and Tgfb3), collagen 3 type α 1 (Col3a1) and NADPH oxidase 4 (Nox4)] was assessed in cardiac tissue from $^{12.5}$SHHF$^{+/+}$eple rats compared with $^{12.5}$SHHF$^{+/+}$ rats (light grey, n = 4) and in $^{12.5}$SHHF$^{cp/cp}$eple rats compared with $^{12.5}$SHHF$^{cp/cp}$ rats by RT-qPCR (dark grey, n = 4). Comparative threshold cycles (C_T) for Sdha, Actb and B2m genes, considered as housekeeping genes, were used for qPCR data normalization. Gene fold regulation is expressed as the ratio of ΔCT of the treated group over the ΔCT of the placebo group of the same genotype at 12.5 months of age. #$P < 0.05$ for the comparison of the untreated and treated animals from the same genotype at the same age by Student's t-test.

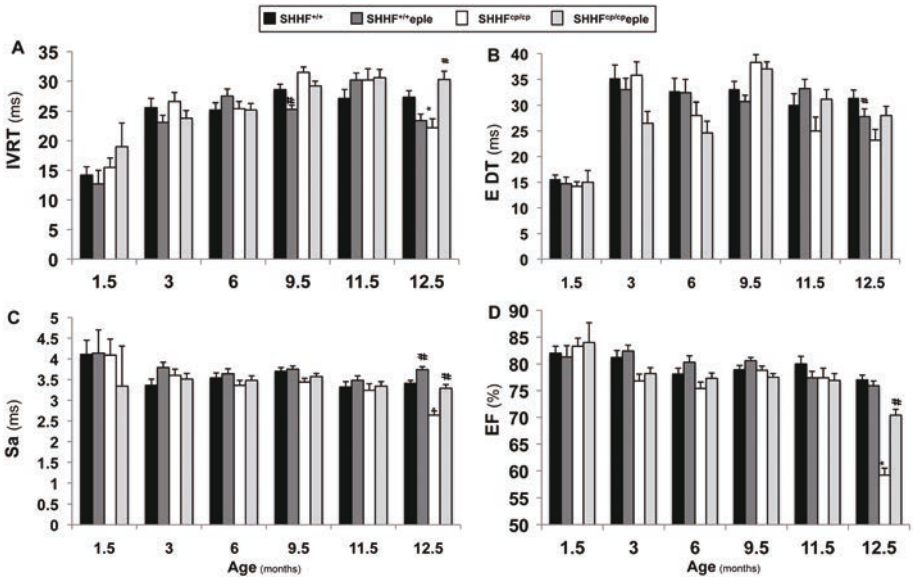

Figure 4

Chronic eple treatment improves SHHF$^{cp/cp}$ cardiac functional parameters. Echocardiographic monitoring of cardiac functional parameters where at 1.5 months of age $n = 9$ SHHF$^{+/+}$ rats were evaluated then $n = 8$ of them at the other time points; $n = 8$ SHHF$^{+/+}$eple were evaluated at each time point; $n = 8$ SHHF$^{cp/cp}$ were evaluated at 1.5, 3 and 6 months, $n = 7$ of them at 9 months and $n = 6$ of them at 11.5 and 12.5 time points. Finally, $n = 10$ SHHF$^{cp/cp}$eple were evaluated from 1.5 to 11. 5 months of age and $n = 11$ of them at 12.5 months. (A) Isovolumic relaxation time (IVRT), (B) E wave deceleration time (EDT), (C) Sa duration (Sa) and (D) ejection fraction (EF). Two-way ANOVA with genotype (SHHF$^{+/+}$ vs. SHHF$^{cp/cp}$) and treatment (placebo vs. eple) was performed, and the significance level was set to $P < 0.0127$. *$P < 0.0127$ for the comparison between the genotypes at the same age, #$P < 0.0127$ for the comparison of the untreated and treated animals from the same genotype at the same age.

$^{+}$BW = 456 ± 14 g] (Figure 5A). Characterization of $^{12.5}$SHHF$^{cp/cp}$ perirenal adipocyte size (mean cross-sectional area) and distribution (median) (inserts within Figure 5B panels) revealed significantly larger adipocyte size and broader distribution than that observed in $^{12.5}$SHHF$^{+/+}$ rats (Figure 5B left panels).

Altogether, the above results indicate that the presence of metabolic disorders in SHHF$^{cp/cp}$ rats are associated with adverse cardiac remodelling in these obese rats as compared with lean SHHF$^{+/+}$ rats, resulting in an impairment of $^{12.5}$SHHF$^{cp/cp}$ diastolic and systolic functions.

Preventive chronic eplerenone monotherapy mainly preserves SHHF$^{cp/cp}$ myocardial structure and function

Preventive effects of eplerenone in SHHF$^{+/+}$eple rats. Initiation of the 11-month eple treatment at 1.5 months of age in lean SHHF$^{+/+}$ rats had preventive effects on their cardiac phenotypes. Chronic MRA treatment significantly and sustainably reduced the hypertrophic remodelling by preventing SW thickening as early as 9.5 months of age (Figure 2B). Although myocardial fibrosis was detectable in $^{12.5}$SHHF$^{+/+}$ rats (Figure 3A, upper left panel), its quantification (Figure 3B) did not reveal any significant effect of eple treatment. Molecular characterization (Figure 3C) of myocardial fibrosis was also assessed by the relative quantification of several transcripts encoding for structural and extracellular matrix proteins [fibronectin (Fn1), vimentin (Vim), transforming growth factor 2 and 3 (Tgfb2 and Tgfb3 respectively), collagen type 3a1 (Col3a1) and NADPH oxidase 4 (Nox4)]. None of these transcripts exhibited a significant reduction in their expression levels. The assessment of SHHF$^{+/+}$ diastolic (IVRT and EDT) and systolic (Sa and EF) cardiac function also demonstrated fairly stable parameters with ageing, none of which were significantly affected by eple treatment (Figure 4 A–D, black and dark grey columns).

Hence, the prevention of LV concentric remodelling observed in lean SHHF$^{+/+}$eple rats suggests that they modestly but significantly benefited from the early initiation of eple treatment.

Greater benefits of eplerenone treatment in obese SHHF$^{cp/cp}$ rats

Chronic MRA alleviated the cardiac eccentric remodelling of SHHF$^{cp/cp}$eple rats by significantly reducing their LV mass at 11.5 months of age (Figure 2C) and heart weight/tibia length ratio at age 12.5 months ($^{12.5}$SHHF$^{cp/cp}$eple HW/TL = 49.5 ± 1.3 mg·mm^{-1} vs. $^{12.5}$SHHF$^{cp/cp}$ HW/TL = 57 ± 1.7 mg·mm^{-1}). Eple treatment also prevented the LV remodelling of $^{12.5}$SHHF$^{cp/cp}$eple myocardium by limiting its dilation and septal thickening (Figure 2A and B). These structural improvements in $^{12.5}$SHHF$^{cp/cp}$eple LV were accompanied by a significant reduction in myocardial fibrosis, initially evaluated and quantified at the histological level (Figure 3A and B, #$P < 0.05$) and subsequently confirmed at the molecular level using RT-qPCR (Figure 3C). Significant down-regulations of Fn1, Vim, Tgfb2, Tgfb3, Col3a1 and Nox4 were demonstrated upon treatment in the $^{12.5}$SHHF$^{cp/cp}$eple myocardium when compared with their $^{12.5}$SHHF$^{cp/cp}$ untreated controls (Figure 3C).

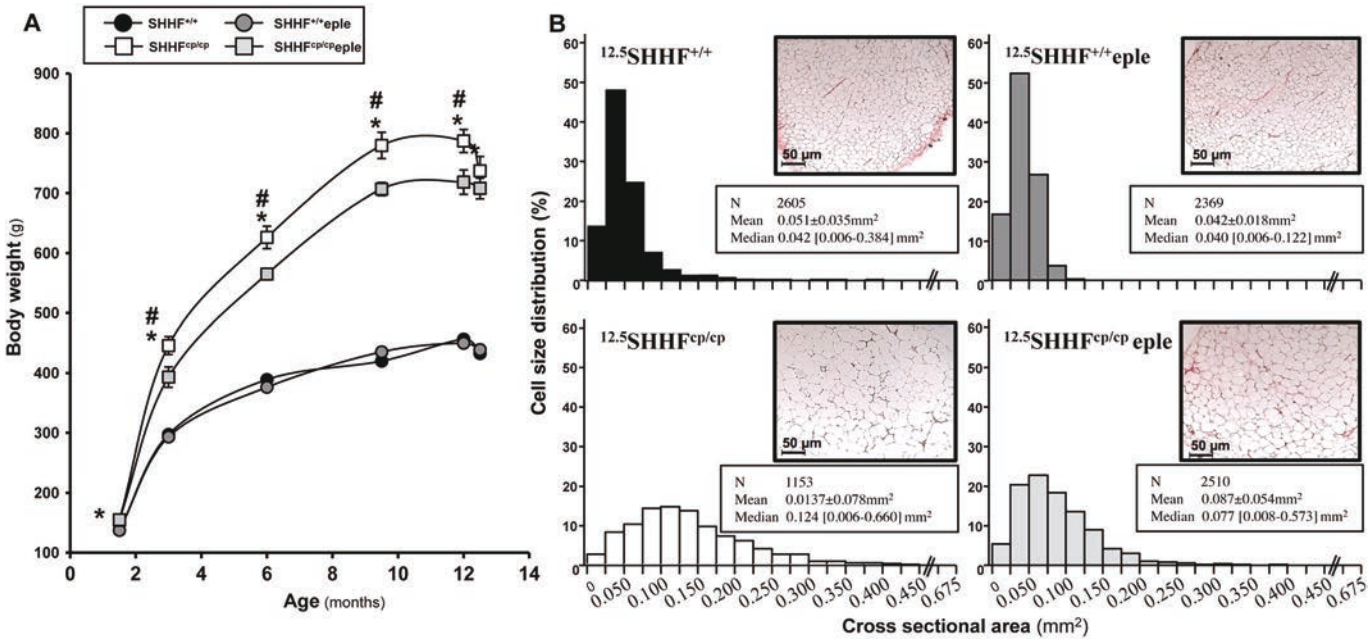

Figure 5

Chronic eple treatment reduces body weight gain and visceral adipocyte hypertrophy. Rats received either MRA (eple, 100 mg·kg^{-1}·day^{-1}) or placebo from the age of 1.5 months up to 12.5 months. (A) Follow-up of animal body weight (BW). At 1.5 months of age $n = 9$, SHHF$^{+/+}$ rats were evaluated then $n = 8$ of them at the other time points; $n = 8$ SHHF$^{+/+}$eple were evaluated at each time point; $n = 8$ SHHF$^{cp/cp}$ were evaluated at 1.5, 3 and 6 months, $n = 7$ of them at 9 months and $n = 6$ of them at 11.5 and 12.5 time points. Finally, $n = 11$ SHHF$^{cp/cp}$eple were evaluated at each time point. *$P < 0.05$ SHHF$^{cp/cp}$ compared with SHHF$^{+/+}$ at the same age; #$P < 0.05$ treated group compared with the untreated group of the same genotype at the same age by Student's *t*-test. (B) Morphological analysis of perirenal VAT dissected at month 12.5. Analysis of VAT sections stained with Sirius red allowing the measurement of the cross-sectional adipocyte area (CSAA, mm^2) and cell size distribution (%) of the adipocyte population from each experimental group (SHHF$^{+/+}$ $n = 5$; SHHF$^{+/+}$eple $n = 4$; SHHF$^{cp/cp}$ $n = 5$; SHHF$^{cp/cp}$ eple $n = 8$).

At 12.5 months of age, chronic eple treatment had no significant effect on myocardial MR transcript expression in either genotype (not shown) but significantly decreased the expression of the Hsd11β1 transcript (encoding for the enzyme converting cortisone into corticosterone) only in $^{12.5}$SHHF$^{cp/cp}$eple rats (Hsd11β1 transcript $2^{-\Delta CT12.5SHHFcp/cpeple}/2^{-\Delta CT12.5SHHFcp/cp} = -1.466$).

At 12.5 months of age, chronic eple treatment had no significant effect on perirenal adipose tissue Hsd11β1 transcript expression in either genotype (not shown). This did not exclude the possible participation of this enzyme to the observed VAT phenotypes at earlier time points than the end of the study, but suggested that the effects on phenotype were mostly as a result of MR antagonism in adipose tissue.

Diastolic function preservation

In HF pathophysiology, the link between structure and function is relatively straightforward in particular for diastolic function, which is adversely affected by LV hypertrophy. In addition to the reduction in cardiac hypertrophy, results relative to cardiac functional parameters (Figure 4A–D) showed that eple prevented the myocardial relaxation impairment already observed in ^{3}SHHF$^{cp/cp}$ rats. At the age of 3 months, diastolic parameters were less altered in the eple group, as demonstrated by a significant increase in EDT upon treatment (^{3}SHHF$^{cp/cp}$eple EDT = 26.5 ± 2.3 ms vs. ^{3}SHHF$^{cp/cp}$ EDT = 35.8 ± 2.6 ms) and a concomitant trend for a smaller E wave velocity ((^{3}SHHF$^{cp/cp}$eple E = 114 mm·s^{-1} vs. ^{3}SHHF$^{cp/cp}$ E = 106 mm·s^{-1}). In the $^{12.5}$SHHF$^{cp/cp}$eple group, treatment also prevented the increase in E/A (not shown) and the decrease in IVRT (Figure 4A).

Systolic function preservation

Eple further improved cardiac systolic function in the $^{12.5}$SHHF$^{cp/cp}$eple group by preventing the drop in Sa wave observed in $^{12.5}$SHHF$^{cp/cp}$ controls ($^{12.5}$SHHF$^{cp/cp}$eple Sa = 3.29 ± 0.09 cm·s^{-1} vs. $^{12.5}$SHHF$^{cp/cp}$ Sa = 2.64 ± 0.10 cm·s^{-1}, $P < 0.0001$) as well as the decrease in EF (Figure 4C and D). Concomitant with the observed alteration in systolic function in obese placebo $^{12.5}$SHHF$^{cp/cp}$ rats, an increase in LV filling pressure was also noted, as shown not only by the decrease in IVRT and EDT (Figure 4A and B) but also by an elevation in E/e′ and E/A ratios, which were prevented by eple treatment (not shown).

Altogether, these results demonstrate that SHHF$^{cp/cp}$eple animals greatly benefited from early eple treatment by reducing the adverse cardiac remodelling observed in their untreated controls. The treatment positively affected both diastolic as well as systolic functions and delayed the onset of HF in the obese rats by preserving the decline in LV function.

Chronic eplerenone further benefits obese SHHF$^{cp/cp}$ rats by greatly improving their metabolic status

While long-term MR antagonism had no effect on SHHF$^{+/+}$eple body weight (BW), eple significantly and sustainably

Table 1

Mineralocorticoid receptor blockade reduces dyslipidemia and preserves adiponectinemia

Experimental group *n*	$^{1.5}SHHF^{+/+}$ *7*	$^{12.5}SHHF^{+/+}$ *10*	$^{12.5}SHHF^{+/+}$eple *8*	$^{1.5}SHHF^{cp/cp}$ *7*	$^{12.5}SHHF^{cp/cp}$ *6*	$^{12.5}SHHF^{cp/cp}$eple *11*	ANOVA Genotype	ANOVA Treatment	ANOVA Interaction
Lipid profile, $g \cdot L^{-1}$	0.69 ± 0.03	0.90 ± 0.25	0.75 ± 0.28	0.93 ± 0.03	4.25 ± 0.33*	2.67 ± 0.24#	<0.05	<0.05	<0.05
Total chol.									
HDL	0.24 ± 0.01	0.25 ± 0.02	0.27 ± 0.02	0.30 ± 0.01	0.56 ± 0.02*	0.50 ± 0.02	<0.05	NS	NS
LDL	0.38 ± 0.03	0.08 ± 0.00	0.08 ± 0.01	0.48 ± 0.03	1.48 ± 0.40*	0.55 ± 0.08#	<0.05	<0.05	<0.05
TG	0.37 ± 0.01	0.61 ± 2.02	0.58 ± 2.26	0.77 ± 0.14	20.5 ± 2.6*	8.26 ± 1.93#	<0.05	<0.05	<0.05
FFA	1.2 ± 0.1	0.4 ± 0.0	0.3 ± 0.1	1.6 ± 0.2	1.0 ± 0.2	1.5 ± 0.3	<0.05	NS	NS
Fasting glycemia, $mmol \cdot L^{-1}$	4.6 ± 0.4	5.7 ± 0.4	6.1 ± 0.4	5.7 ± 0.5	5.4 ± 0.6	6.4 ± 0.4	NS	NS	NS
Fasting insulin, $\mu IU \cdot mL^{-1}$	11 ± 2	12 ± 5	10 ± 5	16 ± 4	52 ± 6*	69 ± 5	<0.05	NS	NS
HOMA-IR index	0.8 ± 0.2	0.9 ± 0.5	0.9 ± 0.5	2.6 ± 0.8	3.6 ± 0.6*	5.4 ± 0.6	<0.05	NS	NS
Ionogram, $mmol \cdot L^{-1}$ Na^+	141 ± 0	143 ± 3	139 ± 3	140 ± 1	146 ± 3	140 ± 2	NS	NS	NS
K^+	4.8 ± 0.2	4.9 ± 0.2	5.2 ± 0.2	4.9 ± 0.1	4.6 ± 0.3	5.0 ± 0.2	NS	NS	NS
Na^+/K^+ ratio	29.9 ± 1.4	30.2 ± 1.9	27.1 ± 2.0	28.9 ± 0.6	33.1 ± 2.3	28.4 ± 1.7	NS	NS	NS
Adiponectin, $\mu g \cdot mL^{-1}$	6.3 ± 0.4	6.3 ± 1.3	7.4 ± 1.2	19.7 ± 1.4	11.9 ± 0.7*	22.7 ± 1.6#	<0.05	<0.05	<0.05
BNP, $pg \cdot mL^{-1}$	135 ± 18	219 ± 25	208 ± 25	102 ± 15	225 ± 29	203 ± 22	NS	NS	NS

HDL, high-density lipoprotein; LDL, low-density lipoprotein; FFA, free fatty acids; TG, triglyceride; Na^+, sodium, K^+, potassium; BNP, brain natriuretic peptide. Values are the mean ± SEM. Two-factor non-parametric ANOVAs analysis with two factors allowed the evaluation of interaction between genotype and treatment at 12.5 months of age. Pairwise comparison for adjusted multiple testing set to $P < 0.0127$ in order to preserve the 5% overall α error rate.

*To compare SHHF cp/cp versus SHHF+/+ at the same time point.

#To compare eple versus placebo for a same genotype; NS, non-significant; *n* represents for the number of samples.

reduced $SHHF^{cp/cp}$eple BW reaching a maximal value at 12-months of age ($^{12}SHHF^{cp/cp}$epleBW = 718 ± 13 g vs. $^{12}SHHF^{cp/cp}$BW = 787 ± 17 g) (Figure 5A). Eple treatment significantly minimized weight gain of $^{12}SHHF^{cp/cp}$-treated rats (563 ± 43 g gained) when compared with $^{12}SHHF^{cp/cp}$-untreated rats (634 ± 27 g gained) and this was achieved without significantly modifying their food and water intake or their 24 h urinary excretion (data not shown). Eple had no impact on the size and distribution of $^{12.5}SHHF^{+/+}$ adipocytes (Figure 5B, upper panels) although chronic MRA treatment resulted in significantly less hypertrophy of $^{12.5}SHHF^{cp/cp}$eple adipocytes than that observed in untreated controls (Figure 5 B, lower panels).

Eple monotherapy partially prevented the respective increases in total cholesterol (−40%), LDL (−65%) and TG (−60%) concentrations as well as the decrease in adiponectin blood concentration observed in $^{12.5}SHHF^{cp/cp}$ controls (Table 1). MRA treatment had no significant effects on either the Na^+/K^+ ratio, excluding any potential toxic effect on salt and water balance due to the long-term use of the MRA (Table 1), or on BNP plasma levels in surviving animals at the end of the study.

Thus, $SHHF^{cp/cp}$eple rats benefited from eple treatment at both the cardiac and metabolic level. Together, these phenotypic improvements participated in a greater survival rate as indicated by the Kaplan–Meier representation where 100% of $SHHF^{cp/cp}$eple rats completed the protocol (Figure 1B).

Correlation of metabolic and cardiac physiological profiles of all experimental groups

The statistical correlations of several metabolic and cardiac physiological parameters of the six experimental groups ($^{1.5}SHHF^{+/+}$; $^{1.5}SHHF^{cp/cp}$; $^{12.5}SHHF^{+/+}$; $^{12.5}SHHF^{+/+}$eple; $^{12.5}SHHF^{cp/cp}$ and $^{12.5}SHHF^{cp/cp}$eple) are presented as a correlogram in Figure 6. This approach allowed a better understanding of the evolution of selected cardiac parameters (vertical columns) using the probability of a significant relationship with metabolic values independently of the age, the genotype and the treatment (horizontal lines). Correlation coefficients (*r*) are systematically ranked between −1 to +1, where −1 value represents a perfect negative correlation between two variables, while + 1 represents a perfect positive correlation. The darker blue and red squares indicate a significant strong positive (from 0.6 to 1) and negative (from −1 to −0.6) correlation, respectively, while squares in light blue and pink denote a significant intermediate correlation (from 0.2 to 0.6 and from −0.6 to −0.2 respectively). The grey squares show the non-significant-matched parameters.

In the present series, regardless of the genotype, the age and the treatment, the high values of the metabolic parameters (Ins, LDL, HDL, Tot Chol and TG serum levels) were systematically and significantly correlated with high heart weight (HW) values and their lower values were statistically correlated with lower HW values. Together, these above-cited parameters exhibit a statistically positive correlation between each other (blue squares). Conversely, Ins, LDL, HDL, total cholesterol and TG serum levels showed a very systematic and significant negative correlation (red squares) with the cardiac ejection fraction (EF), suggesting that when those metabolic parameters rise, the systolic function is depressed.

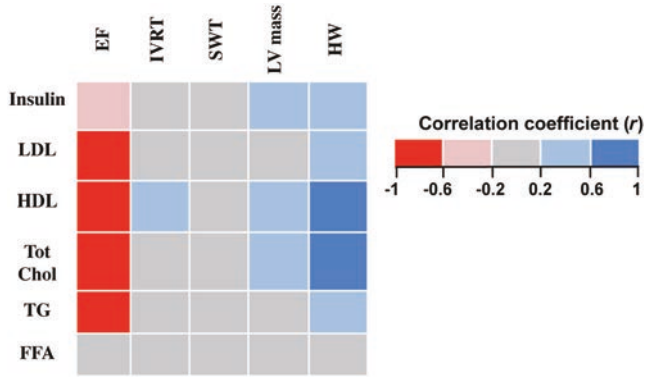

Figure 6

Correlation of metabolic and cardiac physiological profiles of all experimental groups. The CoExpress software was used for calculating correlation coefficients (r) based on Pearson's test between physiological parameters and the corrplot function to elaborate the depicted correlogram. Grey coloured rectangles are poorly correlated and not significant (pVal > 0.05) while the coloured scale bar ranges from red (*r* from −1 to −0.6) to dark blue (*r* from 0.6 to 1) and intermediate values (*ar* from −0.6 to −0.2 in pink and from 0.2 to 0.6 in light blue). Cardiac parameters are represented horizontally with EF denoting ejection fraction; IVRT, isovolumetric relaxation time; SWT, septum wall thickness; LV mass, left ventricle mass; HW, heart weight. Metabolic parameters are represented vertically with LDL, HDL denoting low-density and high-density lipoprotein respectively; Tot Chol, total cholesterol; TG, triglycerides and FFA, free fatty acids.

Discussion and conclusion

The efficacy of eple in preventing the obesity-accelerated progression towards HF was assessed in the present study over a course of the longest treatment duration reported to date in the literature. The design of the present study allowed us to demonstrate long-term sustained effects of eple and their modulation by the presence ($SHHF^{cp/cp}$) or absence ($SHHF^{+/+}$) of metabolic disorders. Using this specific approach, we demonstrated that chronic MR antagonism initiated when young pre-hypertensive SHHF rats are at risk of developing HF but not yet symptomatic was able to sustainably prevent cardiac remodelling in a haemodynamically-independent manner. Incremental benefits were further observed when the preventive treatment was given to pre-hypertensive, overweight and dyslipidaemic $SHHF^{cp/cp}$ rats. Indeed and as suggested by the correlation data, eple had the most striking effects on traits related to obesity by reducing weight gain, adipocyte hypertrophy and dyslipidaemia, all of which contributed to the prevention of cardiac remodelling and alterations in function in $SHHF^{cp/cp}$eple rats. While clinical data are limited regarding the ability of MRA to prevent the risk of developing HF in obese patients, our results strongly suggest that in the context of obesity, the targeted antagonism of MR overactivation appears as a promising therapeutic approach in this setting. Our study provides evidence that will potentially open new avenues for drug repositioning of MRA for the prevention of HF, particularly in high-risk patients presenting obesity-related disorders.

Compared with other studies (Rocha *et al.*, 1998; Bender *et al.*, 2013; Cezar *et al.*, 2013), our data further characterized the anti-fibrotic properties of eple in the context of obesity by

assessing the sustained long-term effects of this MRA. The decrease in Tgfb2 (mostly expressed in epithelial cells) and Tgfb3 (primarily expressed in mesenchymal cells), Col3a1, Fn 1, Nox4 and Vim transcripts upon eple treatment strongly suggests that MR activation is also involved in the deleterious differentiation of cardiac fibroblasts into myofibroblasts. Such differentiation is known to occur during HF development (Cucoranu *et al.*, 2005; Heymans *et al.*, 2015) and during the endothelial-to-mesenchymal transition that is reactivated in the diseased adult heart (Welch-Reardon *et al.*, 2015). The reduced expression of the Nox4 transcript in $^{12.5}$SHHF$^{cp/cp}$eple rats also suggests that the beneficial effect of MRA is partly the result of sustained anti-oxidative stress effects previously reported shortly after the initiation of the treatment (Kuster *et al.*, 2005; Bender *et al.*, 2015).

The eple-induced down-regulation of these transcripts furthermore alleviated the alterations in cardiac diastolic relaxation, LV stiffness, hypertrophy and subsequent dilated remodelling observed in SHHF$^{cp/cp}$eple rats, thus confirming preclinical data obtained when MRA treatment was given for a shorter duration (Rocha *et al.*, 1998; Cezar *et al.*, 2013; Bender *et al.*, 2015). The unique therapeutic opportunity provided by early preventive MRA administration enabled the SHHF$^{cp/cp}$eple rats to be protected from developing diastolic dysfunction as the increase in filling pressures and early impairment of myocardial relaxation were prevented. While the sudden death of the sickest animals in the control SHHF$^{cp/cp}$-untreated group prevented the detection of significant differences in systolic function prior to the last echocardiographic time point, eple treatment nonetheless significantly preserved the systolic function of these SHHF$^{cp/cp}$eple rats. Furthermore, given that the severity of myocardial fibrosis has been associated with long-term mortality in HF patients (Azevedo *et al.*, 2010; Aoki *et al.*, 2011; Fraccarollo *et al.*, 2011), it is likely that myocardial fibrosis caused the lower survival rate observed in untreated animals, while the anti-fibrotic property of eple contributed to the improved survival rate of the SHHF$^{cp/cp}$ eple rats.

Given the pleiotropic activity of the MR, it is likely that the observed beneficial effects may also be related to MR antagonism in other MR target organs in addition to the myocardium and adipose tissues. Because metabolic disorders are well-established risk factors for developing cardiovascular diseases, the authors cannot refute the possibility that the prevention of hepatocellular damage mediated by MRA treatment, demonstrated in non-alcoholic fatty liver disease experimental models by others (Wada *et al.*, 2010, 2013; Pizarro *et al.*, 2015), is also involved in the global improvement of the health of treated rats. Of interest, the efficacy of eple at ameliorating histological steatosis and hepatic fibrosis in mice even allows us to consider the MR as a novel potential therapeutic target for insulin resistance and non-alcoholic liver diseases (Pizarro *et al.*, 2015). Likewise, an improvement in kidney function (Kang *et al.*, 2009; Lian *et al.*, 2012) as well as decreased sympathetic drive and improved baroreflex functions in HF are likely to contribute to the reported beneficial effects of MRA treatment. In addition to this pleiotropic effect of MR, the down-regulation of the Hsd11b1 enzyme in the myocardium upon MRA treatment might also participate in the cardiac phenotype improvement by locally reducing the inflammatory response. Further analyses are required to better comprehend certain discrepancies in the reported metabolic effects of MRA that are difficult to reconcile or inconsistent with previous results reported in the literature, as outlined in Supporting Information Table S4 (Bender *et al.*, 2015; Bostick *et al.*, 2015). Antihypertensive and glucose homeostasis properties of the MRA could have been masked by the complexity of the SHHF strain and/or the 11-month duration of the treatment, highlighting long-term chronic effects rather than an acute response to MRA, as mostly described in the literature. In the SHHF strain, the development of metabolic and hypertensive disorders is genetically determined rather than diet-induced (such as in high-fat/high-fructose and high-salt diets), and several concomitant neuroendocrine alterations (Heyen *et al.*, 2002; Radin *et al.*, 2003; Radin *et al.*, 2008; Przybylski *et al.*, 2010) have been reported in addition to hyperaldosteronism. Moreover, MRAs vary in their effects and some of the differences reported between the effects of spironolactone and eple may result from the fact that eple is devoid of the anti-progesterone, anti-androgenic and anti-glucogenic side effects of spironolactone. Notwithstanding the latter, the eple-induced overall protection reported in the present study is predominantly the result of MR antagonism because eple is only marginally antagonistic to other receptors. The absence of expected insulin-sensitivity properties of the preserved levels of circulating adiponectin could be explained by the fact that one of the adiponectin target organs, the liver, was shown to develop severe non-alcoholic steatosis in the SHHF$^{cp/cp}$ rat (Youcef *et al.*, 2014) that may preclude its favourable response to adiponectin. Of note, such impairments in the benefits of adiponectin have previously been reported in obese experimental models (Hui *et al.*, 2012). Likewise, the absence of BNP regulation upon treatment is likely to be a reflection of the complex relationship between the amount of visceral fat distribution and BNP levels (Clerico *et al.*, 2012).

While the above issues remain to be investigated in the SHHF model and in tissues other than the myocardium and visceral adipocyte pads, eple treatment had conversely striking effects on preventing the development of dyslipidaemia and the decrease in adiponectin concentration in $^{12.5}$SHHF$^{cp/cp}$eple rats, both of which are considered to be good prognostic factors in HF patients. The fact that adiponectin is reported to act directly on cardiomyocytes, alleviating the development of hypertrophy, cardiomyopathy and systolic dysfunction (Goldstein *et al.*, 2009), is also consistent with its participation in the preservation of cardiac function in the present model (Guo *et al.*, 2008; Hirata *et al.*, 2009; Armani *et al.*, 2014).

There is also accumulating evidence suggesting that MR overactivation mediates pathophysiological changes that participate in the development of MetS and the associated decline in cardiovascular function. Clinical reports support the notion that hypertensive and primary hyperaldosteronism patients exhibit more frequent impairment of metabolic signalling, dyslipidaemia and obesity (Manrique *et al.*, 2005; Van Gaal *et al.*, 2006; Sowers, 2007). Corticosterone is an upstream precursor molecule of the mineralocorticoid aldo. Upon eple treatment, the myocardial transcript of the enzyme responsible for its production, Hsd11β1and its urinary levels were decreased. This suggests that eple treatment interrupted the positive feedback loop in which MR activation participates in the up-regulation of Hsd11β1 gene

expression (Nagata *et al.*, 2006). Because aldo is synthesized from an upper precursor, that is, cholesterol, one could also speculate that a similar positive feedback loop is also present between MR activation and regulation of cholesterol levels, which may explain the anti-cholesterol effect of MRA treatment in our experimental model. To the best of our knowledge, the effect of MRA on dyslipidaemia in humans has only been described in the ASCOT clinical trial where MRA treatment reduced hyperlipidaemia (reduction in total and LDL cholesterol levels) in individuals with resistant hypertension (Chapman *et al.*, 2007). This purported MRA effect on dyslipidaemia could potentially benefit from *post hoc* analyses of data collected in large trials evaluating the effect of MRA on HF patients in order to reinforce the data obtained in the small pilot trials by Kosmala *et al.* (2012, 2013). In agreement with *in vitro* as well as the sparse *in vivo* findings, our results indicate that MR activation is involved as a crucial regulator of adipocyte function and hypertrophy (Caprio *et al.*, 2007; Hirata *et al.*, 2009; Wada *et al.*, 2013). More importantly, our findings further demonstrate that the reported reduced adipocyte hypertrophy observed after shorter treatment durations *in vivo* (Caprio *et al.*, 2007; Hirata *et al.*, 2009) was sustained after 11 months and may account in part for the rarely described reduced weight gain previously observed in ^{3}SHHF$^{cp/cp}$eple rats. The fact that the BW of SHHF$^{+/+}$eple rats was not affected by eple treatment indicates that it has very minor effect, if any, on lean body mass.

Obesity and its associated metabolic abnormalities are major risk factors for the development of HF (Rimbaud *et al.*, 2009; Lai *et al.*, 2014). The correlogram of metabolic parameters with the cardiac parameters clearly demonstrate the physiological association between metabolic and cardiac parameters in our experimental model. The increased metabolic values paralleled the increases in cardiac remodelling and diastolic dysfunction (correlation of LV mass and HW with metabolic parameters), while the increased metabolic values paralleled the decrease in systolic function (negative correlation of EF with metabolic parameters). Our results further demonstrated that MRA not only delayed LV remodelling and dysfunction but also improved dyslipidaemia. Together with the improvement in adipocyte hypertrophy in SHHF$^{cp/cp}$ rats, eple was found to have a beneficial effect on lipid homeostasis, which most likely contributed to preserving the quality of cardiac energy sources and the delay in HF development. Eple thus appears to be a promising drug that could prevent ventricular remodelling and cardiac function by preserving cardiac energy metabolism.

Given that late eple administration either rarely (Bender *et al.*, 2015) or mostly fails to reverse cardiac outcomes (Susic *et al.*, 2007; Cezar *et al.*, 2013), the use of eple as a preventive rather than curative drug should be considered and further investigated in HF with preserved EF. Such an early treatment approach was assessed clinically in the treatment of HF with preserved EF using the MRA spironolactone (Pfeffer *et al.*, 2015) but overall only neutral results were obtained. A *post hoc* analysis of the regional variation of this study concluded that the patients from America were the only patients benefiting from spironolactone treatment (Pfeffer *et al.*, 2015). However, the baseline characteristics of these American patients displayed higher body mass index (32.9 vs. 29.4 kg·m^{-2}) and dyslipidaemia (71 vs. 49%) than their Russian/Georgian counterparts. In the present experimental model, SHHF$^{cp/cp}$ and SHHF$^{+/+}$ closely mimicked these patient group differences at baseline, and, likewise, our findings revealed a greater benefit of MRA in the metabolically-affected subgroups of rats.

In summary, the present findings demonstrate that long-term chronic MRA treatment started before the onset of cardiac alterations was beneficial to both lean and obese SHHF rats and contributed in delaying progression to the development of HF symptoms. These latter rats further benefited from the treatment through an improvement in their metabolic parameters. Given the converging evidence of the major role of excessive MR activation as an independent risk factor for metabolic and subsequent cardiovascular disease, our results support the use of MRA as a promising therapeutic strategy for the prevention of cardiac diseases especially in HF patients with altered metabolic parameters.

Acknowledgements

We are thankful to Clément L'Huillier, Arnaud Bianchi and Anne-Laure Leblanc for their expert technical assistance in histology and animal handling. The authors thank Pierre Pothier for the critical reading of the manuscript. This work was funded by Institut National de la Santé et de la Recherche Médicale (Inserm), Région Lorraine, Fondation pour la Recherche Médicale (FRM) comité Lorrain, FP7 FIBRO-TARGETS grant agreement no: 602904. G. Youcef received a salary grant from the Fonds National pour la Recherche (FNR) Luxembourg. We are grateful to Pfizer Inc. (New York, NY) for providing part of the eplerenone.

Author contributions

G.Y., A.O., N.N., A.M., C.D., R.M.R.G., C.L. and A.P. performed the research. A.P., F.Z. and L.V. designed the research study. R.M.R.G., C.L., R.F. and A.M. contributed essential tools. A.P., G.Y., A.O., C.L., R.F., F.Z. and P.L. analysed the data. A.P., G.Y., A.O., F.J., F.Z., P.L. and L.V. wrote the paper.

Conflict of interest

The authors disclose no conflicts of interest.

Declaration of transparency and scientific rigour

This Declaration acknowledges that this paper adheres to the principles for transparent reporting and scientific rigour of preclinical research recommended by funding agencies, publishers and other organizations engaged with supporting research.

References

Alexander SP, Cidlowski JA, Kelly E, Marrion N, Peters JA, Benson HE *et al.* (2015a). The Concise Guide to PHARMACOLOGY 2015/16: Nuclear hormone receptors. Br J Pharmacol 172: 5956–5978.

Alexander SP, Fabbro D, Kelly E, Marrion N, Peters JA, Benson HE *et al.* (2015b). The Concise Guide to PHARMACOLOGY 2015/16: Catalytic receptors. Br J Pharmacol 172: 5979–6023.

Aoki T, Fukumoto Y, Sugimura K, Oikawa M, Satoh K, Nakano M *et al.* (2011). Prognostic impact of myocardial interstitial fibrosis in non-ischemic heart failure. -Comparison between preserved and reduced ejection fraction heart failure. Circ J 75: 2605–2613.

Armani A, Cinti F, Marzolla V, Morgan J, Cranston GA, Antelmi A *et al.* (2014). Mineralocorticoid receptor antagonism induces browning of white adipose tissue through impairment of autophagy and prevents adipocyte dysfunction in high-fat-diet-fed mice. FASEB J 28: 3745–3757.

Azevedo CF, Nigri M, Higuchi ML, Pomerantzeff PM, Spina GS, Sampaio RO *et al.* (2010). Prognostic significance of myocardial fibrosis quantification by histopathology and magnetic resonance imaging in patients with severe aortic valve disease. J Am Coll Cardiol 56: 278–287.

Baldo MP, Forechi L, Morra EA, Zaniqueli D, Machado RC, Lunz W *et al.* (2011). Long-term use of low-dose spironolactone in spontaneously hypertensive rats: effects on left ventricular hypertrophy and stiffness. Pharmacol Rep 63: 975–982.

Bayorh MA, Mann G, Walton M, Eatman D (2006). Effects of enalapril, tempol, and eplerenone on salt-induced hypertension in dahl salt-sensitive rats. Clin Exp Hypertens 28: 121–132.

Bender SB, McGraw AP, Jaffe IZ, Sowers JR (2013). Mineralocorticoid receptor-mediated vascular insulin resistance: an early contributor to diabetes-related vascular disease? Diabetes 62: 313–319.

Bender SB, DeMarco VG, Padilla J, Jenkins NT, Habibi J, Garro M *et al.* (2015). Mineralocorticoid receptor antagonism treats obesity-associated cardiac diastolic dysfunction. Hypertension 65: 1082–1088.

Bostick B, Habibi J, DeMarco VG, Jia G, Domeier TL, Lambert MD *et al.* (2015). Mineralocorticoid receptor blockade prevents Western diet-induced diastolic dysfunction in female mice. Am J Physiol Heart Circ Physiol 308: H1126–H1135.

Caprio M, Feve B, Claes A, Viengchareun S, Lombes M, Zennaro MC (2007). Pivotal role of the mineralocorticoid receptor in corticosteroid-induced adipogenesis. FASEB J 21: 2185–2194.

Caprio M, Antelmi A, Chetrite G, Muscat A, Mammi C, Marzolla V *et al.* (2011). Antiadipogenic effects of the mineralocorticoid receptor antagonist drospirenone: potential implications for the treatment of metabolic syndrome. Endocrinology 152: 113–125.

Cezar MD, Damatto RL, Martinez PF, Lima AR, Campos DH, Rosa CM *et al.* (2013). Aldosterone blockade reduces mortality without changing cardiac remodelling in spontaneously hypertensive rats. Cell Physiol Biochem 32: 1275–1287.

Chapman N, Dobson J, Wilson S, Dahlof B, Sever PS, Wedel H *et al.* (2007). Effect of spironolactone on blood pressure in subjects with resistant hypertension. Hypertension 49: 839–845.

Clark AL, Fonarow GC, Horwich TB (2014). Obesity and the obesity paradox in heart failure. Prog Cardiovasc Dis 56: 409–414.

Clerico A, Giannoni A, Vittorini S, Emdin M (2012). The paradox of low BNP levels in obesity. Heart Fail Rev 17: 81–96.

Cucoranu I, Clempus R, Dikalova A, Phelan PJ, Ariyan S, Dikalov S *et al.* (2005). NAD(P)H oxidase 4 mediates transforming growth factor-beta1-induced differentiation of cardiac fibroblasts into myofibroblasts. Circ Res 97: 900–907.

Curtis MJ, Bond RA, Spina D, Ahluwalia A, Alexander SP, Giembycz MA *et al.* (2015). Experimental design and analysis and their reporting: new guidance for publication in BJP. Br J Pharmacol 172: 3461–3471.

De Keulenaer GW, Brutsaert DL (2011). Are systolic and diastolic heart failure overlapping or distinct phenotypes within the heart failure spectrum? Circulation 123: 1996–2005.

Feraco A, Armani A, Mammi C, Fabbri A, Rosano GM, Caprio M (2013). Role of mineralocorticoid receptor and renin-angiotensin-aldosterone system in adipocyte dysfunction and obesity. J Steroid Biochem Mol Biol 137: 99–106.

Fraccarollo D, Berger S, Galuppo P, Kneitz S, Hein L, Schutz G *et al.* (2011). Deletion of cardiomyocyte mineralocorticoid receptor ameliorates adverse remodelling after myocardial infarction. Circulation 123: 400–408.

Goldstein BJ, Scalia RG, Ma XL (2009). Protective vascular and myocardial effects of adiponectin. Nat Clin Pract Cardiovasc Med 6: 27–35.

Greenberg B, Zannad F, Pitt B (2006). Role of aldosterone blockade for treatment of heart failure and post-acute myocardial infarction. Am J Cardiol 97: 34F–40F.

Guo C, Ricchiuti V, Lian BQ, Yao TM, Coutinho P, Romero JR *et al.* (2008). Mineralocorticoid receptor blockade reverses obesity-related changes in expression of adiponectin, peroxisome proliferator-activated receptor-gamma, and proinflammatory adipokines. Circulation 117: 2253–2261.

Heyen JR, Blasi ER, Nikula K, Rocha R, Daust HA, Frierdich G *et al.* (2002). Structural, functional, and molecular characterization of the SHHF model of heart failure. Am J Physiol Heart Circ Physiol 283: H1775–H1784.

Heymans S, Gonzalez A, Pizard A, Papageorgiou AP, Lopez-Andres N, Jaisser F *et al.* (2015). Searching for new mechanisms of myocardial fibrosis with diagnostic and/or therapeutic potential. Eur J Heart Fail 17: 764–771.

Hirata A, Maeda N, Hiuge A, Hibuse T, Fujita K, Okada T *et al.* (2009). Blockade of mineralocorticoid receptor reverses adipocyte dysfunction and insulin resistance in obese mice. Cardiovasc Res 84: 164–172.

Homma T, Fujisawa M, Arai K, Ishii M, Sada T, Ikeda M (2012). Spironolactone, but not eplerenone, impairs glucose tolerance in a rat model of metabolic syndrome. J Vet Med Sci 74: 1015–1022.

Hui X, Lam KS, Vanhoutte PM, Xu A (2012). Adiponectin and cardiovascular health: an update. Br J Pharmacol 165: 574–590.

Iraqi W, Rossignol P, Angioi M, Fay R, Nuee J, Ketelslegers JM *et al.* (2009). Extracellular cardiac matrix biomarkers in patients with acute myocardial infarction complicated by left ventricular dysfunction and heart failure: insights from the Eplerenone Post-Acute Myocardial Infarction Heart Failure Efficacy and Survival Study (EPHESUS) study. Circulation 119: 2471–2479.

Ishizuka T, Ernsberger P, Liu S, Bedol D, Lehman TM, Koletsky RJ *et al.* (1998). Phenotypic consequences of a nonsense mutation in the leptin receptor gene (fak) in obese spontaneously hypertensive Koletsky rats (SHROB). J Nutr 128: 2299–2306.

Kang YS, Ko GJ, Lee MH, Song HK, Han SY, Han KH *et al.* (2009). Effect of eplerenone, enalapril and their combination treatment on diabetic nephropathy in type II diabetic rats. Nephrol Dial Transplant 24: 73–84.

Kilkenny C, Browne W, Cuthill IC, Emerson M, Altman DG (2010). NC3Rs Reporting Guidelines Working Group. Br J Pharmacol 160: 1577–1579.

Kosmala W, Jedrzejuk D, Derzhko R, Przewlocka-Kosmala M, Mysiak A, Bednarek-Tupikowska G (2012). Left ventricular function impairment in patients with normal-weight obesity: contribution of abdominal fat deposition, profibrotic state, reduced insulin sensitivity, and proinflammatory activation. Circ Cardiovasc Imaging 5: 349–356.

Kosmala W, Przewlocka-Kosmala M, Szczepanik-Osadnik H, Mysiak A, Marwick TH (2013). Fibrosis and cardiac function in obesity: a randomised controlled trial of aldosterone blockade. Heart 99: 320–326.

Kuster GM, Kotlyar E, Rude MK, Siwik DA, Liao R, Colucci WS *et al.* (2005). Mineralocorticoid receptor inhibition ameliorates the transition to myocardial failure and decreases oxidative stress and inflammation in mice with chronic pressure overload. Circulation 111: 420–427.

Lacolley P, Labat C, Pujol A, Delcayre C, Benetos A, Safar M (2002). Increased carotid wall elastic modulus and fibronectin in aldosterone-salt-treated rats: effects of eplerenone. Circulation 106: 2848–2853.

Lai YH, Liu CC, Kuo JY, Hung TC, Wu YJ, Yeh HI *et al.* (2014). Independent effects of body fat and inflammatory markers on ventricular geometry, midwall function, and atrial remodeling. Clin Cardiol 37: 172–177.

Lian M, Hewitson TD, Wigg B, Samuel CS, Chow F, Becker GJ (2012). Long-term mineralocorticoid receptor blockade ameliorates progression of experimental diabetic renal disease. Nephrol Dial Transplant 27: 906–912.

Manrique J, Diaz A, Gavira JJ, Hernandez A, Pujante D, Errasti P (2005). Preliminary results of the effect of treatment of hyperhomocysteinemia and its relationship with inflammation, coagulation status, and endothelial function after renal transplantation. Transplant Proc 37: 3782–3784.

Marzolla V, Armani A, Zennaro MC, Cinti F, Mammi C, Fabbri A *et al.* (2012). The role of the mineralocorticoid receptor in adipocyte biology and fat metabolism. Mol Cell Endocrinol 350: 281–288.

McGrath JC, Lilley E (2015). Implementing guidelines on reporting research using animals (ARRIVE etc.): new requirements for publication in BJP. Br J Pharmacol 172: 3189–3193.

McMurray JJ, Petrie MC, Murdoch DR, Davie AP (1998). Clinical epidemiology of heart failure: public and private health burden. Eur Heart J 19 (Suppl P): P9–16.

Miana M, de Las Heras N, Rodriguez C, Sanz-Rosa D, Martin-Fernandez B, Mezzano S *et al.* (2011). Effect of eplerenone on hypertension-associated renal damage in rats: potential role of peroxisome proliferator activated receptor gamma (PPAR-gamma). J Physiol Pharmacol 62: 87–94.

Nagata K, Obata K, Xu J, Ichihara S, Noda A, Kimata H *et al.* (2006). Mineralocorticoid Receptor Antagonism Attenuates Cardiac Hypertrophy and Failure in Low-Aldosterone Hypertensive Rats. Hypertension 47: 656–664.

Nazarov PV, Reinsbach SE, Muller A, Nicot N, Philippidou D, Vallar L *et al.* (2013). Interplay of microRNAs, transcription factors and target genes: linking dynamic expression changes to function. Nucleic Acids Res 41: 2817–2831.

Pawson AJ, Sharman JL, Benson HE, Faccenda E, Alexander SP, Buneman OP *et al.* (2014). The IUPHAR/BPS guide to PHARMACOLOGY: an expert-driven knowledge base of drug targets and their ligands. Nucleic Acids Res 42: D1098–D1106.

Pfeffer MA, Claggett B, Assmann SF, Boineau R, Anand IS, Clausell N *et al.* (2015). Regional variation in patients and outcomes in the Treatment of Preserved Cardiac Function Heart Failure With an Aldosterone Antagonist (TOPCAT) trial. Circulation 131: 34–42.

Pizarro M, Solis N, Quintero P, Barrera F, Cabrera D, Rojas-de Santiago P *et al.* (2015). Beneficial effects of mineralocorticoid receptor blockade in experimental non-alcoholic steatohepatitis. Liver Int 35: 2129–2138.

Przybylski R, McCune S, Hollis B, Simpson RU (2010). Vitamin D deficiency in the spontaneously hypertensive heart failure [SHHF] prone rat. Nutr Metab Cardiovasc Dis 20: 641–646.

Radin MJ, Holycross BJ, Hoepf TM, McCune SA (2003). Increased salt sensitivity secondary to leptin resistance in SHHF rats is mediated by endothelin. Mol Cell Biochem 242: 57–63.

Radin MJ, Holycross BJ, Hoepf TM, McCune SA (2008). Salt-induced cardiac hypertrophy is independent of blood pressure and endothelin in obese, heart failure-prone SHHF rats. Clin Exp Hypertens 30: 541–552.

Ramirez E, Klett-Mingo M, Ares-Carrasco S, Picatoste B, Ferrarini A, Ruperez FJ *et al.* (2013). Eplerenone attenuated cardiac steatosis, apoptosis and diastolic dysfunction in experimental type-II diabetes. Cardiovasc Diabetol 12: 172.

Rigsby CS, Pollock DM, Dorrance AM (2007). Spironolactone improves structure and increases tone in the cerebral vasculature of male spontaneously hypertensive stroke-prone rats. Microvasc Res 73: 198–205.

Rimbaud S, Garnier A, Ventura-Clapier R (2009). Mitochondrial biogenesis in cardiac pathophysiology. Pharmacol Rep 61: 131–138.

Rocha R, Chander PN, Khanna K, Zuckerman A, Stier CT Jr (1998). Mineralocorticoid blockade reduces vascular injury in stroke-prone hypertensive rats. Hypertension 31: 451–458.

Sowers JR (2007). Metabolic risk factors and renal disease. Kidney Int 71: 719–720.

Susic D, Varagic J, Ahn J, Matavelli L, Frohlich ED (2007). Long-term mineralocorticoid receptor blockade reduces fibrosis and improves cardiac performance and coronary hemodynamics in elderly SHR. Am J Physiol Heart Circ Physiol 292: H175–H179.

van Deursen VM, Damman K, van der Meer P, Wijkstra PJ, Luijckx GJ, van Beek A *et al.* (2014). Co-morbidities in heart failure. Heart Fail Rev 19: 163–172.

Van Gaal LF, Mertens IL, De Block CE (2006). Mechanisms linking obesity with cardiovascular disease. Nature 444: 875–880.

Wada T, Kenmochi H, Miyashita Y, Sasaki M, Ojima M, Sasahara M *et al.* (2010). Spironolactone improves glucose and lipid metabolism by ameliorating hepatic steatosis and inflammation and suppressing enhanced gluconeogenesis induced by high-fat and high-fructose diet. Endocrinology 151: 2040–2049.

Wada T, Miyashita Y, Sasaki M, Aruga Y, Nakamura Y, Ishii Y *et al.* (2013). Eplerenone ameliorates the phenotypes of metabolic syndrome with NASH in liver-specific SREBP-1c Tg mice fed high-fat and high-fructose diet. Am J Physiol Endocrinol Metab 305: E1415–E1425.

Watson LE, Jewell C, Song J, Dostal DE (2013). Echocardiographic effects of eplerenone and aldosterone in hypertensive rats. Front Biosci (Elite Ed) 5: 922–927.

Welch-Reardon KM, Wu N, Hughes CC (2015). A role for partial endothelial-mesenchymal transitions in angiogenesis? Arterioscler Thromb Vasc Biol 35: 303–308.

Youcef G, Olivier A, L'Huillier CP, Labat C, Fay R, Tabcheh L *et al.* (2014). Simultaneous characterization of metabolic, cardiac, vascular and renal phenotypes of lean and obese SHHF rats. PLoS One 9: e96452.

Zennaro MC, Caprio M, Feve B (2009). Mineralocorticoid receptors in the metabolic syndrome. Trends Endocrinol Metab 20: 444–451.

Supporting Information

Additional Supporting Information may be found in the online version of this article at the publisher's web-site:

http://dx.doi.org/10.1111/bph.13479

Figure S1 Carotid hemodynamic assessment.

Table S1 Influence of the eplerenone treatment on urinary aldosterone and corticosterone excretion.
Table S2 Lack of impact of eplerenone treatment on carotic hemodynamic properties.
Table S3 Chronic eplerenone treatment does not impact hemodynamic parameters in SHHF rats.
Table S4 Influence of eplerenone treatment applied as monotherapy in murine models.

Article No.4: MRA treatment reduces MetS-associated OA in SHHF rats

Published in Annals of the Rheumatic Diseases on 2017

Eplerenone treatment alleviates the development of joint lesions in a new rat model of spontaneous metabolic-associated osteoarthritis

Chaohua Deng[1], Arnaud Bianchi[1], Nathalie Presle[1], David Moulin[1], Meriem Koufany[1], Cécile Guillaume[1], Hervé Kempf[1,*], Anne Pizard[2,*]

1. UMR7365 CNRS-Université de Lorraine, IMoPA, Vandoeuvre-les-Nancy, France
2. UMRS-Inserm U1116, Université de Lorraine, Vandoeuvre-les-Nancy, France

***Corresponding authors**

#This part of work has been applied for a patent:

European patent (No. EP16305964.5)

Methods and pharmaceutical compositions for the treatment of osteoarthritis

Inventor, contribution: 25%

ARD Online First, published on May 5, 2017 as 10.1136/annrheumdis-2016-210700

Eplerenone treatment alleviates the development of joint lesions in a new rat model of spontaneous metabolic-associated osteoarthritis

Increasing epidemiological and clinical studies suggest that metabolic syndrome (MetS) plays a role in the incidence and progression of osteoarthritis (OA).[1 2] However, in absence of an appropriate MetS-associated OA experimental model,[3] the MetS contribution to the joint phenotype in OA remains difficult to investigate and the evaluation of potential disease-modifying OA drugs (DMOADs) is complicated. Noteworthy, in contrast to their lean SHHF$^{+/+}$(spontaneously hypertensive heart failure) controls, obese SHHF$^{cp/cp}$ rats, a well-characterised model of MetS,[4] develop drastic metabolic, cardiovascular and renal alterations that are substantially improved through an early chronic mineralocorticoid receptor antagonism (MRA) treatment.[5] Thus, by comparing young (1.5 months) and aged (12.5 months) lean SHHF$^{+/+}$ and obese SHHF$^{cp/cp}$ rats, we sought to evaluate for the first time the potential (1) contribution of MetS to joint alterations and (2) therapeutic benefits derived from chronic MRA treatment by eplerenone (figure 1A).

Rats with no MetS ($^{1.5}$SHHF$^{+/+}$ and $^{12.5}$SHHF$^{+/+}$) or with barely developed MetS ($^{1.5}$SHHF$^{cp/cp}$)[4] displayed normal knee articular phenotype (figure 1Ba,e,i,m and data not shown for young rats). In striking contrast, $^{12.5}$SHHF$^{cp/cp}$ rats, affected by culminating MetS conditions,[5] exhibited knee joints with marked fibrillations from the surface to the middle layer of the cartilage (figure 1B\c,g,k) and moderate to severe loss of proteoglycans (figure 1Bg) and collagen II (figure 1Bk) through the entire thickness of the cartilage. These alterations of the $^{12.5}$SHHF$^{cp/cp}$ knees were associated with pronounced osteophyte formation (figure 1Bc,k) and with fibrosis, inflammation and cellular infiltration of the synovial tissue (figure 1Bc,o). Very interestingly, we could demonstrate that a preventive 11-month eplerenone treatment did not alter the normal knee

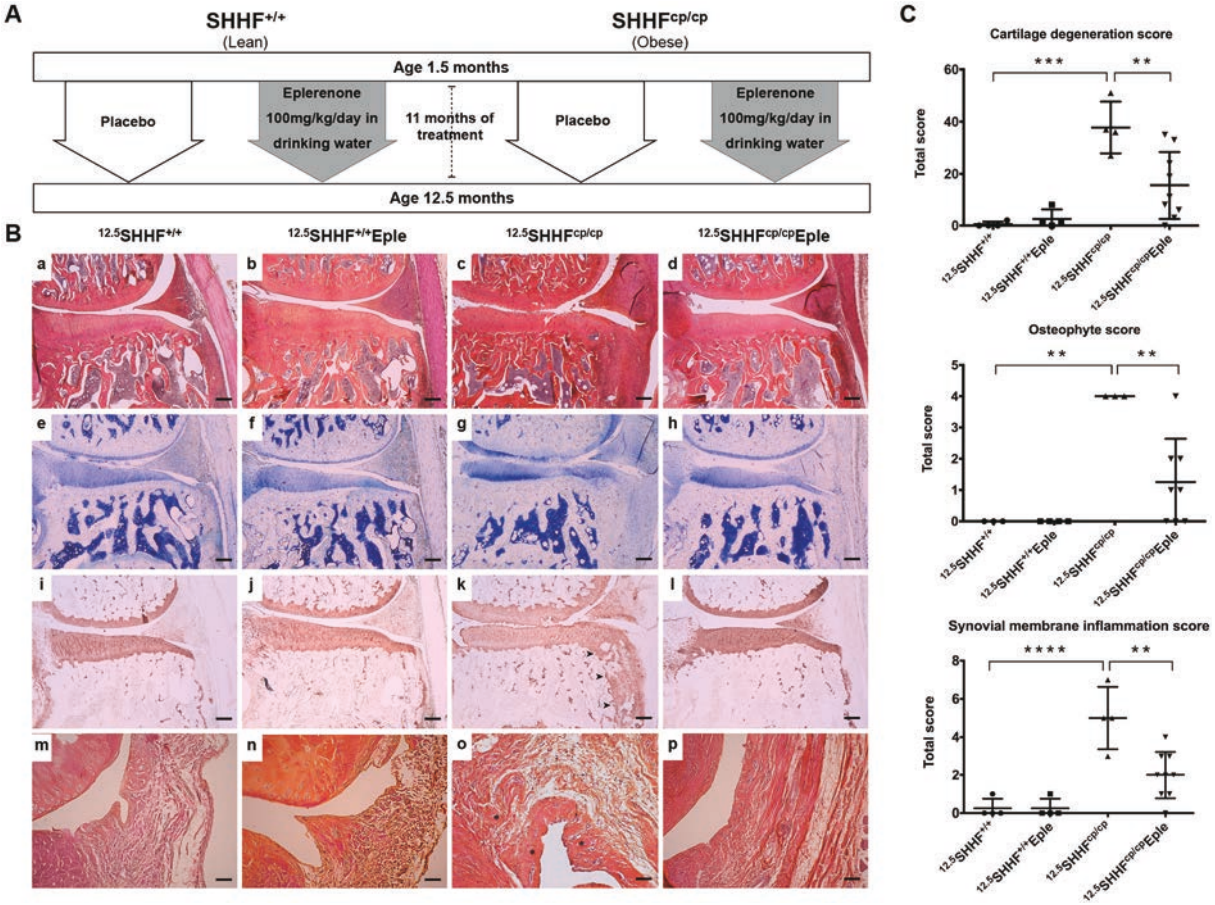

Figure 1 Preventive 11-month treatment with mineralocorticoid receptor antagonist eplerenone alleviated the metabolic syndrome (MetS)-associated joint lesions in SHHF model. (**A**) Experimental design of the study. Lean spontaneously hypertensive heart failure (SHHF$^{+/+}$) and obese SHHF$^{cp/cp}$ rats were divided randomly into treatment groups. Untreated groups (n=4 for SHHF$^{+/+}$ and n=4 for SHHF$^{cp/cp}$) were given placebo and Eple groups (n=4 for SHHF$^{+/+}$ and n=9 for SHHF$^{cp/cp}$) were given 100 mg/kg/day of eplerenone (gift from Pfizer) in drinking water from 1.5 months to 12.5 months of age. Knee joints of 1.5-month-old and 12.5-month-old specimens of each group were collected for histological analysis. (**B**) Representative H&E staining (a–d, m–p), toluidine blue staining (e–h) and collagen II immunohistochemistry (i–l) sections of the knee joint of $^{12.5}$SHHF$^{+/+}$, $^{12.5}$SHHF$^{+/+}$Eple, $^{12.5}$SHHF$^{cp/cp}$ and $^{12.5}$SHHF$^{cp/cp}$Eple rats. In panel k, the arrowheads demarcate osteophyte. In panel o, the arrows point to the infiltration and the asterisks indicate area of fibrosis. Scale bar: 100 µm for magnification ×4 (a–l) and 20 µm for magnification ×20 (m–p). (**C**) Scores for cartilage degradation, osteophyte formation and synovial membrane inflammation in $^{12.5}$SHHF$^{+/+}$, $^{12.5}$SHHF$^{+/+}$Eple, $^{12.5}$SHHF$^{cp/cp}$ and $^{12.5}$SHHF$^{cp/cp}$Eple rats were performed blindly by at least two independent investigators according to OARSI recommendations.[6] Values represent mean±SD. One-way ANOVA with Bonferroni's correction was used for statistical analysis, **p<0.01, ***p<0.001, ****p<0.0001.

phenotype of $^{12.5}$SHHF$^{+/+}$ rats (figure 1Bb,f,j,n) but substantially reduced the cartilage damages, osteophyte formation and synovial inflammation observed in placebo $^{12.5}$SHHF$^{cp/cp}$ rats (compare figure 1Bd,h,l,p with figure 1Bc,g,k,o, respectively). These striking findings were further substantiated by cartilage degeneration, osteophyte formation and synovial membrane inflammation scores, measured according to the lastest OARSI recommendations for histological assessments in rats[6] (figure 1C). Altogether, this establishes that metabolic disorders in obese SHHF$^{cp/cp}$ rats induce changes in the knee joint that are significantly prevented on chronic treatment with MRA eplerenone.

Stratifying OA of various aetiologies to attain precision medicine[7] is yet of limited interest as no efficient and specific DMOAD is available for clinical use.[3 7] In this regard, the present pilot study sustains the proof of concept that preventive and chronic MRA treatment with the well known safety profile drug eplerenone may constitute a promising therapeutic strategy effective for patients with MetS at increased risk of developing knee OA, especially those with abdominal obesity we very recently reported to be better responders to eplerenone.[8] Interestingly, through the known beneficial impact of eplerenone on cardiac[5] and renal (unpublished data) conditions, plus the hereby supported positive effect on the development of MetS-associated cartilage and synovial lesions, MRA could ease mobility of this subfamily of patients with OA. If validated in clinic, such improvement of their life quality might further participate to the decrease of cardiovascular risks in patients with MetS by maintaining physical activity.

In conclusion, we uncovered the SHHF$^{cp/cp}$ strain as a unique spontaneous MetS-associated OA model in rat. Although the bone phenotype remains to be characterised, our work highlights the SHHF model as a novel and attractive instrumental tool to evaluate new preventive and curative therapeutics. Actually, using this model, we evidenced that preventive chronic MRA could positively impede the development of OA-like lesions in the articular and synovial tissues of individuals with MetS. Current and future investigations in vitro, in SHHF models and in patients cohorts will help decipher which and how systemic and/or local modulations of MR-downstream pathways[9] are involved in this uncovered beneficial effect of eplerenone in MetS-induced OA lesions.

Chaohua Deng,[1,2] Arnaud Bianchi,[1,2] Nathalie Presle,[1,2] David Moulin,[1,2,3] Meriem Koufany,[1,2] Cécile Guillaume,[1] Hervé Kempf,[1,2] Anne Pizard[2,3,4,5]

[1]UMR7365 CNRS-Université de Lorraine, IMoPA, Ingénierie Moléculaire et Physiopathologie Articulaire, Vandoeuvre-les-Nancy, France
[2]Fédération de Recherche 3209, Vandoeuvre-les-Nancy, France
[3]CHRU Nancy, Vandoeuvre-les-Nancy, France
[4]UMRS-Inserm U1116, Université de Lorraine, Vandoeuvre-les-Nancy, France
[5]CIC-P1433 Inserm, CHRU Nancy, Vandoeuvre-les-Nancy, France

Correspondence to Dr Hervé Kempf, UMR 7365 CNRS-UL, IMoPA, 9 avenue de la Forêt de Haye, Vandoeuvre-lès-Nancy 54500, France; herve.kempf@inserm.fr and Dr Anne Pizard, UMRS-Inserm U1116, CHRU Nancy, ILCV, 4 rue du Morvan, Vandoeuvre-les-Nancy 54500, France; anne.pizard@inserm.fr

Contributors HK and AP conceived the study. CD, AB, NP, DM, MK, CG and AP performed the experiments. CD, AB, NP, DM, MK, HK and AP interpreted the data. CD, HK and AP wrote the manuscript.

Funding This work was supported by Inserm and Région Lorraine. CD was funded by a China Scholarship Council graduate scholarship.

Disclaimer The sponsors had no role in any experimental part of the study or the writing of the manuscript.

Competing interests None declared.

Provenance and peer review Not commissioned; externally peer reviewed.

To cite Deng C, Bianchi A, Presle N, *et al*. *Ann Rheum Dis* Published Online First: [*please include* Day Month Year]. doi:10.1136/annrheumdis-2016-210700

Received 20 October 2016
Revised 26 February 2017
Accepted 29 March 2017

Ann Rheum Dis 2017;**0**:1–2. doi:10.1136/annrheumdis-2016-210700

REFERENCES

1 Zhuo Q, Yang W, Chen J, *et al*. Metabolic syndrome meets osteoarthritis. *Nat Rev Rheumatol* 2012;8:729–37.
2 Berenbaum F, Griffin TM, Liu-Bryan R. Review: metabolic regulation of inflammation in osteoarthritis. *Arthritis Rheumatol* 2017;69:9–21.
3 Courties A, Gualillo O, Berenbaum F, *et al*. Metabolic stress-induced joint inflammation and osteoarthritis. *Osteoarthritis Cartilage* 2015;23:1955–65.
4 Youcef G, Olivier A, L'Huillier CP, *et al*. Simultaneous characterization of metabolic, cardiac, vascular and renal phenotypes of lean and obese SHHF rats. *PLoS One* 2014;9:e96452.
5 Youcef G, Olivier A, Nicot N, *et al*. Preventive and chronic mineralocorticoid receptor antagonism is highly beneficial in obese SHHF rats. *Br J Pharmacol* 2016;173:1805–19.
6 Gerwin N, Bendele AM, Glasson S, *et al*. The OARSI histopathology initiative - recommendations for histological assessments of osteoarthritis in the rat. *Osteoarthritis Cartilage* 2010;18:24–34.
7 Bijlsma JW, Berenbaum F, Lafeber FP. Osteoarthritis: an update with relevance for clinical practice. *Lancet* 2011;377:2115–26.
8 Olivier A, Pitt B, Girerd N, *et al*. Effect of eplerenone in patients with heart failure and reduced ejection fraction: potential effect modification by abdominal obesity: insight from the EMPHASIS-HF trial. *Eur J Heart Fail* 2017.
9 Jaisser F, Farman N. Emerging roles of the mineralocorticoid receptor in pathology: toward new paradigms in clinical pharmacology. *Pharmacol Rev* 2016;68:49–75.

Eplerenone treatment alleviates the development of joint lesions in a new rat model of spontaneous metabolic-associated osteoarthritis

Chaohua Deng, Arnaud Bianchi, Nathalie Presle, David Moulin, Meriem Koufany, Cécile Guillaume, Hervé Kempf and Anne Pizard

Ann Rheum Dis published online May 5, 2017

Notes

Conclusions

The results of the present study are of utmost importance in two ways:

1. We have uncovered SHHF$^{cp/cp}$ rats as a unique spontaneous metabolic-associated OA model in rat. This has obvious implications for advancing our understanding of 'metabolic OA' as SHHFcp/cp strain may become very instrumental in testing/defining new therapeutics in this context

2. Moreover, we have evidenced that the chronic MRA (by eplerenone) could positively impede or at least slow down the development of OA-lesions in the joints of individuals with metabolic disorders. As a safe and already largely used medication in patients with cardiovascular diseases, MRA may thus constitute the first identified therapeutic strategy effective for OA that potentially may avoid/delay surgical knee replacement. Interestingly, through amelioration of OA-features and consequent relief of associated pain, preventive MRA could increase mobility and life quality of OA patients with MetS and therefore indirectly participate to the decrease of cardiovascular risks in MetS patients by potentially preserving physical activity.

Discussion & Perspective

I. The preventive effects of eplerenone on MetS-associated OA changes: indirect or direct?

In our data presented in ***Article N°4, Deng et al 2017; ARD***, we do not provide evidence for a direct (through MR expressed in the joint tissues) or indirect (through systemic effect) role of MRA in the mitigation of the phenotype. It is obviously a crucial point to decipher through future investigations, and we are currently pursuing our experimental work to answer this question.

Evidence for indirect effects

The beneficial effects of the drug on the cardiac function and metabolic phenotype have been recently reported (***See Article N°3, Youcef et al 2016; BJP***) and a manuscript on the renal phenotype currently in writing will report improvement of the renal function upon eplerenone treatment via for part of it the alteration of protein expression involved in ECM remodeling. Applied as preventive treatment, eplerenone significantly mitigates weight gain in the $SHHF^{cp/cp}$ Eple group while it had no effect on the $SHHF^{+/+}$ gain of weight (**Figure 24**).

As presented in **Figure 24**, $SHHF^{cp/cp}$Eple rats are only 10% lighter than their placebo counterparts and thus still roughly 60% heavier than the $SHHF^{+/+}$ rats, which undoubtedly represent a massive excess of weight as compared to lean $SHHF^{+/+}$. Furthermore, $SHHF^{cp/cp}$Eple rats still have a metabolic syndrome even though with mitigated features as compared to the placebo $SHHF^{cp/cp}$ rats (***See Article N°3, Youcef et al 2016; BJP***). Altogether, the dramatic histologic observations seen in the eplerenone group are unlikely to be exclusively due to the small although significative weight improvement.

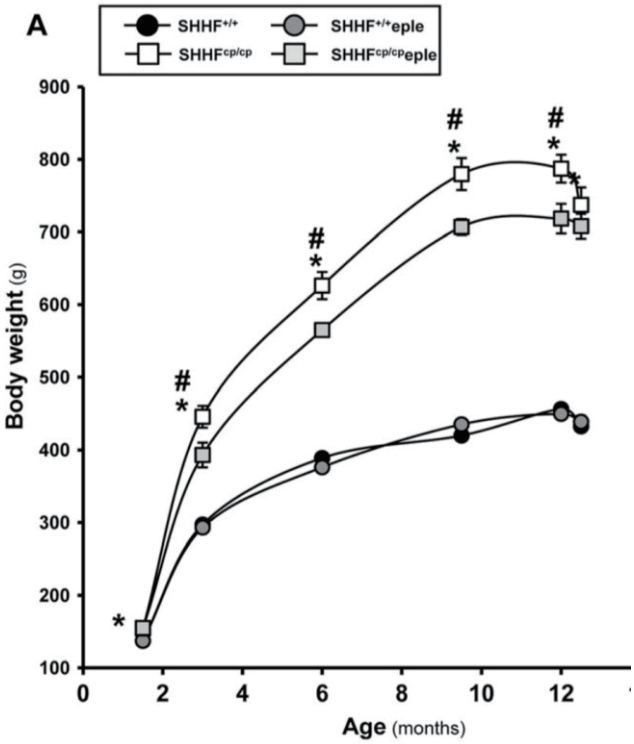

Figure 24 Follow-up of animal body weight during eplerenone treatment.
(Youcef et al., 2016)

The overall beneficial effect of the drug may participate to the quality of life improvement of the treated rats. Indeed, the SHHF$^{cp/cp}$Eple stayed very passive in their cage as they spent most of the day eating while laying on their back, a behavior similar to that observed for the placebo SHHF$^{cp/cp}$ rats. Consequently, although not directly evaluated, it seems unlikely that the muscle strength and mobility are major reasons for the prevention of the OA phenotype observed in SHHF$^{cp/cp}$Eple rats. These preliminary but insufficiently documented observations prompt us to consider telemetric follow-up of the rats' activity during our future experiments as this will be the only unbiased argument for demonstrating a potential impact of eplerenone on the rats' mobility.

Evidence for direct effects

In line with a potential direct beneficial effect of eplerenone on the knee joint, we can mention that some of our preliminary data demonstrate that the MR is expressed in femoral head cartilage from SHHF rats (**Figure 25**) and in primary

articular chondrocytes from Wistar rats (data not shown).

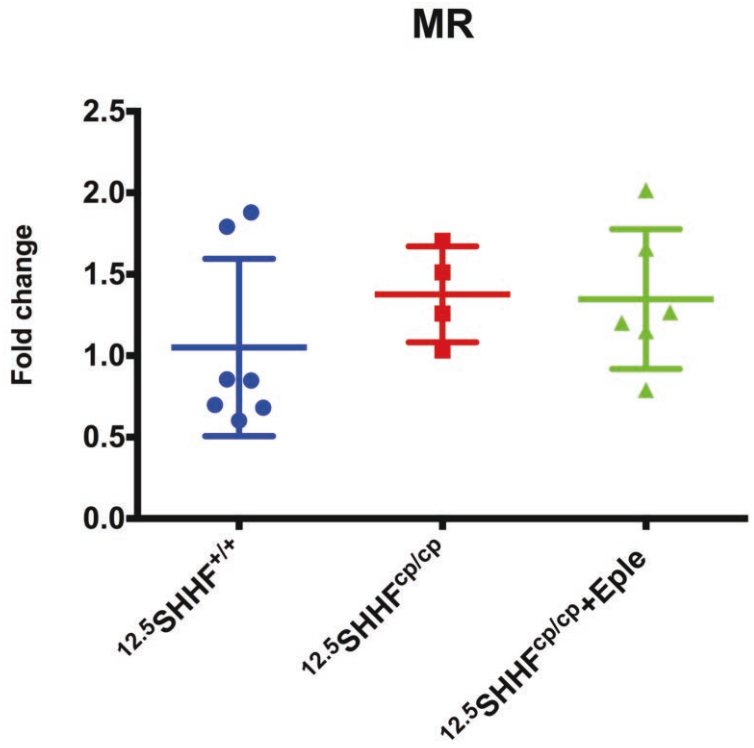

Figure 25 MR gene expression in femoral head cartilage of SHHF rats.
Expression of MR gene in femoral head cartilage from lean SHHF$^{+/+}$ rats (n=7) and from untreated (n=4) or eplerenone treated obese SHHF$^{cp/cp}$ rats (n=6). Values are expressed as mean±SD.

Eplerenone treatment also significantly reduced the inflammatory markers and cartilage degenerative markers that we observed increased in SHHF$^{cp/cp}$ femoral head (**Figure 26**). This suggests that in addition to a probable systemic role (through global health improvement), a direct beneficial impact could also be retrieved from the antagonism of the MR present in the joint.

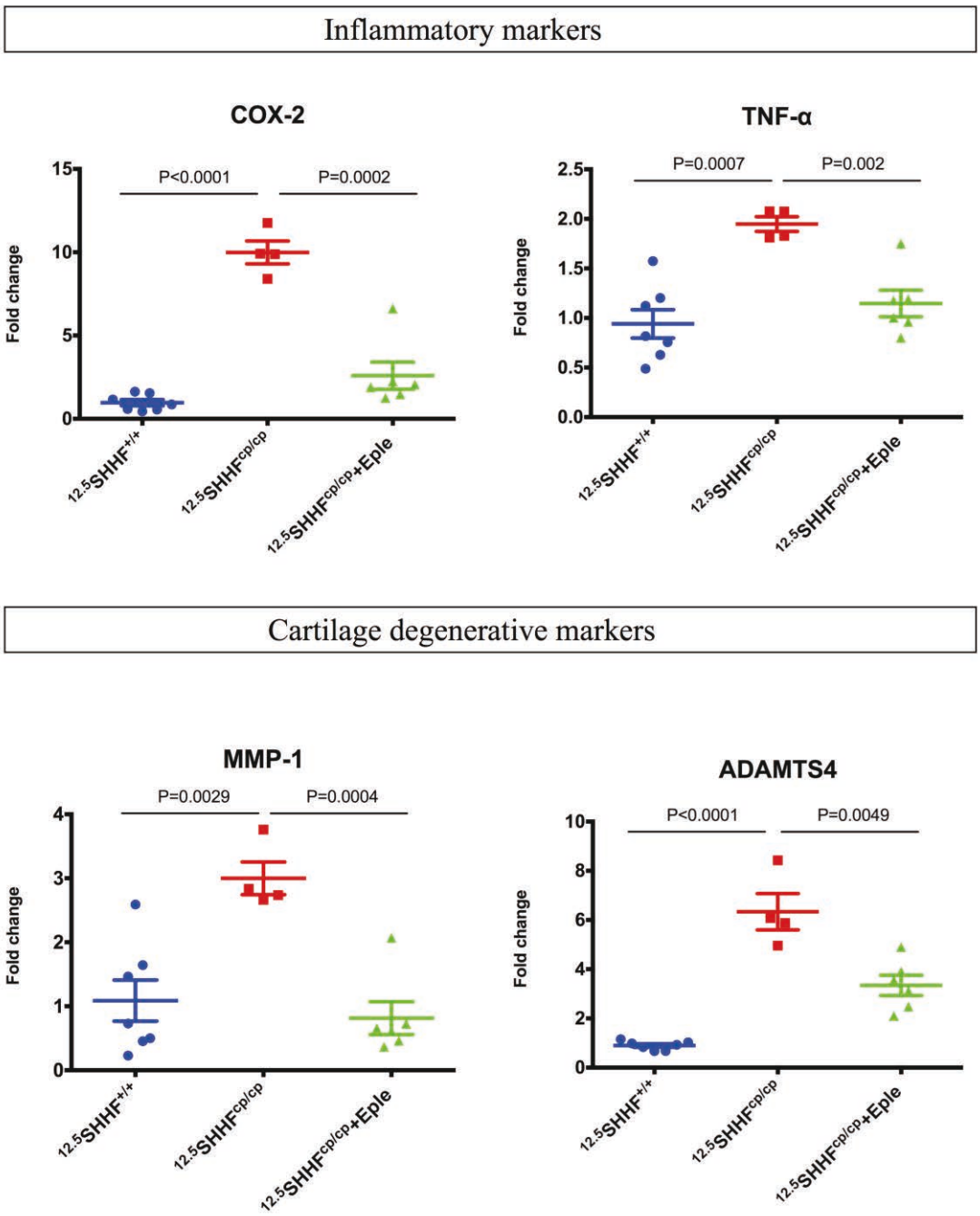

Figure 26 Quantitative PCR results performed mRNA from femoral head cartilage of SHHF rats.

Expression of genes encoding inflammatory and cartilage degenerative markers in femoral head cartilage from lean SHHF$^{+/+}$ rats (n=7) and from untreated (n=4) or eplerenone treated obese SHHF$^{cp/cp}$ rats (n=6).

II. Does Eplerenone have effects on the subchondral bone of the rats?

In addition to osteophyte formation, the subchondral bone alteration is another important hallmark of OA. It would be nice to evaluate in detail exactly how the

subchondral bone is affected in $^{12.5}SHHF^{cp/cp}$ rats and if eplerenone has or not an inhibitory effect on this particular feature. The observations under the microscope of all our specimens (***depicted by representive specimens in Article N°4, Deng et al 2017; ARD)*** do not convince us to draw any unambiguous conclusion on this particular feature. Thus, in contrast to the 3 other parameters (cartilage degradation, osteophyte formation and synovial inflammation), we believe that we should do further investigations to describe the subchondral bone changes. This would highly benefit from an independent complementary analysis by micro-computed tomography (μCT) for instance that would allow to precisely detect the alteration of the tibial bone (subchondral and cortical).

III. SHHF rat model can serve a instrumental tool for the study of MetS-associated OA?

Increasing epidemiological and clinical studies have highlighted the role of MetS in the incidence and progression of OA. However, there is still lack of an appropriate MetS-associated OA experimental models to study the underlying mechanism of this increasing OA subtype and evaluate the potential disease-modifying OA drugs (DMOADs).

In this context, the SHHF rat model is of high interest and is worth further investigation. The advantage of this model is that the colony is composed of control lean rats, $SHHF^{+/+}$, and obese rats, $SHHF^{cp/cp}$, carrying a mutation in the leptin receptor and with the characteristics of MetS as they develop hypertension associated with obesity, dyslipidemia, insulino resistance with elevated levels of aldosterone, a MR ligand. We have uncovered the $SHHF^{cp/cp}$ strain as a unique spontaneous MetS-associated OA model in rat and may serve as a novel and attractive instrumental tool to evaluate new preventive and curative therapeutics (***See Article N°4, Deng et al 2017; ARD***).

The metabolic syndrome in $SHHF^{cp/cp}$ rats develops very early and gradually (Youcef et al., 2014): at 1.5 months, there are already some changes of metabolic

parameters in the plasma of SHHF$^{cp/cp}$ obese rats, such as high-density lipoprotein (HDL), free fatty acids (FFA), insulin, and adiponectin. It will be very interesting and useful to compare the kinetic of MetS and OA development in SHHF$^{cp/cp}$ obese rats, since individual components of MetS such as diabetes and dyslipidemia have been shown importantly linked to the initiation and progression of OA. Thus, it will be of interest to follow the metabolic parameters by analysis of the plasma and the radiographic changes of joint lesions by μCT and magnetic resonance imaging (MRI). In addition, the metabolic and radiographic improvement may indicate sensitive improvements by the drug treatment like eplerenone, earlier before the symptotic and histological changes.

In the present study, the plasmas and urine of rats were kept every three months during the experiment. Thus, it is always possible to follow the kinetic development of plasma values. We are thus planning to detect the CTX-II (Compare C-Telopeptide of Type II Collagen) by the enzyme-linked immunosorbent assay (ELISA) in the plasma and urine.

IV. Eplerenone may constitute a preventive therapeutic strategy for MetS patients at increased risk of developing OA

Eplerenone has been extensively used in cardiovascular field and less in dermatology (psoriasis treatment) and our work opens a new opportunity of using it in OA.

Yet mostly used as curative drug in addition to standard heart failure (HF) care (when HF patient have reduced ejection fraction i.e. the worse phenotype and latest stage of the disease) the therapeutic use of MRA is now being re-positioned to be considered as preventive therapy, in at risk of developing HF population such as obese individuals.

Such repositioning concept is currently tested in the ongoing FP7 funded European HOMAGE clinical trial (see clinicaltrial.gov) where biomarker profiling at risk of developing HF individuals (including obese and MetS patients) should help

stratifying patients according to their likelihood to better respond to a anti-fibrotic MRA therapy (Spironolactone).

The importance of the presence of metabolic disorder in the response to MRA therapy has been recently suggested (Olivier et al., 2017). This very recent post-hoc analysis of the EMPHASIS-HF clinical trial further suggests the importance of targeting abdominally obese patients with MRA. This study allowed us to investigate if the clinical response to eplerenone in mildly symptomatic HF patients varied by abdominal obesity. In Emphasis population, eplerenone improved outcomes in HFrEF patients (HF patients with reduced ejection fraction) with and without abdominal obesity, although the benefit appeared to be more pronounced among those with abdominal obesity (Olivier et al., 2017).

Even though not used in a preventive setting, these data on the influence of obesity in the impact of Eplerenone is in line with precision medicine concept.

Altogether our current data and the identification of a best responder subgroup of abdominally obese patients to Eplerenone in HF trial prompt us to suggest that if clinically tested for its impact on OA development, the first population to be targeted by Eplerenone should be the MetS patients with early stage of OA. Our results do not allow further extrapolation on which other etiology of OA patients might benefit from an MRA treatment as we “only” studied the influence of metabolic disorders.

V. MR is a potential target for the treatment of OA?

First, MR activation is implicated in obesity, inflammation and fibrosis, which are common features in OA. Second, high levels of aldosterone, a ligand of MR, have been described to be involved in obesity, insulin resistance and other features of MetS. Third, the $SHHF^{cp/cp}$ obese rats display hyperaldosteronism in addition to the hallmarks of MetS. Furthermore, we recently demonstrated the beneficial effects of chronic preventive (11 months) MRA eplerenone treatment in both heart failure, MetS features (***See Article N°3, Youcef et al 2016; BJP***) and joint lesions (***See Article N°4, Deng et al 2017; ARD***). Taken together, all these evidences and recent results

highlight the potential key role of MR in OA.

Our preliminary results demonstrated in particular that MRA eplerenone exert anti-inflammatory effect in primary articular chondrocytes from Wistar rats with inflammation. We have also detected the expression of MR in these chondrocytes by qPCR (data not shown). In this context, our ongoing project is to study more specifically the direct role of MR in joint, despite its systemic or indirect beneficial effects in MetS-associated OA.

Recently, a prospective clinical study showed that short-term (2 weeks) of low-dose spironolactone (aldosterone antagonist) can improve the OA-related knee effusion in patients aged around 50 years old (Elsaman et al., 2016). However, another clinical trial revealed that 12 weeks of low-dose spironolactone did not have beneficial effect in older people (around 77 years old) with OA (Mcmurdo et al., 2016). Actually, we are currently investigating withing a OA cohort the therapeutic effects of MRA in patients with OA (KHOALA).

Chapter 3B

Metabolic syndrome components and osteoarthritis: study on chondrocytes

3B.1 Obesity and OA

The association between obesity and the increased risk of OA has been recognized as early as 1988, by the data from the first US national Health and Nutrition Examination Survey (Anderson and FELSON, 1988) and the Framingham Study (FELSON et al., 1988). Since then, the poplulation-based studies have consistently shown a link between obesity and OA (Ackerman and Osborne, 2012; Leyland et al., 2016; Michl et al., 2016; Reyes et al., 2016; Visser et al., 2014; Wen et al., 2016; Yusuf et al., 2010). The mechanical stress and metabolic factors are the main contributors, linking obesity and OA.

Mechanical loading

Increased loading has been shown to inhibit cartilage matrix synthesis and to induce the expression of proinflammatory factors (Chowdhury et al., 2008; Gosset et al., 2006) and degradative enzymes (Fitzgerald et al., 2008). Recent in vivo study provide further evidence for the role of mechanical loading on cartilage. Compression of mice joints leaded to increased fribrillation and periarticular osteophyte formation with increasing load intensity (Ko et al., 2013). High mechanical loading also resulted in significant degenerative changes in rat joint, including a progressive decrease in cartilage aggregate modulus, diminished cellularity and increased histological degeneration (Roemhildt et al., 2013).

Not only cartilage, but also subchondral bone, is subjected to mechanical loading in obese condition. Compressive loading of mouse and rat knee joints could lead to thickening of subchondral cortical bone (Ko et al., 2013; Roemhildt et al., 2013). Furthermore, in guinea-pig, the thickening of subchondral bone was associated with the development and progression of OA. However, the underlying mechanism of compressive loading induced subchondral bone changes is still not clear. Several studies indicated that the osteoblast from subchondral bone may play a role in this process. Cyclic compression on the osteoblasts isolated from non-sclerotic areas of

OA subchondral bone, could induce an inflammatory phenotype resembling that of osteoblasts isolated from OA sclerotic regions (Sanchez et al., 2008; Sanchez et al., 2012). In addition, mechanical compression could stimulate the production of IL-6, prostaglandin E2 (PGE2) and MMPs in osteoblasts (Liu et al., 2006; Sanchez et al., 2012).

Taken together, excessive mechanical loading can greatly affect joint tissues, especially articular cartilage and subchondral bone, and is an important factor in obesity-induced OA in weight-bearing joints.

Metabolic stress

The association between obesity and OA has also been found for hand joints that cannot be explained by increased joint loading, but suggests that metabolic factors contribute to OA (Visser et al., 2014; Yusuf et al., 2010). Loss of body fat is more closely related to symptomatic relief than the loss of body weight in obese patients with knee OA (Toda et al., 1998) and the risk of primary knee and hip replacement for OA relates to both adipose mass and central adiposity (Wang ART 2009), indicating that adiposity may be a more important contributor than increased mechanical loading to the high prevalence of OA in obese population.

Adipose tissue is now regarded as a very active endocrine organ and has been proven to secret a number of adipokines, such as leptin, adiponectin, visfatin and resistin (Gomez et al., 2009), which exhibit inflammatory and degradative effects on joint tissues. Here, I will not discuss in detail the role of individual adipokines in OA, which has been widely reported in a previous review (Neumann et al., 2016).

3B.2 Diabetes and OA

The relationship between diabetes mellitus (DM) and OA has been revealed by recent population-based epidemiological studies (Eymard et al., 2015; Frey et al., 2016; Magnusson et al., 2015; Nieves-Plaza et al., 2013; Schett et al., 2013). Recent two systematic reviews and meta-analysis highlighted a high frequency of OA in

patients with DM, and DM could be an independent risk factor for the incidence and progression of OA (Louati et al., 2015; Williams et al., 2016). A multi-center, longitudinal, prospective observational study showed that medication-treated DM has no effect on OA incidence but reduces OA progression (Shirinsky and Shirinsky, 2017).

Hyperglycemia and insulin resistance, the two major features of DM, may contribute to the relationship between DM and OA.

Hyperglycemia

To date, the results of epidemiological studies examing the link between hyperglycemia and OA remain controversial (Cimmino and Cutolo, 1990; Garessus et al., 2016). However, experimental studies have linked hyperglycemia with both local and systemic toxicities relevant to OA (Berenbaum, 2011). Thus, an independent correlation between OA and hyperglycaemia may potentially exist.

In an experimental DM rat model, characterized by high blood glucose levels due to chemical destruction of pancreatic β-cells, there was a decrease in type II collagen and proteoglycan content in cartilage (Atayde et al., 2012). High glucose concentration may have direct detrimental effect on chondrocytes, because excessive intracellular glucose concentration can activate several different pathways such as polyol, hexosamine, protein kinase C or pentose phosphate pathways, all known to produce advanced glycation end products (AGEs) and reactive oxygen species (ROS).

Accumulation of extracellular AGEs could increase the stiffness and fragility of cartilage and bone (Vashishth et al., 2001; Verzijl et al., 2002). By binding to its receptor, AGEs induce the production of proinflammatory cytokines, proteolytic enzymes and ROS in chondrocytes and synoviocytes (Chen et al., 2013; Franke et al., 2009; Nah et al., 2008; Nah et al., 2007; Rasheed et al., 2011). Increased ROS production is linked to mitochondrial dysfunction and may affect cartilage homeostasis (Henrotin et al., 2003; Vaamonde-García et al., 2012). Finally, human OA chondrocytes were found unable to downregulate the glucose transporter 1

(GLUT-1), one of the main glucose transporters expressed by chondrocytes to adapt glucose incorporation depending on the extracellular concentration (Shikhman et al., 2001), which led to enhanced glucose incorporation and ROS production (Rosa et al., 2009). A recent study showed that high glucose concentration could enhance IL-1β-induced inflammation in cultured murine articular chondrocytes via oxidative stress and the polyol pathway, and chondrocytes from DM patients with OA showed increased responsiveness compared to OA patients without DM (Laiguillon et al., 2015).

Insulin resistance

Hyperinsulinemia is most often caused by insulin resistance at the early stages of DM and may promote cartilage degradation. Serum insulin levels are higher in overweight patients with OA than those without OA (Silveri 1994). Importantly, chondrocytes express the specific high affinity insulin receptor (InsR) that respond to physiologic insulin concentrations. The InsR seems to be more abundant in normal than in OA chondrocytes (Rosa et al., 2011). Besides its important role in chondrogenesis (Phornphutkul et al., 2006), insulin was shown to promote type II collagen and proteoglycan synthesis and to inhibit IL-1β-induced catabolic effects in adult chondrocytes from various species (Cai et al., 2002).

In contrast, a recent study showed that insulin treatment could downregulate autophagy in human normal chondrocytes, and lead to a loss of proteoglycans and an increased MMP-13 and IL-1β expression. Chondrocytes from OA patients with DM exhibite decreased autophagic activity compared to healthy and OA patients without DM (Ribeiro et al., 2016). Further investigations, particularly the animal model with DM, are warranted to underly the link between insulin and autophagy.

3B.3 Hypertension and OA

A population-based study has indicated that hypertension is more prevalent in the OA population compared to the population without OA (75% vs 38%)

(Puenpatom and Victor, 2009), and several epidemiological studies showed the association between hypertension and OA (Engström et al., 2009; Monira Hussain et al., 2014; Yoshimura et al., 2012).

Vascular alterations associated with hypertension may lead to subchondral ischaemia, which may impair nutrient and gas exchange between the articular cartilage and bone, initiating degradative changes in the cartilage (Imhof et al., 2000). Subchondral ischaemia may also induce apoptosis of osteocytes, which might trigger inflammation and bone remodelling. Osteocyte apoptosis was actually found in the necrotic trabeculae of the femoral head in a rat model of hypertension, the Spontaneously Hypertensive rat (Shibahara et al., 2000).

3B.4 Dyslipidemia and OA

Lipids are important nutrients for chondrocytes metabolism, and lipid content constitutes about 1% of articular cartilage. Lipids may be available for chondrocytes by de novo synthesis (Bernstein et al., 2010) or through penetration from synovial fluid (Wang et al., 2013). Dyslipidemia in MetS is characterized by high plasma levels of triglycerides, low levels of HDL, slightly increased levels of low-density lipoprotein (LDL), and increased levels of FFA. Numerous studies have shown the disruption of lipid metabolism in OA.

However, the effects of dyslipidemia on joints remain unclear. Epidemiological studies have reported the positive association between high serum cholesterol and OA (Al-Arfaj, 2003; Davies-Tuck et al., 2009; Hart et al., 1995; Oliviero et al., 2009; Stürmer et al., 1998), whereas other studies found no correlation (Davis 1988, Bagge 1991) (**Summarized in Table 3**).

Population size	Population ethnicity	Study design	Conclusion
1003 women	Chingford population (UK Caucasian)	Cross-sectional	Hypercholesterolemia is associated with both unilateral and bilateral knee OA independent of obesity[10]
3885 adults	American (US)	National Health and Nutrition Examination Survey (NHANES I)	Findings from this study are not supportive of a metabolic link including serum cholesterol between obesity and knee OA[11]
809 OA patients	Southwest Germany	Case-control	This study adds to the evidence regarding the independent role of serum cholesterol as a systemic risk factor for OA[12]
246 OA patients	Saudi Arabia	Cohort	The results showed an association between high serum cholesterol level and both knee and generalized OA[13]
Cohort I: 1148 Cohort II: 1281 Elderly people	Goteborg, Sweden	Cohort	Metabolic factors including triglycerides, cholesterol and blood glucose levels did not correlate to radiographic OA[14]
148 women	Victoria, Australia	Cohort	In this study of asymptomatic middle-aged women with no clinical knee OA, high serum cholesterol and triglyceride levels were associated with the incidence of bone marrow lesions over 2 years[15]
44 patients with RA, psoriatic arthritis and OA and 33 healthy controls	Italy	Case-control	Patients with OA showed the highest concentrations of apolipoprotein A-I and total cholesterol compared to health controls[90]

Table 3 Summary of epidemiological studies regarding the association between serum cholesterol levels and OA.
(Farnaghi et al., 2017)

The chondrocytes of OA cartilage accumulate intracellular lipid, and the elevated level correlates positively with OA severity (Lippiello 1991), indicating the role of lipid deposition in OA. In addition, comparative proteomic study of articular cartilage and chondrocytes from healthy donors and OA patients have demonstrated altered expression of proteins related to lipid metabolism in OA (Wu et al., 2007). A recent study revealed difference in the distribution of lipids in healthy and OA cartilage by using time of flight-secondary ion mass spectrometry (TOF-SIMS): the authors found that cholesterol and several species of fatty acids accumulate in droplets in the superficial area of OA cartilage (Cillero-Pastor et al., 2012). The impaired expression of genes regulating cholesterol effux may explain the abnormal lipid deposition in OA cartilage (Collins-Racie et al., 2009; Tsezou et al., 2010).

Article No.5 (in preparation): EPA reduces inflammation via autophagy

Eicosapentaenoic acid attenuates the inflammatory and degenerative response of rat chondrocyte to palmitate and hyperglycemia via regulation of autophagy

Chaohua Deng[1], Aurore Gemble[1], Cécile Guillaume[1], Anne Pizard[2], Hervé Kempf[1,*] and Arnaud Bianchi[1,*]

1. UMR7365 CNRS-Université de Lorraine, IMoPA, Vandoeuvre-les-Nancy, France
2. UMRS-Inserm U1116, Université de Lorraine, Vandoeuvre-les-Nancy, France

***Corresponding authors**

The association between obesity and an increased risk of OA has been recognized by population-based studies, although the detailed mechanism linking obesity and OA has not been fully elucidated (Reyes et al., 2016). Studies indicate that mechanical and metabolic factors play key role in joint destruction. In the weight-bearing joints, altered biomechanic is the major contributor to OA (Felson et al., 2004). However, the association between obesity and OA in hand cannot be explained by increased joint loading, but is related to metabolic factors (Visser et al., 2014; Yusuf et al., 2010). In the past few years, OA has been linked not only to obesity but also to other cardiovascular risk factors, including DM, dyslipidemia, hypertension and insulin resistance (Yoshimura et al., 2012). All those risk factors constitute the MetS, which has become a major worldwide health issue affecting more than 2 billion individuals across the globe. Compared to OA patients without MetS, epidemiological studies show that MetS patients develop clinical symptoms of OA earlier in life and are subject to increased inflammation and pain in the joints (Engström et al., 2009; Puenpatom and Victor, 2009).

In fact, MetS and obesity are associated with various metabolic alterations that could also contribute alone or in combination to OA pathogenesis, such as disorders in glucose and lipid metabolism. In this context, FFA and glucose are of particular interest, since their circulating levels are elevated in obesity, which consequently play a critical role in other metabolic diseases such as diabetes and insulin resistance (Karpe et al., 2011; Yoshimura et al., 2012). To date, the results of epidemiological studies examing the association between hyperglycemia and OA remain controversial (Cimmino and Cutolo, 1990; Garessus et al., 2016). Experimental studies have linked hyperglycemia with both local and systemic toxicities relevant to OA, mediated by oxidative stress and AGEs (Berenbaum, 2011). Thus, an independent correlation between OA and hyperglycaemia potentially exists. Beside, elevated plasma FFA levels account for a large part of insulin resistance which is associated with several metabolic diseases including DM, hypertension and dyslipidemia (Boden, 2011). Satured FFA have been shown to activate inflammatory signaling in macrophages

(Håversen et al., 2009), astrocytes (Gupta et al., 2012), and skeletal muscle cells (Hirabara et al., 2010). Recently, a study described the abundant distribution of satured FFA plamitic acid and oleic acid in human OA cartilage, compared to healthy cartilage (Cillero-Pastor et al., 2012).

Omega-3 polyunsaturated fatty acids (ω-3 PUFAs) are essential to human health and normal physiology, and deficiencies can lead to chronic diseases (Zhang and Spite, 2012). In particular, increasing evidences from both human and animal studies have demonstrated that ω-3 PUFAs, primarily eicosapentaenoic acid (EPA) and docosahexaenoic acid (DHA), can exert anti-inflammatory effects and have a beneficial role in a variety of human diseases, including diabetes, atherosclerosis, asthma, and arthritis (Di Giuseppe et al., 2014). A recent clinical study suggests that fish oil improves OA symptoms (Hill et al., 2016). In a mouse model of OA, exogenous supplementation of ω-3 PUFAs might delay OA onset while high satured FFA diets might accelerate OA progression (Wu et al., 2015). In fat-1 transgenic mice, enhancement of the synthesis of endogenous n-3 PUFAs from n-6 PUFAs is found, which can delay the incidence of OA, probably through promotion of autophagy and cell survival in cartilage chondrocytes (Huang et al., 2014). However, the underlying mechanisms for the effect of ω-3 PUFAs in OA warrant further investigation.

Taken together, the relationship between hyperglycemia, satured FFA and OA pathophysiology still need to be clarified. In the present study, we examined the individual and combinational effects of glucose and palmitate on rat articular chondrocytes, and the beneficial effect of EPA and possible mechanism.

Material and Methods

(This section will be used in the manscript)

Chondrocyte isolation and culture

Normal articular cartilage was obtained from 6-week-old male Wistar rats (130 to 150 g) killed under dissociative anesthesia (ketamine [Rhône-Mérieux, Lyon, France] and acepromazine [Sanofi Santé Animale, Libourne, France]) in accordance with local ethics committee and national animal care guidelines. Articular cartilage pieces were collected aseptically by joint surgery and were dissected from femoral head caps. Chondrocytes were obtained by sequential digestion with pronase and collagenase B (Roche Diagnostics, Meylan, France). Cells were washed twice in Dulbecco's Phosphate-Buffered Saline (DPBS) without calcium and magnesium (Gibco), and cultured to confluence in 75-cm^2 flasks at 37°C in a humidified atmosphere containing 5% CO_2. Cells were maintained in Dulbecco's modified Eagle's medium (DMEM)/F-12 (Gibco) supplemented with L- glutamine, pen/strep (Invitrogen), heat-inactivated fetal calf serum (FCS) (10%) (Gibco). All experiments were performed with first-passage chondrocytes plated either at 8×10^5 cells per well in 6-well plates or 4×10^5 cells per well in 12-well plates. Normal and high glucose condition are realized by using 1g/L and 4.5 g/L DMEM (Gibco).

RNA isolation, reverse transcription real-time quantitative polymerase chain reaction

Total RNA from cultured chondrocytes was isolated by using RNAeasy kits (Qiagen). 500ng of total RNA was reverse-transcribed for 90 minutes at 37°C in a 20-µL reaction mixture containing 5 mM dNTPs, 100 mM DTT, 0.2 µg/µL random hexamer primers, and 200 U/µL Moloney murine leukemia virus reverse transcriptase (Invitrogen). Quantitative polymerase chain reaction (qPCR) was performed by using SYBR green mix (Bio-Rad) and Via 7 system (Life Science). The results were expressed as the ratio of mRNA level of each gene of interest over the housekeeping gene RPS29.

Western blot

Rat chondrocytes treated were harvested and lysed in RIPA buffer (Thermo scientific) with PDMF. Protein concentration in samples was determined using the BCA protein assay. Protein samples were run on 4%-20% Mini or Midi PROTEAN TGX Precast Protein Gels (Bio-Rad) and transferred to PVDF membrane by the Trans-Blot Turbo Transfer System, according to the manufacturer's instructions (Bio-Rad). After blocking with 5% milk in Tris-buffered saline (TBS)-Tween for at least 1 h, the membranes were incubated overnight at 4°C with primary antibodies. Autophagic activity was determined by using rabbit mAb LC3B (1:1000) (Cell signaling). A rabbit polyclonal antibody against β-actin (1:4000) (Sigma-Aldrich) was used as loading control. After three washings with TBST, the blot was incubated with an anti-rabbit immunoglobulin G conjugated with horseradish peroxidase (1:2000) (Cell signaling) for 1 h at room temperature. After three washings with high salt TBST, ChemiDoc Imaging Systems was used to detect protein bands, according to the manufacturer's recommendations (Bio-Rad).

Measurement of 2-deoxy-D-glucose uptake

Glucose transport from at least 4 different cell cultures was determined by measuring the uptake of 2-deoxy-D-glucose (2-DG) (Sigma Aldrich). Briefly, mature chondrocytes were cultivated in various concentration of glucose for 72h. Chondrocytes were pre-incubated for 4 h in 0.2 % BSA in a Krebs Ringer buffer without glucose, and then incubated with [1,2^{3}H]-2-DG (0.5 µCi/ml, 28 Ci/mmol, Perkin Elmer). The reaction was stopped after 30 min at 37°C. Radioactivity was determined in solubilized cells plus 2.5 ml of TRI-CARB 2100TR scintillation cocktail (Perkin Elmer). Negative controls were obtained by treating cells with 10 µM cytochalasine B (Sigma Aldrich), a specific inhibitor of the facilitated glucose transporters. Results were expressed in nmol of DG/h/µg of protein.

Chondrocyte Proteoglycan Synthesis

To perform anabolism measurements, chondrocytes were cultured in alginate beads. Briefly, cells were suspended in sterile filtered low viscosity alginate (1.2%, w/v) (from Macrocystis pyrifera, Sigma) at a concentration of 5×10^6 cells/ml and slowly expressed through a 22-gauge needle into $CaCl_2$ solution. After instantaneous gelation, the beads were incubated in $CaCl_2$ solution for 15 min and washed two times in 0.15m NaCl and then in DMEM/Ham's F-12 medium. The beads were finally maintained in complete culture medium for 6 days in a humidified atmosphere with 5% CO_2 at 37 °C before further experiments.

The alginate beads were incubated in complete DMEM medium containing only 2% foetal calf serum with 10 μCi/ml radiolabeled sodium sulfate ($Na_2{}^{35}SO_4$) for 4 h at 37 °C. Alginate beads were washed five times with 0.15 mM NaCl and solubilized in a 55 mm citrate buffer (pH 6.8) with 20 mm EDTA. Cells were digested overnight at 60 °C in 0.2 mM NaH_2PO_4 buffer (pH 7.3) containing 0.01 mM EDTA, 0.01 mM cysteine and papain at 6.75 units/ml. The$^{35}SO_4$-labeled proteoglycan content was measured by liquid scintillation with a LKB 1214 counter (Wallac, France).

Statistical analysis

Results are expressed as mean ± SEM. Differences between groups were assessed by two-tailed t test by using the software Prism 6. P values <0.05 were considered significant.

RESULTS

High glucose reduces glucose uptake and sulphate incorporation, and induces degenerative response in chondrocytes

First, we evaluated the effect of high glucose on rat articular chondrocytes. When cultured in high glucose condition for 24 hours, rat chondrocytes showed a decreased incorporation of sulphate, and concommitantly developped a resistance to glucose evidenced by an inhibition of ^{3}H-glucose uptake (**Fig1A**). During the same time, the gene expression of MMP-13 was slightly increased while that of GLUT-3 decreased. No change was observed for IL-6, Aggrecan, IGF-1 or GLUT-1 (**Fig1B**).

When chondrocytes were exposed to high level glucose for 48 hours and 72 hours, only the mRNA level for IGF-1 was up-regulated (**Fig1B**).

Palmitate increases the expression of pro-inflammatory markers and matrix metalloproteinases expression

Then, we analyzed the effects of a saturated free fatty acid, Palmitate (PA), on gene expression of catabolic and anabolic factors in rat articular chondrocytes. Expression of COX-2, mPGES, MMP-3, MMP-13, Col 2 and Aggrecan was assessed in primary rat articular chondrocytes treated with increased concentration of PA (0.1mM, 0.25mM, 0.5mM) for 24 hours. The mRNA levels of COX-2 and mPGES were significantly increased by PA in a dose-dependent manner, compared with untreated cells (**Fig2A&B**). ELISA measurement confirmed the stimulatory effect of PA on the protein expression of COX-2 (data not shown). Consistently, a concomitant increase in the expression of matrix metalloproteinases MMP-3 and MMP-13 was also observed according to the increasing concentrations of PA (**Fig2C&D**). PA treatment did not modify significantly the mRNA expression of Col2, while it seemed to decrease Aggrecan expression slightly (**Fig1E&F**), but without reaching statistical significance.

High glucose treatment worsens the inflammatory and degenerative response induced by palmitate

To determine whether the effects of PA may be more severe in high glucose condition, we evaluated the expression of COX-2, mPGES, MMP-3, MMP-13, Col 2 and Aggrecan, in rat chondrocytes treated with normal glucose (1g/L) or high glucose (4.5g/L), either alone or in combination with PA (0.1mM) for 24 hours. In accordance to what was found in **Fig1B** and **Fig2A**, glucose alone at high level did not induce any significant change in the expression of any of these genes, and PA at 0.1mM with normal glucose condition increased only COX-2 expression significantly (**Fig3**). Surprisingly, PA at 0.1mM associated with high glucose condition not only further induced COX-2 expression, but also significantly increased MMP-3 ($P=0.0275$) and MMP-13 ($P=0.0464$) expression and decreased Aggrecan ($P=0.0318$) expression (**Fig3**).

Palmitate induces chondrocyte apoptosis

PA exhibited a pro-apoptotic effect in rat chondrocytes. There was a significant increased number of apoptotic cells following PA treatment for 48 hours. No obvious difference was noticed between normal and high glucose contidions (**Fig4**).

Eicosapentaenoic acid treatment decreases high glucose and palmitate-induced inflammation and degenerative response

To evaluate whether EPA could prevent in high glucose condition the pro-inflammatory and degenerative effects of PA, we measured the expression of COX-2, mPGES, MMP-3, MMP-13, Col 2 and Aggrecan in rat articular chondrocytes treated with PA at 0.1 mM with increasing EPA concentrations (10μM, 30μM, 60μM, 100μM) for 24 hours. This treatment was applied following a previous exposure of chondrocytes to high glucose level for 72 hours. The preliminary exposure of chondrocytes to high levels of glucose for 72 hours prior to PA treatment results in a

up-regulation of mRNA levels for the inflammatory and degenerative factors. EPA caused a significant reduction in the stimulatory effects of PA and high glucose on the expression of COX-2 and mPGES, as well as MMP-13 (**Fig5A, B&D**). EPA also reduced the expression of MMP-3 induced by PA and high glucose, but without statistical difference (**Fig5C**). EPA treatment did not change the effect of PA and high glucose on Col 2 and Aggrecan expression (**Fig5E&F**).

EPA treatment decreases high glucose and palmitate induced ER stress and autophagy

In order to evaluate the role of autophagy in the inflammatory and degenerative response of chondrocytes to PA and high glucose, we performed western blot analysis to determine the protein level of LC3, a classic marker for autophagosomes localized on the phagophore and autophagosome membrane (Klionsky et al., 2016). After 48 hours treatment with 0.1mM PA in high glucose condition, there was actually a significant increase of LC3II protein levels. Importantly, EPA (30μM) treatment could significantly decrease the expression level of LC3II level (**Fig6B**).

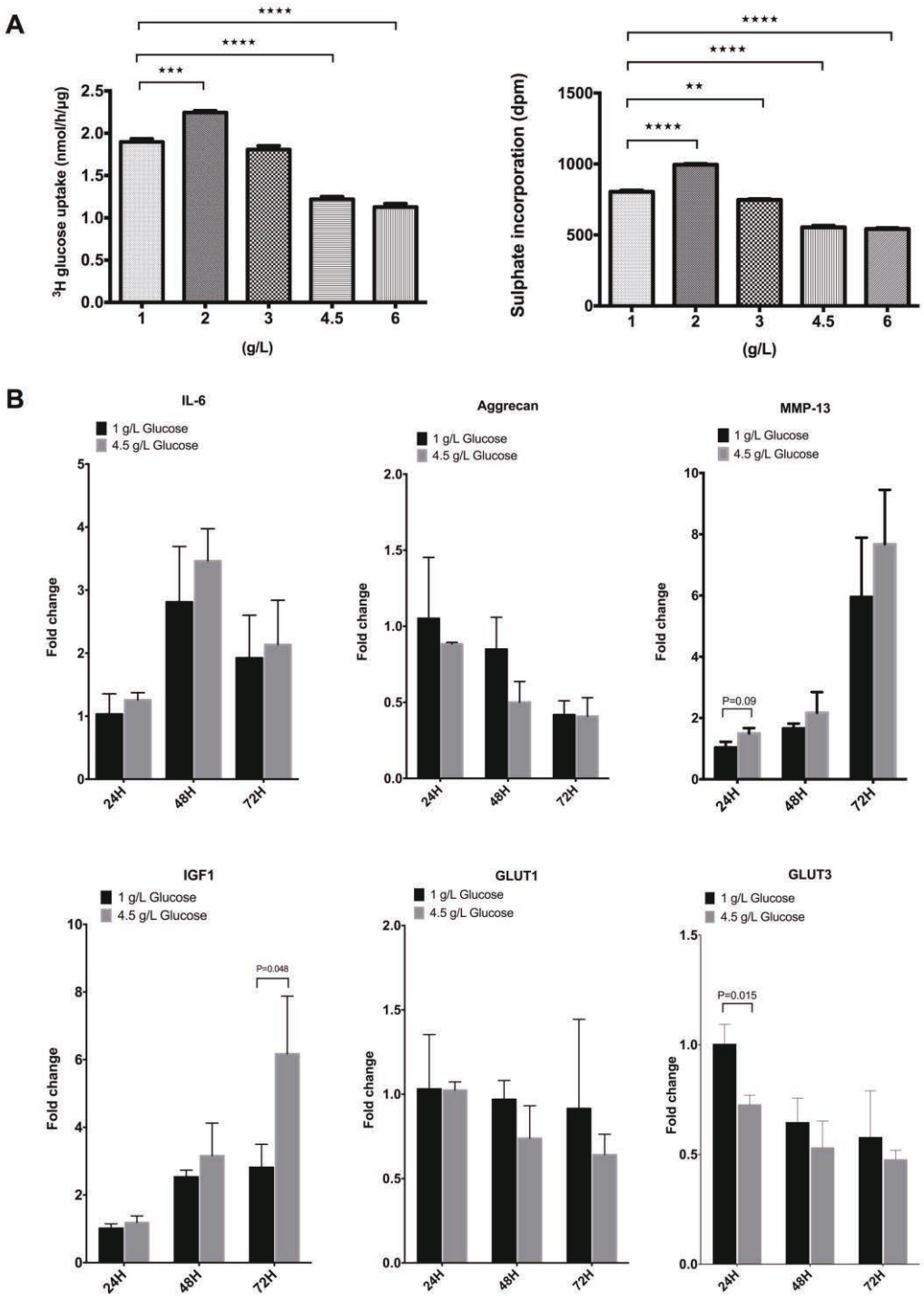

Figure 1. Inhibited glucose uptake and sulphate incorporation and degenerative response induced by high glucose condition. When the rat chondrocytes were cultured under increasing glucose condition for 24 hours, (A) a significant deceased ^{3}H-glucose incorporation and (B) a significant reduced sulphate incorporation were observed at 4.5 g/L of glucose. (C) When the rat chondrocytes were cultured for 24, 48 and 72 hours in high glucose condition (4.5 g/L), mRNA were assessed by qPCR for different markers. Values are expressed as mean±SD. ★, $p<0.05$; ★★, $p<0.01$; ★★★, $p<0.001$; ★★★★, $p<0.0001$. N=3.

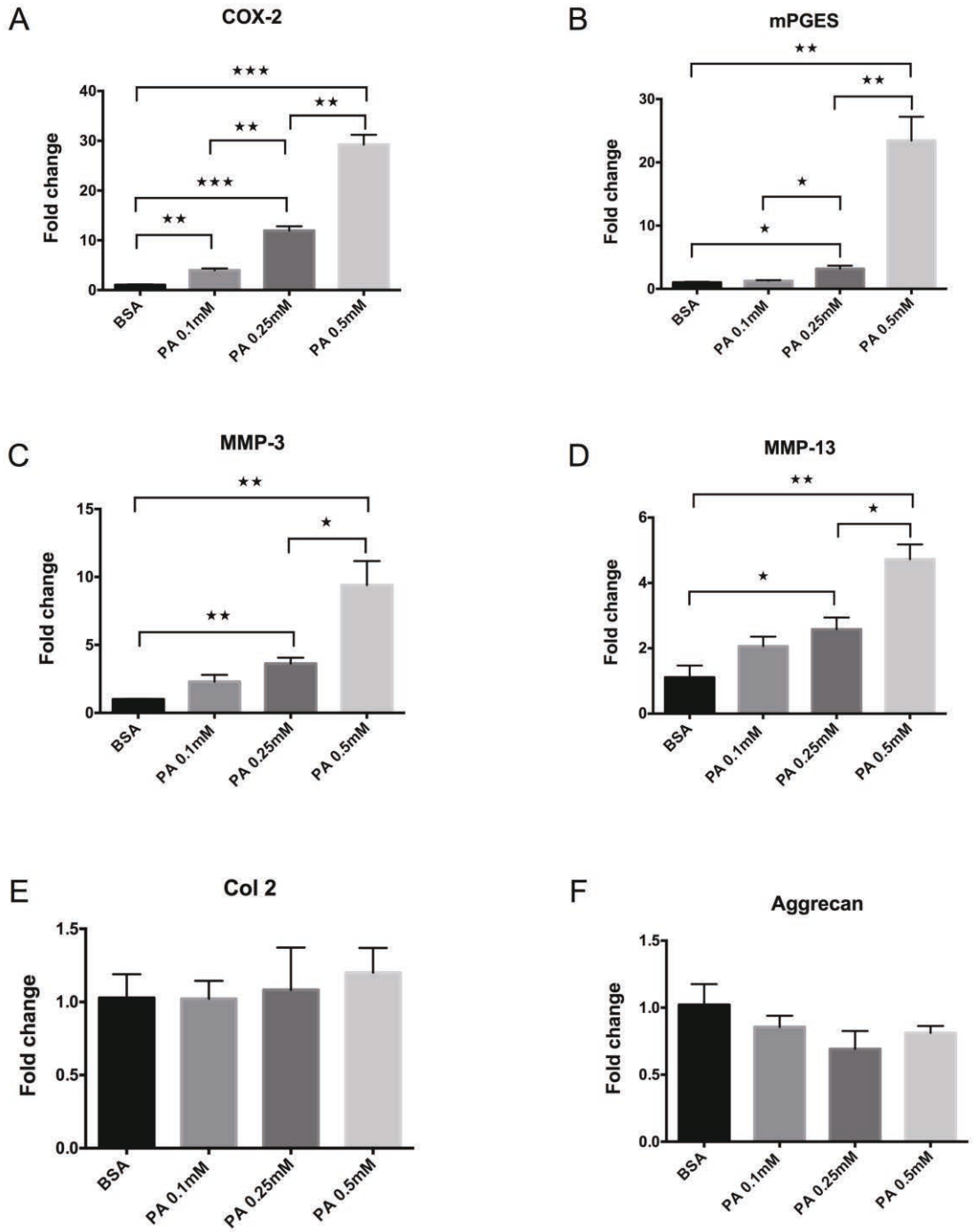

Figure 2. Effect of palmitate on the expression of pro-inflammatory markers, matrix metalloproteinases and chondrocyte markers. After exposure to high glucose for 72 hours, primary rat articular chondrocytes were treated with increasing concentration of palmitate (0.1 mM, 0.25 mM, 0.5 mM) for 24 hours, and mRNA were assessed by qPCR for (A-B) pro-inflammatory markers COX-2 and mPGES, (C-D) matrix metalloproteinases MMP3, MMP13, and (E-F) chondrocyte markers Col 2 and Aggrecan. Values are expressed as mean±SEM. ★, $p<0.05$; ★★, $p<0.01$; ★★★, $p<0.001$. N=3.

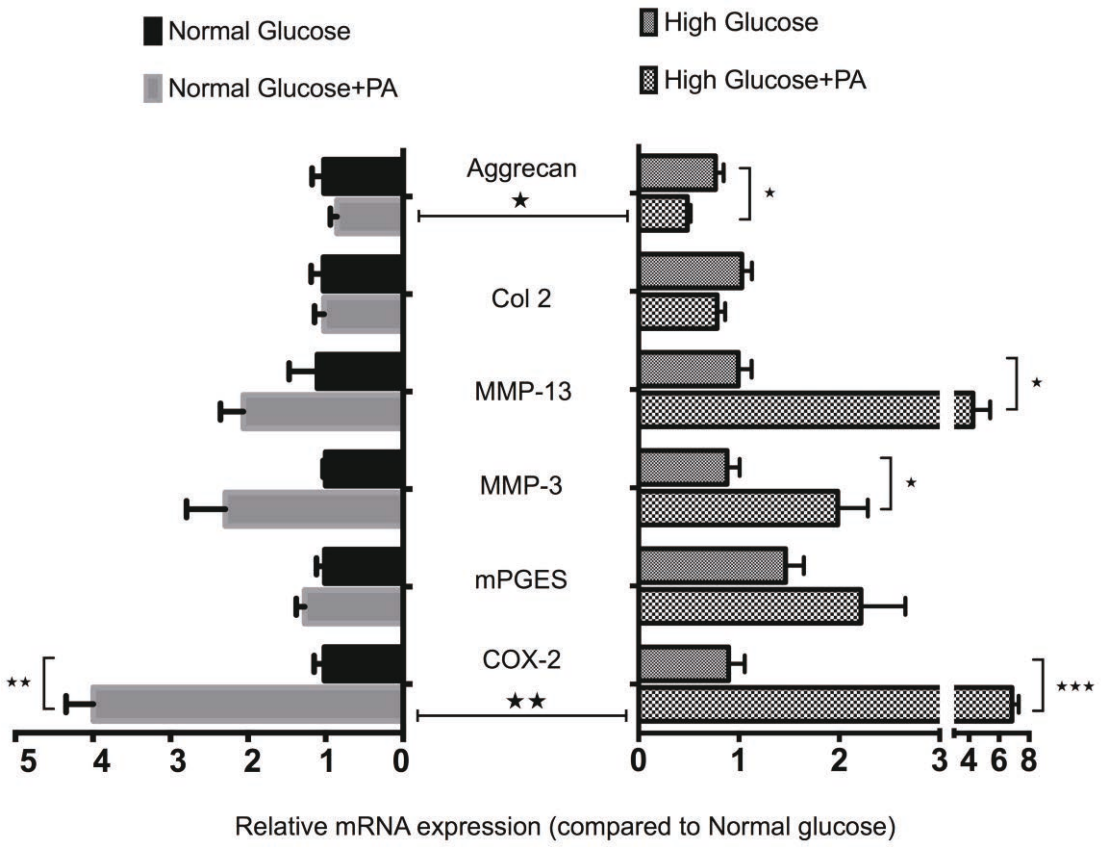

Figure 3. Effect of high glucose and palmitate on the expression of pro-inflammatory markers, matrix metalloproteinases and chondrocyte markers. Primary rat articular chondrocytes treated with normal glucose (1 g/L), high glucose (4.5 g/L), and palmitate (0.1 mM) for 24 hours. Gene expression was determined by qPCR. Values are expressed as mean±SEM. ★, $p<0.05$; ★★, $p<0.01$; ★★★, $p<0.001$; ★★★★, $p<0.0001$

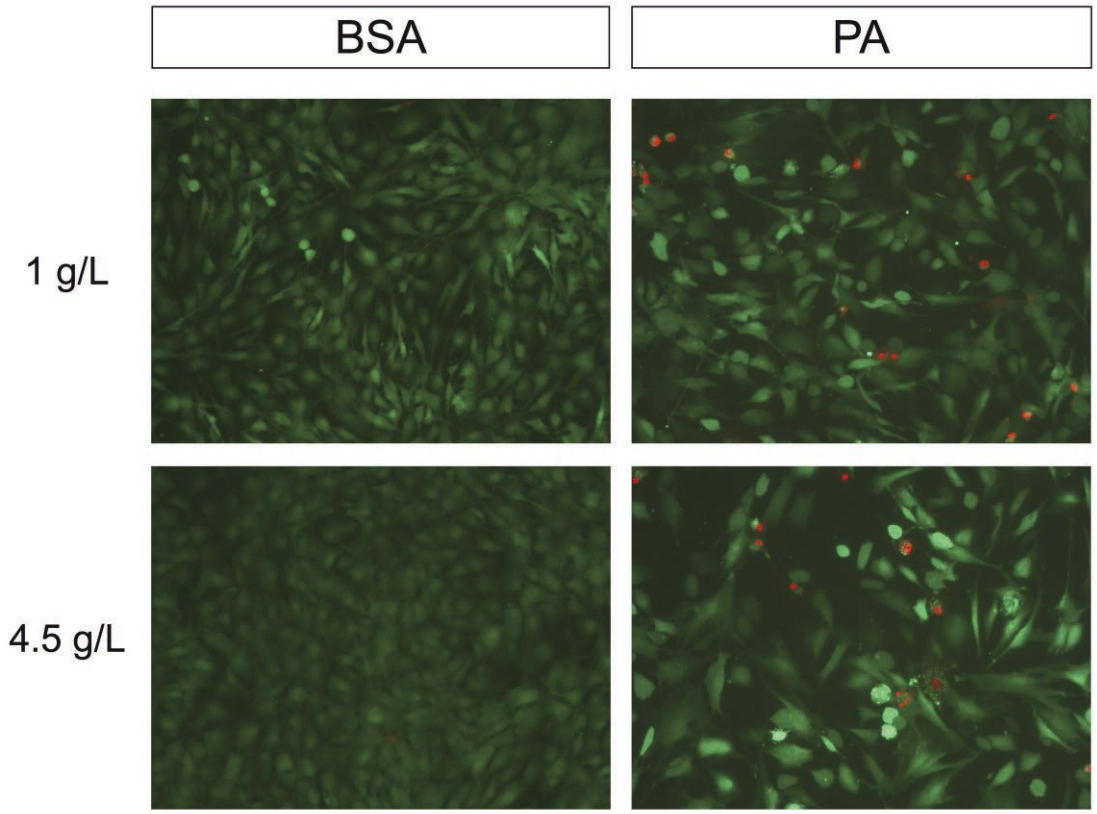

Figure 4. Pro-apoptotic effect of palmitate in chondrocytes. A significant increased amount of dead cells (red) in rat chondrocytes treated with PA at 0.1mM for 48 hours. Live cells: Green (Calcein-AM) ; Apoptotic cells: Red (Propidium Iodide).

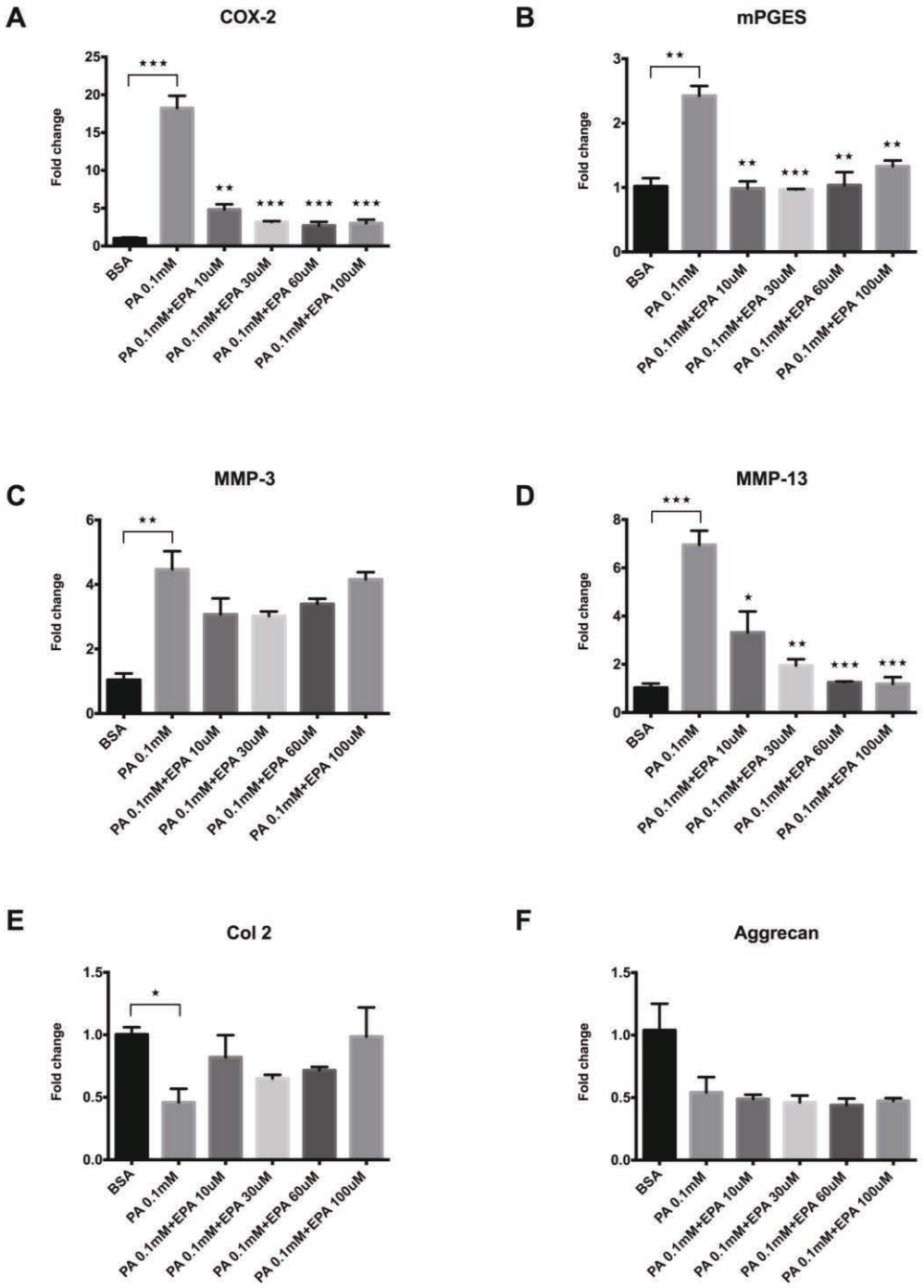

Figure 5. **Effect of EPA on the expression of pro-inflammatory markers, matrix metalloproteinases and chondrocyte markers induced by palmitate and high glucose.** Primary rat articular chondrocytes in high glucose (4.5 g/L) were treated with 0.1 mM palmitate and increasing concentration of EPA (10uM, 30uM, 60uM, 100uM) for 24 hours. (A-B) Pro-inflammatory markers COX-2, mPGES, (C-D) matrix metalloproteinases MMP3, MMP13, and (E-F) chondrocyte markers Col 2, Aggrecan were determined by qPCR. Values are expressed as mean±SEM. ★, $p<0.05$; ★★, $p<0.01$; ★★★, $p<0.001$; ★★★★, $p<0.0001$.

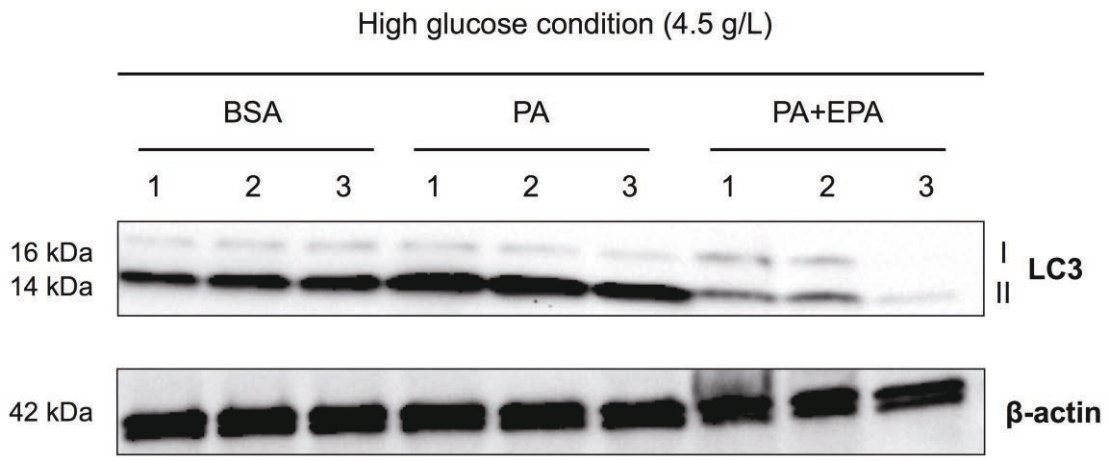

Figure 6. Effect of EPA on high glucose and palmitate induced autophagy. Rat chondrocytes cultured in high glucose condition (4.5 g/L) were treated with 0.1mM palmitate and 30uM EPA for 48 hours. The protein level of autophagy marker LC3 was dertermined by western blot.

Conclusions

Our study shows that PA induces the expression of pro-inflammatory markers and matrix metalloproteinases in rat articular chondrocytes, two hallmarks of OA. In high glucose condition, the chondrocyte response to PA enhanced significantly, suggesting a combined effect of two components of the MetS. The contribution of PA and high glucose to these changes may be due to dysregulated autophagy.

The present study demonstrates for the first time the beneficial effect of EPA to inhibit PA-induced inflammation and cartilage degradation, and provides new potential therapeutic insight for the treatment of OA through targeting autophagy.

Discussion & Perspective

I. Omega-3 fatty acid : a potential therapeutic choice for OA?

ω-3 PUFAs are essential to human health and normal physiology and a number of human and animal studies have demonstrated the anti-inflammatory and beneficial effects in a variety of human diseases, including diabetes, atherosclerosis, asthma, and arthritis (Calder, 2006; Di Giuseppe et al., 2014; Proudman et al., 2008).

A recent clinical study suggests that fish oil (enrich on ω-3 PUFAs) improves OA symptoms (Hill et al., 2016). In mouse models, exogenous supplementation of ω-3 PUFAs might delay OA onset while high satured FFA diets might accelerate OA progression (Wu et al., 2015). In fat-1 transgenic mice, enhancement of the synthesis of endogenous ω-3 PUFAs from ω-6 PUFAs is found, which can delay the incidence of OA (Huang et al., 2014). EPA has been shown to reduce production of inflammatory cytokines induced by IL-1β in bovine chondrocytes (Zainal et al., 2009). EPA can also inhibit oxidative stress-induced human chondrocytes apoptosis and expression of MMP-3 and MMP-13. In addition, intra-articular injection of EPA prevented the progression of DMM-induced OA in mice by inhibiting chondrocytes apoptosis and MMP13 expression (Sakata et al., 2014). However, the underlying mechanisms for the effect of ω-3 PUFAs in OA warrant further investigation.

Recent studies indicating that ω-3 PUFAs can stimulate GPR120, one of the lipid sensing GPCRs (G-protein-coupled receptors) (Da Young Oh et al., 2010; Hirasawa et al., 2004). ω-3 PUFAs are shown to be the ligands for GPR120 and can exert broad anti-inflammatory effects in various macrophage types (Da Young Oh et al., 2010). The anti-inflammatory effects mediated by ω-3 PUFAs are abrogated by GPR120 knockdown (Da Young Oh et al., 2010). These results suggest that GPR120 acts as a receptor/sensor for the anti-inflammatory effect of ω-3 PUFAs. (**Figure 27**)

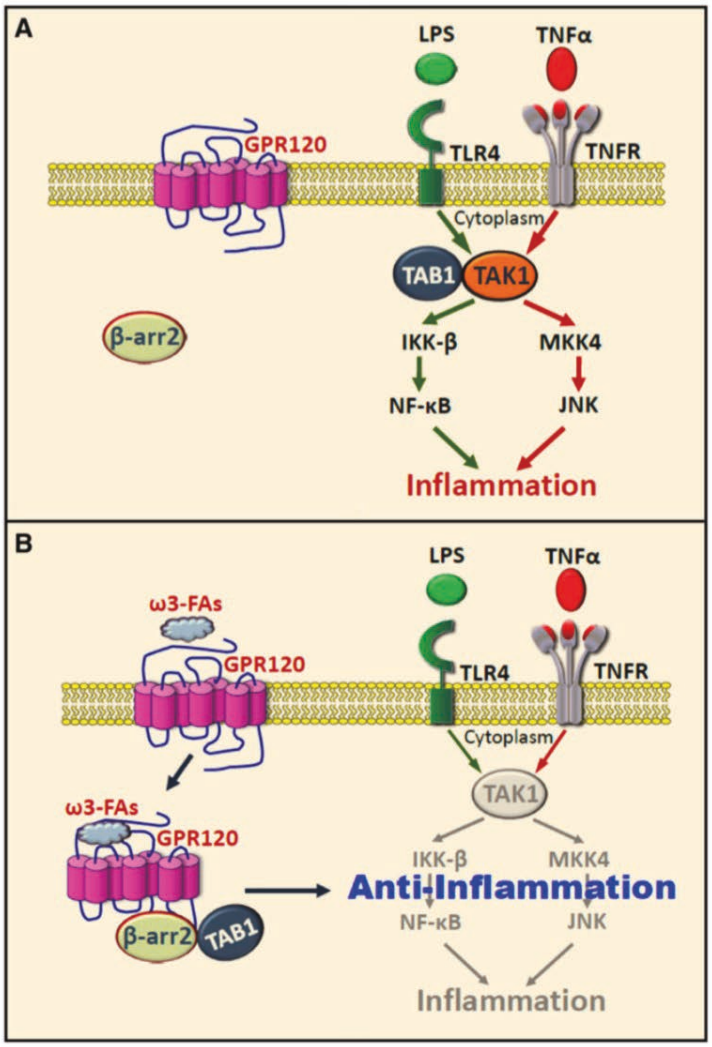

Figure 27 Omega-3 fatty acids and the GPR120 signaling pathway.
(Glass and Olefsky, 2012)

In this context, in order to verify whether the beneficial effect of EPA in the inflammatory and degenerative response induced by PA and high glucose is via GPRRs, we have tested the agonists and antagonists of GPR40 and GPR120 by evaluating the gene expression of COX-2. With the preliminary results, we can see a decrease in the expression of COX-2 mediated by TUG891 at 100 nM, suggesting that GPR120 may be the receptor for the anti-inflammatory effect of EPA. However, the concentration of AH7614 (inhibitor of GPR120) should be increased in further experiment (**Figure 28**).

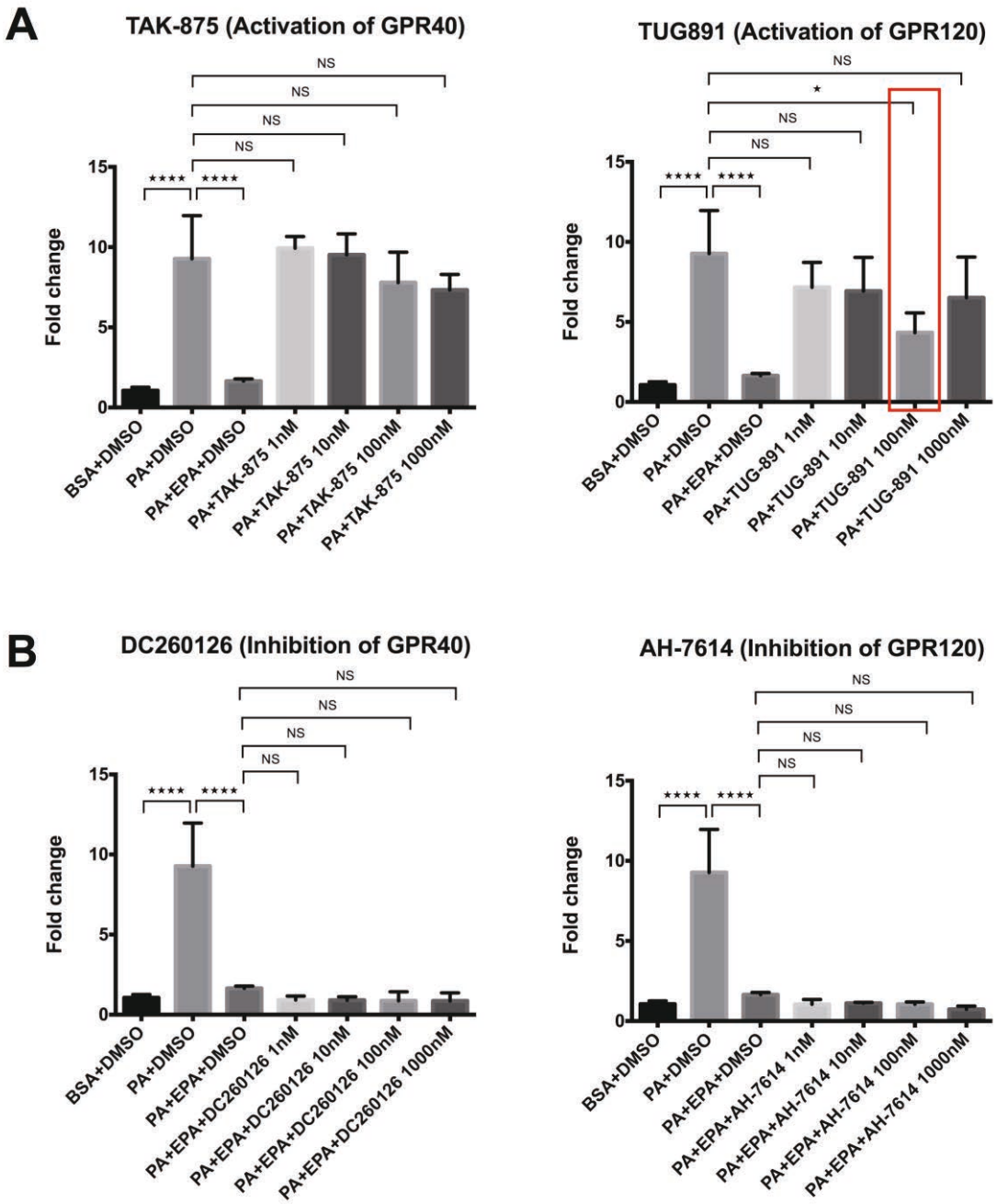

Figure 28 Effect of agonists and antagonists of GPR40 and GPR120 on the expression of COX-2 induced by palmitate and high glucose.

After exposure to high glucose for 72 hours, primary rat articular chondrocytes were treated with 0.1mM PA, 30uM EPA and increasing concentrations of agonists and antagonists of GPR40 and GPR120. (A) Effect of agonists and (B) Effect of antagonists on the expression of COX-2 was determined by qPCR.. Values are expressed as mean±SD. ★, $p<0.05$; ★★★★, $p<0.0001$.

II. Autophagy will be critical therapeutic target in OA?

Autophagy prevents aging-related OA

Autophagy is an important mechanism in normal adult articular cartilage for cellular homeostasis (Caramés et al., 2010). The superficial zone of cartilage shows the strongest signal of autophagy markers, including microtubule-associated protein light chain 3 (LC3), Beclin-1, and ULK1. During the aging process in mouse and human articular cartilage, there is a decreased expression of LC3, Beclin-1, and ULK1, accompanied by increased apoptosis (Caramés et al., 2010; Caramés et al., 2015; Hui et al., 2016). In addition, there is a progressive reduction in the expression of LC3 and concomitant increase in chondrocyte apoptosis and cartilage degradation in aged mice, suggesting a relationship between autophagy and cartilage degeneration (Caramés et al., 2015; Hui et al., 2016). Targeted deletion of the key autophagy marker ATG5 in chondrocytes promoted aging-related OA (Bouderlique et al., 2016). The researchers also found increased chondrocyte apoptosis in ATG5 KO mice, compared with controls (Bouderlique et al., 2016). These obeservational results in cartilage show that the basal autophagic activity decreases with age and may contribute to the increased susceptibility to aging-related OA (Duarte, 2015).

In the initial and early stages of OA, autophagy is increased in chondrocyte and cartilage with increased expression of LC3 and Beclin-1 (Sasaki et al., 2012). However, in late stage of OA, there is increased chondrocyte apoptosis and decreased expression of autophagy genes, including LC3, Beclin-1, ULK1 and ATG5 (Zhang et al., 2015). Conversely, the cell clusters in OA cartilage. The increased autophagy in early stage of OA upon response to mechanical or metabolic stress may repensent a protective and compensatory process, and the destructive damage will occur if the prolonged stress exceeds the capacity of this mechanism.

mTOR is a potential therapeutic target in OA

A key regulator of autophagy initiation is the mammalian target of rapamycin

(mTOR) (**Figure 29**). mTOR is overexpressed in human OA cartilage as well as mouse and dog experimental OA. Cartilage-specific ablation of mTOR resulted in increased autophagy and protected mice from DMM-induced OA associated with a significant reduction in cartilage degradation and apoptosis. Upregulation of mTOR expression resulted in reduced autophagy with increased chondrocyte apoptosis (Zhang et al., 2015). In contrast, chondrocyte specific deletion of ATG5 in mice showed increased chondrocyte apoptosis and acceleration of age-related OA (Bouderlique et al., 2016).

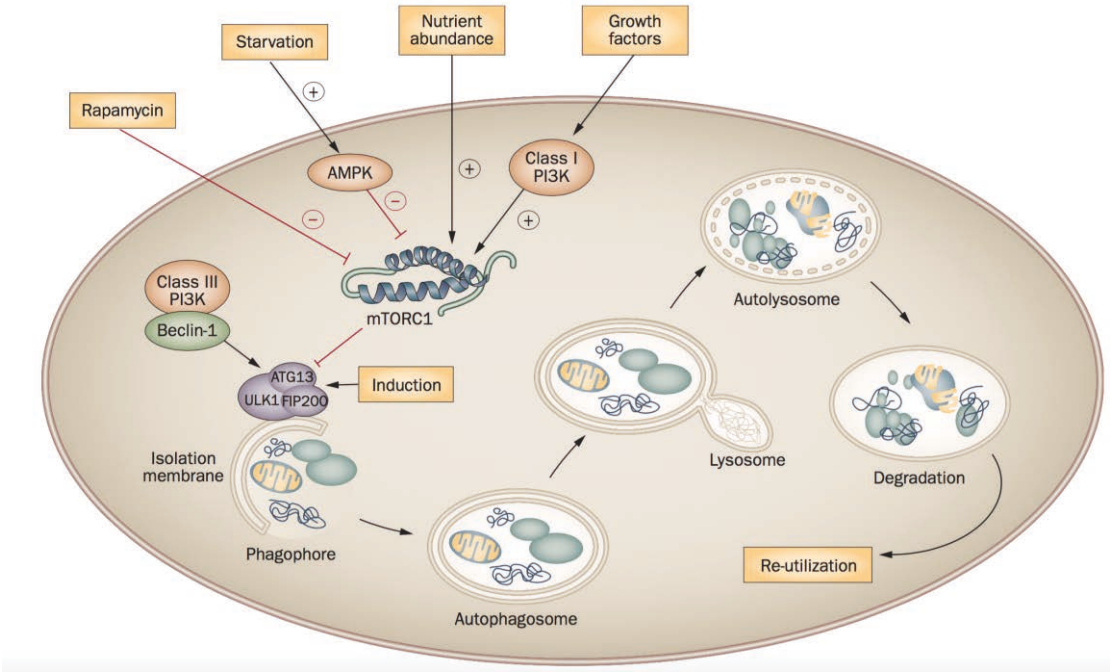

Figure 29 Regulation and execution of autophagy.
(Lotz and Caramés, 2011)

Rapamycin, an mTOR inhibitor and upstream regulators of the mTOR pathway, have been shown to activate autophagy in human chondrocytes and prevent the OA-like changes (Sasaki et al., 2012). In experimental OA mice, when rapamycin was intraperitoneally administered for 10 weeks, the severity of cartilage degradation was significantly reduced associated with a significant decrease in synovitis. Rapamycin treatment also maintained cartilage cellularity and decreased ADAMTS-5 and IL-1β expression in articular cartilage (Caramés et al., 2012). Similarly, local intra-articular

injection of rapamycin in the murine OA model could also significantly reduce the severity of articular degradation (Matsuzaki et al., 2014; Takayama et al., 2014). Reduced mTOR expression and the activation of LC3 was observed in the chondrocytes of rapamycin treated mice (Takayama et al., 2014). Hence, rapamycin could be a novel therapeutic approach for treating patients with OA.

In summary, articular chondrocytes in patients with OA showed inhibited autophagy compared to those of healthy individuals, contibuting directly to progression of OA.

References

Ackerman, I. N. and Osborne, R. H. (2012). Obesity and increased burden of hip and knee joint disease in Australia: results from a national survey. *BMC Musculoskeletal Disorders* **13**, 254.

Adirekkiat, S., Sumethkul, V., Ingsathit, A., Domrongkitchaiporn, S., Phakdeekitcharoen, B., Kantachuvesiri, S., Kitiyakara, C., Klyprayong, P. and Disthabanchong, S. (2010). Sodium thiosulfate delays the progression of coronary artery calcification in haemodialysis patients. *Nephrol. Dial. Transplant.* **25**, 1923–1929.

Akiyama, H., Chaboissier, M.-C., Martin, J. F., Schedl, A. and de Crombrugghe, B. (2002). The transcription factor Sox9 has essential roles in successive steps of the chondrocyte differentiation pathway and is required for expression of Sox5 and Sox6. *Genes Dev.* **16**, 2813–2828.

Al-Arfaj, A. S. (2003). Radiographic osteoarthritis and serum cholesterol. *Saudi Med J* **24**, 745–747.

Anders, H.-J. and Schaefer, L. (2014). Beyond tissue injury-damage-associated molecular patterns, toll-like receptors, and inflammasomes also drive regeneration and fibrosis. *J. Am. Soc. Nephrol.* **25**, 1387–1400.

Anderson, J. J. and FELSON, D. T. (1988). Factors associated with osteoarthritis of the knee in the first national Health and Nutrition Examination Survey (HANES I). Evidence for an association with overweight, race, and physical demands of work. *Am. J. Epidemiol.* **128**, 179–189.

Armani, A., Cinti, F., Marzolla, V., Morgan, J., Cranston, G. A., Antelmi, A., Carpinelli, G., Canese, R., Pagotto, U., Quarta, C., et al. (2014). Mineralocorticoid receptor antagonism induces browning of white adipose tissue through impairment of autophagy and prevents adipocyte dysfunction in high-fat-diet-fed mice. *FASEB J.* **28**, 3745–3757.

Atayde, S. A., Yoshinari, N. H., Nascimento, D. P., Catanozi, S., Andrade, P. C., Velosa, A. P. P., Parra, E. R., Passarelli, M., Nakandakare, E. R., Capelozzi, V. L., et al. (2012). Experimental diabetes modulates collagen remodelling of joints in rats. *Histol. Histopathol.* **27**, 1471–1479.

Bandyopadhyay, P. K., Garrett, J. E., Shetty, R. P., Keate, T., Walker, C. S. and Olivera, B. M. (2002). gamma -Glutamyl carboxylation: An extracellular posttranslational modification that antedates the divergence of molluscs, arthropods, and chordates. *Proc. Natl. Acad. Sci. U.S.A.* **99**, 1264–1269.

Bauersachs, J., Jaisser, F. and Toto, R. (2015). Mineralocorticoid receptor activation and mineralocorticoid receptor antagonist treatment in cardiac and renal diseases. *Hypertension* **65**, 257–263.

Behonick, D. J. and Werb, Z. (2003). A bit of give and take: the relationship between the extracellular matrix and the developing chondrocyte. *Mech. Dev.* **120**, 1327–1336.

Bene, N. C., Alcaide, P., Wortis, H. H. and Jaffe, I. Z. (2014). Mineralocorticoid receptors in immune cells: emerging role in cardiovascular disease. *Steroids* **91**, 38–45.

Bengtsson, T., Aszodi, A., Nicolae, C., Hunziker, E. B., Lundgren-Akerlund, E. and Fässler, R. (2005). Loss of alpha10beta1 integrin expression leads to moderate dysfunction of growth plate chondrocytes. *J. Cell. Sci.* **118**, 929–936.

Berenbaum, F. (2011). Diabetes-induced osteoarthritis: from a new paradigm to a new phenotype. *Ann. Rheum. Dis.* **70**, 1354–1356.

Berenbaum, F., Griffin, T. M. and Liu-Bryan, R. (2017). Review: Metabolic Regulation of Inflammation in Osteoarthritis. *Arthritis Rheumatol* **69**, 9–21.

Bernstein, P., Sticht, C., Jacobi, A., Liebers, C., Manthey, S. and Stiehler, M. (2010). Expression pattern differences between osteoarthritic chondrocytes and mesenchymal stem cells during chondrogenic differentiation. *Osteoarthritis and Cartilage* **18**, 1596–1607.

Bi, W., Deng, J. M., Zhang, Z., Behringer, R. R. and de Crombrugghe, B. (1999). Sox9 is required for cartilage formation. *Nat. Genet.* **22**, 85–89.

Bijlsma, J. W. J., Berenbaum, F. and Lafeber, F. P. J. G. (2011). Osteoarthritis: an update with relevance for clinical practice. *Lancet* **377**, 2115–2126.

Boden, G. (2011). Obesity, insulin resistance and free fatty acids. *Curr Opin Endocrinol Diabetes Obes* **18**, 139–143.

Bonafe, L., Cormier-Daire, V., Hall, C., Lachman, R., Mortier, G., Mundlos, S., Nishimura, G., Sangiorgi, L., Savarirayan, R., Sillence, D., et al. (2015). Nosology and classification of genetic skeletal disorders: 2015 revision. *Am. J. Med. Genet. A* **167A**, 2869–2892.

Bouderlique, T., Vuppalapati, K. K., Newton, P. T., Li, L., Barenius, B. and Chagin, A. S. (2016). Targeted deletion of Atg5 in chondrocytes promotes age-related osteoarthritis. *Ann. Rheum. Dis.* **75**, 627–631.

Briet, M. and Schiffrin, E. L. (2011). The role of aldosterone in the metabolic syndrome. *Curr. Hypertens. Rep.* **13**, 163–172.

Brown, N. J. (2013). Contribution of aldosterone to cardiovascular and renal inflammation and fibrosis. *Nature Publishing Group* 1–11.

Brucculeri, M., Cheigh, J., Bauer, G. and Serur, D. (2005). Long-term intravenous sodium thiosulfate in the treatment of a patient with calciphylaxis. *Semin Dial* **18**, 431–434.

Buchtova, M., Oralova, V., Aklian, A., Masek, J., Vesela, I., Ouyang, Z., Obadalova, T., Konecna, Z., Spoustova, T., Pospisilova, T., et al. (2015). Fibroblast growth factor and canonical WNT/β-catenin signaling cooperate in suppression of chondrocyte differentiation in experimental models of FGFR signaling in cartilage. *Biochim. Biophys. Acta* **1852**, 839–850.

Cabandugama, P. K., Gardner, M. J. and Sowers, J. R. (2017). The Renin Angiotensin Aldosterone System in Obesity and Hypertension: Roles in the Cardiorenal Metabolic Syndrome. *Med. Clin. North Am.* **101**, 129–137.

Cai, L., Okumu, F. W., Cleland, J. L., Beresini, M., Hogue, D., Lin, Z. and Filvaroff, E. H. (2002). A slow release formulation of insulin as a treatment for osteoarthritis. *Osteoarthritis and Cartilage* **10**, 692–706.

Calder, P. C. (2006). n-3 polyunsaturated fatty acids, inflammation, and inflammatory diseases. *Am. J. Clin. Nutr.* **83**, 1505S–1519S.

Caprio, M., Fève, B., Claës, A., Viengchareun, S., Lombès, M. and Zennaro, M.-C. (2007). Pivotal role of the mineralocorticoid receptor in corticosteroid-induced adipogenesis. *FASEB J.* **21**, 2185–2194.

Caramés, B., Hasegawa, A., Taniguchi, N., Miyaki, S., Blanco, F. J. and Lotz, M. (2012). Autophagy activation by rapamycin reduces severity of experimental osteoarthritis. *Ann. Rheum. Dis.* **71**, 575–581.

Caramés, B., Olmer, M., Kiosses, W. B. and Lotz, M. K. (2015). The Relationship of Autophagy Defects to Cartilage Damage During Joint Aging in a Mouse Model. *Arthritis & Rheumatology* **67**, 1568–1576.

Caramés, B., Taniguchi, N., Otsuki, S., Blanco, F. J. and Lotz, M. (2010). Autophagy is a protective mechanism in normal cartilage, and its aging-related loss is linked with cell death and osteoarthritis. *Arthritis Rheum.* **62**, 791–801.

Catena, C., Lapenna, R., Baroselli, S., Nadalini, E., Colussi, G., Novello, M., Favret, G., Melis, A., Cavarape, A. and Sechi, L. A. (2006). Insulin Sensitivity in Patients with Primary Aldosteronism: A Follow-Up Study. *J. Clin. Endocrinol. Metab.* **91**, 3457–3463.

Cavaco, S., Viegas, C. S. B., Rafael, M. S., Ramos, A., Magalhães, J., Blanco, F. J., Vermeer, C. and Simes, D. C. (2016). Gla-rich protein is involved in the

cross-talk between calcification and inflammation in osteoarthritis. *Cell. Mol. Life Sci.* **73**, 1051–1065.

Chen, J., Singh, K., Mukherjee, B. B. and Sodek, J. (1993). Developmental expression of osteopontin (OPN) mRNA in rat tissues: evidence for a role for OPN in bone formation and resorption. *Matrix* **13**, 113–123.

Chen, L., Adar, R., Yang, X., Monsonego, E. O., Li, C., Hauschka, P. V., Yayon, A. and Deng, C. X. (1999). Gly369Cys mutation in mouse FGFR3 causes achondroplasia by affecting both chondrogenesis and osteogenesis. *J. Clin. Invest.* **104**, 1517–1525.

Chen, L., Li, C., Qiao, W., Xu, X. and Deng, C. (2001). A Ser(365)-->Cys mutation of fibroblast growth factor receptor 3 in mouse downregulates Ihh/PTHrP signals and causes severe achondroplasia. *Human Molecular Genetics* **10**, 457–465.

Chen, Y. J., Sheu, M. L., Tsai, K. S., Yang, R. S. and Liu, S. H. (2013). Advanced glycation end products induce peroxisome proliferator-activated receptor γ down-regulation-related inflammatory signals in human chondrocytes via Toll-like receptor-4 and receptor for advanced glycation end products. *PLoS ONE* **8**, e66611.

Chowdhury, T. T., Arghandawi, S., Brand, J., Akanji, O. O., Bader, D. L., Salter, D. M. and Lee, D. A. (2008). Dynamic compression counteracts IL-1beta induced inducible nitric oxide synthase and cyclo-oxygenase-2 expression in chondrocyte/agarose constructs. *Arthritis Res. Ther.* **10**, R35.

Cicone, J. S., Petronis, J. B., Embert, C. D. and Spector, D. A. (2004). Successful treatment of calciphylaxis with intravenous sodium thiosulfate. *Am. J. Kidney Dis.* **43**, 1104–1108.

Cillero-Pastor, B., Eijkel, G., Kiss, A., Blanco, F. J. and Heeren, R. M. A. (2012). Time-of-flight secondary ion mass spectrometry-based molecular distribution distinguishing healthy and osteoarthritic human cartilage. *Anal. Chem.* **84**, 8909–8916.

Cimmino, M. A. and Cutolo, M. (1990). Plasma glucose concentration in symptomatic osteoarthritis: a clinical and epidemiological survey. *Clin. Exp. Rheumatol.* **8**, 251–257.

Cinque, L., Forrester, A., Bartolomeo, R., Svelto, M., Venditti, R., Montefusco, S., Polishchuk, E., Nusco, E., Rossi, A., Medina, D. L., et al. (2015). FGF signalling regulates bone growth through autophagy. *Nature* **528**, 272–275.

Collin, M., Niemann, F. and Jaisser, F. (2014). Mineralocorticoid receptor modulators: a patent review (2007 - 2012). *Expert Opin Ther Pat* **24**, 177–183.

Collins-Racie, L. A., Yang, Z., Arai, M., Li, N., Majumdar, M. K., Nagpal, S., Mounts, W. M., Dorner, A. J., Morris, E. and LaVallie, E. R. (2009). Global analysis of nuclear receptor expression and dysregulation in human osteoarthritic articular cartilage: reduced LXR signaling contributes to catabolic metabolism typical of osteoarthritis. *Osteoarthritis and Cartilage* **17**, 832–842.

Colvin, J. S., Bohne, B. A., Harding, G. W., McEwen, D. G. and Ornitz, D. M. (1996). Skeletal overgrowth and deafness in mice lacking fibroblast growth factor receptor 3. *Nat. Genet.* **12**, 390–397.

Courties, A., Gualillo, O., Berenbaum, F. and Sellam, J. (2015). Metabolic stress-induced joint inflammation and osteoarthritis. *Osteoarthritis and Cartilage* **23**, 1955–1965.

CRANENBURG, E. C. M., van SPAENDONCK-ZWARTS, K. Y., BONAFE, L., MITTAZ CRETTOL, L., RÖDIGER, L. A., DIKKERS, F. G., van ESSEN, A. J., SUPERTI-FURGA, A., ALEXANDRAKIS, E., Vermeer, C., et al. (2011). Circulating matrix γ-carboxyglutamate protein (MGP) species are refractory to vitamin K treatment in a new case of Keutel syndrome. *J. Thromb. Haemost.* **9**, 1225–1235.

Da Young Oh, Talukdar, S., Bae, E. J., Imamura, T., Morinaga, H., Fan, W., Li, P., Lu, W. J., Watkins, S. M. and Olefsky, J. M. (2010). GPR120 Is an Omega-3 Fatty Acid Receptor Mediating Potent Anti-inflammatory and Insulin-Sensitizing Effects. *Cell* **142**, 687–698.

Das, U. N. (2016). Renin-angiotensin-aldosterone system in insulin resistance and metabolic syndrome. *J Transl Int Med* **4**, 66–72.

Davies-Tuck, M. L., Hanna, F., Davis, S. R., Bell, R. J., Davison, S. L., Wluka, A. E., Adams, J. and Cicuttini, F. M. (2009). Total cholesterol and triglycerides are associated with the development of new bone marrow lesions in asymptomatic middle-aged women - a prospective cohort study. *Arthritis Res. Ther.* **11**, R181.

de Frutos, C. A., Vega, S., Manzanares, M., Flores, J. M., Huertas, H., Martínez-Frías, M. L. and Nieto, M. A. (2007). Snail1 is a transcriptional effector of FGFR3 signaling during chondrogenesis and achondroplasias. *Dev. Cell* **13**, 872–883.

Deng, C., Wynshaw-Boris, A., Zhou, F., Kuo, A. and Leder, P. (1996). Fibroblast growth factor receptor 3 is a negative regulator of bone growth. *Cell* **84**, 911–921.

Di Giuseppe, D., Wallin, A., Bottai, M., Askling, J. and Wolk, A. (2014). Long-term intake of dietary long-chain n-3 polyunsaturated fatty acids and risk of

rheumatoid arthritis: a prospective cohort study of women. *Ann. Rheum. Dis.* **73**, 1949–1953.

Divoux, A. and Clément, K. (2011). Architecture and the extracellular matrix: the still unappreciated components of the adipose tissue. *Obesity Reviews* **12**, e494–e503.

Duarte, J. H. (2015). Osteoarthritis: Autophagy prevents age-related OA. *Nature Publishing Group* 1–1.

Dy, P., Wang, W., Bhattaram, P., Wang, Q., Wang, L., Ballock, R. T. and Lefebvre, V. (2012). Sox9 directs hypertrophic maturation and blocks osteoblast differentiation of growth plate chondrocytes. *Dev. Cell* **22**, 597–609.

Eitzinger, N., Surmann-Schmitt, C., Bösl, M., Schett, G., Engelke, K., Hess, A., Mark, von der, K. and Stock, M. (2012). Ucma is not necessary for normal development of the mouse skeleton. *Bone* **50**, 670–680.

El-Maadawy, S., Kaartinen, M. T., Schinke, T., Murshed, M., Karsenty, G. and McKee, M. D. (2003). Cartilage formation and calcification in arteries of mice lacking matrix Gla protein. *Connect. Tissue Res.* **44 Suppl 1**, 272–278.

Ellison, E. H. and Castellino, F. J. (1998). Adsorption of vitamin K-dependent blood coagulation proteins to spread phospholipid monolayers as determined from combined measurements of the surface pressure and surface protein concentration. *Biochemistry* **37**, 7997–8003.

Elsaman, A. M., Radwan, A. R., Mohammed, W. I. and Ohrndorf, S. (2016). Low-dose Spironolactone: Treatment for Osteoarthritis-related Knee Effusion. A Prospective Clinical and Sonographic-based Study. *J. Rheumatol.* **43**, 1114–1120.

Engström, G., Gerhardsson de Verdier, M., Rollof, J., Nilsson, P. M. and Lohmander, L. S. (2009). C-reactive protein, metabolic syndrome and incidence of severe hip and knee osteoarthritis. A population-based cohort study. *Osteoarthritis and Cartilage* **17**, 168–173.

Even, S. E. L., Dulak-Lis, M. G., Touyz, R. M. and Dinh Cat, A. N. (2014). Abstract. *Hormone Molecular Biology and Clinical Investigation* **19**, 1–14.

Eymard, F., Parsons, C., Edwards, M. H., Petit-Dop, F., Reginster, J. Y., Bruyère, O., Richette, P., Cooper, C. and Chevalier, X. (2015). Diabetes is a risk factor for knee osteoarthritis progression. *Osteoarthritis and Cartilage* **23**, 851–859.

Farnaghi, S., Crawford, R., Xiao, Y. and Prasadam, I. (2017). Cholesterol metabolism in pathogenesis of osteoarthritis disease. *Int J Rheum Dis*.

Fellmann, L., Nascimento, A. R., Tibiriça, E. and Bousquet, P. (2013). Murine models for pharmacological studies of the metabolic syndrome. *Pharmacology and Therapeutics* **137**, 331–340.

FELSON, D. T., Anderson, J. J., Naimark, A., Walker, A. M. and Meenan, R. F. (1988). Obesity and knee osteoarthritis. The Framingham Study. *Ann. Intern. Med.* **109**, 18–24.

Felson, D. T., Goggins, J., Niu, J., Zhang, Y. and Hunter, D. J. (2004). The effect of body weight on progression of knee osteoarthritis is dependent on alignment. *Arthritis Rheum.* **50**, 3904–3909.

Fernandes, C., Maynard, B. and Hanna, D. (2014). Successful treatment of calciphylaxis with intravenous sodium thiosulfate in a nonuremic patient: case report and review of therapy side effects. *J Cutan Med Surg* **18**, 356–360.

Feteih, R., Tassinari, M. S. and Lian, J. B. (1990). Effect of sodium warfarin on vitamin K-dependent proteins and skeletal development in the rat fetus. *J. Bone Miner. Res.* **5**, 885–894.

Fitzgerald, J. B., Jin, M., Chai, D. H., Siparsky, P., Fanning, P. and Grodzinsky, A. J. (2008). Shear- and compression-induced chondrocyte transcription requires MAPK activation in cartilage explants. *Journal of Biological Chemistry* **283**, 6735–6743.

Franke, S., Sommer, M., Rüster, C., Bondeva, T., Marticke, J., Hofmann, G., Hein, G. and Wolf, G. (2009). Advanced glycation end products induce cell cycle arrest and proinflammatory changes in osteoarthritic fibroblast-like synovial cells. *Arthritis Res. Ther.* **11**, R136.

Fraser, J. D. and Price, P. A. (1988). Lung, heart, and kidney express high levels of mRNA for the vitamin K-dependent matrix Gla protein. Implications for the possible functions of matrix Gla protein and for the tissue distribution of the gamma-carboxylase. *Journal of Biological Chemistry* **263**, 11033–11036.

Frey, N., Hügle, T., Jick, S. S., Meier, C. R. and Spoendlin, J. (2016). Type II diabetes mellitus and incident osteoarthritis of the hand: a population-based case-control analysis. *Osteoarthritis and Cartilage* **24**, 1535–1540.

Fryns, J. P., van Fleteren, A., Mattelaer, P. and van den Berghe, H. (1984). Calcification of cartilages, brachytelephalangy and peripheral pulmonary stenosis. Confirmation of the Keutel syndrome. *Eur. J. Pediatr.* **142**, 201–203.

Garessus, E. D. G., de Mutsert, R., Visser, A. W., Rosendaal, F. R. and Kloppenburg, M. (2016). No association between impaired glucose metabolism and osteoarthritis. *Osteoarthritis and Cartilage* **24**, 1541–1547.

Garg, R. and Adler, G. K. (2012). Role of mineralocorticoid receptor in insulin resistance. *Current Opinion in Endocrinology & Diabetes and Obesity* **19**, 168–175.

Gerber, H. P., Vu, T. H., Ryan, A. M., Kowalski, J., Werb, Z. and Ferrara, N. (1999). VEGF couples hypertrophic cartilage remodeling, ossification and angiogenesis during endochondral bone formation. *Nat. Med.* **5**, 623–628.

Gheduzzi, D., Boraldi, F., Annovi, G., DeVincenzi, C. P., Schurgers, L. J., Vermeer, C., Quaglino, D. and Ronchetti, I. P. (2007). Matrix Gla protein is involved in elastic fiber calcification in the dermis of pseudoxanthoma elasticum patients. *Lab. Invest.* **87**, 998–1008.

Giacchetti, G., Ronconi, V., Turchi, F., Agostinelli, L., Mantero, F., Rilli, S. and Boscaro, M. (2007). Aldosterone as a key mediator of the cardiometabolic syndrome in primary aldosteronism: an observational study. *J. Hypertens.* **25**, 177–186.

Glass, C. K. and Olefsky, J. M. (2012). Inflammation and Lipid Signaling in the Etiology of Insulin Resistance. *Cell Metabolism* **15**, 635–645.

Gomez, R., Lago, F., Gomez-Reino, J., Dieguez, C. and Gualillo, O. (2009). Adipokines in the skeleton: influence on cartilage function and joint degenerative diseases. *J. Mol. Endocrinol.* **43**, 11–18.

Gosset, M., Berenbaum, F., Levy, A., Pigenet, A., Thirion, S., Saffar, J.-L. and Jacques, C. (2006). Prostaglandin E2 synthesis in cartilage explants under compression: mPGES-1 is a mechanosensitive gene. *Arthritis Res. Ther.* **8**, R135.

Gosset, M., Berenbaum, F., Thirion, S. and Jacques, C. (2008). Primary culture and phenotyping of murine chondrocytes. *Nat Protoc* **3**, 1253–1260.

Gröber, U., Reichrath, J., Holick, M. F. and Kisters, K. (2014). Vitamin K: an old vitamin in a new perspective. *Dermatoendocrinol* **6**, e968490.

Guo, C., Ricchiuti, V., Lian, B. Q., Yao, T. M., Coutinho, P., Romero, J. R., Li, J., Williams, G. H. and Adler, G. K. (2008). Mineralocorticoid receptor blockade reverses obesity-related changes in expression of adiponectin, peroxisome proliferator-activated receptor-gamma, and proinflammatory adipokines. *Circulation* **117**, 2253–2261.

Gupta, S., Knight, A. G., Gupta, S., Keller, J. N. and Bruce-Keller, A. J. (2012). Saturated long-chain fatty acids activate inflammatory signaling in astrocytes. *J. Neurochem.* **120**, 1060–1071.

Hackeng, T. M., Rosing, J., Spronk, H. M. and Vermeer, C. (2001). Total chemical synthesis of human matrix Gla protein. *Protein Sci.* **10**, 864–870.

Hale, J. E., Fraser, J. D. and Price, P. A. (1988). The identification of matrix Gla protein in cartilage. *Journal of Biological Chemistry* **263**, 5820–5824.

Hardin, J. A., Cobelli, N. and Santambrogio, L. (2015). Consequences of metabolic and oxidative modifications of cartilage tissue. *Nat Rev Rheumatol* **11**, 521–529.

Hart, D. J., Doyle, D. V. and Spector, T. D. (1995). Association between metabolic factors and knee osteoarthritis in women: the Chingford Study. *J. Rheumatol.* **22**, 1118–1123.

Håversen, L., Danielsson, K. N., Fogelstrand, L. and Wiklund, O. (2009). Induction of proinflammatory cytokines by long-chain saturated fatty acids in human macrophages. *Atherosclerosis* **202**, 382–393.

Henrotin, Y. E., Bruckner, P. and Pujol, J. P. L. (2003). The role of reactive oxygen species in homeostasis and degradation of cartilage. *Osteoarthritis and Cartilage* **11**, 747–755.

Hill, C. L., March, L. M., Aitken, D., Lester, S. E., Battersby, R., Hynes, K., Fedorova, T., Proudman, S. M., James, M., Cleland, L. G., et al. (2016). Fish oil in knee osteoarthritis: a randomised clinical trial of low dose versus high dose. *Ann. Rheum. Dis.* **75**, 23–29.

Hirabara, S. M., Curi, R. and Maechler, P. (2010). Saturated fatty acid-induced insulin resistance is associated with mitochondrial dysfunction in skeletal muscle cells. *J. Cell. Physiol.* **222**, 187–194.

Hirasawa, A., Tsumaya, K., Awaji, T., Katsuma, S., Adachi, T., Yamada, M., Sugimoto, Y., Miyazaki, S. and Tsujimoto, G. (2004). Free fatty acids regulate gut incretin glucagon-like peptide-1 secretion through GPR120. *Nat. Med.* **11**, 90–94.

Hirata, A., Maeda, N., Hiuge, A., Hibuse, T., Fujita, K., Okada, T., Kihara, S., Funahashi, T. and Shimomura, I. (2009). Blockade of mineralocorticoid receptor reverses adipocyte dysfunction and insulin resistance in obese mice. *Cardiovasc. Res.* **84**, 164–172.

Horton, W. A., Hall, J. G. and Hecht, J. T. (2007). Achondroplasia. *Lancet* **370**, 162–172.

Howe, A. M. and Webster, W. S. (1992). The warfarin embryopathy: a rat model showing maxillonasal hypoplasia and other skeletal disturbances. *Teratology* **46**, 379–390.

Huang, M.-J., Wang, L., Jin, D.-D., Zhang, Z.-M., Chen, T.-Y., Jia, C.-H., Wang, Y., Zhen, X.-C., Huang, B., Yan, B., et al. (2014). Enhancement of the synthesis

of n-3 PUFAs in fat-1 transgenic mice inhibits mTORC1 signalling and delays surgically induced osteoarthritis in comparison with wild-type mice. *Ann. Rheum. Dis.* **73**, 1719–1727.

Hui, W., Young, D. A., Rowan, A. D., Xu, X., Cawston, T. E. and Proctor, C. J. (2016). Oxidative changes and signalling pathways are pivotal in initiating age-related changes in articular cartilage. *Ann. Rheum. Dis.* **75**, 449–458.

Hur, D. J., Raymond, G. V., Kahler, S. G., Riegert-Johnson, D. L., Cohen, B. A. and Boyadjiev, S. A. (2005). A novel MGP mutation in a consanguineous family: review of the clinical and molecular characteristics of Keutel syndrome. *Am. J. Med. Genet. A* **135**, 36–40.

Imhof, H., Sulzbacher, I., Grampp, S., Czerny, C., Youssefzadeh, S. and Kainberger, F. (2000). Subchondral bone and cartilage disease: a rediscovered functional unit. *Invest Radiol* **35**, 581–588.

Inada, M., Wang, Y., Byrne, M. H., Rahman, M. U., Miyaura, C., López-Otín, C. and Krane, S. M. (2004). Critical roles for collagenase-3 (Mmp13) in development of growth plate cartilage and in endochondral ossification. *Proc. Natl. Acad. Sci. U.S.A.* **101**, 17192–17197.

Iraqi, W., Rossignol, P., Angioi, M., Fay, R., Nuee, J., Ketelslegers, J. M., Vincent, J., Pitt, B. and Zannad, F. (2009). Extracellular Cardiac Matrix Biomarkers in Patients With Acute Myocardial Infarction Complicated by Left Ventricular Dysfunction and Heart Failure: Insights From the Eplerenone Post-Acute Myocardial Infarction Heart Failure Efficacy and Survival Study (EPHESUS) Study. *Circulation* **119**, 2471–2479.

Iwata, T., Chen, L., Li, C., Ovchinnikov, D. A., Behringer, R. R., Francomano, C. A. and Deng, C. X. (2000). A neonatal lethal mutation in FGFR3 uncouples proliferation and differentiation of growth plate chondrocytes in embryos. *Human Molecular Genetics* **9**, 1603–1613.

Jaisser, F. and Farman, N. (2016). Emerging Roles of the Mineralocorticoid Receptor in Pathology: Toward New Paradigms in Clinical Pharmacology. *Pharmacol. Rev.* **68**, 49–75.

Kaartinen, M. T., Murshed, M., Karsenty, G. and McKee, M. D. (2007). Osteopontin upregulation and polymerization by transglutaminase 2 in calcified arteries of Matrix Gla protein-deficient mice. *J. Histochem. Cytochem.* **55**, 375–386.

Karpe, F., Dickmann, J. R. and Frayn, K. N. (2011). Fatty acids, obesity, and insulin resistance: time for a reevaluation. *Diabetes* **60**, 2441–2449.

Kasal, D. A. B. and Schiffrin, E. L. (2012). Angiotensin II, Aldosterone, and Anti-Inflammatory Lymphocytes: Interplay and Therapeutic Opportunities. *Int J Hypertens* **2012**, 829786–5.

Kasal, D. A., Barhoumi, T., Li, M. W., Yamamoto, N., Zdanovich, E., Rehman, A., Neves, M. F., Laurant, P., Paradis, P. and Schiffrin, E. L. (2012). T regulatory lymphocytes prevent aldosterone-induced vascular injury. *Hypertension* **59**, 324–330.

Keutel, J., Jörgensen, G. and Gabriel, P. (1971). [A new autosomal-recessive hereditary syndrome. Multiple peripheral pulmonary stenosis, brachytelephalangia, inner-ear deafness, ossification or calcification of cartilages]. *Dtsch. Med. Wochenschr.* **96**, 1676–81 passim.

Khosroshahi, H. E., Sahin, S. C., Akyuz, Y. and Ede, H. (2014). Long term follow-up of four patients with Keutel syndrome. *Am. J. Med. Genet. A* **164A**, 2849–2856.

Klionsky, D. J., Abdelmohsen, K., Abe, A., Abedin, M. J., Abeliovich, H., Acevedo Arozena, A., Adachi, H., Adams, C. M., Adams, P. D., Adeli, K., et al. (2016). Guidelines for the use and interpretation of assays for monitoring autophagy (3rd edition). *Autophagy* **12**, 1–222.

Ko, F. C., Dragomir, C., Plumb, D. A., Goldring, S. R., Wright, T. M., Goldring, M. B. and van der Meulen, M. C. H. (2013). In vivo cyclic compression causes cartilage degeneration and subchondral bone changes in mouse tibiae. *Arthritis Rheum.* **65**, 1569–1578.

Kolkhof, P. and Borden, S. A. (2012). Molecular pharmacology of the mineralocorticoid receptor: prospects for novel therapeutics. *Mol. Cell. Endocrinol.* **350**, 310–317.

Kolkhof, P., Delbeck, M., Kretschmer, A., Steinke, W., Hartmann, E., Bärfacker, L., Eitner, F., Albrecht-Küpper, B. and Schäfer, S. (2014). Finerenone, a novel selective nonsteroidal mineralocorticoid receptor antagonist protects from rat cardiorenal injury. *J. Cardiovasc. Pharmacol.* **64**, 69–78.

Kozhemyakina, E., Lassar, A. B. and Zelzer, E. (2015). A pathway to bone: signaling molecules and transcription factors involved in chondrocyte development and maturation. *Development* **142**, 817–831.

Krakow, D. (2015). Skeletal dysplasias. *Clin Perinatol* **42**, 301–19– viii.

Krakow, D. and Rimoin, D. L. (2010). The skeletal dysplasias. *Genet. Med.* **12**, 327–341.

Krejci, P., Aklian, A., Kaucka, M., Sevcikova, E., Prochazkova, J., Masek, J. K., Mikolka, P., Pospisilova, T., Spoustova, T., Weis, M., et al. (2012). Receptor tyrosine kinases activate canonical WNT/β-catenin signaling via MAP kinase/LRP6 pathway and direct β-catenin phosphorylation. *PLoS ONE* **7**, e35826.

Kulman, J. D., Harris, J. E., Haldeman, B. A. and Davie, E. W. (1997). Primary structure and tissue distribution of two novel proline-rich gamma-carboxyglutamic acid proteins. *Proc. Natl. Acad. Sci. U.S.A.* **94**, 9058–9062.

Kumagai, E., Adachi, H., Jacobs, D. R., Hirai, Y., Enomoto, M., Fukami, A., Otsuka, M., Kumagae, S. I., Nanjo, Y., Yoshikawa, K., et al. (2011). Plasma Aldosterone Levels and Development of Insulin Resistance: Prospective Study in a General Population. *Hypertension* **58**, 1043–1048.

Laiguillon, M. C., Courties, A., Houard, X., Auclair, M., Sautet, A., Capeau, J., Fève, B., Berenbaum, F. and Sellam, J. (2015). Characterization of diabetic osteoarthritic cartilage and role of high glucose environment on chondrocyte activation: toward pathophysiological delineation of diabetes mellitus-related osteoarthritis. *Osteoarthritis and Cartilage* **23**, 1513–1522.

Legeai-Mallet, L., Benoist-Lasselin, C., Munnich, A. and Bonaventure, J. (2004). Overexpression of FGFR3, Stat1, Stat5 and p21Cip1 correlates with phenotypic severity and defective chondrocyte differentiation in FGFR3-related chondrodysplasias. *Bone* **34**, 26–36.

Lentini, S., Heinig, R., Kimmeskamp-Kirschbaum, N. and Wensing, G. (2016). Pharmacokinetics, safety and tolerability of the novel, selective mineralocorticoid receptor antagonist finerenone - results from first-in-man and relative bioavailability studies. *Fundam Clin Pharmacol* **30**, 172–184.

Leroux-Berger, M., Queguiner, I., Maciel, T. T., Ho, A., Relaix, F. and Kempf, H. (2011). Pathologic calcification of adult vascular smooth muscle cells differs on their crest or mesodermal embryonic origin. *J. Bone Miner. Res.* **26**, 1543–1553.

Leung, V. Y. L., Gao, B., Leung, K. K. H., Melhado, I. G., Wynn, S. L., Au, T. Y. K., Dung, N. W. F., Lau, J. Y. B., Mak, A. C. Y., Chan, D., et al. (2011). SOX9 governs differentiation stage-specific gene expression in growth plate chondrocytes via direct concomitant transactivation and repression. *PLoS Genet.* **7**, e1002356.

Leyland, K. M., Judge, A., Javaid, M. K., Diez-Perez, A., Carr, A., Cooper, C., Arden, N. K. and Prieto-Alhambra, D. (2016). Obesity and the Relative Risk of Knee Replacement Surgery in Patients With Knee Osteoarthritis: A Prospective Cohort Study. *Arthritis Rheumatol* **68**, 817–825.

Li, C., Chen, L., Iwata, T., Kitagawa, M., Fu, X. Y. and Deng, C. X. (1999). A Lys644Glu substitution in fibroblast growth factor receptor 3 (FGFR3) causes dwarfism in mice by activation of STATs and ink4 cell cycle inhibitors. *Human Molecular Genetics* **8**, 35–44.

Li, M., Seki, Y., Freitas, P. H. L., Nagata, M., Kojima, T., Sultana, S., Ubaidus, S., Maeda, T., Shimomura, J., Henderson, J. E., et al. (2010). FGFR3 down-regulates PTH/PTHrP receptor gene expression by mediating JAK/STAT signaling in chondrocytic cell line. *J Electron Microsc (Tokyo)* **59**, 227–236.

Liu, J., Liu, T., Zheng, Y., Zhao, Z., Liu, Y., Cheng, H., Luo, S. and Chen, Y. (2006). Early responses of osteoblast-like cells to different mechanical signals through various signaling pathways. *Biochem. Biophys. Res. Commun.* **348**, 1167–1173.

Lotz, M. K. and Caramés, B. (2011). Autophagy and cartilage homeostasis mechanisms in joint health, aging and OA. *Nature Publishing Group* **7**, 579–587.

Louati, K., Vidal, C., Berenbaum, F. and Sellam, J. (2015). Association between diabetes mellitus and osteoarthritis: systematic literature review and meta-analysis. *RMD Open* **1**, e000077.

Luo, G., D'Souza, R., Hogue, D. and Karsenty, G. (1995). The matrix Gla protein gene is a marker of the chondrogenesis cell lineage during mouse development. *J. Bone Miner. Res.* **10**, 325–334.

Luo, G., Ducy, P., McKee, M. D., Pinero, G. J., Loyer, E., Behringer, R. R. and Karsenty, G. (1997). Spontaneous calcification of arteries and cartilage in mice lacking matrix GLA protein. *Nature* **386**, 78–81.

Maes, C., Kobayashi, T., Selig, M. K., Torrekens, S., Roth, S. I., Mackem, S., Carmeliet, G. and Kronenberg, H. M. (2010). Osteoblast precursors, but not mature osteoblasts, move into developing and fractured bones along with invading blood vessels. *Dev. Cell* **19**, 329–344.

Magnusson, K., Hagen, K. B., Østerås, N., Nordsletten, L., Natvig, B. and Haugen, I. K. (2015). Diabetes is associated with increased hand pain in erosive hand osteoarthritis: data from a population-based study. *Arthritis Care Res (Hoboken)* **67**, 187–195.

Marchini, A., Ogata, T. and Rappold, G. A. (2016). A Track Record on SHOX: From Basic Research to Complex Models and Therapy. *Endocr. Rev.* **37**, 417–448.

Maron, B. A., Oldham, W. M., Chan, S. Y., Vargas, S. O., Arons, E., Zhang, Y.-Y., Loscalzo, J. and Leopold, J. A. (2014). Upregulation of steroidogenic acute regulatory protein by hypoxia stimulates aldosterone synthesis in

pulmonary artery endothelial cells to promote pulmonary vascular fibrosis. *Circulation* **130**, 168–179.

Marulanda, J., Eimar, H., McKee, M. D., Berkvens, M., Nelea, V., Roman, H., Borrás, T., Tamimi, F., Ferron, M. and Murshed, M. (2017). Matrix Gla Protein Deficiency Impairs Nasal Septum Growth Causing Midface Hypoplasia. *J. Biol. Chem.* jbc.M116.769802.

Marzolla, V., Armani, A., Feraco, A., De Martino, M. U., Fabbri, A., Rosano, G. and Caprio, M. (2014). Mineralocorticoid receptor in adipocytes and macrophages: a promising target to fight metabolic syndrome. *Steroids* **91**, 46–53.

Matsuzaki, T., Matsushita, T., Tabata, Y., Saito, T., Matsumoto, T., Nagai, K., Kuroda, R. and Kurosaka, M. (2014). Intra-articular administration of gelatin hydrogels incorporating rapamycin-micelles reduces the development of experimental osteoarthritis in a murine model. *Biomaterials* **35**, 9904–9911.

Mayyas, F., Alzoubi, K. H. and Van Wagoner, D. R. (2013). Impact of aldosterone antagonists on the substrate for atrial fibrillation: Aldosterone promotes oxidative stress and atrial structural/electrical remodeling. *International Journal of Cardiology* 1–8.

Mcmurdo, M. E. T., Sumukadas, D., Donnan, P. T., Cvoro, V., Rauchhaus, P., Argo, I., Waldie, H., Littleford, R., Struthers, A. D. and Witham, M. D. (2016). Spironolactone for People Age 70 Years and Older With Osteoarthritic Knee Pain: A Proof-of-Concept Trial. *Arthritis Care Res (Hoboken)* **68**, 716–721.

MD, Y. H., MD, S. D., PhD, S. W. K., MD, T. L. G. and MD, B. F. (2012). Aldosterone and aldosterone: renin ratio associations with insulin resistance and blood pressure in African Americans. *Journal of the American Society of Hypertension* **6**, 56–65.

Meier, M., Weng, L. P., ALEXANDRAKIS, E., Rüschoff, J. and Goeckenjan, G. (2001). Tracheobronchial stenosis in Keutel syndrome. *Eur. Respir. J.* **17**, 566–569.

Meissner, M., Bauer, R., Beier, C., Betz, C., Wolter, M., Kaufmann, R. and Gille, J. (2006). Sodium thiosulphate as a promising therapeutic option to treat calciphylaxis. *Dermatology (Basel)* **212**, 373–376.

Ménard, J. (2004). The 45-year story of the development of an anti-aldosterone more specific than spironolactone. *Mol. Cell. Endocrinol.* **217**, 45–52.

Michl, G. L., Katz, J. N. and Losina, E. (2016). Risk and risk perception of knee osteoarthritis in the US: a population-based study. *Osteoarthritis and Cartilage* **24**, 593–596.

Mitts, T. F., Bunda, S., Wang, Y. and Hinek, A. (2010). Aldosterone and Mineralocorticoid Receptor Antagonists Modulate Elastin and Collagen Deposition in Human Skin. **130**, 2396–2406.

Mizushima, N. and Komatsu, M. (2011). Autophagy: renovation of cells and tissues. *Cell* **147**, 728–741.

Monira Hussain, S., Wang, Y., Cicuttini, F. M., Simpson, J. A., Giles, G. G., Graves, S. and Wluka, A. E. (2014). Incidence of total knee and hip replacement for osteoarthritis in relation to the metabolic syndrome and its components: a prospective cohort study. *Semin. Arthritis Rheum.* **43**, 429–436.

Mosso, L. M., Carvajal, C. A., Maiz, A., Ortiz, E. H., Castillo, C. R., Artigas, R. A. and Fardella, C. E. (2007). A possible association between primary aldosteronism and a lower beta-cell function. *J. Hypertens.* **25**, 2125–2130.

MS, A. V.-R. M., MD, V. S., MD, M. E., MD, R. G. T., MD, E. A. C., MD, N. A. P. F., BS, I. F.-C. and MD, M. M. (2014). Spironolactone to Prevent Peritoneal Fibrosis in Peritoneal Dialysis Patients: A Randomized Controlled Trial. *American Journal of Kidney Diseases* 1–2.

Munroe, P. B., Olgunturk, R. O., Fryns, J. P., Van Maldergem, L., Ziereisen, F., Yuksel, B., Gardiner, R. M. and Chung, E. (1999). Mutations in the gene encoding the human matrix Gla protein cause Keutel syndrome. *Nat. Genet.* **21**, 142–144.

Murshed, M., Schinke, T., McKee, M. D. and Karsenty, G. (2004). Extracellular matrix mineralization is regulated locally; different roles of two gla-containing proteins. *J. Cell Biol.* **165**, 625–630.

Musani, S. K., Vasan, R. S., Bidulescu, A., Liu, J., Xanthakis, V., Sims, M., Gawalapu, R. K., Samdarshi, T. E., Steffes, M., Taylor, H. A., et al. (2013). Aldosterone, C-reactive protein, and plasma B-type natriuretic peptide are associated with the development of metabolic syndrome and longitudinal changes in metabolic syndrome components: findings from the Jackson Heart Study. *Diabetes Care* **36**, 3084–3092.

Nah, S. S., Choi, I. Y., Lee, C. K., Oh, J. S., Kim, Y. G., Moon, H. B. and Yoo, B. (2008). Effects of advanced glycation end products on the expression of COX-2, PGE2 and NO in human osteoarthritic chondrocytes. *Rheumatology (Oxford)* **47**, 425–431.

Nah, S.-S., Choi, I.-Y., Yoo, B., Kim, Y.-G., Moon, H.-B. and Lee, C.-K. (2007). Advanced glycation end products increases matrix metalloproteinase-1, -3, and -13, and TNF-alpha in human osteoarthritic chondrocytes. *FEBS Lett.* **581**, 1928–1932.

Nasi, S., Ea, H.-K., Lioté, F., So, A. and Busso, N. (2016). Sodium Thiosulfate Prevents Chondrocyte Mineralization and Reduces the Severity of Murine Osteoarthritis. *PLoS ONE* **11**, e0158196.

Naski, M. C., Colvin, J. S., Coffin, J. D. and Ornitz, D. M. (1998). Repression of hedgehog signaling and BMP4 expression in growth plate cartilage by fibroblast growth factor receptor 3. *Development* **125**, 4977–4988.

Naski, M. C., Wang, Q., Xu, J. and Ornitz, D. M. (1996). Graded activation of fibroblast growth factor receptor 3 by mutations causing achondroplasia and thanatophoric dysplasia. *Nat. Genet.* **13**, 233–237.

Neacsu, C. D., Grosch, M., Tejada, M., Winterpacht, A., Paulsson, M., Wagener, R. and Tagariello, A. (2011). Ucmaa (Grp-2) is required for zebrafish skeletal development. Evidence for a functional role of its glutamate γ-carboxylation. *Matrix Biol.* **30**, 369–378.

Neumann, E., Junker, S., Schett, G., Frommer, K. and Müller-Ladner, U. (2016). Adipokines in bone disease. *Nat Rev Rheumatol* 1–7.

Nieves-Plaza, M., Castro-Santana, L. E., Font, Y. M., Mayor, A. M. and Vilá, L. M. (2013). Association of hand or knee osteoarthritis with diabetes mellitus in a population of Hispanics from Puerto Rico. *J Clin Rheumatol* **19**, 1–6.

O'Young, J., Liao, Y., Xiao, Y., Jalkanen, J., Lajoie, G., Karttunen, M., Goldberg, H. A. and Hunter, G. K. (2011). Matrix Gla protein inhibits ectopic calcification by a direct interaction with hydroxyapatite crystals. *J. Am. Chem. Soc.* **133**, 18406–18412.

Offiah, A. C. (2015). Skeletal Dysplasias: An Overview. *Endocr Dev* **28**, 259–276.

Olivier, A., Pitt, B., Girerd, N., Lamiral, Z., Machu, J.-L., McMurray, J. J. V., Swedberg, K., van Veldhuisen, D. J., Collier, T. J., Pocock, S. J., et al. (2017). Effect of eplerenone in patients with heart failure and reduced ejection fraction: potential effect modification by abdominal obesity: Insight from the EMPHASIS-HF trial. *Eur. J. Heart Fail.* **13**, 51.

Oliviero, F., Sfriso, P., Baldo, G., Dayer, J.-M., Giunco, S., Scanu, A., Bernardi, D., Ramonda, R., Plebani, M. and Punzi, L. (2009). Apolipoprotein A-I and cholesterol in synovial fluid of patients with rheumatoid arthritis, psoriatic arthritis and osteoarthritis. *Clin. Exp. Rheumatol.* **27**, 79–83.

Onuora, S. (2017). Osteoarthritis: UCMA links cartilage and bone in OA. *Nat Rev Rheumatol* **13**, 130–130.

Orioli, I. M., Castilla, E. E. and Barbosa-Neto, J. G. (1986). The birth prevalence rates for the skeletal dysplasias. *J. Med. Genet.* **23**, 328–332.

Ornitz, D. M. and Legeai-Mallet, L. (2017). Achondroplasia: Development, pathogenesis, and therapy. *Dev. Dyn.* **246**, 291–309.

Ornitz, D. M. and Marie, P. J. (2015). Fibroblast growth factor signaling in skeletal development and disease. *Genes Dev.* **29**, 1463–1486.

Oury, F., Khrimian, L., Denny, C. A., Gardin, A., Chamouni, A., Goeden, N., Huang, Y.-Y., Lee, H., Srinivas, P., Gao, X.-B., et al. (2013). Maternal and Offspring Pools of Osteocalcin Influence Brain Development and Functions. *Cell* **155**, 228–241.

Ovchinnikov, D. (2009). Alcian blue/alizarin red staining of cartilage and bone in mouse. *Cold Spring Harb Protoc* **2009**, pdb.prot5170–pdb.prot5170.

Pan, F., Liu, X.-G., Guo, Y.-F., Chen, Y., Dong, S.-S., Qiu, C., Zhang, Z.-X., Zhou, Q., Yang, T.-L., Guo, Y., et al. (2010). The regulation-of-autophagy pathway may influence Chinese stature variation: evidence from elder adults. *J. Hum. Genet.* **55**, 441–447.

Pannier, S., Mugniery, E., Jonquoy, A., Benoist-Lasselin, C., Odent, T., Jais, J.-P., Munnich, A. and Legeai-Mallet, L. (2010). Delayed bone age due to a dual effect of FGFR3 mutation in Achondroplasia. *Bone* **47**, 905–915.

Pasch, A., Schaffner, T., Huynh-Do, U., Frey, B. M., Frey, F. J. and Farese, S. (2008). Sodium thiosulfate prevents vascular calcifications in uremic rats. *Kidney Int.* **74**, 1444–1453.

Phornphutkul, C., Wu, K.-Y. and Gruppuso, P. A. (2006). The role of insulin in chondrogenesis. *Mol. Cell. Endocrinol.* **249**, 107–115.

Pitt, B., Kober, L., Ponikowski, P., Gheorghiade, M., Filippatos, G., Krum, H., Nowack, C., Kolkhof, P., Kim, S.-Y. and Zannad, F. (2013). Safety and tolerability of the novel non-steroidal mineralocorticoid receptor antagonist BAY 94-8862 in patients with chronic heart failure and mild or moderate chronic kidney disease: a randomized, double-blind trial. *Eur. Heart J.* **34**, 2453–2463.

Pizarro, M., Solís, N., Quintero, P., Barrera, F., Cabrera, D., Rojas-de Santiago, P., Arab, J. P., Padilla, O., Roa, J. C., Moshage, H., et al. (2015). Beneficial effects of mineralocorticoid receptor blockade in experimental non-alcoholic steatohepatitis. *Liver Int* **35**, 2129–2138.

Price, P. A., Rice, J. S. and Williamson, M. K. (1994). Conserved phosphorylation of serines in the Ser-X-Glu/Ser(P) sequences of the vitamin K-dependent matrix Gla protein from shark, lamb, rat, cow, and human. *Protein Sci.* **3**, 822–830.

Price, P. A., Urist, M. R. and Otawara, Y. (1983). Matrix Gla protein, a new gamma-carboxyglutamic acid-containing protein which is associated with the organic matrix of bone. *Biochem. Biophys. Res. Commun.* **117**, 765–771.

Price, P. A., Williamson, M. K., Haba, T., Dell, R. B. and Jee, W. S. (1982). Excessive mineralization with growth plate closure in rats on chronic warfarin treatment. *Proc. Natl. Acad. Sci. U.S.A.* **79**, 7734–7738.

Proudfoot, D. and Shanahan, C. M. (2006). Molecular mechanisms mediating vascular calcification: role of matrix Gla protein. *Nephrology (Carlton)* **11**, 455–461.

Proudman, S. M., Cleland, L. G. and James, M. J. (2008). Dietary Omega-3 Fats for Treatment of Inflammatory Joint Disease: Efficacy and Utility. *Rheumatic Disease Clinics of North America* **34**, 469–479.

Puenpatom, R. A. and Victor, T. W. (2009). Increased prevalence of metabolic syndrome in individuals with osteoarthritis: an analysis of NHANES III data. *Postgrad Med* **121**, 9–20.

Qi, H., Jin, M., Duan, Y., Du, X., Zhang, Y., Ren, F., Wang, Y., Tian, Q., Wang, X., Wang, Q., et al. (2014). FGFR3 induces degradation of BMP type I receptor to regulate skeletal development. *Biochim. Biophys. Acta* **1843**, 1237–1247.

Queisser, N. and Schupp, N. (2012). Aldosterone, oxidative stress, and NF-κB activation in hypertension-related cardiovascular and renal diseases. *Free Radical Biology and Medicine* **53**, 314–327.

Rafael, M. S., Cavaco, S., Viegas, C. S. B., Santos, S., Ramos, A., Willems, B. A. G., Herfs, M., Theuwissen, E., Vermeer, C. and Simes, D. C. (2014). Insights into the association of Gla-rich protein and osteoarthritis, novel splice variants and γ-carboxylation status. *Mol Nutr Food Res* **58**, 1636–1646.

Rasheed, Z., Akhtar, N. and Haqqi, T. M. (2011). Advanced glycation end products induce the expression of interleukin-6 and interleukin-8 by receptor for advanced glycation end product-mediated activation of mitogen-activated protein kinases and nuclear factor-κB in human osteoarthritis chondrocytes. *Rheumatology (Oxford)* **50**, 838–851.

Raucci, A., Laplantine, E., Mansukhani, A. and Basilico, C. (2004). Activation of the ERK1/2 and p38 mitogen-activated protein kinase pathways mediates fibroblast growth factor-induced growth arrest of chondrocytes. *Journal of Biological Chemistry* **279**, 1747–1756.

Reyes, C., Leyland, K. M., Peat, G., Cooper, C., Arden, N. K. and Prieto-Alhambra, D. (2016). Association Between Overweight and Obesity and

Risk of Clinically Diagnosed Knee, Hip, and Hand Osteoarthritis: A Population-Based Cohort Study. *Arthritis Rheumatol* **68**, 1869–1875.

Ribeiro, M., López de Figueroa, P., Blanco, F. J., Mendes, A. F. and Caramés, B. (2016). Insulin decreases autophagy and leads to cartilage degradation. *Osteoarthritis and Cartilage* **24**, 731–739.

Roemhildt, M. L., Beynnon, B. D., Gauthier, A. E., Gardner-Morse, M., Ertem, F. and Badger, G. J. (2013). Chronic in vivo load alteration induces degenerative changes in the rat tibiofemoral joint. *Osteoarthritis and Cartilage* **21**, 346–357.

Rosa, S. C., Gonçalves, J., Judas, F., Mobasheri, A., Lopes, C. and Mendes, A. F. (2009). Impaired glucose transporter-1 degradation and increased glucose transport and oxidative stress in response to high glucose in chondrocytes from osteoarthritic versus normal human cartilage. *Arthritis Res. Ther.* **11**, R80.

Rosa, S. C., Rufino, A. T., Judas, F., Tenreiro, C., Lopes, M. C. and Mendes, A. F. (2011). Expression and function of the insulin receptor in normal and osteoarthritic human chondrocytes: modulation of anabolic gene expression, glucose transport and GLUT-1 content by insulin. *Osteoarthritis and Cartilage* **19**, 719–727.

Sakata, S., Hayashi, S., Fujishiro, T., Kawakita, K., Kanzaki, N., Hashimoto, S., Iwasa, K., Chinzei, N., Kihara, S., Haneda, M., et al. (2014). Oxidative stress-induced apoptosis and matrix loss of chondrocytes is inhibited by eicosapentaenoic acid. *J. Orthop. Res.* **33**, 359–365.

Sanchez, C., Deberg, M. A., Bellahcène, A., Castronovo, V., Msika, P., Delcour, J. P., Crielaard, J. M. and Henrotin, Y. E. (2008). Phenotypic characterization of osteoblasts from the sclerotic zones of osteoarthritic subchondral bone. *Arthritis Rheum.* **58**, 442–455.

Sanchez, C., Pesesse, L., Gabay, O., Delcour, J.-P., Msika, P., Baudouin, C. and Henrotin, Y. E. (2012). Regulation of subchondral bone osteoblast metabolism by cyclic compression. *Arthritis Rheum.* **64**, 1193–1203.

Sasaki, H., Takayama, K., Matsushita, T., Ishida, K., Kubo, S., Matsumoto, T., Fujita, N., Oka, S., Kurosaka, M. and Kuroda, R. (2012). Autophagy modulates osteoarthritis-related gene expression in human chondrocytes. *Arthritis Rheum.* **64**, 1920–1928.

Schett, G., Kleyer, A., Perricone, C., Sahinbegovic, E., Iagnocco, A., Zwerina, J., Lorenzini, R., Aschenbrenner, F., Berenbaum, F., D'Agostino, M.-A., et al. (2013). Diabetes is an independent predictor for severe osteoarthritis: results from a longitudinal cohort study. *Diabetes Care* **36**, 403–409.

Schurgers, L. J., Cranenburg, E. C. M. and Vermeer, C. (2008). Matrix Gla-protein: the calcification inhibitor in need of vitamin K. *Thromb. Haemost.* **100**, 593–603.

Schurgers, L. J., Uitto, J. and Reutelingsperger, C. P. (2013). Vitamin K-dependent carboxylation of matrix Gla-protein: a crucial switch to control ectopic mineralization. *Trends Mol Med* **19**, 217–226.

Sen, U., Vacek, T. P., Hughes, W. M., Kumar, M., Moshal, K. S., Tyagi, N., Metreveli, N., Hayden, M. R. and Tyagi, S. C. (2008). Cardioprotective role of sodium thiosulfate on chronic heart failure by modulating endogenous H2S generation. *Pharmacology* **82**, 201–213.

Shanahan, C. M., Cary, N. R., Salisbury, J. R., Proudfoot, D., Weissberg, P. L. and Edmonds, M. E. (1999). Medial localization of mineralization-regulating proteins in association with Mönckeberg's sclerosis: evidence for smooth muscle cell-mediated vascular calcification. *Circulation* **100**, 2168–2176.

Shapiro, I. M., Layfield, R., Lotz, M., Settembre, C. and Whitehouse, C. (2014). Boning up on autophagy: the role of autophagy in skeletal biology. *Autophagy* **10**, 7–19.

Shiang, R., Thompson, L. M., Zhu, Y. Z., Church, D. M., Fielder, T. J., Bocian, M., Winokur, S. T. and Wasmuth, J. J. (1994). Mutations in the transmembrane domain of FGFR3 cause the most common genetic form of dwarfism, achondroplasia. *Cell* **78**, 335–342.

Shibahara, M., Nishida, K., Asahara, H., Yoshikawa, T., Mitani, S., Kondo, Y. and Inoue, H. (2000). Increased osteocyte apoptosis during the development of femoral head osteonecrosis in spontaneously hypertensive rats. *Acta Med. Okayama* **54**, 67–74.

Shikhman, A. R., Brinson, D. C., Valbracht, J. and Lotz, M. K. (2001). Cytokine Regulation of Facilitated Glucose Transport in Human Articular Chondrocytes. *The Journal of Immunology* **167**, 7001–7008.

Shin, D. (2014). Association between metabolic syndrome, radiographic knee osteoarthritis, and intensity of knee pain: results of a national survey. *J. Clin. Endocrinol. Metab.* **99**, 3177–3183.

Shirinsky, I. V. and Shirinsky, V. S. (2017). Effects of medication-treated diabetes on incidence and progression of knee osteoarthritis: a longitudinal analysis of the Osteoarthritis Initiative data. *Rheumatol. Int.* **34**, 1899–9.

Shung, C.-Y., Ota, S., Zhou, Z.-Q., Keene, D. R. and Hurlin, P. J. (2012). Disruption of a Sox9-β-catenin circuit by mutant Fgfr3 in thanatophoric dysplasia type II. *Human Molecular Genetics* **21**, 4628–4644.

Sindelka, G., Widimský, J., Haas, T., Prázný, M., Hilgertová, J. and Skrha, J. (2000). Insulin action in primary hyperaldosteronism before and after surgical or pharmacological treatment. *Exp. Clin. Endocrinol. Diabetes* **108**, 21–25.

Singh, G., Miller, J. D., Lee, F. H., Pettitt, D. and Russell, M. W. (2002). Prevalence of cardiovascular disease risk factors among US adults with self-reported osteoarthritis: data from the Third National Health and Nutrition Examination Survey. *Am J Manag Care* **8**, S383–91.

Stickens, D., Behonick, D. J., Ortega, N., Heyer, B., Hartenstein, B., Yu, Y., Fosang, A. J., Schorpp-Kistner, M., Angel, P. and Werb, Z. (2004). Altered endochondral bone development in matrix metalloproteinase 13-deficient mice. *Development* **131**, 5883–5895.

Stock, M., Menges, S., Eitzinger, N., Geßlein, M., Botschner, R., Wormser, L., Distler, A., Schlötzer-Schrehardt, U., Dietel, K., Distler, J., et al. (2017). A Dual Role of Upper Zone of Growth Plate and Cartilage Matrix-Associated Protein in Human and Mouse Osteoarthritic Cartilage: Inhibition of Aggrecanases and Promotion of Bone Turnover. *Arthritis Rheumatol*.

Stürmer, T., Sun, Y., Sauerland, S., Zeissig, I., Günther, K. P., Puhl, W. and Brenner, H. (1998). Serum cholesterol and osteoarthritis. The baseline examination of the Ulm Osteoarthritis Study. *J. Rheumatol.* **25**, 1827–1832.

Su, W. C., Kitagawa, M., Xue, N., Xie, B., Garofalo, S., Cho, J., Deng, C., Horton, W. A. and Fu, X. Y. (1997). Activation of Stat1 by mutant fibroblast growth-factor receptor in thanatophoric dysplasia type II dwarfism. *Nature* **386**, 288–292.

Sun, L.-F. and Chen, X. (2012). Tracheobronchial stenosis in Keutel syndrome. *Indian Pediatr* **49**, 759.

Sunnerhagen, M., Drakenberg, T., Forsen, S. and Stenflo, J. (1996). Effect of Ca2+ on the structure of vitamin K-dependent coagulation factors. *Haemostasis* **26 Suppl 1**, 45–53.

Surmann-Schmitt, C., Dietz, U., Kireva, T., Adam, N., Park, J., Tagariello, A., Onnerfjord, P., Heinegård, D., Schlötzer-Schrehardt, U., Deutzmann, R., et al. (2008). Ucma, a novel secreted cartilage-specific protein with implications in osteogenesis. *Journal of Biological Chemistry* **283**, 7082–7093.

Tagariello, A., Luther, J., Streiter, M., Didt-Koziel, L., Wuelling, M., Surmann-Schmitt, C., Stock, M., Adam, N., Vortkamp, A. and Winterpacht, A. (2008). Ucma--A novel secreted factor represents a highly specific marker for distal chondrocytes. *Matrix Biol.* **27**, 3–11.

Takayama, K., Kawakami, Y., Kobayashi, M., Greco, N., Cummins, J. H., Matsushita, T., Kuroda, R., Kurosaka, M., Fu, F. H. and Huard, J. (2014). Local intra-articular injection of rapamycin delays articular cartilage degeneration in a murine model of osteoarthritis. *Arthritis Res. Ther.* **16**, 269–10.

Thomas, W., Dooley, R. and Harvey, B. J. (2009). Aldosterone as a renal growth factor. *Steroids* **75**, 550–554.

Toda, Y., Toda, T., Takemura, S., Wada, T., Morimoto, T. and Ogawa, R. (1998). Change in body fat, but not body weight or metabolic correlates of obesity, is related to symptomatic relief of obese patients with knee osteoarthritis after a weight control program. *J. Rheumatol.* **25**, 2181–2186.

Tsezou, A., Iliopoulos, D., Malizos, K. N. and Simopoulou, T. (2010). Impaired expression of genes regulating cholesterol efflux in human osteoarthritic chondrocytes. *J. Orthop. Res.* **28**, 1033–1039.

Urbanet, R., Nguyen Dinh Cat, A., Feraco, A., Venteclef, N., Mogrhabi, El, S., Sierra-Ramos, C., Alvarez de la Rosa, D., Adler, G. K., Quilliot, D., Rossignol, P., et al. (2015). Adipocyte Mineralocorticoid Receptor Activation Leads to Metabolic Syndrome and Induction of Prostaglandin D2 Synthase. *Hypertension* **66**, 149–157.

Usher, M. G., Duan, S. Z., Ivaschenko, C. Y., Frieler, R. A., Berger, S., Schütz, G., Lumeng, C. N. and Mortensen, R. M. (2010). Myeloid mineralocorticoid receptor controls macrophage polarization and cardiovascular hypertrophy and remodeling in mice. *J. Clin. Invest.* **120**, 3350–3364.

Vaamonde-García, C., Riveiro-Naveira, R. R., Valcárcel-Ares, M. N., Hermida-Carballo, L., Blanco, F. J. and López-Armada, M. J. (2012). Mitochondrial dysfunction increases inflammatory responsiveness to cytokines in normal human chondrocytes. *Arthritis Rheum.* **64**, 2927–2936.

Vashishth, D., Gibson, G. J., Khoury, J. I., Schaffler, M. B., Kimura, J. and Fyhrie, D. P. (2001). Influence of nonenzymatic glycation on biomechanical properties of cortical bone. *Bone* **28**, 195–201.

Verzijl, N., DeGroot, J., Ben, Z. C., Brau-Benjamin, O., Maroudas, A., Bank, R. A., Mizrahi, J., Schalkwijk, C. G., Thorpe, S. R., Baynes, J. W., et al. (2002). Crosslinking by advanced glycation end products increases the stiffness of the collagen network in human articular cartilage: a possible mechanism through which age is a risk factor for osteoarthritis. *Arthritis Rheum.* **46**, 114–123.

Viegas, C. S. B., Cavaco, S., Neves, P. L., Ferreira, A., João, A., Williamson, M. K., Price, P. A., Cancela, M. L. and Simes, D. C. (2009). Gla-rich protein is a

novel vitamin K-dependent protein present in serum that accumulates at sites of pathological calcifications. *Am. J. Pathol.* **175**, 2288–2298.

Viegas, C. S. B., Rafael, M. S., Enriquez, J. L., Teixeira, A., Vitorino, R., Luís, I. M., Costa, R. M., Santos, S., Cavaco, S., Neves, J., et al. (2015). Gla-rich protein acts as a calcification inhibitor in the human cardiovascular system. *Arterioscler. Thromb. Vasc. Biol.* **35**, 399–408.

Viegas, C. S. B., Simes, D. C., Laizé, V., Williamson, M. K., Price, P. A. and Cancela, M. L. (2008). Gla-rich protein (GRP), a new vitamin K-dependent protein identified from sturgeon cartilage and highly conserved in vertebrates. *Journal of Biological Chemistry* **283**, 36655–36664.

Visser, A. W., Ioan-Facsinay, A., de Mutsert, R., Widya, R. L., Loef, M., de Roos, A., le Cessie, S., Heijer, den, M., Rosendaal, F. R., Kloppenburg, M., et al. (2014). Adiposity and hand osteoarthritis: the Netherlands Epidemiology of Obesity study. *Arthritis Res. Ther.* **16**, R19.

Vuppalapati, K. K., Bouderlique, T., Newton, P. T., Kaminskyy, V. O., Wehtje, H., Ohlsson, C., Zhivotovsky, B. and Chagin, A. S. (2015). Targeted Deletion of Autophagy Genes Atg5 or Atg7 in the Chondrocytes Promotes Caspase-Dependent Cell Death and Leads to Mild Growth Retardation. *J. Bone Miner. Res.* **30**, 2249–2261.

Wajih, N., Borras, T., Xue, W., Hutson, S. M. and Wallin, R. (2004). Processing and transport of matrix gamma-carboxyglutamic acid protein and bone morphogenetic protein-2 in cultured human vascular smooth muscle cells: evidence for an uptake mechanism for serum fetuin. *Journal of Biological Chemistry* **279**, 43052–43060.

Wang, X., Qi, H., Wang, Q., Zhu, Y., Wang, X., Jin, M., Tan, Q., Huang, Q., Xu, W., Li, X., et al. (2015). FGFR3/fibroblast growth factor receptor 3 inhibits autophagy through decreasing the ATG12-ATG5 conjugate, leading to the delay of cartilage development in achondroplasia. *Autophagy* **11**, 1998–2013.

Wang, Y., Wei, L., Zeng, L., He, D. and Wei, X. (2013). Nutrition and degeneration of articular cartilage. *Knee Surg Sports Traumatol Arthrosc* **21**, 1751–1762.

Wen, L., Kang, J.-H., Yim, Y.-R., Kim, J.-E., Lee, J.-W., Lee, K.-E., Park, D.-J., Kim, T.-J., Park, Y.-W., Kweon, S.-S., et al. (2016). Associations between body composition measurements of obesity and radiographic osteoarthritis in older adults: Data from the Dong-gu Study. *BMC Musculoskeletal Disorders* **17**, 192.

Whaley-Connell, A., Johnson, M. S. and Sowers, J. R. (2010). Aldosterone: role in the cardiometabolic syndrome and resistant hypertension. *Prog Cardiovasc Dis* **52**, 401–409.

Wieland, H. A., Michaelis, M., Kirschbaum, B. J. and Rudolphi, K. A. (2005). Osteoarthritis - an untreatable disease? *Nat Rev Drug Discov* **4**, 331–344.

Williams, M. F., London, D. A., Husni, E. M., Navaneethan, S. and Kashyap, S. R. (2016). Type 2 diabetes and osteoarthritis: a systematic review and meta-analysis. *J. Diabetes Complicat.* **30**, 944–950.

Wong, M. and Carter, D. R. (2003). Articular cartilage functional histomorphology and mechanobiology: a research perspective. *Bone* **33**, 1–13.

Wong, S. K., Chin, K.-Y., Suhaimi, F. H., Fairus, A. and Ima-Nirwana, S. (2016). Animal models of metabolic syndrome: a review. *Nutrition & Metabolism* 1–12.

Wu, C.-L., Jain, D., McNeill, J. N., Little, D., Anderson, J. A., Huebner, J. L., Kraus, V. B., Rodriguiz, R. M., Wetsel, W. C. and Guilak, F. (2015). Dietary fatty acid content regulates wound repair and the pathogenesis of osteoarthritis following joint injury. *Ann. Rheum. Dis.* **74**, 2076–2083.

Wu, J., Liu, W., Bemis, A., Wang, E., Qiu, Y., Morris, E. A., Flannery, C. R. and Yang, Z. (2007). Comparative proteomic characterization of articular cartilage tissue from normal donors and patients with osteoarthritis. *Arthritis Rheum.* **56**, 3675–3684.

Yagami, K., Suh, J. Y., Enomoto-Iwamoto, M., Koyama, E., Abrams, W. R., Shapiro, I. M., Pacifici, M. and Iwamoto, M. (1999). Matrix GLA protein is a developmental regulator of chondrocyte mineralization and, when constitutively expressed, blocks endochondral and intramembranous ossification in the limb. *J. Cell Biol.* **147**, 1097–1108.

Yang, L., Tsang, K. Y., Tang, H. C., Chan, D. and Cheah, K. S. E. (2014). Hypertrophic chondrocytes can become osteoblasts and osteocytes in endochondral bone formation. *Proc. Natl. Acad. Sci. U.S.A.* **111**, 12097–12102.

Yoshimura, N., Muraki, S., Oka, H., Tanaka, S., Kawaguchi, H., Nakamura, K. and Akune, T. (2012). Accumulation of metabolic risk factors such as overweight, hypertension, dyslipidaemia, and impaired glucose tolerance raises the risk of occurrence and progression of knee osteoarthritis: a 3-year follow-up of the ROAD study. *Osteoarthritis and Cartilage* **20**, 1217–1226.

Youcef, G., Olivier, A., L'Huillier, C. P. J., Labat, C., Fay, R., Tabcheh, L., Toupance, S., Rodriguez-Guéant, R.-M., Bergerot, D., Jaisser, F., et al. (2014). Simultaneous Characterization of Metabolic, Cardiac, Vascular and Renal Phenotypes of Lean and Obese SHHF Rats. *PLoS ONE* **9**, e96452–14.

Youcef, G., Olivier, A., Nicot, N., Muller, A., Deng, C., Labat, C., Fay, R., Rodriguez-Guéant, R.-M., Leroy, C., Jaisser, F., et al. (2016). Preventive and

chronic mineralocorticoid receptor antagonism is highly beneficial in obese SHHF rats. *Br. J. Pharmacol.* **173**, 1805–1819.

Young, M. J. and Rickard, A. J. (2012). Mechanisms of mineralocorticoid salt-induced hypertension and cardiac fibrosis. *Mol. Cell. Endocrinol.* **350**, 248–255.

Yusuf, E., Nelissen, R. G., Ioan-Facsinay, A., Stojanovic-Susulic, V., DeGroot, J., van Osch, G., Middeldorp, S., Huizinga, T. W. J. and Kloppenburg, M. (2010). Association between weight or body mass index and hand osteoarthritis: a systematic review. *Ann. Rheum. Dis.* **69**, 761–765.

Zainal, Z., Longman, A. J., Hurst, S., Duggan, K., Caterson, B., Hughes, C. E. and Harwood, J. L. (2009). Relative efficacies of omega-3 polyunsaturated fatty acids in reducing expression of key proteins in a model system for studying osteoarthritis. *Osteoarthritis and Cartilage* **17**, 896–905.

Zennaro, M.-C., Caprio, M. and Fève, B. (2009). Mineralocorticoid receptors in the metabolic syndrome. *Trends Endocrinol. Metab.* **20**, 444–451.

Zhang, L., Hao, J.-B., Ren, L.-S., Ding, J.-L. and Hao, L.-R. (2014). The aldosterone receptor antagonist spironolactone prevents peritoneal inflammation and fibrosis. *Laboratory Investigation* **94**, 839–850.

Zhang, M. J. and Spite, M. (2012). Resolvins: anti-inflammatory and proresolving mediators derived from omega-3 polyunsaturated fatty acids. *Annu. Rev. Nutr.* **32**, 203–227.

Zhang, Y., Vasheghani, F., Li, Y.-H., Blati, M., Simeone, K., Fahmi, H., Lussier, B., Roughley, P., Lagares, D., Pelletier, J.-P., et al. (2015). Cartilage-specific deletion of mTOR upregulates autophagy and protects mice from osteoarthritis. *Ann. Rheum. Dis.* **74**, 1432–1440.

Zhong, H., Liu, F., Dai, X., Zhou, L. and Fu, P. (2013). Sodium thiosulfate protects human aortic smooth muscle cells from osteoblastic transdifferentiation via high-level phosphate. *Kaohsiung J. Med. Sci.* **29**, 587–593.

Zhou, Z.-Q., Ota, S., Deng, C., Akiyama, H. and Hurlin, P. J. (2015). Mutant activated FGFR3 impairs endochondral bone growth by preventing SOX9 downregulation in differentiating chondrocytes. *Human Molecular Genetics* **24**, 1764–1773.

Zhuo, Q., Yang, W., Chen, J. and Wang, Y. (2012). Metabolic syndrome meets osteoarthritis. *Nat Rev Rheumatol* **8**, 729–737.

Ziereisen, F., De Munter, C. and Perlmutter, N. (1993). The Keutel syndrome. Report of a case and review of the literature. *Pediatr Radiol* **23**, 314–315.

Résumé

Modification du phénotype des chondrocytes dans la plaque de croissance et le cartilage articulaire: de la physiologie à la pathologie

Cartilage est un tissu unique, caractérisé par la matrice extracellulaire abondante et un seul type de cellule, le chondrocytes. Les modifications du phénotype chondrocytes, tels que la prolifération et de l'hypertrophie, sont des événements physiologiques survenant au cours du développement squelettique et cartilage articulaire adulte.

Dans la plaque de croissance, la division active et l'expansion des chondrocytes est le mécanisme principal lors du processus de l'ossification endochondrale. Les chondrocytes jouent un rôle essentiel dans ce processus. Le comportement et les caractéristiques cellulaires des chondrocytes de la plaque de croissance sont régulées à tous les stades de l'ossification endochondrale par un réseau complexe d'interactions entre les hormones circulantes, les facteurs de croissance produits localement et la matrice extracellulaire sécrétée par les chondrocytes.

Dans le cartilage articulaire, les chondrocytes forment des régions morphologiquement distinctes et maintiennent l'équilibre entre production et dégradation des composants de la matrice extracellulaire.

Cependant, l'altération pathologique du phénotype des chondrocytes pourrait entraîner de nombreuses maladies squelettiques et articulaires humaines, y compris les chondrodysplasies et l'arthrose. Dans ce contexte, mon projet de doctorat a été conçu pour étudier I) les modifications des phénotypes chondrocytaires déclenchés par les déterminants génétiques et le stress métabolique et par conséquent II) la participation des deux conditions pathologiques au développement de la maladie et/ou à la progression.

Mots-Clés: Phénotype chondrocytaire, Cartilage, Matrix Gla Protein, Syndrome métabolique

Abstract

Modification of chondrocyte phenotype in growth plate and articular cartilage : from physiology to pathology

Cartilage is a unique tissue characterized by abundant extracellular matrix and a single cell type, the chondrocyte. Modifications of chondrocyte phenotype, such as proliferation and hypertrophy, are physiological events occuring during skeletal development and in adult articular cartilage.

In growth plate cartilage, the active division and expansion of chondrocytes is the primary mechanism during the process of endochondral bone formation. Chondrocytes play a central role in this process, through a combination of proliferation, extracellular matrix secretion and hypertrophy. The behaviour and cellular features of growth plate chondrocytes are regulated at all stages of endochondral ossification by a complex network of interactions between circulating hormones, locally produced growth factors and the extracellular matrix secreted by the chondrocytes.

In articular cartilage, the chondrocytes form morphologically distinct regions, including a superficial region of flattened cells, a sparsely populated middle layer, and a deep zone of hypertrophic chondrocytes. In mature articular cartilage, these chondrocytes maintain the balance of production and degradation of extracellular matrix components.

However, pathological alteration of chondrocyte phenotype could lead to numerous human skeletal and articular diseases, including chondrodysplasias and osteoarthritis. In this context, my PhD project was designed to study I) the modifications of chondrocyte phenotypes triggered by genetic determinants and metabolic stress and consequently II) the participation of both pathologic conditions to disease development and/or progression.

Keywords: Chondrocyte phenotype, Cartilage, Matrix Gla protein, Metabolic syndrome